Characterizing iron sensing and overload in health and disease

Edouard Charlebois

Microbiology and Immunology, McGill University, Montreal

December 2022

A thesis submitted to McGill University in partial fulfillment of the requirements

of the degree of Doctor of Philosophy

©Edouard Charlebois, 2022

Abstract

Iron's ability to participate in redox reactions has made it indispensable for many cellular processes including oxygen transport, DNA synthesis, and development in practically all living organisms. Iron in the circulation is transported and kept inert by transferrin to prevent the undesired formation of dangerous radicals produced by Fenton chemistry. In mammals, systemic iron homeostasis is regulated by the liver-derived peptide hormone hepcidin (gene name: *HAMP*) which functions by preventing cellular iron export through ferroportin. Consequently, sustained elevated hepcidin production results in hypoferremia due to cellular iron retention whereas abrogated expression results in iron accumulation in the bloodstream and, subsequently, in tissues. *HAMP* transcription is regulated by bone morphogenetic proteins (BMP), namely BMP6 and BMP2, produced by the liver's sinusoidal endothelial cells (LSEC) and proinflammatory interleukin-6 (IL-6). This thesis has aimed to address how LSECs finetune BMP expression in response to iron fluctuations, how inflammatory hypoferremia can be restored in the context of iron overload, and how iron overload influences the progression of the intramacrophage protozoan parasite *Leishmania*. To address the first question, we utilized mice with endothelial-specific ablation of transferrin receptor 1, a receptor involved in regulated transferrin-bound iron import. Knockout animals demonstrated physiological expression of *Hamp* and *Bmp6* messenger RNA (mRNA) and retained the ability to induce their expression in response to iron challenge. Both *Hamp* and *Bmp6* mRNAs correlated with non-transferrin bound iron (NTBI) accumulation during iron loading. Single cell transcriptomics revealed a profound effect of dietary iron absorption compared to transferrin-bound iron injection on the reprogramming of LSECs and revealed that dietary iron intake activates target genes of the antioxidant transcription factor nuclear factor erythroid 2-related factor 2 (*Nfe2l2*) which regulates BMP transcription. These data suggest that LSECs sense iron fluctuations primarily by NTBI. We then explored hepcidin's regulatory network using hemojuvelin (gene name: *HJV*) knockout animals. These mice present with severe systemic iron overload triggered from the inactivation of this BMP co-receptor and ensuing disruption of *Hamp* expression. We sought to dissect whether iron overload, lack of HJV, or both triggered the observed lack of inflammatory hypoferremia. Iron depletion in *Hjv*$^{-/-}$ animals did not rescue *Hamp* expression in response to lipopolysaccharide (LPS). However, iron-depleted

knockout mice were more sensitive to synthetic hepcidin treatment. Polysome profiling revealed elevated ferroportin translation in iron loaded conditions. Treatment with concurrent LPS, which inhibited ferroportin transcription, and synthetic hepcidin, which degraded cell surface ferroportin, managed to induce a successful hypoferremic response in iron loaded animals suggesting that ferroportin renewal is the limiting factor for hypoferremia in these. Finally, experiments using *Hjv*$^{-/-}$ animals infected with *Leishmania major* revealed that these were transiently protected from cutaneous leishmaniasis. Acute intraperitoneal infection with *L. major* revealed increased expression of the cytokines and chemokines *Il1b*, *Tnf*a, *Cxcl2*, and *Ccl2* in peritoneal cells suggesting a possible role for these in transient protection. Taken together, this work has broadened our understanding of homeostatic iron sensing, uncovered the main driver preventing inflammatory hypoferremia during iron overload, and expanded our understanding of iron's role in leishmaniasis.

Résumé

Chez les mammifères, la capacité du fer à participer aux réactions d'oxydoréduction l'a rendu indispensable à de nombreux processus cellulaires, notamment le transport de l'oxygène, la synthèse de l'ADN et le développement. Le fer présent dans la circulation est transporté et maintenu inerte par la transferrine pour éviter la formation indésirable de radicaux dangereux produits par la chimie de Fenton. L'homéostasie systémique du fer est maintenue par l'hormone dérivée du foie, l'hepcidine (gène : *HAMP*), qui fonctionne en empêchant l'exportation du fer par la ferroportine. Par conséquent, une production élevée et soutenue d'hepcidine entraîne une hypoferrémie due à la rétention du fer, tandis qu'une expression réduite entraîne une accumulation de fer dans le sang et, ensuite, dans les tissus. La transcription de *HAMP* est régulée par les protéines morphogénétiques osseuses (BMP), notamment BMP6 et BMP2, produites par les cellules endothéliales sinusoïdales du foie (LSEC) et l'interleukine-6 (IL-6) inflammatoire. Cette thèse a eu pour objectif d'étudier comment les LSEC ajustent l'expression des BMP en réponse aux fluctuations du fer, comment l'hypoferrémie inflammatoire peut être restaurée dans un contexte de surcharge en fer, et comment la surcharge en fer influence la progression du parasite protozoaire intramacrophage *Leishmania*. Premièrement, nous avons utilisé des souris dont le récepteur 1 de la transferrine a été éliminé de l'endothélium. Les animaux knockout manifestaient une expression physiologique de l'ARN messager (ARNm) de *Hamp* et de *Bmp6* et conservaient la capacité d'induire leur expression en réponse à un défi ferreux. Les ARNm de *Hamp* et de *Bmp6* sont corrélés au fer non lié à la transferrine (NTBI) qui s'accumule pendant la charge en fer. La transcriptomique unicellulaire a révélé un effet profond du fer alimentaire par rapport à l'injection de fer lié à la transferrine sur la programmation des LSEC en activant les gènes cibles du facteur de transcription antioxydant *Nfe2l2* qui régule la transcription de BMP. Ces résultats suggèrent que les LSECs détectent les fluctuations du fer principalement par le NTBI. Ensuite, nous avons exploré le réseau de régulation de l'hepcidine en utilisant des animaux knockout pour l'hémojuveline (HJV) qui présentent une surcharge en fer systémique sévère déclenchée par l'inactivation de ce co-récepteur de BMP et la perte d'expression de *Hamp* qui s'ensuit. Nous voulions déterminer si la surcharge en fer, l'absence de HJV, ou les deux, étaient à l'origine de l'absence d'hypoferrémie inflammatoire. Une carence en fer chez les animaux $Hjv^{-/-}$ n'a pas pu

sauver l'expression de *Hamp* induit par le lipopolysaccharide (LPS). Cependant, les souris knockout dépourvues de fer étaient plus sensibles au traitement d'hepcidine synthétique. Le profilage des polysomes a révélé une traduction élevée de la ferroportine dans des conditions de charge en fer. Un traitement simultané par LPS, lequel inhibe la transcription de la ferroportine, et par l'hepcidine synthétique, lequel dégrade la ferroportine de surface cellulaire, a réussi à induire une réponse hypoferrémique chez les animaux chargés en fer, ce qui suggère que le renouvellement de la ferroportine est le facteur limitant de l'hypoferrémie chez ces derniers. Enfin, des expériences utilisant des animaux *Hjv*$^{-/-}$ infectés par *Leishmania major* ont révélé que ceux-ci étaient transitoirement protégés de la leishmaniose cutanée. L'infection intrapéritonéale par *L. major* a révélé une augmentation de l'expression des cytokines et des chimiokines *Il1b, Tnfa, Cxcl2* et *Ccl2* dans les cellules péritonéales, ce qui suggère un rôle possible de ces dernières dans la protection transitoire. Dans l'ensemble, ce travail a permis d'élargir notre compréhension de la détection systémique du fer, de découvrir le principal moteur empêchant l'hypoferrémie inflammatoire pendant la surcharge en fer, et d'élargir notre compréhension du rôle du fer dans la leishmaniose.

Acknowledgements

I would like to begin by acknowledging the funding obtained from the Canadian Institutes of Health Research (CIHR) during the first year of my Master's degree and from the *Fonds de recherche du Québec – Santé* (FRQS) during the second year as well as over the course of my doctorate.

The work presented herein would not have been possible without the help, guidance, and mentorship of many remarkable people. I begin by thanking my supervisor, Kostas Pantopoulos, for his incredible support over these past 6 years. Our journey together began on a somewhat difficult pass. I had no idea what I was doing, was placed under the supervision of a renegade student, and the lab's funds were running dry. To everyone's amazement, we pulled through for each of these problems. I quickly learned the necessary skills to perform robust, reproducible experiments thanks to the expert supervision of your wonderful research associate Carine Fillebeen, we quickly realized that we needed to be more careful which students we accepted into the lab, and, by overcoming these two challenges in addition to persevering in the face of adversity, managed to secure important funds that would help keep the lab running during my doctorate. From there, we made important contributions to the field of iron metabolism which led us on many adventures together including to Alberta in western Canada and to Heidelberg in Germany. These experiences helped shape me into the scientist I am today. Of course, this was only made possible by your easygoing, approachable, and determined attitude. The initial reticence to approach the supervisor that all students face quickly evaporated. Thank you for always being available to answer my questions despite the answers not always being what I want to hear! My goal was to leave the lab in a better place than the one I found it. I hope I've managed to achieve this.

It is impossible to think I would have lasted more than a week in academia without the help of Carine. Carine, you are our lab mom through and through. You stand as a beacon of experience guiding us along our path through the twists and turns of graduate studies. You somehow always have valuable input when we show you our results which don't make any sense most of the time. It is impossible to put into words how amazing it is to have you help us without ever complaining even if you are visibly frustrated with us at times. You may not know it, but you brighten our days immeasurably. The treats and sweets you bring us help keep us sane through the darkest times.

Much like a mother, a lot of the work you do is underappreciated and unrecognized until the students (children) have grown. Having done a bit of my own mouse tag and tailing and genotyping, I know how thankless this job can be. The current students have no idea how lucky they are to have you. I've tried my best to keep you laughing and entertained in return, but I know this is a small reward for an immense responsibility. Thank you for shaping me into the adult I have become today. You keep joking that I will forget about you, but I'm not sure anyone could forget someone so exceptional.

Of course, I would also like to thank my co-supervisor, Martin Olivier, for his expertise in leishmaniasis which was invaluable for the success of our project together. Martin, your passion for leishmaniasis is second to none. Although at times it is difficult to keep up with such enthusiasm, you always have interesting ideas to share deepening our love for *Leishmania* as well. Thank you for inviting us into your world. It has also been a pleasure to spend time with you during lab activities and at scientific conferences. Cartagena was an amazing experience full of wonderful science. Your ability to form bonds with other researchers has helped expand our connections in the field tremendously furthering our knowledge as a result.

My journey as a graduate student has been marked by many exceptional colleagues and friends. Despite not being a molecular biologist by training, Ageliki, I like to think you have taught me more than I have taught you. You arrived as a bewildered post-doc, but your amazing quality to draw people in helped you quickly bond with our lab and learn the necessary skills to succeed. You have been one of my closest confidants through my journey as a graduate student. Thank you for always being there when I needed to discuss difficult subjects whether they were about lab work, our supervisor, or boring adult topics like finding jobs. I envy your ability to explore outside of your comfort zone. Leaving your country to come work in an academic lab miles away from home is no simple task. I truly appreciate all the activities you have introduced me to like cross country skiing and climbing. Without you, my extracurricular life would have been much more depressing.

To the present and past Pantopoulos lab members, John, Maria, Wen, Yupeng, Sofiya, and Sabrina – thank you for helping me along the way and I know you are in good hands! Maria, your joyful nature was indispensable to life in the lab. You and your infectious laugh have been sorely

missed ever since you graduated. Yupeng, thank you in particular for the help on the *Leishmania* project. I am confident you have the making of a great scientist if you put your mind to it.

To the present and past members of the Olivier lab, Line, George, Amy, Victoria, Andrea, and Carlos – thank you so much for supporting me through unfamiliar territory. Line, you are a shining beacon of happiness for all of us. I have never met someone as joyful as you and I hope you continue to radiate your inspiring energy. Victoria, I could not have survived many of these experiments without you. Your organization and planning are like no other.

I would like to thank my advisory committee members Stéphanie Lehoux and Maziar Divangahi for providing me with essential advice and taking the time to try to understand my projects even when they are quite confusing. Their ideas and comments were greatly appreciated and helped expand my knowledge in the field.

A substantial amount of work would not have been possible without the help of the community at the Lady Davis Institute. I would like to thank the Schiffrin lab for allowing us to use their equipment, the Topisirovic lab, in particular Predrag and Sam, for showing me how to use the polysome fractionator, Mike Giovinazzo for his countless guidance whenever a common room machine equipment broke or was difficult to use, and both Naciba Benlimame and Lilian Canetti for their help with immunohistochemistry and immunofluorescence sample processing. A special thank you to Kathy Forner, Veronique Michaud, and Yvhans Chery of the animal facility for all the help they provided with animal procedures.

Finally, I would like to thank my family for being so patient with me. I know it is difficult to understand that science and doctorate degrees are a lengthy process. But good things come to those who wait – or so they say. Thank you for supporting me through these long years despite being part of a world that is completely foreign to most. This thesis could not have been possible without your patience and understanding.

Table of Contents

List of Tables and Figures

CHAPTER 1

CHAPTER 2

Main Figures

Supplemental Figures and Tables

CHAPTER 3

Main Figures

Supplemental Figures and Tables

CHAPTER 4

Main Figures

Supplemental Figures and Tables

Keywords and Definitions

Keyword	Definition
Anemia	Condition characterized by low red blood cell count and low hemoglobin.
Bone morphogenetic proteins (BMP)	Signaling molecules part of the TGF-β superfamily.
Ferroportin (FPN, *SLC40A1*)	The sole elemental iron exporter responsible for iron flow from cells to the bloodstream.
Hemochromatosis	Diseases of excess body iron and reduced hepcidin expression.
Hemojuvelin (*HJV*)	A RGM family BMP co-receptor important for hepcidin signaling.
Hepcidin (*HAMP*)	A liver-derived peptide hormone that controls iron efflux by binding and degrading ferroportin.
Holo/apo-transferrin	Transferrin bound to (holo) or devoid (apo) of iron.
Hypoferremia	A state characterized by lowered levels of serum iron compared to healthy individuals or animals.
Leishmaniasis	A condition resulting from infection with the intra-macrophage protozoan parasite of genus *Leishmania.*
Non-transferrin bound iron (NTBI)	Iron bound to small molecule carriers (citrate or acetate) or peptides other than transferrin (albumin).
Transferrin	A peptide ferric iron carrier found in the circulation.
Transferrin receptor 1	The cellular iron gate responsible for regulated uptake of transferrin-bound iron.

List of Abbreviations

Abbreviation	Full Name
°C	Degree Celsius
2-ME	2-mercaptoethanol
AB	Alberta
ABCG2	ATP-binding cassette sub-family G member 2 protein
ALAS2	5-aminolevulinic acid synthase 2
AML12	Alpha mouse liver 12
ANOVA	Analysis of variance
ARE	Antioxidant response element
AUC	Area under curve
BC	B lymphocyte
BMP	Bone morphogenetic protein
BMPR	Bone morphogenetic protein receptor
BSL	Biosafety level
CA	California
CCAC	Canadian Council on Animal Care
CCL	Chemokine (C-C motif) ligand
CD	Cluster of differentiation
CDC14A	Cell division cycle 14A
CDC42BPA	Myotonic dystrophy protein kinase-like alpha
cDNA	Complementary deoxyribonucleic acid
CE-ICP-MS	Capillary electrophoresis-inductively coupled plasma mass spectrometry
CIHR	Canadian Institutes of Health Research
CO_2	Carbon dioxide
CROT	Carnitine O-Octanoyltransferase
CUL1	Cullin 1
CXCL	Chemokine (C-X-C motif) ligand
CYBRD1	Duodenal cytochrome b
DAPI	4′,6-diamidino-2-phenylindole
DEG	Differentially expressed gene
DFO	Desferrioxamine
Diff-Quik	Differential Quik
DMT1	Divalent metal transporter 1
DNA	Deoxyribonucleic acid
EC	Endothelial cell
ELISA	Enzyme-linked immunosorbent assay
EMSA	Electrophoretic mobility shift assay

ERFE	Erythroferrone
EV	Extracellular vesicle
FAC	Ferric ammonium citrate
FBS	Fetal bovine serum
FBXL5	F-Box and leucine rich repeat protein 5
FC	Fold change
Fl	Floxed
FLVCR	Feline leukemia virus subgroup C cellular receptor
FPN	Ferroportin
FRQS	Fonds de recherche du Québec - santé
FSL1	Synthetic diacylated lipoprotein, Pam2CGDPKHPKSF
FTH1	Ferritin heavy chain
FTL	Ferritin light chain
FTMT	Mitochondrial ferritin
GCP2	Glutamate carboxypeptidase II
GEO	Gene Expression Omnibus
GM-CSF	Granulocyte-macrophage colony-stimulating factor
GO	Gene ontology
GPI	Glycophosphatidylinositol
GPX	Glutathione peroxidase
GSVA	Gene set variation analysis
H&E	Haematoxylin and eosin
Hamp	Hepcidin
HbR	Hemoglobin receptor
HCP1	Heme carrier protein 1
HECT	Homologous to the E6-AP carboxyl terminus
HEK293H	Human embryonic kidney 293 with good adherence
HEK293T	Human embryonic kidney 293 with mutated large T antigen
HEPES	4-(2-hydroxyethyl)-1-piperazineethanesulfonic acid
HERC2	HECT and RLD domain-containing E3 ubiquitin ligase
HFE	Homeostatic iron regulator
HID	High iron diet
HIF	Hypoxia inducible factor
HJV	Hemojuvelin
HMOX	Heme oxygenase
hnRNP K	Heterogeneous nuclear ribonucleoprotein K
HPLC	High-performance liquid chromatography
HRE	Hypoxia response element
HRG1	Heme-responsive gene 1
HRI	Heme-regulated eIF2α kinase
HRP	Horseradish peroxidase

Huh7	Human hepatoma cell line 7
Id	Inhibitor of DNA binding
IDD	Iron deficient diet
IFNγ	Interferon gamma
IL	Interleukin
INHBB	Inhibin subunit beta b
iNOS	Inducible nitric oxide synthase
IP	Intraperitoneal
IRE	Iron response element
IRIDA	Iron-refractory iron-deficiency anemia
IRP	Iron regulatory protein
IRT	Iron regulated transporter
IV	Intravenous
JAK	Janus kinase
kDa	Kilodalton
LCN	Lipocalin
LFR1	*Leishmania* ferric reductase 1
LHR1	Leishmania heme response 1
LIC	Liver iron content
LIP	Labile iron pool
LIR1	*Leishmania* iron regulator 1
LIT1	*Leishmania* iron transporter 1
LmFLVCRB	*Leishmania* feline leukemia virus subgroup C cellular receptor b
LN	Lymph node
Log	Logarithm
LPS	Lipopolysaccharide
LSEC	Liver sinusoidal endothelial cell
LTCC	L-type calcium channel
MA	Massachusetts
MAF	Musculoaponeurotic Fibrosarcoma
MCH	Mean corpuscular hemoglobin
MCV	Mean corpuscular volume
mG	membrane-Green
MHC	Major histocompatibility complex
MLN	Mesenteric lymph node
mRNA	Messenger ribonucleic acid
MSigDB	Molecular Signature Database
mT	membrane-Tomato
mTOR	Mammalian target of rapamycin
Myc	MYC Proto-Oncogene, BHLH Transcription Factor
NAD	Nicotinamide adenine dinucleotide

NCOA4	Nuclear receptor coactivator 4
NEO1	Neogenin
NF-κB	Nuclear factor-κB
NOS2	Nitric oxide synthase 2
NRAMP1	Natural resistance associated macrophage protein 1
NRF2/NFE2L2	Nuclear Factor Erythroid 2-Related Factor 2
NSERC	Natural Sciences and Engineering Research Council of Canada
NTA	Nitrilotriacetate
NTBI	Non-transferrin bound iron
OD	Optical density
OXPHOS	Oxidative phosphorylation
P47PHOX	Neutrophil cytosolic factor 1
PBS	Phosphate-buffered saline
PCBP	Poly-C binding protein
pH	Potential hydrogen
PV	Parasitophorous vacuole
QC	Quebec
qPCR	Quantitative polymerase chain reaction
Rab	Ras-associated binding
RBC	Red blood cell
RCC1	Regulator of chromosome condensation 1-protein
RDW	Red cell distribution width
RGM	Repulsive guidance molecule
RLD	RCC1 like domain
RNA	Ribonucleic acid
RNF217	Ring finger protein217
ROS	Reactive oxygen species
RPMI	Roswell Park memorial Institute medium
RT	Room temperature
scRNA-Seq	Single cell RNA sequencing
SD	Standard Diet
SDM	Schneider's Drosophila Medium
SDS-PAGE	Sodium dodecyl-sulfate polyacrylamide gel electrophoresis
SEM	Standard error of the mean
Sf9	Spodoptera frugiperda 9
SIC	Spleen iron content
siRNA	Short interfering ribonucleic acid
SKP1	S-phase kinase associated protein 1
SLC	Solute carrier
SMAD	Small mother against decapentaplegic
SOCS	Suppressor of cytokine signaling

STAT	Signal transducers and activators of transcription
STEAP3	Six-transmembrane epithelial antigen of the prostate 3
TBS	Tris-buffered saline
TBS-T	TBS containing Tween-20
TEK	Tyrosine Kinase, Endothelial
Tf	Transferrin
TFA	Trifluoroacetic acid
TFR	Transferrin receptor
Tg	Transgene
TGF-β	Transforming growth factor β
Th	T helper
TIBC	Total iron binding capacity
TLR	Toll-like receptor
TMPRSS6	Transmembrane serine protease 6
TNFα	Tumor necrosis factor α
TTCC	T-type calcium channel
TTP	Tristetraprolin
UMAP	Uniform manifold approximation and projection
UMG	University Medical Center Göttingen
USA	United States of America
USF2	Upstream stimulatory factor 2
UTR	Untranslated region
v/v	Volume by volume
w/v	Weight by volume
WT	Wild type
ZIP	ZRT/IRT like protein
ZnMP	Zinc(II) mesoporphyrin IX
ZRT	Zinc transporter protein
µg	Microgram
µl	Microliter
µm	Micrometer

Contribution of Authors

The candidate has chosen to submit a manuscript-based thesis. This thesis contains three original manuscripts and is in accordance with the guidelines for thesis preparation provided by the Faculty of Graduate and Postdoctoral Studies of McGill University. The candidate, Edouard Charlebois, is recognized as the principal author and to have performed the majority of the work of the manuscripts presented. The specific contributions of authors are as follows:

Chapter 1 and 5

The literature review and general discussion are novel and written in its entirety by EC and reviewed by KP.

Chapter 2

Charlebois E, Fillebeen CC, Presley JF, Cagnone G, Lisi V, Lavallee VP, Joyal JS, & Pantopoulos P. Liver sinusoidal endothelial cells induce BMP6 expression in response to non-transferrin bound iron. *Blood*. 2022.

Permission to reprint this article for theses is granted under the American Society of Hematology copyright agreement available online.

EC was involved in all aspects of the study. EC performed experiments, delineated cell populations for single cell experiments, helped guide the generation of single cell figures, and helped guide analysis of data for single cell work.

CCF provided help with breeding mice and with experimental design.

JP stained slides for immunofluorescence and generated images at the confocal.

GC performed the bulk of the bioinformatics analysis of single cell sequencing experiments, generated figures related to single cell experiments, and wrote part of the results and methods section under the supervision of JSJ.

VL and VPL performed and supervised, respectively, the generation of single-cell RNA sequencing libraries.

KP helped design and supervise experiments and wrote the manuscript.

*Slides for immunofluorescence were processed by Lilian Canetti of the pathology department of the Jewish General Hospital.

**Measurements of serum iron parameters were performed by the Biochemistry Department of the Montreal Jewish General Hospital.

Chapter 3

Charlebois E, Fillebeen C, Katsarou A, Rabinovich A, Wisniewski K, Venkataramani V, Michalke B, Velentza A, & Pantopoulos, P. A crosstalk between hepcidin and IRE/IRP pathways controls ferroportin expression and determines serum iron levels in mice. *eLife*. 2022.

This manuscript is reprinted from the journal eLife with permissions granted by the Creative Commons Attribution (CC BY) license.

EC was involved in all aspects of the study. EC performed most experiments and generated all figures.

CF helped breed mouse colonies, placed mice on diets, and was indispensable for electromobility shift assays involving radioactivity.

AK helped collect samples.

AR, KW, and AV generated and provided synthetic hepcidin used in experiments.

VV and MB analyzed samples for iron speciation.

KP designed the study and wrote the manuscript.

*Slides for immunohistochemistry and Perls staining were processed by Dr. Naciba Benlimame and Lilian Canetti of the pathology department of the Montreal Jewish General Hospital.

**Measurements of serum iron parameters were performed by the Biochemistry Department of the Montreal Jewish General Hospital.

Chapter 4

Charlebois E, Li Y, Wagner V, Pantopoulos K, & Olivier M. Genetic iron overload hampers development of cutaneous leishmaniasis in mice. *International Journal of Molecular Sciences*. 2023.

This manuscript is reprinted from the International Journal of Molecular Sciences with permissions granted by the Creative Commons Attribution (CC BY) license.

EC was involved in all aspects of this study. EC performed experiments, generated all figures, and wrote the first draft of the manuscript.

YL helped perform qPCR experiments and analyze data for parasite load.

VW helped collect samples for footpad parasite load measurements.

KP supervised the study, provided guidance, and edited the manuscript.

MO helped with animal injections, measuring footpads, collecting intraperitoneal lavage samples, and designed the study.

*Multiplex assays were performed by EVE Technologies.

**Measurements of serum iron parameters were performed by the Biochemistry Department of the Montreal Jewish General Hospital.

Contributions to Original Knowledge

The work presented herein contributes to original knowledge in the field of iron metabolism, iron restriction as a form of innate immunity, and iron's function in leishmaniasis. The specific contributions are as follows:

In **Chapter 2**, we explored how liver sinusoidal endothelial cell iron acquisition affects their ability to sense iron and produce the iron-sensitive bone morphogenetic protein 6 (BMP6) by ablating the cellular iron gate transferrin receptor 1 (Tfr1) in mice. Our study revealed the following:

1. Lack of endothelial Tfr1 did not hinder basal levels of *Bmp6* messenger RNA (mRNA) expression in mice.
2. *Bmp6* mRNA expression can be induced by dietary iron loading and by iron-bound transferrin in knockout animals.
3. Non-transferrin bound iron correlates with expression of *Bmp6*.
4. Endothelial cells undergo extensive reprogramming in response to dietary iron and activate nuclear factor erythroid 2-related factor 2 (Nfe2l2) as revealed by single cell transcriptomics.

In **Chapter 3**, we investigated the crosstalk between iron and inflammatory signaling necessary for activation of the liver peptide hormone hepcidin (Hamp) responsible for controlling systemic iron homeostasis. We demonstrated that:

1. Genetic and dietary iron overload impair the ability for animals to produce a successful hypoferremic response resulting from inflammatory challenge necessary to withhold iron from invading pathogens.
2. Treatment with supraphysiological doses of synthetic Hamp alone is not enough to produce hypoferremia in iron loaded animals.
3. The cellular iron exporter ferroportin is extensively transcribed and translated during iron overload.

4. Hypoferremia can only be induced in conditions of iron overload when combination treatment of an inflammatory agent and synthetic hepcidin are used to disrupt both transcription and cell surface expression of ferroportin.

In **Chapter 4**, we sought to study the progression of leishmaniasis in a model of severe genetic iron overload lacking expression of Hamp. This model provides a unique look at leishmaniasis because macrophages, *Leishmania*'s host cell, lack iron stores due to unregulated expression of ferroportin. We showed that:

1. Genetically iron overloaded animals demonstrate a transient resistance to cutaneous leishmaniasis in footpads.
2. Acute exposure to intraperitoneal *Leishmania major* failed to induce interferon gamma expression in the liver of knockout animals whereas their intraperitoneal cells demonstrated increased mRNA expression of *Il1b*, *TNFa*, *Cxcl2*, and *Ccl2*.
3. Parasite burden of *L. infantum* in genetically iron overloaded mice matched control animals in spleens and livers, despite the former expressing elevated ferroportin protein levels suggesting that this protein is not a determinant of protection.

Taken together, these results outline the importance of continued basic research in the field of iron metabolism including iron's importance for pathogen growth and development. This work helps guide production of therapies for patients suffering from iron overload and strategies for treating patients with leishmaniasis.

Chapter 1: Literature Review and Research Objectives

Iron has been a crucial element for the development of life on earth. Primitive organisms existed in an environment rich in iron and sulfur with little oxygen. These elements were used to generate iron-sulfur clusters as an accessible form of electron transport with many different metabolic functions[1]. Iron found in the earth's mantle was crucial for generation of simple life as well as to maintain adequate water supplies on the planet's surface for eventual evolution of complex life[2]. The appearance of photosynthetic cyanobacteria approximately 2.4 billion years ago brought a rise in atmospheric oxygen and subsequent drop in bioavailable ferrous (Fe^{2+}) iron due to its oxidation to ferric (Fe^{3+}) iron necessitating life to adapt by creating antioxidant mechanisms and improving iron acquisition methods[3]. At all points, iron within organisms was required to be carefully regulated to control its participation in Fenton chemistry[4], the products of which are highly aggressive hydroxyl radicals which are potent oxidants. The details of Fenton chemistry are outlined below[5].

$$Fe^{2+} + H_2O_2 \rightarrow Fe^{3+} + {}^{\bullet}OH + OH^-$$

$${}^{\bullet}OH + H_2O_2 \rightarrow HO_2^{\bullet} + H_2O$$

$$Fe^{2+} + {}^{\bullet}OH \rightarrow Fe^{3+} + OH^-$$

$$Fe^{3+} + HO_2^{\bullet} \rightarrow Fe^{2+} + O_2 + H^+$$

$${}^{\bullet}OH + {}^{\bullet}OH \rightarrow H_2O_2$$

$$\text{Organic pollutant} + {}^{\bullet}OH \rightarrow \text{Degraded products}$$

The term reactive oxygen species (ROS) has been broadly used to describe the different oxygen radicals, including those produced by iron, within cells. Used by practically all living organisms, iron's ability to readily accept and donate electrons has made it indispensable for oxygen transport, cellular metabolism, DNA synthesis, innate immunity, growth, and development[6]. Hence, from simple to complex organisms, many strategies have been developed to fulfill iron requirements while maintaining relative safety.

1.1 Ferritin and iron storage

A logical solution to the problem of iron's reactivity is to maintain areas of storage where it can be kept inert, and this is achieved by ferritin. This was the first description of a protein with a role in iron metabolism. Ferritin is a ferroxidase first isolated in 1937 from horse spleens due to its abundance and the second protein ever to be crystallized[7]. Ferritin has homologs in all organisms except for yeast. This enzyme is unique in that it stores its own product[8]. In humans, ferritin forms a shell of 24 subunits of two different sizes, dubbed light (gene name: *FTL*) and heavy (gene name: *FTH1*) chain subunits, which are 19 kDa and 21 kDa, respectively[9]. Despite being relatively close in size, these two subunits are only roughly 50% similar in sequence likely having diverged during evolution from a common ancestral gene[10,11]. Moreover, both ferritins maintain relatively similar three-dimensional structure aiding it to form its shell-like shape. Studies have shown that FTH1 appears be the main catalytic component for ferroxidation[12]. Homopolymers of this subunit can oxidize and store iron faster than physiological ferritin complexes and this subunit maintains its oxidation activity even when the polypeptide ends are truncated by a few amino acids[13]. Additionally, the carboxy terminal of the heavy chain forming the hydrophobic channel plays a role in iron core formation[13]. FTL would simply aid the nucleation of the iron core[12,14] as FTL homopolymers do not properly store iron[15]. The importance of FTH1 is underlined by attempts to generate knockouts and their early embryonic lethal phenotype[16]. Speculations propose that ferritin plays a critical role in cardiac development since lethality occurs at day 9.5 when FTH1 expression is highest in cardiac cells[16].

Ferritin complexes can store up to 4500 atoms of iron in the form of ferric oxyhydroxide[9]. This creates an inert repository of iron that can be quickly accessed within cells during periods of iron demand. Characteristically, because of ferric iron's low solubility and generally oxidized state, cells must convert iron to its ferrous form only when it is ready to be used or transported to its target site. It is currently thought that ferritin is primarily cytosolic[17]. However, there are reports of its localization being punctate[18-20] and even associated with vesicles[21,22]. In mammals, ferritin iron stores can easily be retrieved by "ferritinophagy", a process which is mediated by Nuclear Receptor Coactivator 4 (gene name: *NCOA4*) and involves the formation of autolysosomes[23-25]. Experimentally, ferritinophagy can be induced by iron chelation[26] and inhibited by iron supplementation[27]. Mechanistically, NCOA4 is under a dual control mechanism between binding

with FTH1 and the HECT and RLD domain-containing E3 ubiquitin protein ligase 2 (gene name: *HERC2*)[28]. Under conditions of iron repletion, HERC2 binds and degrades NCOA4 preventing ferritinophagy. Of critical importance, HERC2 and both ferritin subunits contain structural motifs known as iron responsive elements (IREs) in the untranslated regions (UTRs) of their mRNAs controlling their posttranscriptional expression based on intracellular iron flux[29,30]. These sequences together with iron regulatory proteins (IRPs) form the basis of the IRE-IRP iron translational regulatory system[30] (described in further detail in section 1.4). Briefly, low iron availability causes IRPs to bind to IREs while iron influx causes release. Thus, when positioned in the 5' UTRs of mRNA, IRP binding to IREs from low iron availability represses translation, while 3' IREs cause stabilization of mRNAs. Ferritin was demonstrated to contain an IRE in its 5' UTR and was the first protein described to be regulated posttranscriptionally by iron[29].

A third unique ferritin that exists within mitochondria was described at the turn of the century. This form is encoded by the intronless mitochondrial ferritin gene (gene name: *FTMT*) making it likely a processed pseudogene that arose as a retrotranscript[31,32]. Importantly, FTMT lacks the IREs present in FTH1 and FTL suggesting that it is not iron regulated posttranscriptionally despite high homology to FTH1 suggesting similar function[33]. As such, overexpression studies have shown its function to include iron storage, regulating iron distribution between cytosol and mitochondria, and preventing ROS formation within mitochondria[32,34]. Levels of FTMT were highest in tissues with high metabolic activity including the testis, kidney, heart, and brain[35]. However, mice deficient in FTMT are viable, show no obvious differences in serum iron parameters and fertility, and is not essential for siderocyte formation[36]. Thus, focus has been placed on studying the role of FTMT in the brain where associations have been made with Parkinson's disease and Alzheimer's disease[37,38].

Interestingly, ferritin can also be found in the serum of mammals though this ferritin tends to be iron poor[39,40]. Despite being iron deficient, serum ferritin has been used as a marker of iron status within humans as it adequately reflects iron stores in the liver[41]. It is, however, important to note that serum ferritin levels are easily influenced by inflammation[42], liver disease[42], and malignancies[43] requiring it to be paired with other tests for accurate diagnosis. Serum ferritin can be secreted from a number of cells including but not limited to hepatocytes[44], hepatoma cells[45], macrophages[18,46,47], neuroblastoma cells[48], oligodendrocytes[49], and astrocytes[50]. FTL is

predominantly recovered in serum as demonstrated by reactivity with anti-FTL antibodies and with little anti-FTH1 reactivity[51]. The primary source of serum ferritin appears to be macrophages having also ruled out the possibility that ferritin simply leaks out from damaged cells [18,52]. Since ferritin lacks a classical secretory signal peptide, its mechanism of excretion from cells has long been enigmatic with focus on nonclassical pathways involving lysosomal secretion[18], secretory autophagy, or multivesicular body-exosomes[53]. Recent work has clearly defined an involvement of the extracellular vesicle (EV) secretion pathway in release of ferritin from cells involving iron regulation of CD63, a tetraspanin heavily expressed in EVs[54]. However, ferritin found in EVs is iron-rich[53] and, while this would provide a novel mechanism for paracrine iron communication, this fails to explain the iron-poor ferritin found directly in the serum. Serum ferritin has the capacity to bind concanavalin A, a lectin which readily binds glycopeptides, suggesting that this form of ferritin is glycosylated[51,55]. A reason for its abundance in the serum remains to be determined.

1.2 Transferrin and the iron highway

About a decade after the crystallization of ferritin, in 1947, transferrin, a 76 kDa glycoprotein conserved among vertebrates, was first described for its capacity to bind iron in human plasma[56]. This protein is composed of two lobes at the N- and C- termini, both with unique iron binding affinities and high homology, connected by a short-linking region[57,58]. Thus, transferrin can bind two ferric iron ions. Transferrin is produced primarily by the liver's hepatocytes[59] but is also found in the testis's Sertoli cells[60], in the endoderm of the mouse visceral yolk sac[61], and in the fetal liver as early as 11 days following gestation[62]. Transferrin can bind a variety of ions with differing affinities including aluminum, cadmium, gallium, and zinc and functions similarly to ferritin in that it keeps these inert[63]. However, its primary physiological role is for efficient, targeted delivery of plasma iron to organs in the transferrin cycle with the additional immunological benefit of sequestering this ion in the circulation making it more difficult to access for invading pathogens. However, it should be noted that some protozoa and bacteria have developed mechanisms for transferrin-bound iron uptake[64,65].

Once diferric transferrin, referred to as holo-transferrin, binds to its ubiquitously expressed cognate receptor, transferrin receptor 1 (TFR1, gene name: *TFRC*), it is endocytosed via clathrin-coated vesicles[66,67]. Upon removal of clathrin, subsequent endosome acidification leads to

conformational changes in TFR1 and transferrin causing the release of iron from transferrin[68] with the newly iron-free transferrin, dubbed apo-transferrin, now tightly bound to TFR1 in acidic conditions[69]. While transferrin and TFR1 are eventually recycled to the cell surface[69,70], ferric iron released must first be reduced by the ferrireductase six-transmembrane epithelial antigen of prostate 3 (gene name: *STEAP3*)[71] to allow it to pass through the hydrophilic channels of divalent metal-ion transporter-1 (DMT1; gene name *Slc11a2*). DMT1 is electrogenic requiring proton co-transport to move iron across the membrane which is aptly provided by the acidic environment of the endosome[72,73]. Upon exit from the endosome, iron must be carefully escorted by the metallochaperones poly-C binding proteins 1 and 2 (gene names: *PCBP1*, *PCBP2*) to avoid toxicity from the previously mentioned Fenton chemistry[74,75]. PCBPs belong to the family of hnRNP K RNA binding proteins and PCBP1 and PCBP2 appear to play the most significant role in iron shepherding despite all forms of PCBPs demonstrating some capability for iron transport[75]. Focus has been on these two isoforms as these are ubiquitously expressed at high levels in all mammalian cells. The action of these iron chaperones has been extensively studied with respect to delivery of iron to ferritin, but PCBPs may also deliver iron to the "labile iron pool" (LIP) or directly to non-heme enzymes[76]. The LIP refers to the subset of iron that is kinetically exchangeable, available for immediate use in chemical reactions, and serves as the basis for iron cofactor synthesis, assembly, and insertion[77,78]. Thus, the LIP is the first fraction of iron that is chelated upon treatment with iron chelators and is the portion with the most redox active subset of iron which is not stored in ferritin. Interestingly, PCBPs do not play a direct role in delivery of iron to mitochondria, the center of heme and iron-sulfur cluster synthesis[76]. Instead, PCBP1 depletion in mice appears to indirectly reduce mitochondrial heme production by decreasing ferritin iron stores[79]. Thus, the exact mechanism of directed mitochondrial iron acquisition remains enigmatic. The reason this protein has evolved functions of iron transport and RNA binding is also an interesting question.

1.3 Canonical iron uptake through transferrin receptors

TFR1 belongs to a family of receptors and enzymes known as the TFR/GCP2 family and is found in practically all vertebrates[80]. This family contains at least seven members of which the most important for iron metabolism are TFR1 and transferrin receptor 2 (TFR2) but also includes glutamate carboxypeptidase II (GCP2). TFR1 is homodimer composed of type II integral

membrane glycoproteins and can bind two molecules of holo-transferrin for internalization by endocytosis[67]. The importance of both TFR1 and GCP2 was underlined by their lethal phenotype in whole-body knockouts[81,82]. TFR1 knockout animals died at embryonic day 12.5 and analysis of embryos suggested that TFR1 was crucial for iron uptake of red blood cells as well as for neuronal development[81]. Much like ferritin and of clinical relevance, TFR1 can also be found in the serum as a truncated form[83]. Its ratio compared with serum ferritin has been demonstrated to accurately determine patient iron levels while distinguishing between simple iron deficiency and anemia from inflammation[84]. Importantly, TFR1 was revealed to be posttranscriptionally regulated by iron shortly after ferritin[85]. The notable difference between these two genes being TFR1's five IRE motifs are in its 3' UTR suggesting that its mRNA is stabilized in the absence of intracellular iron, and this is reflected in the increased mRNA copy numbers observed under these conditions[86,87]. Additionally, it was later discovered that TFR1 could be controlled by hypoxia and iron deficiency by a hypoxia response element (HRE) in its promoter[88]. This sequence can be bound by hypoxia inducible factors 1α and 2α (HIF-1α and HIF-2α, gene names: *HIF1A* and *HIF2A*) which are stabilized in the presence of hypoxia[89]. Interestingly, iron chelation can mimic hypoxia suggesting overlap between these pathways[90]. To further demonstrate the complex interplay between hypoxia and iron metabolism, HIF-2α has been shown to be regulated by an IRE sequence resulting in iron-dependent control of erythropoiesis[91].

Since its discovery, many conditional knockouts of TFR1 have been generated with a plethora of interesting phenotypes. As expected, knockout of TFR1 in mouse muscle leads to decreased iron stores in muscle and, surprisingly, in adipose tissue and liver[92]. This is accompanied by changes in systemic metabolic regulation as normal energy production in muscle is disrupted causing a switch to fatty acid β oxidation. Mice lacking TFR1 in muscle showed significant growth retardation and typically died around day 13. Inactivation of TFR1 in the intestinal epithelium led to pleiotropic effects[93]. This conditional knockout was similarly fated to early death suggesting a critical role for this receptor during development for epithelial barrier maintenance. Moreover, this study demonstrated that TFR1 played a homeostatic role in intestinal epithelial cells preserving proliferation of intestinal epithelial cells progenitors, lipid handling, stem cell marker expression, and controlling epithelial-to-mesenchymal cell transition[93]. Interestingly, iron administration had no effect but knockin with a TFR1 allele that lacks receptor function could rescue this phenotype. A final knockout from this group demonstrated that cardiac TFR1 is also essential for survival[94].

Mice lacking TFR1 in cardiomyocytes died within 11 days of birth which could be saved by aggressive iron treatment as well as supplementation with nicotinamide riboside to induce nicotinamide adenine dinucleotide (NAD) production. These results demonstrate the importance of cardiac iron uptake with implications for cardiac failure resulting from iron deficiency.

Recent models of TFR1 deficiency have discovered more niche roles for this receptor. One such example is the disruption of TFR1 in muscle satellite cells leading to impaired skeletal muscle regeneration paired with ferroptosis[95]. Ferroptosis is an iron-dependent form of regulated cell death characterized by accumulation of lipid-based reactive oxygen species when glutathione-dependent lipid peroxide repair systems are compromised[96]. Recent evidence also offers a role for TFR1 in bone mass maintenance[97]. Ablation of TFR1 in myeloid osteoclast precursors led to increases in trabecular bone mass specifically in female mice while disruption in differentiated osteoclasts resulted in increases in trabecular bone volume in both genders with a greater effect in females[97]. This phenotype was attributed to attenuated mitochondrial metabolism and cytoskeletal organization[97]. Interestingly, despite impressive phenotypes observed in the conditional knockouts mentioned, ablation of TFR1 on hepatocytes resulted in a mild phenotype[98,99]. These mice were predisposed to developing microcytic anemia from an iron-deficient diet and had slightly lower liver iron stores with relatively normal markers of iron homeostasis. Treatment of isolated primary hepatocytes from these mice with radioactively labeled holo-transferrin demonstrated that these cells could still gather roughly 60% of the iron[98]. Taken together, these results suggest that, in the absence of TFR1, hepatocytes are still able to acquire iron bound to transferrin through another mechanism perhaps related to TFR2.

For many years, it was thought that TFR1 was the only receptor for transferrin. It was not until 1999 that TFR2 was described as a receptor with high homology to TFR1. Notably, TFR2 has two isoforms, a full-length α and short length β form[100] and is stabilized when bound to transferrin[101,102]. While the β form is expressed ubiquitously at low levels, the α form is expressed primarily in hepatocytes[100] and erythroid precursors[103]. This full length variant is 45% identical and 66% similar to TFR1 in its extracellular domain[100]. Despite its ability to efficiently incorporate transferrin-bound iron into cells, TFR2 has been predominantly described as an iron sensor as it exhibits an approximately 25-fold lower binding affinity than TFR1 for its substrate[104] and is not iron-regulated at a transcriptional level[103,105]. TFR2's role can be better appreciated by studying

knockout animal models. Whole-body knockout of TFR2 does not lead to an impairment in iron uptake but instead results in an iron overload phenotype explained in greater detail in section 1.10[106]. Similar to TFR1 conditional osteoclast knockouts, TFR2 ablation can also lead to increases in bone mass suggesting that TFR2 normally limits bone formation[107]. This phenotype was attributed to TFR2's ability to bind bone morphogenetic proteins (BMPs) to inhibit heterotopic ossification[107]. Deletion of the β form of TFR2 in mice resulted in a transient anemia early in life with otherwise normal iron homeostasis and liver iron followed by severe spleen iron accumulation with downregulation of the cellular iron exporter ferroportin (gene name: *SLC40A1*) later in life[108]. A TFR2 conditional knockout of the β form in macrophages was then generated and a similar decrease in ferroportin expression despite unaltered body iron homeostasis was observed suggesting that this receptor plays a noncanonical role in regulation of these cells[109].

1.4 Cellular iron regulation by iron regulatory proteins

An important consequence of iron import in cells is the modulation of the IRE/IRP system and subsequent cellular posttranscriptional reprogramming. IREs are highly conserved 25-30 nucleotide motifs through evolution of metazoa with ferritin's IRE being the most prevalent suggesting that it is the ancestral version of this motif[110]. To reiterate, expression of TFR1 is enhanced by iron-deprivation in contrast to ferritin due to the IRE-IRP system[29,86,111,112]. Where 5' UTR IRE sequences will inhibit translation upon iron depletion and consequent IRP binding, 3' sequences will stabilize mRNA transcripts[113]. Two distinct IRPs have been extensively described, IRP1 (gene name: *ACO1*) and IRP2 (gene name: *IREB2*). IRP1 is bifunctional; when an iron-sulfur cluster is present in its active site, the enzyme functions as aconitase in the tricarboxylic acid cycle[114]. Loss of the iron-sulfur cluster restores its nucleotide binding activity. IRP1 deficiency results in pulmonary hypertension, cardiac hypertrophy, fibrosis, and transient polycythemia due to relief of HIF-2α suppression[91,115,116]. Feeding *Irp1*-deficient animals an iron-deficient diet results in high mortality through further stabilization of HIF-2α causing abdominal hemorrhages[115]. On the other hand, mice lacking IRP2 present with microcytic anemia, largely normal livers and kidneys, tissue iron redistribution, and adult-onset progressive neurodegeneration[117,118]. Surprisingly, disruption of the iron-sulfur cluster assembly machinery activated IRP2 which promoted iron loading in a manner that was independent of IRP1[119]. The differences in observed phenotypes between both knockouts suggest a nonredundant role for both

IRPs. As expected, knockout of both IRP1 and IRP2 results in embryonic lethality before stage E6.5 in mice[120].

IRPs are regulated by ubiquitination which controls their abundance by degradation. IRP2 is targeted for degradation by the E3 ubiquitin ligase complex SKP1-CUL1-FBXL5[121,122]. FBXL5, an F-box protein containing a conserved F-box domain in its leucine-rich region[123], has an iron core causing it to destabilize in the absence of iron[121,122]. Thus, under iron-replete conditions, IRP2 is released from IRE motifs and subsequently targeted for proteasomal degradation by the FBXL5-containing E3 ubiquitin ligase complex. IRP1 may also be targeted for degradation by FBXL5 in the presence of iron when it is mutated to prevent iron-sulfur cluster binding[124,125]. However, under physiological iron-replete conditions, IRP1's iron-sulfur cluster will bind the target area of FBXL5 protecting it from degradation and allowing it to perform its function as aconitase. Taken together, the IRE-IRP system is critical for balancing cellular iron homeostasis.

Since the discovery of the IREs in ferritin and TFR1, many IRE elements have been described in other genes including 5-aminolevulinic acid synthase 2 (gene name: *ALAS2*), cell division cycle 14A (gene name: *CDC14A*), mitochondrial aconitase, HIF-2α, ferroportin, DMT1, myotonic dystrophy protein kinase-like alpha (gene name: *CDC42BPA*), and CD63[54,113,126]. This outlines the importance of iron for many different cellular processes. Furthermore, of these genes, ferroportin's IRE was described before its function had been elucidated and has been shown to be of vital importance for balancing iron flux from both the diet and iron recycling processes[127].

1.5 Dietary iron uptake

Thus far, the intricacies of cellular iron metabolism have been discussed illustrating the careful balance that must be maintained for proper cellular function. The only point of entry for iron is through the diet. Crucially, mammals lack excretory mechanisms for iron necessitating meticulous regulation. As such, regulatory mechanisms controlling dietary iron uptake have developed over the course of evolution. On average, humans will obtain roughly 1-2 mg of iron from the diet to replenish loss due to cellular desquamation. Dietary iron is taken up by enterocytes through few specialized cell-surface proteins aimed to either transport heme or non-heme iron. Non-heme iron uptake, especially the reductive system, has been extensively characterized and is summarized in figure 1.1. The process involves uptake in enterocytes by the previously mentioned metal transporter DMT1 which is abundant in these and upregulated under low iron conditions[128].

However, iron in the diet is generally present in the ferric form and must first be reduced by the duodenal cytochrome b (gene name: *CYBRD1*)[129,130]. Additionally, non-heme iron absorption is believed to be aided by ascorbic acid found in gastric juice[131]. Notably, CYBRD1 may bind ascorbic acid which has been shown to play an important role for its ferrireductase function[132,133].

In contrast, heme iron, which is readily bioavailable and highly abundant in meat and fish, is taken up at the brush-border membrane of enterocytes possibly by heme carrier protein 1 (HCP1, gene name: *SLC46A1*)[134,135]. The ability of HCP1 to also transport folate has put it in question as the primary importer of heme but no other molecule implicated in heme transport has been shown to be relevant for enterocyte heme absorption and this remains an important question in the field[136,137]. Once inside enterocytes, the heme ring containing iron can then be degraded by heme oxygenases 1 and 2[138] (gene name: *HMOX1* and *HMOX2*) to release iron for storage or use within enzymes. It is also possible for heme to be exported directly by either feline leukemia virus subgroup C cellular receptor 1 (gene name: *FLVCR1*) or ATP-binding cassette sub-family G member 2 protein (gene name: *ABCG2*) to the circulation or back to the lumen, respectively, although transport by FLVCR1 has not been shown to be relevant in enterocytes[139-141]. Export of labile iron from enterocytes at the basolateral membrane is handled by ferroportin, the sole iron exporter described to date[127,142,143]. Yet, as discussed, ferroportin transcripts are posttranscriptionally negatively regulated by the IRE/IRP system under conditions of iron depletion. This raises the issue of iron entry into the bloodstream under conditions of iron deficiency when it is required most. This question has been resolved in part by the discovery of ferroportin isoforms lacking an IRE sequence which are highly expressed in iron-deprived enterocytes[144]. An additional layer of hypoxia-related regulation of IRP1 has also been shown to play a role in keeping ferroportin expressed in enterocytes during iron shortage[145]. Following its release into the bloodstream, iron must be oxidized by ferroxidases such as the transmembrane hephaestin (gene name: *HEPH*) or plasma ceruloplasmin (gene name: *CP*) to allow binding to transferrin[146-148]. Iron absorption has been shown to be more efficient in the upper intestinal tract, specifically the duodenum and proximal jejunum, and this is thought to be due to expression profiles of iron uptake and export machinery[149-151]. Experiments from a much simpler time when patients could be fed radiolabeled meals revealed that nonheme iron uptake is more regulated than heme iron and that the latter is a significant source of iron for body iron stores as reflected by

serum ferritin[152]. Despite our current understanding of iron trafficking in enterocytes, the possibility that other uncharacterized receptors exist is still possible.

Enterocyte-specific animal knockouts are rather rare due to the severe phenotypes resulting from disrupted iron homeostasis. One recent study using tamoxifen-inducible enterocyte-specific ferroportin knockout mice, which quickly become anemic, demonstrated that no other pathways function for iron export even when these mice are fed a 1% ferric citrate diet[153]. This study provided evidence disproving the possibility of paracellular iron absorption caused by citrate disrupting tight junctions between enterocytes. Another study has demonstrated that enterocyte-specific disruption of ferritinophagy results in protection from genetic iron overload suggesting that iron stores in enterocytes are critical for regulating circulating iron[154]. Thus, enterocytes play a pivotal role in maintaining homeostatic iron balance. Disturbances at any level in these can cause repercussions in our ability to gather iron or prevent it from accumulating beyond safety thresholds.

1.6 Non-transferrin bound iron and iron-related pathologies

Normal transferrin saturation in humans hovers around 30%[155]. As the saturation of transferrin progressively increases above this level, the buffers capacity to efficiently sequester iron begins to wane[156]. This results in the presence of non-transferrin bound iron (NTBI), a form of iron originally described in thalassemia patients for its low molecular weight and ability to be easily chelated from the blood[157]. In reality, NTBI is a misnomer as it also refers to iron that is not bound to heme or ferritin in the serum but rather to small molecule carriers or peptides such as citrate[158,159], acetate[159], or albumin[156,160]. There are, in fact, multiple forms of NTBI described depending on whether they require a mild mobilizing agent such as nitrilotriacetic acid for chelation or are directly chelatable[161]. It is also likely that various forms of NTBI are found at different concentrations depending on the etiological cause of iron overload and its duration. Current debates highlight the possibility of finding low levels of NTBI even under normal conditions which could rapidly fluctuate postprandial and possibly play a role in iron sensing.

Clinically, NTBI has been a product observed in many iron-related pathologies including thalassemias[157,162], which are diseases of impaired globin synthesis, transfusion-related iron overload when treating thalassemias or sickle cell diseases[163], and hemochromatoses[164-166], a broad term referring to diseases of excess iron in the body, as well as other conditions such as diabetes[167].

Compared to the highly regulated and generally time-consuming process of transferrin-bound iron uptake, NTBI is taken up by cells in seconds[168]. One exception to this rule is hemoglobin producing cells such as erythroid cells which display a seemingly astonishing speed for incorporation of transferrin-bound iron on the order of a few minutes[169]. Nevertheless, radioactively labeled iron experiments have demonstrated that holo-transferrin can take up to 50 minutes to be cleared from the circulation in rodents while NTBI takes approximately 10 seconds[168]. Though direct evidence framing NTBI as the key player of pathology in hemochromatosis and other diseases remains to be shown, current theories suggest that uptake of NTBI is the cause for iron accumulation over time in tissues, such as the heart and pancreas, due to iron-independent regulation of its transporters[170,171]. A prime example is the resulting cardiomyopathy observed in hemochromatosis patients[172,173] as well as the elevated risks of joint-related damage in humans and mice[174,175]. Moreover, pancreatic acinar cells appear particularly prone to NTBI uptake as seen in mouse models of hemochromatosis which develop pancreatic failure[176,177].

1.7 Non-transferrin bound iron transporters

It took several decades from the initial discovery of NTBI in 1976 to the identification of candidates responsible for its rapid uptake[77]. Of particular interest was its uptake by the liver considering this organ is the principal site of iron storage. Early studies in the 1960s had shown that, once the transferrin buffer was saturated, the liver was the primary site of iron uptake following further NTBI injection[178]. The earliest implicated NTBI transporters were L-type calcium channels[179] (LTCCs) and DMT1[180]. The latter was of particular interest as it was the first characterized mammalian iron transporter[181] and had just been implicated in endosomal transport of free iron following endocytosis of transferrin[72]. DMT1 has 12 transmembrane helices with an aqueous cavity and a metal-ion binding site formed between residues in α-helices 1 and 6[182]. However, the potential for DMT1 to be a physiologically significant NTBI cell surface transporter was quickly dismissed due to its function requiring an acidic environment found only in endosomes for maximal efficiency[72] until the discovery of the multiple isoforms of DMT1[183]. Despite having found an isoform of DMT1 that localizes to the plasma membrane and can actively transport iron at pH 7.5[183,184], this isoform was found to contain an IRE in the 3' region of its mRNA sequence suggesting that its expression decreases under conditions of iron overload when NTBI would be present in the serum[185]. This evidence considered with hepatocyte-specific inactivation

of DMT1 not preventing liver iron loading have demonstrated that it is dispensable for NTBI uptake[186].

Early studies also implicated LTCCs in NTBI uptake. Iron was initially reported to interfere with calcium uptake in these pore-forming voltage-gated channels[187] followed by studies demonstrating a promising role in iron absorption in the heart compared to liver cells[179,188]. Thus, most of the research regarding iron transport of these channels has focused on the heart for its involvement in iron-dependent cardiomyopathy. The best evidence supporting NTBI uptake activity of these receptors has been through experiments using calcium channel blockers[188-190]. In these trials, treatment with blockers could significantly reduce cardiac iron absorption by roughly 30-50%. Transgenic mouse models have also corroborated the role of LTCCs in iron trafficking showing that overexpression of LTCCs in mice results in heart iron loading[188]. Only about a decade later were another set of calcium channels, T-type calcium channels (TTCCs), implicated in NTBI uptake. These are not usually expressed in the heart but can be found under conditions causing hypertrophy[191] and thalassemia[192,193]. Studies have shown that blocking these channels can also result in decreased cardiac iron uptake, albeit never fully preventing it. Unfortunately, knockout models have been unsuccessful as ablation of LTCCs is lethal in the heart even when induced in adult mice[194,195]. Despite this lethal phenotype, some therapeutic success observed in controlling iron load of the heart by blocking these channels in humans[196-199].

Liver NTBI uptake seems to be primarily controlled by the ZRT/IRT like protein (ZIP) family of which 14 members have been described in mammals. The first member to be described in this family, iron-regulated transporter 1, was initially described for its importance in iron uptake in *Arabidopsis*[200]. The members of this highly conserved family of proteins feature eight transmembrane domains and, importantly, nine of these have a histidine-rich motifs in their fourth and fifth transmembrane domains[200]. This motif is altered in both ZIP14 (gene name: *SLC39A14*) and ZIP8 (gene name: *SLC39A8*) in the fifth transmembrane domain where the first histidine residue is replaced by a glutamic acid which may affect its ion transport range[201]. It should be noted that early studies in ZIPs found an association with ZIP2 (gene name: *SLC39A2*) and iron homeostasis implicating it as an iron importer[202]. Later, a screen in transfected HEK293T cells assessed the ability of all ZIP family proteins to transport iron and found that, other than ZIP8 and ZIP14, only ZIP2 was capable of increasing iron load[203]. ZIP2 is unique in that it does not seem to

require iron to be reduced for uptake[203]. Yet, whether ZIP2 is of physiologically relevant in iron uptake remains in question as recent studies suggest that it plays a minimal role[204]. Little other evidence has been brought forth proposing ZIP2 as a major contributor of NTBI trafficking.

Great focus has been placed on ZIP14 as the liver NTBI transporter because of its prominent transcript expression in this tissue[205]. Early studies working with ZIP14 showed a clear involvement in NTBI uptake as seen by radioactively labelled iron uptake in HEK 293H, Sf9, and AML12 cell lines[206]. This transporter clearly localized to the cell membrane, overexpression led to iron accumulation, iron uptake was inhibited by ferrous iron chelators, and siRNA suppression resulted in decreased iron loading[206]. Despite zinc being the preferred substrate for ZIP14, iron is efficiently taken up by this transporter under a subset of conditions which include temperature-dependence, pH-sensitivity, calcium-dependence, and inhibition by cobalt, manganese and zinc as demonstrated in the heterologous expression system of *Xenopus laevis* oocytes[207]. Given the abundance of NTBI during iron overload conditions, this transporter could presumably be responsible for rapid iron uptake in the liver. Further evidence for its involvement in NTBI trafficking includes its iron-dependent expression in the rat liver[185] as well as its overexpression in many tissues of infants with neonatal hemochromatosis including the pancreas and heart[208]. Intriguingly, a screen to determine which ZIPs were iron regulated revealed that only ZIP5 is upregulated by iron while ZIP6, ZIP7, and ZIP10 are downregulated in the presence of iron loading at the mRNA level[209]. An important corollary of these results is that transcript levels are not necessarily indicative of protein expression and involvement in iron metabolism. Neither Zip14, ZIP8, nor ZIP2 appeared to be transcriptionally regulated by iron. ZIP14 appears to be controlled largely posttranscriptionally as seen by its proteasomal degradation *in vitro* following iron chelation[210].

The function of ZIP14 has been extensively characterized *in vivo* using knockout mice. Interestingly, *Slc39a14*$^{-/-}$ mice were viable, exhibited growth retardation, skeletal abnormalities[211], and did not show any major perturbations in iron metabolism except for roughly ~35% lower liver iron at early ages suggesting that other ZIPs could accommodate for lack of ZIP14 or that NTBI was relatively absent under normal conditions[212]. Work done crossing *Slc39a14*$^{-/-}$ with either the *Hfe*$^{-/-}$ mouse model of relatively mild hemochromatosis or the *Hjv*$^{-/-}$ mouse model of severe hemochromatosis demonstrated a clear redistribution of iron loading[212]. In both models, livers

were spared of iron loading while kidneys accumulated iron instead. In conditions of severe genetic iron overload, spleen was also targeted for iron loading while pancreas was relatively spared, particularly in the acinar cells, in absence of ZIP14 suggesting a role for this transporter in pancreas as well. To further complicate these data, dietary iron loading caused disproportionate iron loading in pancreas, heart, kidney, and spleen. It should be noted that dietary iron loading had relatively little effect on plasma NTBI suggesting that the observed increase in pancreatic iron could be due to transferrin bound iron in the experimental timeframe. Taken together, ZIP14 appears to be the main pathway of NTBI uptake in the parenchymal cells of the liver as well as the acinar cells of the pancreas and that, in the absence of the liver clearing NTBI from the serum, this iron accumulates quickly in other tissues in a ZIP14-independent manner.

ZIP8 is the other likely candidate for NTBI uptake due to its similarity to ZIP14. ZIP8 mRNA distribution differs significantly from ZIP14 suggesting that it plays a nonredundant role in iron transport[213]. It is most highly expressed in the lung and placenta whereas, in the liver, its expression is roughly ten times less than ZIP14[213]. Similar to ZIP14, ZIP8 protein levels have been shown to increase *in vitro* whereas its mRNA levels are not significantly altered by iron treatment[213]. Curiously, the subcellular localization of ZIP8 appears to differ from ZIP14 wherein the former localizes primarily to the apical membrane[214] while the latter to the basolateral membrane in hepatocytes[185]. Currently, little work has been published on ZIP8 knockout animals as it has been noted in two separate studies with mice with reduced ZIP8 expression in the placenta, yolk sac, and fetus were not viable[215,216]. It is concluded that ZIP8 may play an important role for fetus development and organogenesis. In a recent study focused on manganese metabolism using whole-body inducible and hepatocyte-specific ZIP8 knockouts, iron levels in liver, kidney, heart, and brain were found to be normal[214]. Nevertheless, it would be important to study whole-body inducible knockouts or conditional ZIP8 knockouts in other organs such as the liver, lung, kidney, testis, and pancreas under conditions of iron overload.

1.8 Systemic control of iron distribution by hepcidin

Thus far, mechanisms for iron storage, transport, distribution, and uptake have been described. Yet, the focus of this thesis is centralized on the final piece and orchestrator of systemic iron flow. At the turn of the century, one of the most groundbreaking discoveries in iron metabolism was made with the discovery of the liver-derived peptide hormone hepcidin (gene

name: *HAMP*). This peptide was originally isolated from urine in search of liver-derived antimicrobials[217] and plasma ultrafiltrate in a screen to find novel cysteine-rich antimicrobial peptides[218]. Unprocessed prepro-peptide is 84 amino acids long and undergoes cleavage to remove its 24 amino acid-long endoplasmic reticulum targeting sequence forming pro-hepcidin which is then cleaved at the C-terminus producing 20, 22, and 25 amino acid length peptides[217,219]. These peptides differ in the length of their amino terminals and the 20 and 25 amino acid isoforms are the major species[217]. Shortly after these reports, a hybridization screen searching for proteins upregulated during dietary iron loading found that hepcidin was among these[220]. This was followed by a study in upstream stimulatory factor 2 (USF2) knockout mice, which display a hemochromatosis-like phenotype, where these mice had aberrantly low levels of hepcidin[221]. True to the hypothesis that the phenotype observed in the USF2 mice was due to dysregulated hepcidin expression, transgenic overexpression of hepcidin led to severe microcytic hypochromic anemia resulting in lethality early in life[222]. Shortly after, the first mutations in the human hepcidin gene were described and associated with the severe form of hereditary hemochromatosis that develops early in life known as juvenile hemochromatosis[223].

Notably, two highly similar hepcidin genes have been described in mice, *Hepc1* and *Hepc2*, where only one is present in humans[224]. However, transgenic overexpression of the second hepcidin gene in mice did not lead to any observable iron-related phenotypes suggesting that it does not play a significant role in iron metabolism[224]. Importantly, work aimed at mimicking the effects of hepcidin for therapeutic use demonstrated that only the first 7-9 amino acids of the N-terminal of this peptide are required to maintain its activity on systemic iron homeostasis[225]. It took four years before the first investigation into its mechanism of action was reported[226]. It is now understood that hepcidin will bind to ferroportin, occlude its channel, and target it for internalization by ubiquitination and subsequent lysosomal degradation[226-228]. Of note, ferroportin's stability at the cell surface is dependent on ceruloplasmin levels as well as lysine 253, the target for ubiquitination[229]. Recent work uncovered ring finger protein 217 (gene name: *RNF217*) as the E3 ubiquitin ligase necessary for ubiquitination of ferroportin[230]. By inducing the degradation of ferroportin, hepcidin controls the flux of systemic iron by controlling the quantity of iron distributed to the circulation by iron-recycling macrophages of the reticuloendothelial system, hepatocytes storing iron, and enterocytes obtaining iron from the diet[231-233].

1.9 Inflammatory regulation of hepcidin

As a result of its central role in iron metabolism, hepcidin must be carefully regulated. Hepcidin is primarily controlled at the level of transcription by two major pathways: inflammation and iron. Its inflammatory regulation was shown in early studies demonstrating its upregulation by lipopolysaccharide[220] (LPS), turpentine[234], and bacterial infection in fish[235]. It has since been hypothesized that expression of this peptide and the resulting anemia are intended to withhold iron from invading extracellular pathogens. However, the broadness of expression of inflammatory cytokines has led to many maladaptive hepcidin responses when inflammation is persistent. For example, patients with chronic illnesses such as rheumatoid arthritis, tuberculosis, systemic fungal infections, and malignancies eventually develop anemia. This condition was dubbed anemia of chronic disease later to be renamed anemia of inflammation[236]. Hepcidin's first implication in these conditions was in patients with type 1a glycogen storage diseases[237]. These patients lack expression of glucose-6-phosphatase which impairs glucose homeostasis requiring continuous glucose supplementation. Despite effective treatment, aging patients eventually develop a number of secondary conditions including hepatic inflammation, hepatic adenomas, and anemia[237]. Expression of hepcidin mRNA was greatly elevated in patient's adenomas where inflammation is present[237]. It was noted that mice with transgenic overexpression of hepcidin resulted in a similar phenotype to that of patients with chronic inflammation accumulating iron in tissue macrophages with relatively low liver iron[238]. Eventually, a model of anemia of inflammation in mice was developed utilizing heat-killed *Brucella abortus*. These mice developed anemia within a two-week timeframe without serious illness while preventing effects of erythropoiesis-stimulating agents[239]. This study demonstrated that silencing of hepcidin mRNA could effectively control anemia caused by *Brucella abortus*, and this was corroborated using an antihepcidin antibody to neutralize hepcidin[239]. Later findings demonstrated that genetic knockout of the hepcidin gene could effectively control the development of anemia of inflammation using this model[240,241].

From observations in patients stemmed studies on the inflammatory regulation of hepcidin. An early study established hepcidin as a type 2 acute-phase protein with its induction being closely linked to interleukin (IL) -6 *in vitro* but not IL-1 or tumor necrosis factor α (gene name: *TNF*)[242]. Although this study discounted the role of IL-1 and TNFα in hepcidin regulation, other work demonstrated a possible function of IL-1[243,244] as well as IL-22[245]. The biological implications of

IL-1 induction of hepcidin remain in question, however, with a study suggesting that IL-1 may be relevant during hypoxia[246]. As for IL-22, exogenous administration of this cytokine resulted in significant upregulation of hepcidin *in vivo*[247]. Yet, the physiological relevance of this cytokine also remains uncertain as it seems to only play a minor role during LPS-driven inflammation which causes endogenous production of IL-6[248]. Work with IL-6 knockout mice suggests that this signaling molecule is required and sufficient for hepcidin induction. Knockout animals failed to induce hepcidin in response to turpentine[249], were protected from development of anemia of inflammation[240], and completely lacked hepcidin mRNA expression in response to bacterial *Streptococcus pneumoniae* as well as influenza virus PR8[250]. Importantly, IL-6 has been shown to induce signal transducer and activator of transcription 3 (STAT3) phosphorylation which results in binding to the conserved element in the hepcidin promoter necessary for inflammatory transcriptional activation of hepcidin[251-253]. Other inducers of STAT3 such as type I interferons have been shown to also induce hepcidin[254-256]. Thus, the IL-6/STAT3 signaling axis is widely regarded as the primary pathway of inflammatory hepcidin induction.

1.10 Hepcidin's intricate iron regulatory network

The more intuitive yet complex form of regulation of this hormone is by iron itself and is summarized in figure 1.2. The first studies into the regulation of hepcidin indicated that anemia and hypoxia were involved suggesting a role of iron in hepcidin's regulation[234]. Yet, elucidating the signaling cascade involved in its iron regulation was only made possible by studying mutations in patients with hemochromatosis. The first mutations to be described were in homeostatic iron regulator (gene name: *HFE*), a nonclassical major histocompatibility complex (MHC) class I molecule[257,258]. This protein was shown to be highly expressed in the liver suggesting that it could play a role in modulating hepcidin's expression[259]. Studies in humans revealed a strong association between hemochromatosis and a singular point mutation resulting in a substitution mutation (C282Y) in *HFE*[257]. This mutation disrupts a disulfide bond preventing its association with β_2-microglobulin and thus eliminates its presence at the cell surface. In mice, β_2-microglobulin disruption causes iron overload suggesting a role of MHC class I molecules in iron regulation[260,261]. Yet, patient studies revealed an incredible frequency of the *HFE* C282Y mutation in with homozygosity anywhere between 83% to 100%[262-264]. Predictably, knockout of HFE in mice also led to a hemochromatosis phenotype[265].

Characterization of HFE uncovered a possible mechanism for this protein in iron metabolism as it complexes with the iron receptor TFR1 both *in vitro* and at the placental membrane[266-269]. This interaction was favorable at physiological pH and reduced binding affinity of TFR1 for holo-transferrin suggesting a role in iron absorption of intestinal epithelial cells[268,270]. Consequently, hypotheses at the time of discovery indicated that this interaction may regulate iron uptake. However, this did not account for the disrupted hepcidin expression and the increased rather than decreased iron absorption that were later observed. However, it remained unclear by which mechanism a nonclassical MHC Class I molecule could act to regulate hepcidin.

It was not until the characterization of mutations in the gene hemojuvelin (gene name *HJV*) which result in juvenile hemochromatosis[271-274] that the signaling pathway could begin to be elucidated. HJV is a member of the repulsive guidance molecule (RGM) family of proteins originally described for axonal guidance[275]. At an mRNA level, its expression is predominantly in skeletal muscle, heart, and liver[271,276]. Genetic knockout of HJV in mice led to a much more severe iron loading phenotype than HFE knockout similar to observations in humans[277]. Moreover, hepcidin expression is aberrantly low in mice lacking HJV[277,278] and in humans with mutations in this gene[271]. HJV shares roughly 50% sequence identity to other RGM family members, RGMA and RGMB[275,279]. Importantly, it contains the major structural features of RGM family proteins such as a glycophosphatidylinositol (GPI) anchor, an N-terminal sequence, a proteolytic cleavage site, and a partial Willebrand factor type D domain[280-282]. Work with both RGMA and RGMB had demonstrated that these function as BMP co-receptors[283,284] providing a basis for investigating a possible role of BMPs in hepcidin's signaling cascade as well as HJV as a BMP co-receptor. BMPs represent a large subfamily of the transforming growth factor β (TGF-β) superfamily and, as their name implies, were originally described for their pivotal role in osteogenesis[285]. Briefly, signaling begins when BMPs bind and form complexes with two type I and two type II serine/threonine kinase receptors[286]. Activated type II receptors will then phosphorylate type I receptors which phosphorylate small mother against decapentaplegic (SMAD) proteins. BMPs signal via SMAD1/5/8 whereas TGFβ signals through SMAD2/3. Phosphorylated SMADs will then form heteromeric complexes with SMAD4, translocate to the nucleus, and modulate gene transcription. At the same time as BMPs were being investigated for their role in hepcidin's regulation, a serendipitous observation of early lethality and severe iron overload in hepatocyte-specific SMAD4 mouse knockouts was made[287]. It was then demonstrated that HJV functions as a BMP

co-receptor that controls levels of phosphorylated SMAD1/5/8 opening the gate of understanding for hepcidin's iron regulation[288]. Functional genomic screens in search of iron regulated transcripts involved in the BMP/SMAD pathway revealed that BMP6 was the primary iron-regulated BMP present in the liver[289]. Assuredly, BMP6 mutant mice developed severe iron overload to a degree similar to HJV knockout animals[290,291], while knockout of the BMP receptors had differential results leading to variable levels of iron overload depending on which and the number of receptors disrupted[292,293].

The source of BMPs as well as the number of BMPs involved in iron homeostasis remained in question for some time. Considering endothelial cells were producers of BMPs in other systems, these were a natural candidate for investigation. Investigations into liver cell type populations revealed that liver sinusoidal endothelial cells expressed the most BMP6 mRNA and that only knockout in these resulted in hemochromatosis[294,295]. Additionally, gene expression profiling studies demonstrated that BMP2 was produced specifically in the liver's endothelial cells[296,297]. Studies in BMP6 knockout animals suggested that there could be another BMP capable of inducing hepcidin expression in its absence[298]. Taken together, these findings led to generation of liver sinusoidal endothelial-specific knockout of BMP2 resulting in a clear iron overload phenotype similar to BMP6 knockout animals[299,300]. This finding was corroborated with an association between BMP2 polymorphisms and penetrance of the iron overload phenotype in homozygous C282Y *HFE* in hemochromatosis patients[301,302]. Thus, mutations in BMP2 may predispose patients with other compounding mutations to developing iron overload. Critically, recent studies in double BMP2/6 knockout animals have shown that iron overload is not aggravated in these suggesting that BMP2/6 can work collaboratively likely as heterodimers[303]. Much focus has been placed on understanding the triggers of BMP production. One possible candidate that has been recently proposed is nuclear factor erythroid 2–related factor 2 (gene name: *NFE2L2*), a transcription factor regulating antioxidant response elements (AREs), since AREs have been found intron 1 of BMP6[304]. BMPs in other tissues such as osteoblasts and esophageal basal cells have been associated with activation of NFE2L2 suggesting that these could be linked in other tissues as well[305-307]. Yet, in these models, BMP2 has been proposed as an activator of NFE2L2 whereas the inverse is presented in the context of iron homeostasis.

The discovery of BMP6 as a primary iron-regulated BMP critical for the hepcidin signaling cascade also helped elucidate HFE's function, although current understanding remains wanting. HFE-deficient animals have reduced levels of phosphorylated SMAD1/5/8 despite having elevated BMP6 mRNA transcripts suggesting that HFE plays a key role in regulating this pathway[308-310]. These results were corroborated in humans with HFE-associated hemochromatosis[311,312]. However, HFE has been described as an auxiliary molecule in the BMP signaling cascade as its deficiency can be overcome by supraphysiological doses of exogenous BMP6 and the iron overload phenotype associated with its disruption is relatively mild[313]. HFE was shown to interact with the BMP receptor, BMPR1A, inhibiting its degradation and increasing its cell surface expression[314]. Thus, possible interactions between HFE and other iron proteins has been the subject of much research. One hypothesis suggests that TFR1 sequestering HFE on the surface of hepatocytes would limit HFE's ability to signal to hepcidin. Following an iron bolus, TFR1 would bind holo-transferrin displacing HFE, allowing its signaling function to occur. During iron deficiency, TFR1 would be highly expressed at the cell surface functionally sequestering HFE and preventing hepcidin induction. Work by our group with hepatocyte-specific ablation of TFR1 in mice has supported this hypothesis since mutant mice had severely increased hepcidin relative to liver iron content suggesting that these mice do not properly sense iron levels[315]. Importantly, following a 12-week course of iron-deficient diet, knockout mice expressed noticeable hepcidin mRNA whereas littermate controls did not, demonstrating consistency with the TFR1/HFE interaction regulating hepcidin expression. TFR1 would function as a mechanism to finetune hepcidin expression with the help of HFE. Our results were corroborated in a separate study using hepatocytic TFR1 knockout mice crossed with HFE knockout mice or β-thalassemia mice[99]. Ablation of TFR1 did not affect the iron phenotype of HFE knockout mice but was able to ameliorate hepcidin deficiency and liver iron loading in a model of β-thalassemia intermedia demonstrating relevance of the interaction between TFR1 and HFE.

Considering TFR2 had lower binding affinity for holo-transferrin and its disruption led to hemochromatosis phenotypes, it was an early candidate for investigation in hepcidin's regulatory cascade. Indeed, disruption of TFR2 led to decreased phosphorylated SMAD1/5/8 signaling resulting in decreased hepcidin induction[309,310]. *In vitro* studies demonstrated that TFR2 could bind to HFE by co-immunoprecipitation[316,317] and the binding domain of HFE was then shown to be important for hepcidin's response to holo-transferrin in hepatic cells lines and primary

hepatocytes[318]. Later co-immunoprecipitation studies also demonstrated that these molecules interact with HJV in hepatic cell lines[319]. However, the relevance of these interactions at the cell surface *in vivo* remains to be demonstrated. Overexpression of HFE in TFR2 knockout mice resulted in increased hepcidin mRNA expression[320] suggesting that HFE is sufficient for hepcidin induction. Importantly, a patient study of two siblings with juvenile hemochromatosis symptoms revealed that simultaneous disruption of both HFE and TFR2 would compound the iron overload phenotype[321]. This was later corroborated in a mouse model where knockout of both HFE and TFR2 resulted in further severe iron loading[309].

Hepcidin must also be regulated under conditions of erythropoietic demand such as blood loss to account for the rapid loss of iron and the immense need of this element in production of healthy red blood cells. Although it was long known that iron regulation and erythropoiesis were interconnected, the exact mediator remained elusive until the discovery of erythroferrone (gene name: *ERFE*)[322]. This erythroblast-produced hormone was shown to be inversely correlated to hepcidin in response to phlebotomy and the erythropoiesis-stimulating agent erythropoietin[322]. Importantly, this hormone was overexpressed in mouse models of β-thalassemia, a hemoglobinopathy characterized by reduction in β-globin chain synthesis, suggesting a key role in iron homeostasis[323]. Ablation of ERFE in this model restored hepcidin levels, modestly reduced iron loading, but failed to rescue anemia. The mechanism of action of ERFE in regulation hepcidin was initially thought to be related to its transforming growth factor (TGF) -β family properties possibly by binding to membrane-bound receptors but was later shown to be due to its ability to sequester BMPs[324,325]. Functional studies demonstrated that ERFE could partially inhibit BMP2 but primarily acted as a ligand trap by binding to BMP6 and BMP2/6 heterodimers resulting in the observed decrease in hepcidin expression during erythropoietic demand[325].

While most of the membrane-bound proteins described have been positive regulators of hepcidin expression, transmembrane serine protease 6 (gene name: *TMPRSS6*) negatively regulates hepcidin by proteolytically cleaving HJV from the cell surface[326-329]. TMPRSS6 is predominantly produced in hepatocytes and stabilized under conditions of iron deficiency with no regulation at the mRNA level[330,331]. Inactivation of this protein results in inappropriately elevated hepcidin and subsequent iron-refractory iron-deficiency anemia (IRIDA), a hypochromic microcytic anemia that typically does not improve with oral iron treatment but can be rescued by

parenteral iron[329]. In line with this protein's function, overexpression of TMPRSS6 led to a strong inhibitory effect on hepcidin transcription[328]. Work with different mouse knockout models has brought important conclusions about its function. For example, dual BMP6 and TMPRSS6 knockout phenocopy single BMP6 knockout suggesting that TMPRSS6 functions in the BMP6/HJV pathway[332]. However, inactivation of HFE or TFR2 and TMPRSS6 did not result in improvement of anemia seen in single TMPRSS6 mutant mice suggesting that these function in separately from each other[333]. Importantly, inactivation of both HJV and TMPRSS6 results in iron overload similar to single HJV knockouts[334]. Yet, overexpression of TMPRSS6 in dual HJV/TMPRSS6 knockouts was still able to suppress hepcidin suggesting a role of TMPRSS6 independent of HJV[335]. This overexpression model was also used to show that TMPRSS6 could cleave other members of the hepcidin signaling machinery such as BMP receptors, HFE, and TFR2, but little other evidence has been proposed demonstrating physiological function[335]. To determine if TMPRSS6's function was solely based on its proteolytic activity, mutant mice with nonproteolytic enzyme were generated and still managed to suppress hepcidin expression[336]. This was in line with some observed IRIDA-causing mutations in humans which could still traffic to the cell surface and cleave HJV[337,338]. These findings suggest that both its proteolytic activity as well as some other undescribed functions of this protein are important for iron regulation.

Finally, neogenin (gene name: *NEO1*) has also been shown to be essential for regulation of hepcidin. Disruption of this protein in mice resulted in iron overload, low levels of hepcidin, and reduced BMP signaling[339]. This study revealed that NEO1 inhibits the shedding of HJV, although evidence contradicting this function has been proposed[340]. NEO1's co-expression with BMP receptors and HJV suggests that it works in conjunction with these. NEO1's crystal structure showing that it can bind both HJV and BMP2 simultaneously along with the clustering of this complex observed using live-cell super-resolution fluorescence microscopy suggests that it functions as a scaffold for HJV and by doing so prevents its cleavage from the cell membrane[341]. Mutant mice without the binding site for NEO1 on HJV revealed the importance of this interaction for hepcidin signaling[340,342]. Interference in the binding activity led to significantly reduced ability to induce BMP signaling and hepcidin expression. However, residual signaling also implies that HJV can at least partially function without NEO1. Similarly, expression of a NEO1 mutant that could not bind HJV corroborated these results[340]. As such, the various functions of NEO1 remain to be concretely delineated.

There remain a few key unanswered questions in liver iron sensing with important recent developments. Namely, what is the trigger for endothelial production of BMPs? Early studies determined that BMP6 expression correlated with liver iron and less so with transferrin saturation[343]. Molecularly, there are only a few known candidates that could be responsible for iron sensing in endothelial cells assuming iron acquisition and storage are triggers. One of these is TFR1 and is the subject of the **second chapter** of this thesis. Since TFR1 is considered the cellular iron gate and based on its function as part of the hepcidin cascade in hepatocytes as previously described[315], it was rationalized that this receptor could potentially play a role in iron sensing for endothelial cells. As such, endothelial-specific TFR1 knockout mice have been generated to address this question.

1.11 Crosstalk between hepcidin's regulatory pathways

Crosstalk between hepcidin's BMP-driven iron regulated pathway and IL-6-driven inflammatory pathway has been an interesting subject of investigation. The inflammation-induced TGF-β signaling molecule inhibin subunit beta B (gene name: *INHBB*) has been proposed as a possible link between inflammation and BMP signaling for its strong induction by LPS in mice[344]. Although *in vitro* studies demonstrated that INHBB could activate SMAD1/5/8 signaling triggering hepcidin gene activation[345,346], *in vivo* work with INHBB knockout mice demonstrated that these retained their ability to induce physiological levels of hepcidin in response to LPS thus putting in question the relevance of this molecule for connecting iron and inflammation[344]. Another prospect for this crosstalk lies in the proximity of both SMAD and STAT enhancer elements in hepcidin's promoter. This has raised the possibility that these interact with each other. Supporting this, mutations in the proximal BMP response element of the hepcidin promoter have been shown to weaken its induction by IL-6 in luciferase reporter assays[347]. Other evidence proposed demonstrating a crosstalk was shown in mice deficient in the type I BMP receptor, BMPR1A, which fail to induce hepcidin in response to IL-6[348]. Moreover, observations in hepatocytic SMAD4 knockout mice suggested that SMAD signaling was required for IL-6-driven inflammatory induction of hepcidin[287]. These results provided a strong case for a communication between these two pathways.

However, a plethora of studies have shown that LPS could still induce hepcidin in mouse models with impaired BMP/SMAD signaling pathways albeit to varying extents. Disruption of

SMAD1/5/8 resulted in severely decreased baseline levels of hepcidin that could still increase almost 5-fold by LPS stimulation[349]. Studies in HJV and BMP6 knockout animals noted that these animals could still induce hepcidin in response to LPS although final hepcidin levels remained lower than wild-type controls[278,350]. Interestingly, work with BMP2 knockout animals demonstrated that BMP2 expression was reduced by LPS while maintaining physiological levels of hepcidin induction by the endotoxin suggesting a partially redundant role in inflammation for this signaling molecule[351]. Recent work by our group has aimed to better characterize the crosstalk between BMP6/HJV/SMAD and IL-6/JAK/STAT signaling. Hemojuvelin knockout mice were utilized to study the depth of inflammatory hypoferremia that could be achieved when BMP/HJVSMAD signaling is abrogated[352]. Despite a relative increase in hepcidin in response to LPS as previously reported[278], residual hepcidin expression was insufficient to induce a hypoferremic response, described here as a reduction in serum iron below wild-type mice on standard diet. Similar results were observed in knockout mice infected with live *Escherichia coli* SP15 or treated with the toll-like receptor 2/6 agonist FSL1. Work with cultured primary murine hepatocytes revealed that large enough doses of BMPs could overcome the lack of hemojuvelin at the cell surface and that IL-6 functions in a synergistic manner with BMP signaling[352]. Notably, placing wild-type animals on iron-deficient diet to physiologically diminish BMP/SMAD signaling demonstrated that LPS-driven inflammation could only minimally induce hepcidin under these conditions and could not further reduce serum iron. Taken together, these results suggest that inflammatory hepcidin signaling is synergistic with the iron-controlled BMP/SMAD pathway relying on it for proper basal hepcidin maintenance.

Curiously, *in vitro* work with Huh7 human hepatoma cells and primary mouse hepatocytes revealed that inorganic iron treatment had an opposite effect of that observed *in vivo*[353]. To recapitulate the effects of iron deficiency on hepcidin and SMAD signaling observed *in vivo,* cells were treated with desferrioxamine, an iron chelator. Unexpectedly, this only had a modest effect on hepcidin induction by BMPs and IL-6 suggesting that signaling does not strongly depend on hepatocellular iron levels. This contrasted with cells treated with ferric ammonium citrate, a potent source of inorganic iron, which then failed to induce hepcidin and SMAD phosphorylation in response to BMPs and IL-6. Markers of oxidative stress were elevated in iron-treated cells hinting that this may be responsible for the observed lack of response in accordance with previous reports[354,355]. The follow-up study to these observations sought to dissect the effect of iron-loading

and dysfunctional BMP/HJV/SMAD signaling *in vivo* by modulating dietary iron intake in both wild-type and knockout mice to ultimately deduce why iron loaded animals do not produce a successful hypoferremic response and is the subject of the **third chapter** of this thesis.

1.12 Leishmaniasis etiology and life cycle

Iron is of particular importance in immunity as almost every organism requires it as a cofactor for enzymes. As such, there is a constant competition between host and pathogen for its acquisition. *Leishmania* spp. are the causative agent of leishmaniasis[356]. These protozoan parasites of the *Trypanosomatidae* family are endemic in nearly 100 countries with roughly 0.7-1 million new cases reported each year. Recent estimates suggest that 12 million people are infected with this parasite and that 1 billion people are at risk with these numbers growing due to climate change and forced displacement due to conflict. Sandflies of the genus *Phlebotomus* were the first insects to be implicated in transmission of *Leishmania* in the 30s and 40s[357,358]. While *Phlebotomus* sandflies dominate the western hemisphere, the eastern hemisphere is plagued by sandflies of the *Lutzomyia* genus which are capable of transmitting leishmaniasis in their own right[359]. At least 20 species of *Leishmania* can cause disease in humans ranging from mild cutaneous, disfiguring mucocutaneous, or visceral disease[360]. Cutaneous lesions are self-limiting and generally self-healing but can, in rare cases, progress to severe disseminated cutaneous leishmaniasis, while mucocutaneous and visceral disease require treatment for parasite clearance. Visceral leishmaniasis is lethal in 95% of cases, if untreated, infecting bone marrow, spleen, and liver. Disease etiology is linked to the infecting parasite species with some species causing multiple forms of disease. For example, cutaneous disease may be caused by *L. major*, *L. mexicana*, *L. amazonensis*, while *L. donovani* and *L. infantum* may cause visceral disease to name a few.

Treatment of leishmaniasis has improved greatly over the past decades but remains complicated for many. For over 70 years, antimonial drugs have been the first line of treatment for this disease. However, these require long treatment courses and come with many debilitating side effects, while resistance to antimonials is on the rise. The rise of new treatments including liposomal amphotericin B, Miltefosine, and Paromomycin have provided alternatives to patients failing antimonial treatment[361-363]. Similarly, these treatments may also require long treatment courses, come with significant side effects, and are prone to resistance[364]. Unfortunately, there are still no vaccines for leishmaniasis[365].

Leishmania's life cycle is depicted in figure 1.3. Briefly, the cycle begins with the bite of an infected female sandfly. When the sandfly takes a blood meal, flagellated metacyclic promastigotes are regurgitated into the bloodstream[366]. These are engulfed by macrophages, *Leishmania*'s primary host cell, or neutrophils. Neutrophils are eventually phagocytosed by macrophages providing a secondary form of entry for parasites into macrophages known as the trojan horse mechanism[367-369]. Parasites are contained in membrane-bound parasitophorous vacuoles (PVs) within macrophages where they differentiate from promastigotes to non-motile amastigotes. The differentiation process begins in the hours following uptake and takes at least 5 days[370,371]. Eventually, amastigotes are released from their host cell and may infect other macrophages. The cycle completes when infected macrophages are ingested by sandflies. Parasites will then revert to the promastigote stage within the sandfly midgut until reinfection.

1.13 Leishmania's niche in the macrophage

The PV is a unique site as it is permissive to *Leishmania* growth despite host efforts to eradicate it. Interestingly, morphology of PVs may vary depending on the species of *Leishmania*[372]. *L. major* and *L. infantum* segregate into individual PVs unlike *L. amazonensis* which form large communal PVs[373,374]. Macrophages infected with multiple species of parasite may also fuse their PVs even if this may lead to failure of differentiation for species that prefer to be isolated[375]. PVs are hybrid compartments containing elements from the endoplasmic reticulum as well as the endocytic compartments[376]. The toxin, ricin, that uses a retrograde pathway to enter the cytosol by passing through the endoplasmic reticulum was shown to enter PVs in infected cells[376]. This observation adds and additional layer of complexity to understanding *Leishmania*'s intracellular niche.

PVs must acquire iron from the environment to satisfy *Leishmania*'s requirement for growth. The three main forms of iron present in PVs include transferrin-bound iron, hemoglobin, and heme. *Leishmania* possesses no known siderophore-like molecules for scavenging iron from transferrin[377]. Yet, parasites may obtain iron from transferrin or other chelates as was shown in radioactivity studies using Fe^{59}-bound transferrin but prefer iron that is reduced rather than oxidized[377,378]. Since iron present on transferrin is oxidized, the parasite relies on its recently described ferrireductase *Leishmania* ferric reductase 1 (gene name: *LFR1*) for acquisition once iron is freed from transferrin[379]. Although holo-transferrin has been detected within PVs using

electron microscopy[380], a separate study demonstrated that TFR1 is scarcely detected on PV membranes[372]. Current understanding suggests that continuous fusion of endolysosomes containing holo-transferrin-bound TFR1, heme, or hemoglobin may be an important source of iron for the parasite, but more work is required to fully uncover the significance of this pathway. Supporting this hypothesis, infection with *L. donovani* was shown to deplete the labile iron pool within hours of infection in a macrophage cell line leading to induction of TFR1 expression[381]. The exact mechanism remains to be elucidated, but the rapid depletion of the labile iron pool suggests a process for transport of free iron to the PV that may be relevant early during infection as opposed to acquisition of transferrin-bound iron as infection progresses. The only characterized iron transporter on PVs is natural resistance-associated macrophage protein 1 (NRAMP1, gene name: *SLC11A1*)[382,383]. The multitude of experiments associating NRAMP1 with resistance to intracellular infection and modulation of cytosolic iron have revealed that this transporter likely exports iron from the PV[384-388]. Thus, parasite iron transporters must compete with NRAMP1. Notably, recent work suggests that NRAMP1 may be targeted by hepcidin for degradation and that parasite may use this to their advantage to retain iron within PVs[389].

Heme from hemoglobin or hemoglobin itself may be another source of iron for parasites within PVs. Macrophages may scavenge heme and hemoglobin from the circulation using CD91 and CD163, respectively[390,391]. Once internalized, these cells use heme-responsive gene 1 (HRG1; gene name *SLC48A1*) during erythrophagocytosis to transport heme from digested hemoglobin in the phagolysosome to the cytosol[392]. As such, parasite heme acquisition machinery must also contend with this transporter in PVs. Parasites may alter host macrophage function to increase erythrophagocytosis as seen in experimental models of visceral leishmaniasis in mice infected with *L. donovani*[393]. This is accompanied with an increase in HMOX1 expression to help control production of ROS which are harmful to parasite replication[394,395]. Heme is of particular importance for *Leishmania* as, like many members of the trypanosomatid family, these lack the biosynthetic pathways required to produce their own despite relying on oxidative phosphorylation for energy production[396].

1.14 Leishmania's surface iron molecules

Current evidence has demonstrated two independent pathways for *Leishmania*'s heme acquisition. The first involves clathrin-dependent endocytosis for hemoglobin using the

hemoglobin receptor on the parasite's flagellar pocket[397,398]. This receptor is regulated by Rab5 and Rab7[399-401]. Once internalized, hemoglobin would be rapidly degraded in lysosomes where heme can then be exported to the cytosol by the heme transporter *Leishmania* heme response 1 (gene name: *LHR1*)[402]. The second pathway involves direct transport via the plasma membrane using LHR1 or the leishmanial orthologue of FLVCR2, LmFLVCRb[403,404]. Thus, LHR1 plays a key role in heme uptake through its presence at both the cell surface and in endolysosomes. Recent work studying the uptake of a heme analogue, Zinc(II) Mesoporphyrin IX demonstrated that uptake of this molecule does not depend on a proton gradient but rather on the monovalent cations Na^+ and K^+ [405]. Moreover, uptake efficiency of ZnMP appears to vary between species of *Leishmania* and does not correlate with gene expression of the heme transporters LHR1 and LmFLVCRB[405]. Once *Leshmania* has obtained heme, however, it is unclear how and if iron is extracted for cellular use.

Leishmania may also obtain free iron to incorporate into enzymes and possesses specialized transporters to achieve this goal (Figure 1.4). Once ZIPs were demonstrated to transport iron in mammals, genome studies in *Leishmania major* revealed a ZIP homologue known as *Leishmania* iron transporter 1 (gene name: *LIT1*) expressed in amastigotes[406]. Knockout of this transporter resulted in severely impaired parasite replication and inability to induce productive infections in mice revealing a critical role for direct import of iron[407]. LIT1 works closely with LFR1 since iron must be reduced to pass through this transporter. Likewise, deletion of LFR1 results in impaired parasite infectivity due to inability to properly differentiate to the amastigote form[379]. Overexpression of LFR1 in these studies demonstrated that the subsequent increase in ferrous iron reduced parasite viability, possibly by production of ROS, which could be rescued by disruption of LIT1[379]. Importantly, both molecules are regulated transcriptionally by iron showing marked upregulation when deprived of this element. Since *Leishmania* spp. have no known iron storage molecule, they must carefully control their intracellular iron levels using the major facilitator superfamily protein *Leishmania* iron regulator 1 (gene name: *LIR1*) to prevent iron toxicity. This transporter has been characterized as a cell surface iron exporter which maintains iron homeostasis within the parasite as null mutants have greatly increased intracellular iron[408,409].

Subverting host molecules is an important strategy for parasite survival. *Leishmania* must manipulate the host's iron content as was seen with depletion of the labile iron pool[381]. Additionally, this parasite will also modulate expression of the cellular iron exporter ferroportin

and of IRPs[410]. Radioactive labeling of proteins revealed that *L. donovani* can inhibit translation of ferroportin increasing intracellular iron content favoring parasite growth. Decreased translation resulted from IRP activation which then bound ferroportin's IRE in the 5' UTR.

1.15 Immune responses to Leishmania

Parasite clearance depends on the immune response triggered by the host. Th1 cells have been associated with intracellular parasite killing and protection through the production of IL-2 and interferon gamma (IFNγ, gene name *IFNG*), of which the latter may cause upregulation of inducible nitric oxide synthase (iNOS, gene name *NOS2*) to produce nitric oxide. Th2 responses typically result in susceptibility by generating anti-inflammatory cytokines such as IL-4, -5, and -10. Notably, different mouse strains have been demonstrated to mount separate responses to infection with *L. major* resulting in either parasite clearance or chronic infection[411,412]. Thus, C57BL/6 mice will eventually clear parasite by mounting an effective Th1 response, while BALB/c mice will produce a Th2 response resulting in susceptibility. It should be noted that while this trend holds true for *L. major* infection, it does not reflect observations by other species and even strains of *Leishmania*[413,414]. Moreover, cytokines and their effects on leishmaniasis have been extensively studied. However, many cytokines have been associated with both protection and susceptibility depending on context. This is the case for IL-6 which in adoptive IL-6-deficient dendritic cell transfer experiments was shown to be crucial for resistance[415], while *in vitro* experiments using IL-6 pretreatment demonstrated that this could lead to downmodulation of macrophage activity by inhibiting oxygen-dependent mechanisms as well as others[416]. Similarly, IFNγ is largely thought to be a key cytokine involved in protection against leishmaniasis for its ability to trigger nitric oxide production in macrophages[417]. Yet, its expression was found to be elevated in the later phases of cutaneous and mucosal leishmaniasis suggesting that it may be insufficient for control of parasite once it is established[418]. Thus, consideration for parasite species and experimental timeframes must be made before associating cytokines with disease outcomes.

1.16 Competition between host and Leishmania for iron

The role of iron on parasite growth has been investigated *in vivo* using chelators, dietary iron supplementation, and modification of host genetics. One strategy used in patients suffering from hemochromatosis has been to treat them with chelators of iron such as desferrioxamine (DFO)[419]. Unfortunately, this chelator has a relatively short half-life in the circulation requiring

several treatments over the course of multiple days and suffers from side effects such as hypotension hindering its feasibility in chronic conditions[419-421]. However, it has successfully been used in cell culture and animals to model the effects of iron chelation. Treatment of macrophages with DFO prior and during infection with *L. donovani* or *L. major* demonstrated no significant reduction in parasite growth[422,423]. This was in contrast with several *in vitro* studies showing a suppression of *Leishmania* growth by DFO treatment depending on dose[380,381,423,424]. In mice treated with DFO, cutaneous lesions caused by *L. major* were only slightly delayed[425], while liver and spleen disease burden from *L. chagasi* infection appeared to be significantly reduced[426]. Moreover, restricting dietary iron intake in mice appeared to have no effect on *L. infantum*-induced visceral disease[427]. Taken together, these rather conflicting results suggest that cellular iron restriction may function to restrict parasite growth when the chelator is present in large enough concentration which may be harder to achieve continuously *in vivo*. It should be noted that timing of treatment may also play an important role.

On the other hand, iron loading therapies have proven to be more useful at controlling parasite growth through the production of ROS. The original study demonstrating an effect of iron used a series of 10 iron dextran injections where mice were inoculated in hind footpads 5 days after the first injection[425]. Iron dextran is known to be targeted to macrophages and deliver large amounts of iron to these cells[428]. A dose of 8 mg of iron per day was enough to completely prevent growth of *L. major* in mice footpads. Analysis at 14 weeks demonstrated that *IFNG* and *NOS2* were both upregulated in iron-treated mice[425]. IFNγ has been shown to play a critical role in host immunity as disruption of NF-κB results in susceptibility to cutaneous leishmaniasis due to impaired IFNγ-producing $CD4^+$ T cell proliferation[429]. Subsequently, a study demonstrated that parasite growth in the ear dermis could be restored by antioxidant treatments and that neutrophils and $IL\text{-}12^+$ leukocytes were necessary for protection[430]. Based on evidence that NF-κB could be regulated by iron[431], this group also suggested a role for iron-induced NF-κB activation, T cell proliferation, and generation of IFNγ-producing T cells in immunity against leishmaniasis[432]. Iron dextran injections were also used to demonstrate protection against visceral leishmaniasis caused by *L. infantum*[427]. Despite seeing a clear difference in both liver and spleen parasite burden, it was not clear which cytokines may be involved to cause this observation but disruption of *NOS2* and neutrophil cytosolic factor 1 (gene name: *NCF1*), both involved in production of ROS, rescued the

ability for the parasite to grow in the presence of iron. Importantly, HFE knockout mice, which model hereditary hemochromatosis, did not show any parasite restriction during infection.

The focus of the **fourth chapter** of this thesis is to dissect whether the rapid iron clearance phenotype observed in macrophages of juvenile hemochromatosis mouse models disrupts parasite growth. This will further our understanding of iron's role in parasite growth and will provide insight for iron supplementation therapies in areas endemic with leishmaniasis.

1.17 Rationale and research objectives

Herein, we have attempted to fill the knowledge gaps concerning mammalian iron sensing and further our understanding of the necessary conditions to produce inflammatory hypoferremia. Moreover, iron plays many paramount roles in determining the success of pathogenic infections such as in leishmaniasis. Therefore, this thesis has aimed to:

1. Examine the mechanisms by which our bodies sense iron using endothelial-specific TFR1 knockouts,
2. Dissect the underlying iron-related mechanism preventing inflammatory hypoferremia under conditions of iron overload, and
3. Study the development of *Leishmania* spp. in a mouse model of juvenile hemochromatosis.

Addressing these aims will help further our understanding of systemic iron homeostasis and of iron in immunity. Of particular importance, there is a necessity for novel therapies targeting iron overload and for a deeper understanding of how iron networks can be modulated to control leishmaniasis.

1.18 References

1. Beinert H, Holm RH, Münck E. Iron-Sulfur Clusters: Nature's Modular, Multipurpose Structures. *Science*. 1997;277(5326):653-659.
2. Wade J, Byrne DJ, Ballentine CJ, Drakesmith H. Temporal variation of planetary iron as a driver of evolution. *Proceedings of the National Academy of Sciences*. 2021;118(51):e2109865118.
3. Knoll AH, Nowak MA. The timetable of evolution. *Science Advances*. 2017;3(5).
4. Fenton HJH. LXXIII.—Oxidation of tartaric acid in presence of iron. *Journal of the Chemical Society, Transactions*. 1894;65:899-910.
5. Ameta R, K. Chohadia A, Jain A, Punjabi PB. Chapter 3 - Fenton and Photo-Fenton Processes. In: Ameta SC, Ameta R, eds. Advanced Oxidation Processes for Waste Water Treatment: Academic Press; 2018:49-87.
6. Ganz T. Systemic Iron Homeostasis. 2013;93(4):1721-1741.
7. Laufberger V. Sur la cristallisation de la ferritine. *Soc Chim Biol*. 1937;19:1575-1582.
8. Bakker GR, Boyer RF. Iron incorporation into apoferritin. The role of apoferritin as a ferroxidase. *J Biol Chem*. 1986;261(28):13182-13185.
9. Munro HN, Linder MC. Ferritin: structure, biosynthesis, and role in iron metabolism. *Physiol Rev*. 1978;58(2):317-396.
10. Dörner MH, Salfeld J, Will H, Leibold EA, Vass JK, Munro HN. Structure of human ferritin light subunit messenger RNA: comparison with heavy subunit message and functional implications. *Proceedings of the National Academy of Sciences*. 1985;82(10):3139-3143.
11. Boyd D, Vecoli C, Belcher DM, Jain SK, Drysdale JW. Structural and functional relationships of human ferritin H and L chains deduced from cDNA clones. *J Biol Chem*. 1985;260(21):11755-11761.
12. Santambrogio P, Levi S, Cozzi A, Corsi B, Arosio P. Evidence that the specificity of iron incorporation into homopolymers of human ferritin L- and H-chains is conferred by the nucleation and ferroxidase centres. *Biochem J*. 1996;314(1):139-144.
13. Levi S, Luzzago A, Cesareni G, et al. Mechanism of ferritin iron uptake: activity of the H-chain and deletion mapping of the ferro-oxidase site. A study of iron uptake and ferro-oxidase activity of human liver, recombinant H-chain ferritins, and of two H-chain deletion mutants. *J Biol Chem*. 1988;263(34):18086-18092.
14. Levi S, Yewdall SJ, Harrison PM, et al. Evidence of H- and L-chains have co-operative roles in the iron-uptake mechanism of human ferritin. *Biochem J*. 1992;288(2):591-596.
15. Albertini A, Arosio P, Levi S, et al. Analysis of Ferritins in Lymphoblastoid Cell Lines and in the Lens of. *Blood*. 1998;91(11):4180-4187.
16. Ferreira C, Bucchini D, Martin M-E, et al. Early Embryonic Lethality of H Ferritin Gene Deletion in Mice. *J Biol Chem*. 2000;275(5):3021-3024.
17. Speyer BE, Fielding J. Ferritin as a cytosol iron transport intermediate in human reticulocytes. *Br J Haematol*. 1979;42(2):255-267.
18. Cohen LA, Gutierrez L, Weiss A, et al. Serum ferritin is derived primarily from macrophages through a nonclassical secretory pathway. *Blood, The Journal of the American Society of Hematology*. 2010;116(9):1574-1584.
19. Leichtmann-Bardoogo Y, Cohen LA, Weiss A, et al. Compartmentalization and regulation of iron metabolism proteins protect male germ cells from iron overload. *American Journal of Physiology-Endocrinology and Metabolism*. 2012;302(12):E1519-E1530.

20. Vanoaica L, Darshan D, Richman L, Schümann K, Kühn LC. Intestinal Ferritin H Is Required for an Accurate Control of Iron Absorption. *Cell Metab*. 2010;12(3):273-282.
21. Van Deurs B, Von Bülow F, Møller M. Vesicular transport of cationized ferritin by the epithelium of the rat choroid plexus. *J Cell Biol*. 1981;89(1):131-139.
22. Clough G, Michel CC. The role of vesicles in the transport of ferritin through frog endothelium. *The Journal of Physiology*. 1981;315(1):127-142.
23. Dowdle WE, Nyfeler B, Nagel J, et al. Selective VPS34 inhibitor blocks autophagy and uncovers a role for NCOA4 in ferritin degradation and iron homeostasis in vivo. *Nat Cell Biol*. 2014;16(11):1069-1079.
24. Mancias JD, Wang X, Gygi SP, Harper JW, Kimmelman AC. Quantitative proteomics identifies NCOA4 as the cargo receptor mediating ferritinophagy. *Nature*. 2014;509(7498):105-109.
25. Kidane TZ, Sauble E, Linder MC. Release of iron from ferritin requires lysosomal activity. *American Journal of Physiology-Cell Physiology*. 2006;291(3):C445-C455.
26. Asano T, Komatsu M, Yamaguchi-Iwai Y, Ishikawa F, Mizushima N, Iwai K. Distinct Mechanisms of Ferritin Delivery to Lysosomes in Iron-Depleted and Iron-Replete Cells. *Molecular and Cellular Biology*. 2011;31(10):2040-2052.
27. Gryzik M, Srivastava A, Longhi G, et al. Expression and characterization of the ferritin binding domain of Nuclear Receptor Coactivator-4 (NCOA4). *Biochimica et Biophysica Acta (BBA) - General Subjects*. 2017;1861(11, Part A):2710-2716.
28. Mancias JD, Pontano Vaites L, Nissim S, et al. Ferritinophagy via NCOA4 is required for erythropoiesis and is regulated by iron dependent HERC2-mediated proteolysis. *Elife*. 2015;4.
29. Hentze MW, Rouault TA, Caughman SW, Dancis A, Harford JB, Klausner RD. A cis-acting element is necessary and sufficient for translational regulation of human ferritin expression in response to iron. *Proceedings of the National Academy of Sciences*. 1987;84(19):6730-6734.
30. Hentze MW, Caughman SW, Casey JL, et al. A model for the structure and functions of iron-responsive elements. *Gene*. 1988;72(1-2):201-208.
31. Zheng H, Bhavsar D, Dugast I, Zappone E, Drysdale J. Conserved mutations in human ferritin H pseudogenes: a second functional sequence or an evolutionary quirk? *Biochim Biophys Acta*. 1997;1351(1):150-156.
32. Drysdale J, Arosio P, Invernizzi R, et al. Mitochondrial Ferritin: A New Player in Iron Metabolism. *Blood Cells Mol Dis*. 2002;29(3):376-383.
33. Levi S, Corsi B, Bosisio M, et al. A Human Mitochondrial Ferritin Encoded by an Intronless Gene. *J Biol Chem*. 2001;276(27):24437-24440.
34. Corsi B, Cozzi A, Arosio P, et al. Human Mitochondrial Ferritin Expressed in HeLa Cells Incorporates Iron and Affects Cellular Iron Metabolism. *J Biol Chem*. 2002;277(25):22430-22437.
35. Santambrogio P, Biasiotto G, Sanvito F, Olivieri S, Arosio P, Levi S. Mitochondrial Ferritin Expression in Adult Mouse Tissues. *Journal of Histochemistry & Cytochemistry*. 2007;55(11):1129-1137.
36. Bartnikas TB, Campagna DR, Antiochos B, Mulhern H, Pondarré C, Fleming MD. Characterization of mitochondrial ferritin-deficient mice. *Am J Hematol*. 2010;85(12):958-960.

37. Wu W-S, Zhao Y-S, Shi Z-H, et al. Mitochondrial Ferritin Attenuates β-Amyloid-Induced Neurotoxicity: Reduction in Oxidative Damage Through the Erk/P38 Mitogen-Activated Protein Kinase Pathways. *Antioxidants & Redox Signaling*. 2012;18(2):158-169.
38. Shi Z-H, Nie G, Duan X-L, et al. Neuroprotective Mechanism of Mitochondrial Ferritin on 6-Hydroxydopamine–Induced Dopaminergic Cell Damage: Implication for Neuroprotection in Parkinson's Disease. *Antioxidants & Redox Signaling*. 2010;13(6):783-796.
39. Worwood M, Dawkins S, Wagstaff M, Jacobs A. The purification and properties of ferritin from human serum. *Biochem J*. 1976;157(1):97-103.
40. Arosio P, Yokota M, Drysdale JW. Characterization of Serum Ferritin in Iron Overload: Possible Identity to Natural Apoferritin. *Br J Haematol*. 1977;36(2):199-207.
41. Walters GO, Miller FM, Worwood M. Serum ferritin concentration and iron stores in normal subjects. *J Clin Pathol*. 1973;26(10):770-772.
42. Lipschitz DA, Cook JD, Finch CA. A Clinical Evaluation of Serum Ferritin as an Index of Iron Stores. *New England Journal of Medicine*. 1974;290(22):1213-1216.
43. Marcus DM, Zinberg N. Measurement of Serum Ferritin by Radioimmunoassay: Results in Normal Individuals and Patients With Breast Cancer2. *JNCI: Journal of the National Cancer Institute*. 1975;55(4):791-795.
44. Ghosh S, Hevi S, Chuck SL. Regulated secretion of glycosylated human ferritin from hepatocytes. *Blood*. 2004;103(6):2369-2376.
45. Tran TN, Eubanks SK, Schaffer KJ, Zhou CYJ, Linder MC. Secretion of Ferritin by Rat Hepatoma Cells and Its Regulation by Inflammatory Cytokines and Iron. *Blood*. 1997;90(12):4979-4986.
46. Wesselius LJ, Nelson ME, Skikne BS. Increased release of ferritin and iron by iron-loaded alveolar macrophages in cigarette smokers. *American Journal of Respiratory and Critical Care Medicine*. 1994;150(3):690-695.
47. Yuan X-M, Li W, Baird SK, Carlsson M, Melefors Ö. Secretion of ferritin by iron-laden macrophages and influence of lipoproteins. *Free Radic Res*. 2004;38(10):1133-1142.
48. Selig R, Madafiglio J, Haber M, Norris M, White L, Stewart B. Ferritin production and desferrioxamine cytotoxicity in human neuroblastoma cell lines. *Anticancer Res*. 1993;13(3):721-725.
49. Mukherjee C, Kling T, Russo B, et al. Oligodendrocytes provide antioxidant defense function for neurons by secreting ferritin heavy chain. *Cell Metab*. 2020;32(2):259-272. e210.
50. Greco TM, Seeholzer SH, Mak A, Spruce L, Ischiropoulos H. Quantitative mass spectrometry-based proteomics reveals the dynamic range of primary mouse astrocyte protein secretion. *J Proteome Res*. 2010;9(5):2764-2774.
51. Santambrogio P, Cozzi A, Levi S, Arosio P. Human serum ferritin G-peptide is recognized by anti-L ferritin subunit antibodies and concanavalin-A. *Br J Haematol*. 1987;65(2):235-237.
52. Blake DR, Bacon PA, Eastham EJ, Brigham K. Synovial fluid ferritin in rheumatoid arthritis. *Br Med J*. 1980;281(6242):715-716.
53. Truman-Rosentsvit M, Berenbaum D, Spektor L, et al. Ferritin is secreted via 2 distinct nonclassical vesicular pathways. *Blood*. 2018;131(3):342-352.
54. Yanatori I, Richardson DR, Dhekne HS, Toyokuni S, Kishi F. CD63 is regulated by iron via the IRE-IRP system and is important for ferritin secretion by extracellular vesicles. *Blood*. 2021;138(16):1490-1503.

55. Cragg SJ, Wagstaff M, Worwood M. Detection of a glycosylated subunit in human serum ferritin. *Biochem J*. 1981;199(3):565-571.
56. Schade AL, Caroline L. An iron-binding component in human blood plasma. *Science*. 1946;104(2702):340-341.
57. MacGillivray RT, Mendez E, Shewale JG, Sinha SK, Lineback-Zins J, Brew K. The primary structure of human serum transferrin. The structures of seven cyanogen bromide fragments and the assembly of the complete structure. *J Biol Chem*. 1983;258(6):3543-3553.
58. Gomme PT, McCann KB, Bertolini J. Transferrin: structure, function and potential therapeutic actions. *Drug Discov Today*. 2005;10(4):267-273.
59. Idzerda RL, Huebers H, Finch CA, McKnight GS. Rat transferrin gene expression: tissue-specific regulation by iron deficiency. *Proceedings of the National Academy of Sciences*. 1986;83(11):3723-3727.
60. Skinner MK, Griswold MD. Secretion of Testicular Transferrin by Cultured Sertoli Cells is Regulated by Hormones and Retinoids. *Biol Reprod*. 1982;27(1):211-221.
61. Meehan RR, Barlow DP, Hill RE, Hogan BL, Hastie ND. Pattern of serum protein gene expression in mouse visceral yolk sac and foetal liver. *The EMBO Journal*. 1984;3(8):1881-1885.
62. Ekblom P, Thesleff I. Control of kidney differentiation by soluble factors secreted by the embryonic liver and the yolk sac. *Dev Biol*. 1985;110(1):29-38.
63. Messori L, Kratz F. Transferrin - From inorganic biochemistry to medicine. *Metal Based Drugs*. 1994;1(2-3):161-167.
64. Schryvers AB, Morris LJ. Identification and characterization of the transferrin receptor from Neisseria meningitidis. *Mol Microbiol*. 1988;2(2):281-288.
65. Steverding D, Stierhof YD, Fuchs H, Tauber R, Overath P. Transferrin-binding protein complex is the receptor for transferrin uptake in Trypanosoma brucei. *J Cell Biol*. 1995;131(5):1173-1182.
66. Lawrence CM, Ray S, Babyonyshev M, Galluser R, Borhani DW, Harrison SC. Crystal Structure of the Ectodomain of Human Transferrin Receptor. *Science*. 1999;286(5440):779-782.
67. Sullivan AL, Grasso JA, Weintraub LR. Micropinocytosis of Transferrin by Developing Red Cells: An Electron-microscopic Study Utilizing Ferritin-conjugated Transferrin and Ferritin-conjugated Antibodies to Transferrin. *Blood*. 1976;47(1):133-143.
68. Princiotto JV, Zapolski EJ. Functional heterogeneity and pH-dependent dissociation properties of human transferrin. *Biochimica et Biophysica Acta (BBA) - General Subjects*. 1976;428(3):766-771.
69. Dautry-Varsat A, Ciechanover A, Lodish HF. pH and the recycling of transferrin during receptor-mediated endocytosis. *Proceedings of the National Academy of Sciences*. 1983;80(8):2258-2262.
70. Van Renswoude J, Bridges KR, Harford JB, Klausner RD. Receptor-mediated endocytosis of transferrin and the uptake of fe in K562 cells: identification of a nonlysosomal acidic compartment. *Proceedings of the National Academy of Sciences*. 1982;79(20):6186-6190.
71. Ohgami RS, Campagna DR, Greer EL, et al. Identification of a ferrireductase required for efficient transferrin-dependent iron uptake in erythroid cells. *Nat Genet*. 2005;37(11):1264-1269.
72. Gunshin H, Mackenzie B, Berger UV, et al. Cloning and characterization of a mammalian proton-coupled metal-ion transporter. *Nature*. 1997;388(6641):482-488.

73. Sacher A, Cohen A, Nelson N. Properties of the mammalian and yeast metal-ion transporters DCT1 and Smf1p expressed in Xenopus laevis oocytes. *J Exp Biol*. 2001;204(6):1053-1061.
74. Shi H, Bencze KZ, Stemmler TL, Philpott CC. A Cytosolic Iron Chaperone That Delivers Iron to Ferritin. *Science*. 2008;320(5880):1207-1210.
75. Leidgens S, Bullough KZ, Shi H, et al. Each Member of the Poly-r(C)-binding Protein 1 (PCBP) Family Exhibits Iron Chaperone Activity toward Ferritin. *J Biol Chem*. 2013;288(24):17791-17802.
76. Frey AG, Nandal A, Park JH, et al. Iron chaperones PCBP1 and PCBP2 mediate the metallation of the dinuclear iron enzyme deoxyhypusine hydroxylase. *Proceedings of the National Academy of Sciences*. 2014;111(22):8031-8036.
77. Jacobs A. An Intracellular Transit Iron Pool. Ciba Foundation Symposium 51 - Iron Metabolism; 1977:91-106.
78. Epsztejn S, Kakhlon O, Glickstein H, Breuer W, Cabantchik ZI. Fluorescence Analysis of the Labile Iron Pool of Mammalian Cells. *Anal Biochem*. 1997;248(1):31-40.
79. Ryu M-S, Zhang D, Protchenko O, Shakoury-Elizeh M, Philpott CC. PCBP1 and NCOA4 regulate erythroid iron storage and heme biosynthesis. *J Clin Invest*. 2017;127(5):1786-1797.
80. Lambert LA, Mitchell SL. Molecular Evolution of the Transferrin Receptor/Glutamate Carboxypeptidase II Family. *J Mol Evol*. 2007;64(1):113-128.
81. Levy JE, Jin O, Fujiwara Y, Kuo F, Andrews N. Transferrin receptor is necessary for development of erythrocytes and the nervous system. *Nat Genet*. 1999;21(4):396-399.
82. Tsai G, Dunham KS, Drager U, et al. Early embryonic death of glutamate carboxypeptidase II (NAALADase) homozygous mutants. *Synapse*. 2003;50(4):285-292.
83. Shih YJ, Baynes RD, Hudson BG, Flowers CH, Skikne BS, Cook JD. Serum transferrin receptor is a truncated form of tissue receptor. *J Biol Chem*. 1990;265(31):19077-19081.
84. Punnonen K, Irjala K, Rajamäki A. Serum Transferrin Receptor and Its Ratio to Serum Ferritin in the Diagnosis of Iron Deficiency. *Blood*. 1997;89(3):1052-1057.
85. Casey JL, Di Jeso B, Rao K, Klausner RD, Harford JB. Two genetic loci participate in the regulation by iron of the gene for the human transferrin receptor. *Proceedings of the National Academy of Sciences*. 1988;85(6):1787-1791.
86. Casey JL, Hentze MW, Koeller DM, et al. Iron-Responsive Elements: Regulatory RNA Sequences That Control mRNA Levels and Translation. *Science*. 1988;240(4854):924-928.
87. Rao K, Harford JB, Rouault T, McClelland A, Ruddle FH, Klausner RD. Transcriptional regulation by iron of the gene for the transferrin receptor. *Molecular and Cellular Biology*. 1986;6(1):236-240.
88. Lok CN, Ponka P. Identification of a Hypoxia Response Element in the Transferrin Receptor Gene. *J Biol Chem*. 1999;274(34):24147-24152.
89. Huang LE, Gu J, Schau M, Bunn HF. Regulation of hypoxia-inducible factor 1α is mediated by an O ₂ -dependent degradation domain via the ubiquitin-proteasome pathway. *Proceedings of the National Academy of Sciences*. 1998;95(14):7987-7992.
90. Wang G, Semenza G. Desferrioxamine induces erythropoietin gene expression and hypoxia-inducible factor 1 DNA-binding activity: implications for models of hypoxia signal transduction. *Blood*. 1993;82(12):3610-3615.
91. Wilkinson N, Pantopoulos K. IRP1 regulates erythropoiesis and systemic iron homeostasis by controlling HIF2α mRNA translation. *Blood*. 2013;122(9):1658-1668.

92. Barrientos T, Laothamatas I, Koves TR, et al. Metabolic Catastrophe in Mice Lacking Transferrin Receptor in Muscle. *EBioMedicine*. 2015;2(11):1705-1717.
93. Chen AC, Donovan A, Ned-Sykes R, Andrews NC. Noncanonical role of transferrin receptor 1 is essential for intestinal homeostasis. 2015;112(37):11714-11719.
94. Xu W, Barrientos T, Mao L, Rockman Howard A, Sauve Anthony A, Andrews Nancy C. Lethal Cardiomyopathy in Mice Lacking Transferrin Receptor in the Heart. *Cell Reports*. 2015;13(3):533-545.
95. Ding H, Chen S, Pan X, et al. Transferrin receptor 1 ablation in satellite cells impedes skeletal muscle regeneration through activation of ferroptosis. *Journal of Cachexia, Sarcopenia and Muscle*. 2021;12(3):746-768.
96. Scott, Kathryn, Michael, et al. Ferroptosis: An Iron-Dependent Form of Nonapoptotic Cell Death. *Cell*. 2012;149(5):1060-1072.
97. Das BK, Wang L, Fujiwara T, et al. Transferrin receptor 1-mediated iron uptake regulates bone mass in mice via osteoclast mitochondria and cytoskeleton. *eLife*. 2022;11:e73539.
98. Fillebeen C, Charlebois E, Wagner J, et al. Transferrin receptor 1 controls systemic iron homeostasis by fine-tuning hepcidin expression to hepatocellular iron load. *Blood*. 2019;133(4):344-355.
99. Xiao X, Moschetta GA, Xu Y, et al. Regulation of iron homeostasis by hepatocyte TFR1 requires HFE and contributes to hepcidin suppression in β-thalassemia. *Blood*. 2022.
100. Kawabata H, Yang R, Hirama T, et al. Molecular Cloning of Transferrin Receptor 2. *J Biol Chem*. 1999;274(30):20826-20832.
101. Johnson MB, Enns CA. Diferric transferrin regulates transferrin receptor 2 protein stability. *Blood*. 2004;104(13):4287-4293.
102. Robb A, Wessling-Resnick M. Regulation of transferrin receptor 2 protein levels by transferrin. *Blood*. 2004;104(13):4294-4299.
103. Kawabata H, Germain RS, Ikezoe T, et al. Regulation of expression of murine transferrin receptor 2. *Blood*. 2001;98(6):1949-1954.
104. West AP, Bennett MJ, Sellers VM, Andrews NC, Enns CA, Bjorkman PJ. Comparison of the Interactions of Transferrin Receptor and Transferrin Receptor 2 with Transferrin and the Hereditary Hemochromatosis Protein HFE. *J Biol Chem*. 2000;275(49):38135-38138.
105. Kawabata H, Germain RS, Vuong PT, Nakamaki T, Said JW, Koeffler HP. Transferrin Receptor 2-α Supports Cell Growth Both in Iron-chelated Cultured Cells and in Vivo. *J Biol Chem*. 2000;275(22):16618-16625.
106. Camaschella C, Roetto A, Calì A, et al. The gene TFR2 is mutated in a new type of haemochromatosis mapping to 7q22. *Nat Genet*. 2000;25(1):14-15.
107. Rauner M, Baschant U, Roetto A, et al. Transferrin receptor 2 controls bone mass and pathological bone formation via BMP and Wnt signalling. *Nature Metabolism*. 2019;1(1):111-124.
108. Roetto A, Di Cunto F, Pellegrino RM, et al. Comparison of 3 Tfr2-deficient murine models suggests distinct functions for Tfr2-α and Tfr2-β isoforms in different tissues. *Blood*. 2010;115(16):3382-3389.
109. Rishi G, Secondes ES, Wallace DF, Subramaniam VN. Normal systemic iron homeostasis in mice with macrophage-specific deletion of transferrin receptor 2. *American Journal of Physiology-Gastrointestinal and Liver Physiology*. 2016;310(3):G171-G180.
110. Piccinelli P, Samuelsson T. Evolution of the iron-responsive element. *RNA*. 2007;13(7):952-966.

111. Hentze MW, Caughman SW, Rouault TA, et al. Identification of the Iron-Responsive Element for the Translational Regulation of Human Ferritin mRNA. *Science*. 1987;238(4833):1570-1573.
112. Müllner EW, Kühn LC. A stem-loop in the 3′ untranslated region mediates iron-dependent regulation of transferrin receptor mRNA stability in the cytoplasm. *Cell*. 1988;53(5):815-825.
113. Wilkinson N, Pantopoulos K. The IRP/IRE system in vivo: insights from mouse models. *Front Pharmacol*. 2014;5:176.
114. Hentze MW, Rouault TA, Harford JB, Klausner RD. Oxidation-Reduction and the Molecular Mechanism of a Regulatory RNA-Protein Interaction. *Science*. 1989;244(4902):357-359.
115. Ghosh Manik C, Zhang D-L, Jeong Suh Y, et al. Deletion of Iron Regulatory Protein 1 Causes Polycythemia and Pulmonary Hypertension in Mice through Translational Derepression of HIF2α. *Cell Metab*. 2013;17(2):271-281.
116. Anderson Sheila A, Nizzi Christopher P, Chang Y-I, et al. The IRP1-HIF-2α Axis Coordinates Iron and Oxygen Sensing with Erythropoiesis and Iron Absorption. *Cell Metab*. 2013;17(2):282-290.
117. Galy B, Ferring D, Minana B, et al. Altered body iron distribution and microcytosis in mice deficient in iron regulatory protein 2 (IRP2). *Blood*. 2005;106(7):2580-2589.
118. Cooperman SS, Meyron-Holtz EG, Olivierre-Wilson H, Ghosh MC, McConnell JP, Rouault TA. Microcytic anemia, erythropoietic protoporphyria, and neurodegeneration in mice with targeted deletion of iron-regulatory protein 2. *Blood*. 2005;106(3):1084-1091.
119. Terzi EM, Sviderskiy VO, Alvarez SW, Whiten GC, Possemato R. Iron-sulfur cluster deficiency can be sensed by IRP2 and regulates iron homeostasis and sensitivity to ferroptosis independent of IRP1 and FBXL5. *Science Advances*. 2021;7(22):eabg4302.
120. Smith SR, Ghosh MC, Ollivierre-Wilson H, Hang Tong W, Rouault TA. Complete loss of iron regulatory proteins 1 and 2 prevents viability of murine zygotes beyond the blastocyst stage of embryonic development. *Blood Cells Mol Dis*. 2006;36(2):283-287.
121. Vashisht AA, Zumbrennen KB, Huang X, et al. Control of Iron Homeostasis by an Iron-Regulated Ubiquitin Ligase. *Science*. 2009;326(5953):718-721.
122. Salahudeen AA, Thompson JW, Ruiz JC, et al. An E3 Ligase Possessing an Iron-Responsive Hemerythrin Domain Is a Regulator of Iron Homeostasis. *Science*. 2009;326(5953):722-726.
123. Jin J, Cardozo T, Lovering RC, Elledge SJ, Pagano M, Harper JW. Systematic analysis and nomenclature of mammalian F-box proteins. *Genes & Development*. 2004;18(21):2573-2580.
124. Wang J, Fillebeen C, Chen G, Biederbick A, Lill R, Pantopoulos K. Iron-Dependent Degradation of Apo-IRP1 by the Ubiquitin-Proteasome Pathway. *Molecular and Cellular Biology*. 2007;27(7):2423-2430.
125. Johnson NB, Deck KM, Nizzi CP, Eisenstein RS. A synergistic role of IRP1 and FBXL5 proteins in coordinating iron metabolism during cell proliferation. *J Biol Chem*. 2017;292(38):15976-15989.
126. Cmejla R, Petrak J, Cmejlova J. A novel iron responsive element in the 3′UTR of human MRCKα. *Biochemical and Biophysical Research Communications*. 2006;341(1):158-166.
127. Abboud S, Haile DJ. A Novel Mammalian Iron-regulated Protein Involved in Intracellular Iron Metabolism. *J Biol Chem*. 2000;275(26):19906-19912.

128. Canonne-Hergaux F, Gruenheid S, Ponka P, Gros P. Cellular and Subcellular Localization of the Nramp2 Iron Transporter in the Intestinal Brush Border and Regulation by Dietary Iron. *Blood*. 1999;93(12):4406-4417.
129. McKie AT, Barrow D, Latunde-Dada GO, et al. An Iron-Regulated Ferric Reductase Associated with the Absorption of Dietary Iron. *Science*. 2001;291(5509):1755-1759.
130. Latunde-Dada GO, Simpson RJ, McKie AT. Duodenal Cytochrome B Expression Stimulates Iron Uptake by Human Intestinal Epithelial Cells. *The Journal of Nutrition*. 2008;138(6):991-995.
131. Conrad ME, Schade SG. Ascorbic acid chelates in iron absorption: a role for hydrochloric acid and bile. *Gastroenterology*. 1968;55:35-45.
132. Su D, Asard H. Three mammalian cytochromes b561 are ascorbate-dependent ferrireductases. *FEBS J*. 2006;273(16):3722-3734.
133. Latunde-Dada GO, Van der Westhuizen J, Vulpe CD, Anderson GJ, Simpson RJ, McKie AT. Molecular and Functional Roles of Duodenal Cytochrome B (Dcytb) in Iron Metabolism. *Blood Cells Mol Dis*. 2002;29(3):356-360.
134. Shayeghi M, Latunde-Dada GO, Oakhill JS, et al. Identification of an Intestinal Heme Transporter. *Cell*. 2005;122(5):789-801.
135. Blanc SL, Garrick MD, Arredondo M. Heme carrier protein 1 transports heme and is involved in heme-Fe metabolism. *American Journal of Physiology-Cell Physiology*. 2012;302(12):C1780-C1785.
136. Qiu A, Jansen M, Sakaris A, et al. Identification of an intestinal folate transporter and the molecular basis for hereditary folate malabsorption. *Cell*. 2006;127(5):917-928.
137. Nakai Y, Inoue K, Abe N, et al. Functional characterization of human proton-coupled folate transporter/heme carrier protein 1 heterologously expressed in mammalian cells as a folate transporter. *J Pharmacol Exp Ther*. 2007;322(2):469-476.
138. Maines MD, Trakshel GM, Kutty RK. Characterization of two constitutive forms of rat liver microsomal heme oxygenase. Only one molecular species of the enzyme is inducible. *J Biol Chem*. 1986;261(1):411-419.
139. Quigley JG, Yang Z, Worthington MT, et al. Identification of a Human Heme Exporter that Is Essential for Erythropoiesis. *Cell*. 2004;118(6):757-766.
140. Keel SB, Doty RT, Yang Z, et al. A Heme Export Protein Is Required for Red Blood Cell Differentiation and Iron Homeostasis. *Science*. 2008;319(5864):825-828.
141. Krishnamurthy P, Ross DD, Nakanishi T, et al. The Stem Cell Marker Bcrp/ABCG2 Enhances Hypoxic Cell Survival through Interactions with Heme*. *J Biol Chem*. 2004;279(23):24218-24225.
142. Donovan A, Brownlie A, Zhou Y, et al. Positional cloning of zebrafish ferroportin1 identifies a conserved vertebrate iron exporter. *Nature*. 2000;403(6771):776-781.
143. McKie AT, Marciani P, Rolfs A, et al. A Novel Duodenal Iron-Regulated Transporter, IREG1, Implicated in the Basolateral Transfer of Iron to the Circulation. *Mol Cell*. 2000;5(2):299-309.
144. Zhang D-L, Hughes RM, Ollivierre-Wilson H, Ghosh MC, Rouault TA. A Ferroportin Transcript that Lacks an Iron-Responsive Element Enables Duodenal and Erythroid Precursor Cells to Evade Translational Repression. *Cell Metab*. 2009;9(5):461-473.
145. Anderson ER, Taylor M, Xue X, et al. Intestinal HIF2α promotes tissue-iron accumulation in disorders of iron overload with anemia. *Proc Natl Acad Sci U S A*. 2013;110(50):E4922-E4930.

146. Vulpe CD, Kuo Y-M, Murphy TL, et al. Hephaestin, a ceruloplasmin homologue implicated in intestinal iron transport, is defective in the sla mouse. *Nat Genet*. 1999;21(2):195-199.
147. HOLMBERG CG, Laurell C. Investigations in serum copper. *III: Cae*. 1951.
148. Curzon G, O'reilly S. A coupled iron-caeruloplasmin oxidation system. *Biochemical and Biophysical Research Communications*. 1960;2(4):284-286.
149. Chowrimootoo G, Gillett M, Debnam ES, Srai SK, Epstein O. Iron-transferrin binding to isolated guinea pig enterocytes and the regional localisation of intestinal iron transfer during ontogeny. *Biochimica et Biophysica Acta (BBA) - General Subjects*. 1992;1116(3):256-260.
150. Muir A, Hopfer U. Regional specificity of iron uptake by small intestinal brush-border membranes from normal and iron-deficient mice. *American Journal of Physiology-Gastrointestinal and Liver Physiology*. 1985;248(3):G376-G379.
151. Balusikova K, Dostalikova-Cimburova M, Tacheci I, Kovar J. Expression profiles of iron transport molecules along the duodenum. *Journal of Cellular and Molecular Medicine*. 2022;26(10):2995-3004.
152. Lynch S, Skikne B, Cook J. Food iron absorption in idiopathic hemochromatosis. *Blood*. 1989;74(6):2187-2193.
153. Hanudel MR, Czaya B, Wong S, et al. Enteral ferric citrate absorption is dependent on the iron transport protein ferroportin. *Kidney Int*. 2022;101(4):711-719.
154. Das NK, Jain C, Sankar AD, et al. Modulation of the HIF2-NCOA4 axis in enterocytes attenuates iron loading in a mouse model of hemochromatosis. *Blood*. 2022.
155. Cazzola M, Huebers H, Sayers M, MacPhail A, Eng M, Finch C. Transferrin saturation, plasma iron turnover, and transferrin uptake in normal humans. *Blood*. 1985;66(4):935-939.
156. van der Heul C, van Eijk HG, Wiltink WF, Leijnse B. The binding of iron to transferrin and to other serum components at different degrees of saturation with iron. *Clin Chim Acta*. 1972;38(2):347-353.
157. Hershko C, Graham G, Bates GW, Rachmilewitz EA. Non-Specific Serum Iron in Thalassaemia: an Abnormal Serum Iron Fraction of Potential Toxicity. *Br J Haematol*. 1978;40(2):255-263.
158. May PM, Williams DR. Computer simulation of chelation therapy Plasma mobilizing index as a replacement for effective stability constant. *FEBS Lett*. 1977;78(1):134-138.
159. Grootveld M, Bell JD, Halliwell B, Aruoma OI, Bomford A, Sadler PJ. Non-transferrin-bound iron in plasma or serum from patients with idiopathic hemochromatosis. *J Biol Chem*. 1989;264(8):4417-4422.
160. Esposito BP. Labile plasma iron in iron overload: redox activity and susceptibility to chelation. 2003;102(7):2670-2677.
161. Breuer W, Ermers MJJ, Pootrakul P, Abramov A, Hershko C, Ioav Cabantchik Z. Desferrioxamine-chelatable iron (DCI), a component of serum non-transferrin-bound iron (NTBI) used for assessing iron chelation therapy. *Transfus Sci*. 2000;23(3):241-242.
162. Anuwatanakulchai M, Wasi P, Pootrakul P, Thuvasethakul P. Non-Transferrin Plasma Iron in β-Thalassaemia/Hb E and Haemoglobin H Diseases. *Scand J Haematol*. 1984;32(2):153-158.
163. Wang WC, Ahmed N, Hanna M. Non-transferrin-bound iron in long-term transfusion in children with congenital anemias. *The Journal of Pediatrics*. 1986;108(4):552-557.
164. Aruoma O, Bomford A, Polson R, Halliwell B. Nontransferrin-bound iron in plasma from hemochromatosis patients: effect of phlebotomy therapy. *Blood*. 1988;72(4):1416-1419.

165. Gosriwatana I, Loreal O, Lu S, Brissot P, Porter J, Hider RC. Quantification of Non-Transferrin-Bound Iron in the Presence of Unsaturated Transferrin. *Anal Biochem*. 1999;273(2):212-220.
166. Loréal O, Gosriwatana I, Guyader D, Porter J, Brissot P, Hider RC. Determination of non-transferrin-bound iron in genetic hemochromatosis using a new HPLC-based method. *J Hepatol*. 2000;32(5):727-733.
167. Aljwaid H, White DL, Collard KJ, Moody AJ, Pinkney JH. Non-transferrin-bound iron is associated with biomarkers of oxidative stress, inflammation and endothelial dysfunction in type 2 diabetes. *J Diabetes Complications*. 2015;29(7):943-949.
168. Craven CM, Alexander J, Eldridge M, Kushner JP, Bernstein S, Kaplan J. Tissue distribution and clearance kinetics of non-transferrin-bound iron in the hypotransferrinemic mouse: a rodent model for hemochromatosis. *Proceedings of the National Academy of Sciences*. 1987;84(10):3457-3461.
169. Zhang AS, Sheftel AD, Ponka P. Intracellular kinetics of iron in reticulocytes: evidence for endosome involvement in iron targeting to mitochondria. *Blood*. 2005;105(1):368-375.
170. Wright TL, Brissot P, Ma WL, Weisiger RA. Characterization of non-transferrin-bound iron clearance by rat liver. *J Biol Chem*. 1986;261(23):10909-10914.
171. Kaplan J, Jordan I, Sturrock A. Regulation of the transferrin-independent iron transport system in cultured cells. *J Biol Chem*. 1991;266(5):2997-3004.
172. Cutler DJ, Isner JM, Bracey AW, et al. Hemochromatosis heart disease: An unemphasized cause of potentially reversible restrictive cardiomyopathy. *The American Journal of Medicine*. 1980;69(6):923-928.
173. Dabestani A, Child JS, Perloff JK, Figueroa WG, Schelbert HR, Engel TR. Cardiac Abnormalities in Primary Hemochromatosis. *Ann N Y Acad Sci*. 1988;526(1):234-244.
174. Bardou-Jacquet E, Lainé F, Guggenbuhl P, et al. Worse Outcomes of Patients With HFE Hemochromatosis With Persistent Increases in Transferrin Saturation During Maintenance Therapy. *Clin Gastroenterol Hepatol*. 2017;15(10):1620-1627.
175. Doyard M, Chappard D, Leroyer P, Roth M-P, Loréal O, Guggenbuhl P. Decreased Bone Formation Explains Osteoporosis in a Genetic Mouse Model of Hemochromatosiss. *PLoS One*. 2016;11(2):e0148292.
176. Lunova M, Schwarz P, Nuraldeen R, et al. Hepcidin knockout mice spontaneously develop chronic pancreatitis owing to cytoplasmic iron overload in acinar cells. *The Journal of Pathology*. 2017;241(1):104-114.
177. Altamura S, Kessler R, Gröne H-J, et al. Resistance of Ferroportin to Hepcidin Binding causes Exocrine Pancreatic Failure and Fatal Iron Overload. *Cell Metab*. 2014;20(2):359-367.
178. Wheby MS, Jones LG. ROLE OF TRANSFERRIN IN IRON ABSORPTION*. *J Clin Invest*. 1963;42(7):1007-1016.
179. Tsushima RG, Wickenden AD, Bouchard RA, Oudit GY, Liu PP, Backx PH. Modulation of Iron Uptake in Heart by L-Type Ca2+ Channel Modifiers. *Circulation Research*. 1999;84(11):1302-1309.
180. Garrick LM, Dolan KG, Romano MA, Garrick MD. Non-transferrin-bound iron uptake in Belgrade and normal rat erythroid cells. *J Cell Physiol*. 1999;178(3):349-358.
181. Fleming MD, Trenor CC, Su MA, et al. Microcytic anaemia mice have a mutation in Nramp2, a candidate iron transporter gene. *Nat Genet*. 1997;16(4):383-386.

182. Ehrnstorfer IA, Manatschal C, Arnold FM, Laederach J, Dutzler R. Structural and mechanistic basis of proton-coupled metal ion transport in the SLC11/NRAMP family. *Nature Communications*. 2017;8(1):14033.
183. Hubert N, Hentze MW. Previously uncharacterized isoforms of divalent metal transporter (DMT)-1: Implications for regulation and cellular function. *Proceedings of the National Academy of Sciences*. 2002;99(19):12345-12350.
184. Yanatori I, Tabuchi M, Kawai Y, Yasui Y, Akagi R, Kishi F. Heme and non-heme iron transporters in non-polarized and polarized cells. *BMC Cell Biol*. 2010;11(1):39.
185. Nam H, Wang CY, Zhang L, et al. ZIP14 and DMT1 in the liver, pancreas, and heart are differentially regulated by iron deficiency and overload: implications for tissue iron uptake in iron-related disorders. *Haematologica*. 2013;98(7):1049-1057.
186. Wang C-Y, Knutson MD. Hepatocyte divalent metal-ion transporter-1 is dispensable for hepatic iron accumulation and non-transferrin-bound iron uptake in mice. *Hepatology*. 2013;58(2):788-798.
187. Winegar BD, Kelly R, Lansman JB. Block of current through single calcium channels by Fe, Co, and Ni. Location of the transition metal binding site in the pore. *J Gen Physiol*. 1991;97(2):351-367.
188. Oudit GY, Sun H, Trivieri MG, et al. L-type Ca2+ channels provide a major pathway for iron entry into cardiomyocytes in iron-overload cardiomyopathy. *Nat Med*. 2003;9(9):1187-1194.
189. Crowe S, Bartfay WJ. Amlodipine Decreases Iron Uptake and Oxygen Free Radical Production in the Heart of Chronically Iron Overloaded Mice. *Biol Res Nurs*. 2002;3(4):189-197.
190. Otto-Duessel M, Brewer C, Wood JC. Interdependence of cardiac iron and calcium in a murine model of iron overload. *Translational Research*. 2011;157(2):92-99.
191. Martı ´ nez MaL, Heredia MaP, Delgado C. Expression of T-type Ca2+Channels in Ventricular Cells from Hypertrophied Rat Hearts. *J Mol Cell Cardiol*. 1999;31(9):1617-1625.
192. Kumfu S, Chattipakorn S, Srichairatanakool S, Settakorn J, Fucharoen S, Chattipakorn N. T-type calcium channel as a portal of iron uptake into cardiomyocytes of beta-thalassemic mice. *Eur J Haematol*. 2011;86(2):156-166.
193. Kumfu S, Chattipakorn S, Chinda K, Fucharoen S, Chattipakorn N. T-type calcium channel blockade improves survival and cardiovascular function in thalassemic mice. *Eur J Haematol*. 2012;88(6):535-548.
194. Rosati B, Yan Q, Lee MS, et al. Robust L-type calcium current expression following heterozygous knockout of the Cav1.2 gene in adult mouse heart. *The Journal of Physiology*. 2011;589(13):3275-3288.
195. Seisenberger C, Specht V, Welling A, et al. Functional Embryonic Cardiomyocytes after Disruption of the L-type α1C (Ca 1.2) Calcium Channel Gene in the Mouse. *J Biol Chem*. 2000;275(50):39193-39199.
196. Fernandes JL, Sampaio EF, Fertrin K, et al. Amlodipine Reduces Cardiac Iron Overload in Patients with Thalassemia Major: A Pilot Trial. *The American Journal of Medicine*. 2013;126(9):834-837.
197. Fernandes JL, Loggetto SR, Veríssimo MPA, et al. A randomized trial of amlodipine in addition to standard chelation therapy in patients with thalassemia major. *Blood*. 2016;128(12):1555-1561.

198. Khaled A, Salem HA, Ezzat D, Seif HM, Rabee H. <p>A randomized controlled trial evaluating the effects of amlodipine on myocardial iron deposition in pediatric patients with thalassemia major</p&gt. *Drug Des Devel Ther*. 2019;Volume 13:2427-2436.
199. Gupta V, Kumar I, Raj V, Aggarwal P, Agrawal V. Comparison of the effects of calcium channel blockers plus iron chelation therapy versus chelation therapy only on iron overload in children and young adults with transfusion-dependent thalassemia: A randomized double-blind placebo-controlled trial. *Pediatr Blood Cancer*. 2022;69(6):e29564.
200. Eide D, Broderius M, Fett J, Guerinot ML. A novel iron-regulated metal transporter from plants identified by functional expression in yeast. *Proceedings of the National Academy of Sciences*. 1996;93(11):5624-5628.
201. Taylor KM, Morgan HE, Smart K, et al. The Emerging Role of the LIV-1 Subfamily of Zinc Transporters in Breast Cancer. *Mol Med*. 2007;13(7-8):396-406.
202. Peters JL, Dufner-Beattie J, Xu W, et al. Targeting of the mouse Slc39a2 (Zip2) gene reveals highly cell-specific patterns of expression, and unique functions in zinc, iron, and calcium homeostasis. *Genesis*. 2007;45(6):339-352.
203. Zhang W, Knutson M. Iron transport ability of the Slc39a (ZIP) family of metal-ion transporters. *The FASEB Journal*. 2012;26(S1):641.624-641.624.
204. Franz MC, Pujol-Giménez J, Montalbetti N, et al. Reassessment of the Transport Mechanism of the Human Zinc Transporter SLC39A2. *Biochemistry*. 2018;57(26):3976-3986.
205. Taylor KM, Morgan HE, Johnson A, Nicholson RI. Structure–function analysis of a novel member of the LIV-1 subfamily of zinc transporters, ZIP14. *FEBS Lett*. 2005;579(2):427-432.
206. Liuzzi JP, Aydemir F, Nam H, Knutson MD, Cousins RJ. Zip14 (Slc39a14) mediates non-transferrin-bound iron uptake into cells. *Proceedings of the National Academy of Sciences*. 2006;103(37):13612-13617.
207. Pinilla-Tenas JJ, Sparkman BK, Shawki A, et al. Zip14 is a complex broad-scope metal-ion transporter whose functional properties support roles in the cellular uptake of zinc and nontransferrin-bound iron. *American Journal of Physiology-Cell Physiology*. 2011;301(4):C862-C871.
208. Bonilla S, Prozialeck JD, Malladi P, et al. Neonatal iron overload and tissue siderosis due to gestational alloimmune liver disease. *J Hepatol*. 2012;56(6):1351-1355.
209. Nam H, Knutson MD. Effect of dietary iron deficiency and overload on the expression of ZIP metal-ion transporters in rat liver. *Biometals*. 2012;25(1):115-124.
210. Zhao N, Zhang A-S, Worthen C, Knutson MD, Enns CA. An iron-regulated and glycosylation-dependent proteasomal degradation pathway for the plasma membrane metal transporter ZIP14. *Proceedings of the National Academy of Sciences*. 2014;111(25):9175-9180.
211. Hojyo S, Fukada T, Shimoda S, et al. The Zinc Transporter SLC39A14/ZIP14 Controls G-Protein Coupled Receptor-Mediated Signaling Required for Systemic Growth. *PLoS One*. 2011;6(3):e18059.
212. Jenkitkasemwong S, Wang C-Y, Coffey R, et al. SLC39A14 Is Required for the Development of Hepatocellular Iron Overload in Murine Models of Hereditary Hemochromatosis. *Cell Metab*. 2015;22(1):138-150.

213. Wang C-Y, Jenkitkasemwong S, Duarte S, et al. ZIP8 Is an Iron and Zinc Transporter Whose Cell-surface Expression Is Up-regulated by Cellular Iron Loading. *J Biol Chem*. 2012;287(41):34032-34043.
214. Lin W, Vann DR, Doulias P-T, et al. Hepatic metal ion transporter ZIP8 regulates manganese homeostasis and manganese-dependent enzyme activity. *J Clin Invest*. 2017;127(6):2407-2417.
215. Wang B, He L, Dong H, Dalton TP, Nebert DW. Generation of a Slc39a8 hypomorph mouse: Markedly decreased ZIP8 Zn2+/(HCO3-)2 transporter expression. *Biochemical and Biophysical Research Communications*. 2011;410(2):289-294.
216. Gálvez-Peralta M, He L, Jorge-Nebert LF, et al. ZIP8 Zinc Transporter: Indispensable Role for Both Multiple-Organ Organogenesis and Hematopoiesis In Utero. *PLoS One*. 2012;7(5):e36055.
217. Park CH, Valore EV, Waring AJ, Ganz T. Hepcidin, a Urinary Antimicrobial Peptide Synthesized in the Liver. *J Biol Chem*. 2001;276(11):7806-7810.
218. Krause A, Neitz S, Mägert H-J, et al. LEAP-1, a novel highly disulfide-bonded human peptide, exhibits antimicrobial activity. *FEBS Lett*. 2000;480(2-3):147-150.
219. Cocciolillo S, Sebastiani G, Blostein M, Pantopoulos K. Chapter 18: Liver Hormones. In: Litwack G, ed. Hormonal Signaling in Biology and Medicine: Comprehensive Modern Endocrinology: Academic Press; 2020:425-444.
220. Pigeon C, Ilyin G, Courselaud B, et al. A New Mouse Liver-specific Gene, Encoding a Protein Homologous to Human Antimicrobial Peptide Hepcidin, Is Overexpressed during Iron Overload. *J Biol Chem*. 2001;276(11):7811-7819.
221. Nicolas G, Bennoun M, Devaux I, et al. Lack of hepcidin gene expression and severe tissue iron overload in upstream stimulatory factor 2 (USF2) knockout mice. *Proceedings of the National Academy of Sciences*. 2001;98(15):8780-8785.
222. Nicolas G, Bennoun M, Porteu A, et al. Severe iron deficiency anemia in transgenic mice expressing liver hepcidin. *Proceedings of the National Academy of Sciences*. 2002;99(7):4596-4601.
223. Roetto A, Papanikolaou G, Politou M, et al. Mutant antimicrobial peptide hepcidin is associated with severe juvenile hemochromatosis. *Nat Genet*. 2003;33(1):21-22.
224. Lou D-Q, Nicolas Gl, Lesbordes J-C, et al. Functional differences between hepcidin 1 and 2 in transgenic mice. *Blood*. 2004;103(7):2816-2821.
225. Preza GC, Ruchala P, Pinon R, et al. Minihepcidins are rationally designed small peptides that mimic hepcidin activity in mice and may be useful for the treatment of iron overload. *J Clin Invest*. 2011;121(12):4880-4888.
226. Nemeth E, Tuttle MS, Powelson J, et al. Hepcidin regulates cellular iron efflux by binding to ferroportin and inducing its internalization. *Science*. 2004;306(5704):2090-2093.
227. Billesbølle CB, Azumaya CM, Kretsch RC, et al. Structure of hepcidin-bound ferroportin reveals iron homeostatic mechanisms. *Nature*. 2020.
228. Qiao B, Sugianto P, Fung E, et al. Hepcidin-induced endocytosis of ferroportin is dependent on ferroportin ubiquitination. *Cell Metab*. 2012;15(6):918-924.
229. De Domenico I, Ward DM, Di Patti MCB, et al. Ferroxidase activity is required for the stability of cell surface ferroportin in cells expressing GPI-ceruloplasmin. *The EMBO Journal*. 2007;26(12):2823-2831.
230. Jiang L, Wang J, Wang K, et al. RNF217 regulates iron homeostasis through its E3 ubiquitin ligase activity by modulating ferroportin degradation. *Blood*. 2021.

231. Donovan A, Lima CA, Pinkus JL, et al. The iron exporter ferroportin/Slc40a1 is essential for iron homeostasis. *Cell Metab*. 2005;1(3):191-200.
232. Knutson MD, Oukka M, Koss LM, Aydemir F, Wessling-Resnick M. Iron release from macrophages after erythrophagocytosis is up-regulated by ferroportin 1 overexpression and down-regulated by hepcidin. *Proceedings of the National Academy of Sciences*. 2005;102(5):1324-1328.
233. Delaby C, Pilard N, Gonçalves AS, Beaumont C, Canonne-Hergaux Fo. Presence of the iron exporter ferroportin at the plasma membrane of macrophages is enhanced by iron loading and down-regulated by hepcidin. *Blood*. 2005;106(12):3979-3984.
234. Nicolas G, Chauvet C, Viatte L, et al. The gene encoding the iron regulatory peptide hepcidin is regulated by anemia, hypoxia, and inflammation. *J Clin Invest*. 2002;110(7):1037-1044.
235. Shike H, Lauth X, Westerman ME, et al. Bass hepcidin is a novel antimicrobial peptide induced by bacterial challenge. *Eur J Biochem*. 2002;269(8):2232-2237.
236. Weiss G, Ganz T, Goodnough LT. Anemia of inflammation. *Blood*. 2019;133(1):40-50.
237. Weinstein DA, Roy CN, Fleming MD, Loda MF, Wolfsdorf JI, Andrews NC. Inappropriate expression of hepcidin is associated with iron refractory anemia: implications for the anemia of chronic disease. *Blood*. 2002;100(10):3776-3781.
238. Roy CN, Mak HH, Akpan I, Losyev G, Zurakowski D, Andrews NC. Hepcidin antimicrobial peptide transgenic mice exhibit features of the anemia of inflammation. *Blood*. 2007;109(9):4038-4044.
239. Sasu BJ, Cooke KS, Arvedson TL, et al. Antihepcidin antibody treatment modulates iron metabolism and is effective in a mouse model of inflammation-induced anemia. *Blood*. 2010;115(17):3616-3624.
240. Gardenghi S, Renaud TM, Meloni A, et al. Distinct roles for hepcidin and interleukin-6 in the recovery from anemia in mice injected with heat-killed Brucella abortus. *Blood*. 2014;123(8):1137-1145.
241. Kim A, Fung E, Parikh SG, et al. A mouse model of anemia of inflammation: complex pathogenesis with partial dependence on hepcidin. *Blood*. 2014;123(8):1129-1136.
242. Nemeth E, Valore EV, Territo M, Schiller G, Lichtenstein A, Ganz T. Hepcidin, a putative mediator of anemia of inflammation, is a type II acute-phase protein. *Blood*. 2003;101(7):2461-2463.
243. Lee P, Peng H, Gelbart T, Wang L, Beutler E. Regulation of hepcidin transcription by interleukin-1 and interleukin-6. *Proceedings of the National Academy of Sciences*. 2005;102(6):1906-1910.
244. Inamura J, Ikuta K, Jimbo J, et al. Upregulation of hepcidin by interleukin-1β in human hepatoma cell lines. *Hepatol Res*. 2005;33(3):198-205.
245. Armitage AE, Eddowes LA, Gileadi U, et al. Hepcidin regulation by innate immune and infectious stimuli. *Blood*. 2011;118(15):4129-4139.
246. Silva I, Peccerella T, Mueller S, Rausch V. IL-1 beta-mediated macrophage-hepatocyte crosstalk upregulates hepcidin under physiological low oxygen levels. *Redox Biology*. 2019;24:101209.
247. Smith CL, Arvedson TL, Cooke KS, et al. IL-22 Regulates Iron Availability In Vivo through the Induction of Hepcidin. *The Journal of Immunology*. 2013;191(4):1845-1855.
248. Wallace DF, Subramaniam VN. Analysis of IL-22 contribution to hepcidin induction and hypoferremia during the response to LPS in vivo. *Int Immunol*. 2015;27(6):281-287.

249. Nemeth E, Rivera S, Gabayan V, et al. IL-6 mediates hypoferremia of inflammation by inducing the synthesis of the iron regulatory hormone hepcidin. *J Clin Invest*. 2004;113(9):1271-1276.
250. Rodriguez R, Jung C-L, Gabayan V, et al. Hepcidin Induction by Pathogens and Pathogen-Derived Molecules Is Strongly Dependent on Interleukin-6. *Infection and Immunity*. 2014;82(2):745-752.
251. Wrighting DM, Andrews NC. Interleukin-6 induces hepcidin expression through STAT3. *Blood*. 2006;108(9):3204-3209.
252. Verga Falzacappa MV, Vujic Spasic M, Kessler R, Stolte J, Hentze MW, Muckenthaler MU. STAT3 mediates hepatic hepcidin expression and its inflammatory stimulation. *Blood*. 2007;109(1):353-358.
253. Pietrangelo A, Dierssen U, Valli L, et al. STAT3 is required for IL-6-gp130-dependent activation of hepcidin in vivo. *Gastroenterology*. 2007;132(1):294-300.
254. Ryan JD, Altamura S, Devitt E, et al. Pegylated interferon-α induced hypoferremia is associated with the immediate response to treatment in hepatitis C. *Hepatology*. 2012;56(2):492-500.
255. Zhang X, Rovin BH. Hepcidin expression by human monocytes in response to adhesion and pro-inflammatory cytokines. *Biochimica et Biophysica Acta (BBA) - General Subjects*. 2010;1800(12):1262-1267.
256. Bartolomei G, Cevik RE, Marcello A. Modulation of hepatitis C virus replication by iron and hepcidin in Huh7 hepatocytes. *J Gen Virol*. 2011;92(9):2072-2081.
257. Feder JN, Gnirke A, Thomas W, et al. A novel MHC class I–like gene is mutated in patients with hereditary haemochromatosis. *Nat Genet*. 1996;13(4):399-408.
258. Jouanolle AM, Fergelot P, Gandon G, Yaouanq J, Gall JYL, David V. A candidate gene for hemochromatosis: frequency of the C282Y and H63D mutations. *Hum Genet*. 1997;100(5):544-547.
259. Frazer DM, Vulpe CD, McKie AT, et al. Cloning and gastrointestinal expression of rat hephaestin: relationship to other iron transport proteins. *American Journal of Physiology-Gastrointestinal and Liver Physiology*. 2001;281(4):G931-G939.
260. de Sousa M, Reimão R, Lacerda R, Hugo P, Kaufmann SHE, Porto G. Iron overload in β2-microglobulin-deficient mice. *Immunol Lett*. 1994;39(2):105-111.
261. Santos M, Schilham MW, Rademakers LH, Marx JJ, de Sousa M, Clevers H. Defective iron homeostasis in beta 2-microglobulin knockout mice recapitulates hereditary hemochromatosis in man. *J Exp Med*. 1996;184(5):1975-1985.
262. Bridle KR, Frazer DM, Wilkins SJ, et al. Disrupted hepcidin regulation in HFE-associated haemochromatosis and the liver as a regulator of body iron homoeostasis. *The Lancet*. 2003;361(9358):669-673.
263. Jouanolle AM, Gandon G, Jézéquel P, et al. Haemochromatosis and HLA–H. *Nat Genet*. 1996;14(3):251-252.
264. Jazwinska EC, Cullen LM, Busfield F, et al. Haemochromatosis and HLA–H. *Nat Genet*. 1996;14(3):249-251.
265. Ahmad KA, Ahmann JR, Migas MC, et al. Decreased Liver Hepcidin Expression in the Hfe Knockout Mouse. *Blood Cells Mol Dis*. 2002;29(3):361-366.
266. Bennett MJ, Lebrón JA, Bjorkman PJ. Crystal structure of the hereditary haemochromatosis protein HFE complexed with transferrin receptor. *Nature*. 2000;403(6765):46-53.

267. Parkkila S, Waheed A, Britton RS, et al. Association of the transferrin receptor in human placenta with HFE, the protein defective in hereditary hemochromatosis. *Proceedings of the National Academy of Sciences*. 1997;94(24):13198-13202.
268. Feder JN, Penny DM, Irrinki A, et al. The hemochromatosis gene product complexes with the transferrin receptor and lowers its affinity for ligand binding. *Proceedings of the National Academy of Sciences*. 1998;95(4):1472-1477.
269. Gross CN, Irrinki A, Feder JN, Enns CA. Co-trafficking of HFE, a Nonclassical Major Histocompatibility Complex Class I Protein, with the Transferrin Receptor Implies a Role in Intracellular Iron Regulation. *J Biol Chem*. 1998;273(34):22068-22074.
270. Parkkila S, Waheed A, Britton RS, et al. Immunohistochemistry of HLA-H, the protein defective in patients with hereditary hemochromatosis, reveals unique pattern of expression in gastrointestinal tract. *Proceedings of the National Academy of Sciences*. 1997;94(6):2534-2539.
271. Papanikolaou G, Samuels ME, Ludwig EH, et al. Mutations in HFE2 cause iron overload in chromosome 1q–linked juvenile hemochromatosis. *Nat Genet*. 2004;36(1):77-82.
272. Lanzara C, Roetto A, Daraio F, et al. Spectrum of hemojuvelin gene mutations in 1q-linked juvenile hemochromatosis. *Blood*. 2004;103(11):4317-4321.
273. Lee PL, Beutler E, Rao SV, Barton JC. Genetic abnormalities and juvenile hemochromatosis: mutations of the HJV gene encoding hemojuvelin. *Blood*. 2004;103(12):4669-4671.
274. Huang FW, Rubio-Aliaga I, Kushner JP, Andrews NC, Fleming MD. Identification of a novel mutation (C321X) in HJV. *Blood*. 2004;104(7):2176-2177.
275. Monnier PP, Sierra A, Macchi P, et al. RGM is a repulsive guidance molecule for retinal axons. *Nature*. 2002;419(6905):392-395.
276. Rodriguez Martinez A, Niemelä O, Parkkila S. Hepatic and extrahepatic expression of the new iron regulatory protein hemojuvelin. *Haematologica*. 2004;89(12):1441-1445.
277. Huang FW, Pinkus JL, Pinkus GS, Fleming MD, Andrews NC. A mouse model of juvenile hemochromatosis. *J Clin Invest*. 2005;115(8):2187-2191.
278. Niederkofler V. Hemojuvelin is essential for dietary iron sensing, and its mutation leads to severe iron overload. *J Clin Invest*. 2005;115(8):2180-2186.
279. Samad TA, Srinivasan A, Karchewski LA, et al. DRAGON: A Member of the Repulsive Guidance Molecule-Related Family of Neuronal- and Muscle-Expressed Membrane Proteins Is Regulated by DRG11 and Has Neuronal Adhesive Properties. *The Journal of Neuroscience*. 2004;24(8):2027-2036.
280. Zhang A-S, West AP, Wyman AE, Bjorkman PJ, Enns CA. Interaction of Hemojuvelin with Neogenin Results in Iron Accumulation in Human Embryonic Kidney 293 Cells*. *J Biol Chem*. 2005;280(40):33885-33894.
281. Lin L, Goldberg YP, Ganz T. Competitive regulation of hepcidin mRNA by soluble and cell-associated hemojuvelin. *Blood*. 2005;106(8):2884-2889.
282. Niederkofler V, Salie R, Sigrist M, Arber S. Repulsive Guidance Molecule (RGM) Gene Function Is Required for Neural Tube Closure But Not Retinal Topography in the Mouse Visual System. *The Journal of Neuroscience*. 2004;24(4):808-818.
283. Samad TA, Rebbapragada A, Bell E, et al. DRAGON, a Bone Morphogenetic Protein Co-receptor. *J Biol Chem*. 2005;280(14):14122-14129.

284. Babitt JL, Zhang Y, Samad TA, et al. Repulsive Guidance Molecule (RGMa), a DRAGON Homologue, Is a Bone Morphogenetic Protein Co-receptor. *J Biol Chem*. 2005;280(33):29820-29827.
285. Joyce ME, Roberts AB, Sporn MB, Bolander ME. Transforming growth factor-beta and the initiation of chondrogenesis and osteogenesis in the rat femur. *J Cell Biol*. 1990;110(6):2195-2207.
286. Shi Y, Massagué J. Mechanisms of TGF-β Signaling from Cell Membrane to the Nucleus. *Cell*. 2003;113(6):685-700.
287. Wang R-H, Li C, Xu X, et al. A role of SMAD4 in iron metabolism through the positive regulation of hepcidin expression. *Cell Metab*. 2005;2(6):399-409.
288. Babitt JL, Huang FW, Wrighting DM, et al. Bone morphogenetic protein signaling by hemojuvelin regulates hepcidin expression. *Nat Genet*. 2006;38(5):531-539.
289. Kautz L, Meynard D, Monnier A, et al. Iron regulates phosphorylation of Smad1/5/8 and gene expression of Bmp6, Smad7, Id1, and Atoh8 in the mouse liver. *Blood*. 2008;112(4):1503-1509.
290. Andriopoulos B, Jr., Corradini E, Xia Y, et al. BMP6 is a key endogenous regulator of hepcidin expression and iron metabolism. *Nat Genet*. 2009;41(4):482-487.
291. Meynard D, Kautz L, Darnaud V, Canonne-Hergaux F, Coppin H, Roth M-P. Lack of the bone morphogenetic protein BMP6 induces massive iron overload. *Nat Genet*. 2009;41(4):478-481.
292. Steinbicker AU, Bartnikas TB, Lohmeyer LK, et al. Perturbation of hepcidin expression by BMP type I receptor deletion induces iron overload in mice. *Blood*. 2011;118(15):4224-4230.
293. Mayeur C, Leyton PA, Kolodziej SA, Yu B, Bloch KD. BMP type II receptors have redundant roles in the regulation of hepatic hepcidin gene expression and iron metabolism. *Blood*. 2014;124(13):2116-2123.
294. Canali S, Zumbrennen-Bullough KB, Core AB, et al. Endothelial cells produce bone morphogenetic protein 6 required for iron homeostasis in mice. *Blood*. 2017;129(4):405-414.
295. Rausa M, Pagani A, Nai A, et al. Bmp6 Expression in Murine Liver Non Parenchymal Cells: A Mechanism to Control their High Iron Exporter Activity and Protect Hepatocytes from Iron Overload? *PLoS One*. 2015;10(4):e0122696.
296. Géraud C, Schledzewski K, Demory A, et al. Liver sinusoidal endothelium: A microenvironment-dependent differentiation program in rat including the novel junctional protein liver endothelial differentiation-associated protein-1. *Hepatology*. 2010;52(1):313-326.
297. Daniel, Ginsberg M, Israely E, et al. Molecular Signatures of Tissue-Specific Microvascular Endothelial Cell Heterogeneity in Organ Maintenance and Regeneration. *Dev Cell*. 2013;26(2):204-219.
298. Latour C, Besson-Fournier C, Meynard D, et al. Differing impact of the deletion of hemochromatosis-associated molecules HFE and transferrin receptor-2 on the iron phenotype of mice lacking bone morphogenetic protein 6 or hemojuvelin. *Hepatology*. 2016;63(1):126-137.
299. Koch P-S, Olsavszky V, Ulbrich F, et al. Angiocrine Bmp2 signaling in murine liver controls normal iron homeostasis. *Blood*. 2017;129(4):415-419.

300. Canali S, Wang C-Y, Zumbrennen-Bullough KB, Bayer A, Babitt JL. Bone morphogenetic protein 2 controls iron homeostasis in mice independent of Bmp6. *Am J Hematol*. 2017;92(11):1204-1213.
301. Radio FC, Majore S, Aurizi C, et al. Hereditary hemochromatosis type 1 phenotype modifiers in Italian patients. The controversial role of variants in HAMP, BMP2, FTL and SLC40A1 genes. *Blood Cells Mol Dis*. 2015;55(1):71-75.
302. Milet J, Le Gac G, Scotet V, et al. A common SNP near BMP2 is associated with severity of the iron burden in HFE p.C282Y homozygous patients: A follow-up study. *Blood Cells Mol Dis*. 2010;44(1):34-37.
303. Xiao X, Dev S, Canali S, et al. Endothelial Bone Morphogenetic Protein 2 (Bmp2) Knockout Exacerbates Hemochromatosis in Homeostatic Iron Regulator (Hfe) Knockout Mice but not Bmp6 Knockout Mice. *Hepatology*. 2020.
304. Lim PJ, Duarte TL, Arezes J, et al. Nrf2 controls iron homoeostasis in haemochromatosis and thalassaemia via Bmp6 and hepcidin. *Nature Metabolism*. 2019;1(5):519-531.
305. Ma S, Paiboonrungruan C, Yan T, Williams KP, Major MB, Chen XL. Targeted therapy of esophageal squamous cell carcinoma: the NRF2 signaling pathway as target. *Ann N Y Acad Sci*. 2018;1434(1):164-172.
306. Rai D, Tripathi AK, Sardar A, et al. A novel BMP2 secretagogue ameliorates glucocorticoid induced oxidative stress in osteoblasts by activating NRF2 dependent survival while promoting Wnt/β-catenin mediated osteogenesis. *Free Radical Biology and Medicine*. 2022;190:124-147.
307. Jiang M, Ku W-Y, Zhou Z, et al. BMP-driven NRF2 activation in esophageal basal cell differentiation and eosinophilic esophagitis. *The Journal of Clinical Investigation*. 2015;125(4):1557-1568.
308. Corradini E, Garuti C, Montosi G, et al. Bone Morphogenetic Protein Signaling Is Impaired in an Hfe Knockout Mouse Model of Hemochromatosis. *Gastroenterology*. 2009;137(4):1489-1497.
309. Corradini E, Rozier M, Meynard D, et al. Iron Regulation of Hepcidin Despite Attenuated Smad1,5,8 Signaling in Mice Without Transferrin Receptor 2 or Hfe. *Gastroenterology*. 2011;141(5):1907-1914.
310. Wallace DF, Summerville L, Crampton EM, Frazer DM, Anderson GJ, Subramaniam VN. Combined deletion of Hfe and transferrin receptor 2 in mice leads to marked dysregulation of hepcidin and iron overload. *Hepatology*. 2009;50(6):1992-2000.
311. Bolondi G, Garuti C, Corradini E, et al. Altered hepatic BMP signaling pathway in human HFE hemochromatosis. *Blood Cells Mol Dis*. 2010;45(4):308-312.
312. Ryan JD, Ryan E, Fabre A, Lawless MW, Crowe J. Defective bone morphogenic protein signaling underlies hepcidin deficiency in HFE hereditary hemochromatosis. *Hepatology*. 2010;52(4):1266-1273.
313. Corradini E, Schmidt PJ, Meynard D, et al. BMP6 Treatment Compensates for the Molecular Defect and Ameliorates Hemochromatosis in Hfe Knockout Mice. *Gastroenterology*. 2010;139(5):1721-1729.
314. Wu X-g, Wang Y, Wu Q, et al. HFE interacts with the BMP type I receptor ALK3 to regulate hepcidin expression. *Blood*. 2014;124(8):1335-1343.
315. Fillebeen C, Charlebois E, Wagner J, et al. Transferrin receptor 1 controls systemic iron homeostasis by fine-tuning hepcidin expression to hepatocellular iron load. *Blood*. 2019.

316. Chen J, Chloupková M, Gao J, Chapman-Arvedson TL, Enns CA. HFE Modulates Transferrin Receptor 2 Levels in Hepatoma Cells via Interactions That Differ from Transferrin Receptor 1-HFE Interactions. *J Biol Chem*. 2007;282(51):36862-36870.
317. Goswami T, Andrews NC. Hereditary Hemochromatosis Protein, HFE, Interaction with Transferrin Receptor 2 Suggests a Molecular Mechanism for Mammalian Iron Sensing. *J Biol Chem*. 2006;281(39):28494-28498.
318. Gao J, Chen J, Kramer M, Tsukamoto H, Zhang A-S, Enns CA. Interaction of the Hereditary Hemochromatosis Protein HFE with Transferrin Receptor 2 Is Required for Transferrin-Induced Hepcidin Expression. *Cell Metab*. 2009;9(3):217-227.
319. D'Alessio F, Hentze MW, Muckenthaler MU. The hemochromatosis proteins HFE, TfR2, and HJV form a membrane-associated protein complex for hepcidin regulation. 2012;57(5):1052-1060.
320. Gao J, Chen J, De Domenico I, et al. Hepatocyte-targeted HFE and TFR2 control hepcidin expression in mice. *Blood*. 2010;115(16):3374-3381.
321. Pietrangelo A, Caleffi A, Henrion J, et al. Juvenile hemochromatosis associated with pathogenic mutations of adult hemochromatosis genes. *Gastroenterology*. 2005;128(2):470-479.
322. Kautz L, Jung G, Valore EV, Rivella S, Nemeth E, Ganz T. Identification of erythroferrone as an erythroid regulator of iron metabolism. *Nat Genet*. 2014;46(7):678-684.
323. Kautz L, Jung G, Du X, et al. Erythroferrone contributes to hepcidin suppression and iron overload in a mouse model of β-thalassemia. *Blood*. 2015;126(17):2031-2037.
324. Arezes J, Foy N, McHugh K, et al. Erythroferrone inhibits the induction of hepcidin by BMP6. *Blood*. 2018;132(14):1473-1477.
325. Wang C-Y, Xu Y, Traeger L, et al. Erythroferrone lowers hepcidin by sequestering BMP2/6 heterodimer from binding to the BMP type I receptor ALK3. *Blood*. 2020;135(6):453-456.
326. Silvestri L, Pagani A, Nai A, De Domenico I, Kaplan J, Camaschella C. The Serine Protease Matriptase-2 (TMPRSS6) Inhibits Hepcidin Activation by Cleaving Membrane Hemojuvelin. *Cell Metab*. 2008;8(6):502-511.
327. Finberg KE, Heeney MM, Campagna DR, et al. Mutations in TMPRSS6 cause iron-refractory iron deficiency anemia (IRIDA). *Nat Genet*. 2008;40(5):569-571.
328. Du X, She E, Gelbart T, et al. The Serine Protease TMPRSS6 Is Required to Sense Iron Deficiency. *Science*. 2008;320(5879):1088-1092.
329. Folgueras AR, de Lara FM, Pendás AM, et al. Membrane-bound serine protease matriptase-2 (Tmprss6) is an essential regulator of iron homeostasis. *Blood*. 2008;112(6):2539-2545.
330. Zhang A-S, Anderson SA, Wang J, et al. Suppression of hepatic hepcidin expression in response to acute iron deprivation is associated with an increase of matriptase-2 protein. *Blood*. 2011;117(5):1687-1699.
331. Zhao N, Nizzi CP, Anderson SA, et al. Low Intracellular Iron Increases the Stability of Matriptase-2. *J Biol Chem*. 2015;290(7):4432-4446.
332. Lenoir A, Deschemin J-C, Kautz L, et al. Iron-deficiency anemia from matriptase-2 inactivation is dependent on the presence of functional Bmp6. *Blood*. 2011;117(2):647-650.
333. Lee P, Hsu M-H, Welser-Alves J, Peng H. Severe microcytic anemia but increased erythropoiesis in mice lacking Hfe or Tfr2 and Tmprss6. *Blood Cells Mol Dis*. 2012;48(3):173-178.

334. Finberg KE, Whittlesey RL, Fleming MD, Andrews NC. Down-regulation of Bmp/Smad signaling by Tmprss6 is required for maintenance of systemic iron homeostasis. *Blood*. 2010;115(18):3817-3826.
335. Wahedi M, Wortham AM, Kleven MD, et al. Matriptase-2 suppresses hepcidin expression by cleaving multiple components of the hepcidin induction pathway. *J Biol Chem*. 2017;292(44):18354-18371.
336. Enns CA, Jue S, Zhang A-S. The Ectodomain of Matriptase-2 Plays an Important Non-Proteolytic Role in Suppressing Hepcidin Expression in Mice. *Blood*. 2020.
337. De Falco L, Silvestri L, Kannengiesser C, et al. Functional and Clinical Impact of Novel Tmprss6 Variants in Iron-Refractory Iron-Deficiency Anemia Patients and Genotype–Phenotype Studies. *Hum Mutat*. 2014;35(11):1321-1329.
338. McDonald CJ, Ostini L, Bennett N, et al. Functional analysis of matriptase-2 mutations and domains: insights into the molecular basis of iron-refractory iron deficiency anemia. *American Journal of Physiology-Cell Physiology*. 2015;308(7):C539-C547.
339. Lee D-H, Zhou L-J, Zhou Z, et al. Neogenin inhibits HJV secretion and regulates BMP-induced hepcidin expression and iron homeostasis. *Blood*. 2010;115(15):3136-3145.
340. Enns CA, Jue S, Zhang A-S. Hepatocyte neogenin is required for hemojuvelin-mediated hepcidin expression and iron homeostasis in mice. *Blood*. 2021;138(6):486-499.
341. Healey EG, Bishop B, Elegheert J, Bell CH, Padilla-Parra S, Siebold C. Repulsive guidance molecule is a structural bridge between neogenin and bone morphogenetic protein. *Nat Struct Mol Biol*. 2015;22(6):458-465.
342. Zhao N, Maxson JE, Zhang RH, Wahedi M, Enns CA, Zhang A-S. Neogenin Facilitates the Induction of Hepcidin Expression by Hemojuvelin in the Liver. *J Biol Chem*. 2016;291(23):12322-12335.
343. Corradini E, Meynard D, Wu Q, et al. Serum and liver iron differently regulate the bone morphogenetic protein 6 (BMP6)-SMAD signaling pathway in mice. 2011;54(1):273-284.
344. Besson-Fournier C, Gineste A, Latour C, et al. Hepcidin upregulation by inflammation is independent of Smad1/5/8 signaling by activin B. *Blood*. 2017;129(4):533-536.
345. Besson-Fournier C, Latour C, Kautz L, et al. Induction of activin B by inflammatory stimuli up-regulates expression of the iron-regulatory peptide hepcidin through Smad1/5/8 signaling. *Blood*. 2012;120(2):431-439.
346. Canali S, Core AB, Zumbrennen-Bullough KB, et al. Activin B Induces Noncanonical SMAD1/5/8 Signaling via BMP Type I Receptors in Hepatocytes: Evidence for a Role in Hepcidin Induction by Inflammation in Male Mice. *Endocrinology*. 2016;157(3):1146-1162.
347. Casanovas G, Mleczko-Sanecka K, Altamura S, Hentze MW, Muckenthaler MU. Bone morphogenetic protein (BMP)-responsive elements located in the proximal and distal hepcidin promoter are critical for its response to HJV/BMP/SMAD. *J Mol Med*. 2009;87(5):471-480.
348. Mayeur C, Lohmeyer LK, Leyton P, et al. The type I BMP receptor Alk3 is required for the induction of hepatic hepcidin gene expression by interleukin-6. *Blood*. 2014;123(14):2261-2268.
349. Wang C-Y, Xiao X, Bayer A, et al. Ablation of Hepatocyte Smad1, Smad5, and Smad8 Causes Severe Tissue Iron Loading and Liver Fibrosis in Mice. *Hepatology*. 2019;70(6):1986-2002.

350. Latour C, Besson-Fournier C, Gourbeyre O, Meynard D, Roth MP, Coppin H. Deletion of BMP6 worsens the phenotype of HJV-deficient mice and attenuates hepcidin levels reached after LPS challenge. *Blood*. 2017;130(21):2339-2343.
351. Wang CY, Canali S, Bayer A, Dev S, Agarwal A, Babitt JL. Iron, erythropoietin, and inflammation regulate hepcidin in Bmp2 -deficient mice, but serum iron fails to induce hepcidin in Bmp6 -deficient mice. *Am J Hematol*. 2018.
352. Fillebeen C, Wilkinson N, Charlebois E, Katsarou A, Wagner J, Pantopoulos K. Hepcidin-mediated hypoferremic response to acute inflammation requires a threshold of Bmp6/Hjv/Smad signaling. *Blood*. 2018;132(17):1829-1841.
353. Charlebois E, Pantopoulos K. Iron overload inhibits BMP/SMAD and IL-6/STAT3 signaling to hepcidin in cultured hepatocytes. *PLoS One*. 2021;16(6):e0253475.
354. Ahmed ST, Ivashkiv LB. Inhibition of IL-6 and IL-10 Signaling and Stat Activation by Inflammatory and Stress Pathways. *The Journal of Immunology*. 2000;165(9):5227-5237.
355. Chen L, Ma B, Liu X, Hao Y, Yang X, Liu M. H2O2 induces oxidative stress damage through the BMP-6/SMAD/hepcidin axis. *Development, Growth & Differentiation*. 2020;62(2):139-146.
356. Burza S, Croft SL, Boelaert M. Leishmaniasis. *The Lancet*. 2018;392(10151):951-970.
357. Adler S, Ber M. Transmission of Leishmania tropica by the Bite of Phlebotomus papatasii. *Nature*. 1941;148(3747):227-227.
358. Shortt HE, Smith ROA, Swaminath CS, Krishnan KV. Transmission of Indian Kala-Azar by the Bite of Phebotomus argentipes. *Indian J Med Res*. 1931;18(4):1373-1375 pp.
359. Coelho MDV, Falcao AR. Experimental Transmission of Leishmania braziliensis. I. Transmission by Inoculation of Triturated Phlebotomus longipalpis Infected Experimentally. *Rev Inst Med Trop Sao Paulo*. 1962;4(3):159-162.
360. Pearson RD, Sousa AdQ. Clinical Spectrum of Leishmaniasis. *Clin Infect Dis*. 1996;22(1):1-13.
361. Saravolatz LD, Bern C, Adler-Moore J, et al. Liposomal Amphotericin B for the Treatment of Visceral Leishmaniasis. *Clin Infect Dis*. 2006;43(7):917-924.
362. Berman J. Miltefosine to treat leishmaniasis. *Expert Opin Pharmacother*. 2005;6(8):1381-1388.
363. den Boer M, Davidson RN. Treatment options for visceral leishmaniasis. *Expert Rev Anti Infect Ther*. 2006;4(2):187-197.
364. Pérez-Victoria FJ, Sánchez-Cañete MP, Seifert K, et al. Mechanisms of experimental resistance of Leishmania to miltefosine: Implications for clinical use. *Drug Resistance Updates*. 2006;9(1):26-39.
365. Ghorbani M, Farhoudi R. Leishmaniasis in humans: drug or vaccine therapy? *Drug Des Devel Ther*. 2017;Volume 12:25-40.
366. Olivier M, Minguez-Menendez A, Fernandez-Prada C. Leishmania Viannia guyanensis. *Trends Parasitol*. 2019;35(12):1018-1019.
367. Laskay T, van Zandbergen G, Solbach W. Neutrophil granulocytes as host cells and transport vehicles for intracellular pathogens: Apoptosis as infection-promoting factor. *Immunobiology*. 2008;213(3):183-191.
368. Van Zandbergen G, Klinger M, Mueller A, et al. Cutting Edge: Neutrophil Granulocyte Serves as a Vector for *Leishmania* Entry into Macrophages. *The Journal of Immunology*. 2004;173(11):6521-6525.

369. Peters NC, Egen JG, Secundino N, et al. In Vivo Imaging Reveals an Essential Role for Neutrophils in Leishmaniasis Transmitted by Sand Flies. *Science*. 2008;321(5891):970-974.
370. Galvao-Quintao L, Alfieri SC, Ryter A, Rabinovitch M. Intracellular differentiation of Leishmania amazonensis promastigotes to amastigotes: presence of megasomes, cysteine proteinase activity and susceptibility to leucine-methyl ester. *Parasitology*. 1990;101(1):7-13.
371. Courret N, Frehel C, Prina E, Lang T, Antoine JC. Kinetics of the intracellular differentiation of Leishmania amazonensis and internalization of host MHC molecules by the intermediate parasite stages. *Parasitology*. 2001;122(3):263-279.
372. Courret N, FréHel C, Gouhier N, et al. Biogenesis of *Leishmania*-harbouring parasitophorous vacuoles following phagocytosis of the metacyclic promastigote or amastigote stages of the parasites. *J Cell Sci*. 2002;115(11):2303-2316.
373. Castro R, Scott K, Jordan T, et al. The ultrastructure of the parasitophorous vacuole formed by *Leishmania Major*. *J Parasitol*. 2006;92(6):1162-1170.
374. Antoine J-C, Prina E, Lang T, Courret N. The biogenesis and properties of the parasitophorous vacuoles that harbour Leishmania in murine macrophages. *Trends Microbiol*. 1998;6(10):392-401.
375. Real F, Mortara RA, Rabinovitch M. Fusion between Leishmania amazonensis and Leishmania major Parasitophorous Vacuoles: Live Imaging of Coinfected Macrophages. *PLoS Negl Trop Dis*. 2010;4(12):e905.
376. Ndjamen B, Kang B-H, Hatsuzawa K, Kima PE. Leishmania parasitophorous vacuoles interact continuously with the host cell's endoplasmic reticulum; parasitophorous vacuoles are hybrid compartments. *Cell Microbiol*. 2010;12(10):1480-1494.
377. Wilson ME, Vorhies RW, Andersen KA, Britigan BE. Acquisition of iron from transferrin and lactoferrin by the protozoan Leishmania chagasi. *Infection and Immunity*. 1994;62(8):3262-3269.
378. Wilson ME, Lewis TS, Miller MA, McCormick ML, Britigan BE. Leishmania chagasi: uptake of iron bound to lactoferrin or transferrin requires an iron reductase. *Exp Parasitol*. 2002;100(3):196-207.
379. Flannery AR, Huynh C, Mittra B, Mortara RA, Andrews NW. LFR1 Ferric Iron Reductase of Leishmania amazonensis Is Essential for the Generation of Infective Parasite Forms. *J Biol Chem*. 2011;286(26):23266-23279.
380. Borges VM, Vannier-Santos MA, De Souza W. Subverted transferrin trafficking in Leishmania- infected macrophages. *Parasitol Res*. 1998;84(10):811-822.
381. Das NK, Biswas S, Solanki S, Mukhopadhyay CK. Leishmania donovani depletes labile iron pool to exploit iron uptake capacity of macrophage for its intracellular growth. *Cell Microbiol*. 2009;11(1):83-94.
382. Atkinson, Barton. High level expression of Nramp1^{G169} in RAW264.7 cell transfectants: analysis of intracellular iron transport. *Immunology*. 1999;96(4):656-662.
383. Kuhn DE, Lafuse WP, Zwilling BS. Iron transport into Mycobacterium avium-containing phagosomes from an Nramp1Gly169-transfected RAW264.7 macrophage cell line. *Journal of Leukocyte Biology*. 2001;69(1):43-49.
384. Canonne-Hergaux F, Gruenheid S, Govoni G, Gros P. The Nramp1 Protein and Its Role in Resistance to Infection and Macrophage Function. *Proc Assoc Am Physicians*. 1999;111(4):283-289.

385. Fritsche G, Nairz M, Theurl I, et al. Modulation of macrophage iron transport by Nramp1 (Slc11a1). *Immunobiology*. 2008;212(9):751-757.
386. Nairz M, Fritsche G, Crouch M-LV, Barton HC, Fang FC, Weiss G. Slc11a1 limits intracellular growth of Salmonella enterica sv. Typhimurium by promoting macrophage immune effector functions and impairing bacterial iron acquisition. *Cell Microbiol*. 2009;11(9):1365-1381.
387. Bucheton B, Abel L, Kheir MM, et al. Genetic control of visceral leishmaniasis in a Sudanese population: candidate gene testing indicates a linkage to the NRAMP1 region. *Genes & Immunity*. 2003;4(2):104-109.
388. Castellucci L, Jamieson SE, Miller EN, et al. CXCR1 and SLC11A1polymorphisms affect susceptibility to cutaneous leishmaniasis in Brazil: a case-control and family-based study. *BMC Med Genet*. 2010;11(1):10.
389. Banerjee S, Datta R. Leishmania infection triggers hepcidin-mediated proteasomal degradation of Nramp1 to increase phagolysosomal iron availability. *Cell Microbiol*. 2020.
390. Hvidberg V, Maniecki MB, Jacobsen C, Højrup P, Møller HJ, Moestrup SK. Identification of the receptor scavenging hemopexin-heme complexes. *Blood*. 2005;106(7):2572-2579.
391. Kristiansen M, Graversen JH, Jacobsen C, et al. Identification of the haemoglobin scavenger receptor. *Nature*. 2001;409(6817):198-201.
392. White C, Yuan X, Schmidt Paul J, et al. HRG1 Is Essential for Heme Transport from the Phagolysosome of Macrophages during Erythrophagocytosis. *Cell Metab*. 2013;17(2):261-270.
393. Morimoto A, Omachi S, Osada Y, et al. Hemophagocytosis in Experimental Visceral Leishmaniasis by Leishmania donovani. *PLoS Negl Trop Dis*. 2016;10(3):e0004505.
394. Saha S, Basu M, Guin S, et al. Leishmania donovani Exploits Macrophage Heme Oxygenase-1 To Neutralize Oxidative Burst and TLR Signaling–Dependent Host Defense. *The Journal of Immunology*. 2019;202(3):827-840.
395. Pham N-K, Mouriz J, Kima PE. Leishmania pifanoi Amastigotes Avoid Macrophage Production of Superoxide by Inducing Heme Degradation. *Infection and Immunity*. 2005;73(12):8322-8333.
396. Chin Shen C, Kwang-Poo C. Heme requirement and acquisition by extracellular and intracellular stages of Leishmania mexicana amazonensis. *Molecular and Biochemical Parasitology*. 1985;16(3):267-276.
397. Agarwal S, Rastogi R, Gupta D, Patel N, Raje M, Mukhopadhyay A. Clathrin-mediated hemoglobin endocytosis is essential for survival of Leishmania. *Biochim Biophys Acta*. 2013;1833(5):1065-1077.
398. Krishnamurthy G, Vikram R, Singh SB, et al. Hemoglobin Receptor in *Leishmania* Is a Hexokinase Located in the Flagellar Pocket *J Biol Chem*. 2005;280(7):5884-5891.
399. Singh SB, Tandon R, Krishnamurthy G, et al. Rab5-mediated endosome–endosome fusion regulates hemoglobin endocytosis in Leishmania donovani. *The EMBO Journal*. 2003;22(21):5712-5722.
400. Rastogi R, Verma JK, Kapoor A, Langsley G, Mukhopadhyay A. Rab5 Isoforms Specifically Regulate Different Modes of Endocytosis in Leishmania. *J Biol Chem*. 2016;291(28):14732-14746.
401. Patel N, Singh SB, Basu SK, Mukhopadhyay A. Leishmania requires Rab7-mediated degradation of endocytosed hemoglobin for their growth. *Proceedings of the National Academy of Sciences*. 2008;105(10):3980-3985.

402. Cabello-Donayre M, Malagarie-Cazenave S, Campos-Salinas J, et al. Trypanosomatid parasites rescue heme from endocytosed hemoglobin through lysosomal HRG transporters. *Mol Microbiol*. 2016;101(6):895-908.
403. Huynh C, Yuan X, Miguel DC, et al. Heme Uptake by Leishmania amazonensis Is Mediated by the Transmembrane Protein LHR1. *PLoS Pathogens*. 2012;8(7):e1002795.
404. Cabello-Donayre M, Orrego LM, Herráez E, et al. Leishmania heme uptake involves LmFLVCRb, a novel porphyrin transporter essential for the parasite. *Cellular and Molecular Life Sciences*. 2020;77(9):1827-1845.
405. Cabello-Donayre M, Orrego LM, Herráez E, García-Hernández R, Pérez-Victoria JM. New Insights on Heme Uptake in Leishmania spp. *Int J Mol Sci*. 2022;23(18):10501.
406. Huynh C, Sacks DL, Andrews NW. A Leishmania amazonensis ZIP family iron transporter is essential for parasite replication within macrophage phagolysosomes. *J Exp Med*. 2006;203(10):2363-2375.
407. Jacques I, Andrews NW, Huynh C. Functional characterization of LIT1, the Leishmania amazonensis ferrous iron transporter. *Molecular and Biochemical Parasitology*. 2010;170(1):28-36.
408. Laranjeira-Silva MF, Wang W, Samuel TK, et al. A MFS-like plasma membrane transporter required for Leishmania virulence protects the parasites from iron toxicity. *PLOS Pathogens*. 2018;14(6):e1007140.
409. Sarkar A, Andrews NW, Laranjeira-Silva MF. Intracellular iron availability modulates the requirement for Leishmania Iron Regulator 1 (LIR1) during macrophage infections. *Int J Parasitol*. 2019;49(6):423-427.
410. Das NK, Sandhya S, G VV, et al. Leishmania donovani inhibits ferroportin translation by modulating FBXL5-IRP2 axis for its growth within host macrophages. *Cell Microbiol*. 2018:e12834.
411. Heinzel FP, Sadick MD, Holaday BJ, Coffman RL, Locksley RM. Reciprocal expression of interferon gamma or interleukin 4 during the resolution or progression of murine leishmaniasis. Evidence for expansion of distinct helper T cell subsets. *J Exp Med*. 1989;169(1):59-72.
412. Scott P, Natovitz P, Coffman RL, Pearce E, Sher A. Immunoregulation of cutaneous leishmaniasis. T cell lines that transfer protective immunity or exacerbation belong to different T helper subsets and respond to distinct parasite antigens. *J Exp Med*. 1988;168(5):1675-1684.
413. Anderson CF, Mendez S, Sacks DL. Nonhealing Infection despite Th1 Polarization Produced by a Strain of Leishmania major in C57BL/6 Mice. *The Journal of Immunology*. 2005;174(5):2934-2941.
414. Ji J, Sun J, Qi H, Soong L. Analysis of T helper cell responses during infection with Leishmania amazonensis. *The American journal of tropical medicine and hygiene*. 2002;66(4):338-345.
415. Stäger S, Maroof A, Zubairi S, Sanos SL, Kopf M, Kaye PM. Distinct roles for IL-6 and IL-12p40 in mediating protection against *Leishmania donovani* and the expansion of IL-10+ CD4+ T cells. *Eur J Immunol*. 2006;36(7):1764-1771.
416. Hatzigeorgiou DE, He S, Sobel J, Grabstein KH, Hafner A, Ho JL. IL-6 down-modulates the cytokine-enhanced antileishmanial activity in human macrophages. *The Journal of Immunology*. 1993;151(7):3682-3692.

417. Murray HW, Rubin BY, Rothermel CD. Killing of intracellular Leishmania donovani by lymphokine-stimulated human mononuclear phagocytes. Evidence that interferon-gamma is the activating lymphokine. *J Clin Invest*. 1983;72(4):1506-1510.
418. Ribeiro-De-Jesus A, Almeida RP, Lessa H, Bacellar O, Carvalho EM. Cytokine profile and pathology in human leishmaniasis. *Brazilian Journal of Medical and Biological Research*. 1998;31(1):143-148.
419. Bentur Y, McGuigan M, Koren G. Deferoxamine (Desferrioxamine). *Drug Saf*. 1991;6(1):37-46.
420. Allain P, Mauras Y, Chaleil D, et al. Pharmacokinetics and renal elimination of desferrioxamine and ferrioxamine in healthy subjects and patients with haemochromatosis. *Br J Clin Pharmacol*. 1987;24(2):207-212.
421. Summers MR, Jacobs A, Tudway D, Perera P, Ricketts C. Studies in Desferrioxamine and Ferrioxamine Metabolism in Normal and Iron-Loaded Subjects. *Br J Haematol*. 1979;42(4):547-555.
422. Murray HW, Granger AM, Teitelbaum RF. Gamma interferon-activated human macrophages and Toxoplasma gondii, Chlamydia psittaci, and Leishmania donovani: antimicrobial role of limiting intracellular iron. *Infection and Immunity*. 1991;59(12):4684-4686.
423. Filardy AA, Costa-Da-Silva AC, Koeller CM, et al. Infection with Leishmania major Induces a Cellular Stress Response in Macrophages. *PLoS One*. 2014;9(1):e85715.
424. Segovia M, Navarro A, Artero JM. The effect of liposome-entrapped desferrioxamine on *Leishmania donovani in vitro*. *Annals of Tropical Medicine & Parasitology*. 1989;83(4):357-360.
425. Bisti S, Konidou G, Papageorgiou F, Milon Ge, Boelaert JR, Soteriadou K. The outcome of Leishmania major experimental infection in BALB / c mice can be modulated by exogenously delivered iron. *Eur J Immunol*. 2000;30(12):3732-3740.
426. Malafaia G, Marcon LdN, Pereira LdF, Pedrosa ML, Rezende SA. Leishmania chagasi: Effect of the iron deficiency on the infection in BALB/c mice. *Exp Parasitol*. 2011;127(3):719-723.
427. Vale-Costa S, Gomes-Pereira S, Teixeira CM, et al. Iron Overload Favors the Elimination of Leishmania infantum from Mouse Tissues through Interaction with Reactive Oxygen and Nitrogen Species. *PLoS Negl Trop Dis*. 2013;7(2):e2061.
428. Richter GW. The cellular transformation of injected colloidal iron complexes into ferritin and hemosiderin in experimental animals. *J Exp Med*. 1959;109(2):197-216.
429. Artis D, Speirs K, Joyce K, et al. NF-κB1 Is Required for Optimal $CD4^+$ Th1 Cell Development and Resistance to *Leishmania major*. *The Journal of Immunology*. 2003;170(4):1995-2003.
430. Bisti S, Konidou G, Boelaert J, Lebastard M, Soteriadou K. The prevention of the growth of Leishmania major progeny in BALB/c iron-loaded mice: a process coupled to increased oxidative burst, the amplitude and duration of which depend on initial parasite developmental stage and dose. *Microb Infect*. 2006;8(6):1464-1472.
431. Xiong S, She H, Takeuchi H, et al. Signaling Role of Intracellular Iron in NF-κB Activation. *J Biol Chem*. 2003;278(20):17646-17654.
432. Bisti S, Soteriadou K. Is the reactive oxygen species-dependent-NF-κB activation observed in iron-loaded BALB/c mice a key process preventing growth of Leishmania major progeny and tissue-damage? *Microb Infect*. 2006;8(6):1473-1482.

1.19 Figures

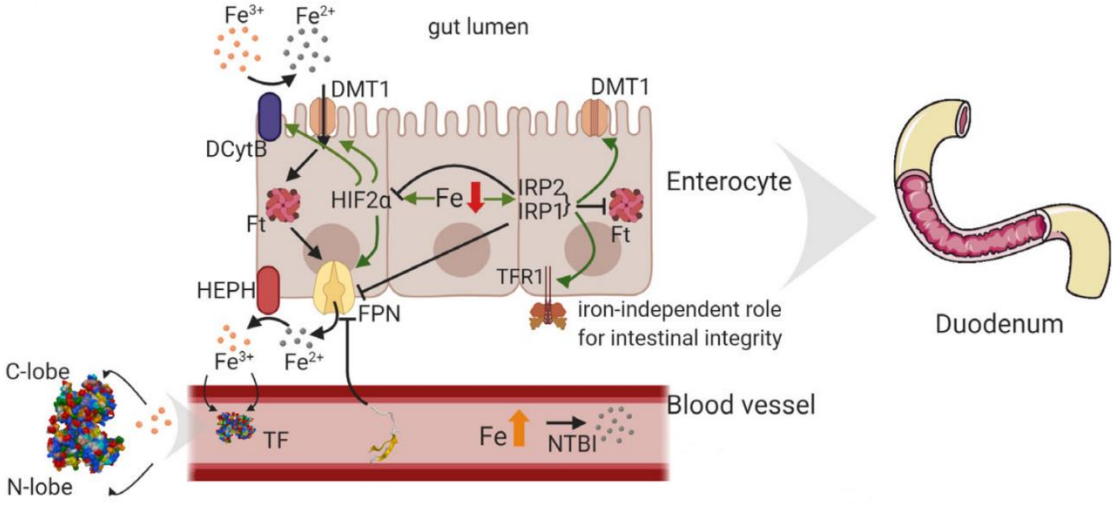

Figure 1.1: Dietary elemental iron uptake.
Ferric (Fe3+) iron in the gut is reduced by duodenal cytochrome b (DCytB; CYBRD1), and then imported by enterocytes using divalent metal transporter 1 (DMT1). Iron can be stored in ferritin (Ft) or exported by ferroportin (FPN) directly to the bloodstream. Additionally, enterocyte iron content dictates IRP activity regulating expression of hypoxia inducible factor 2α (HIF2α), ferritin, ferroportin, and transferrin receptor 1 (TFR1). Once iron enters the bloodstream, it is oxidized by hephaestin (HEPH) or ceruloplasmin (CP) and binds transferrin in a diferric manner for transport. Non-transferrin bound iron (NTBI) is present under conditions of elevated transferrin saturation.

Reproduced from: Mleczko-Sanecka K, Silvestri L. Cell-type-specific insights into iron regulatory processes. *Am J Hematol*. 2021;96(1):110-127 with permission from John Wiley and Sons, ©Copyright John Wiley and Sons, 2022 License number: 5444800166052.

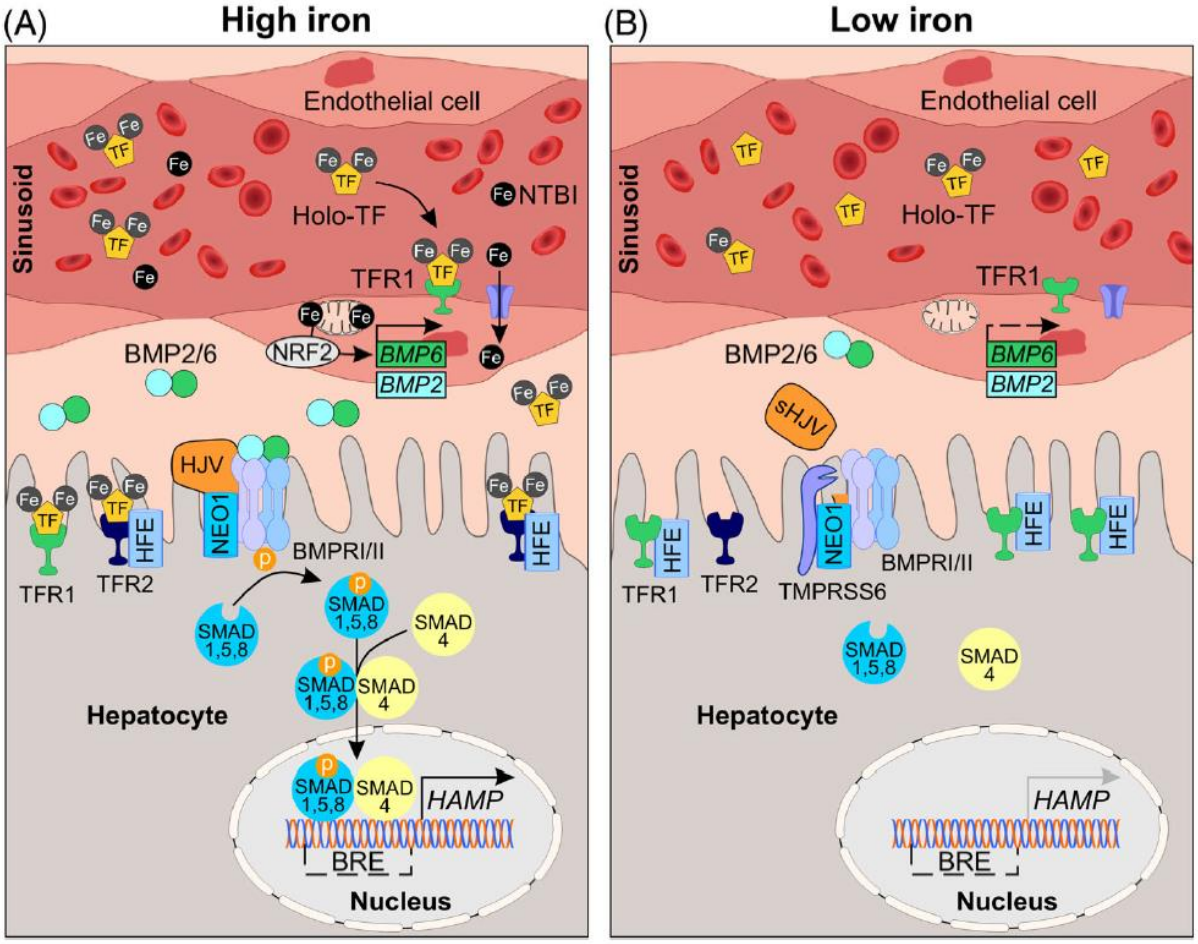

Figure 1.2: Hepcidin's iron regulatory network.
(A) Under conditions of elevated iron in the circulation, transferrin is saturated and non-transferrin bound iron is present. These will enter endothelial cells causing oxidative stress and promoting *NFE2L2* (NRF2) activation and subsequent BMP6 transcription. BMP2 and BMP6 bind tightly to their cognate receptors BMPRI/II as heterodimers in the presence of the co-receptor HJV. Together with the scaffolding protein NEO1, these work to phosphorylate SMAD1/5/8 which will then bind SMAD4, translocate to the nucleus, and induce *HAMP* transcription. TFR2 may bind to HFE and be stabilized by holo-transferrin to help amplify SMAD phosphorylation. (B) Under conditions of iron deficiency, BMP production is halted, HJV is cleaved from the cell surface by TMPRSS6, and *HAMP* expression is absent. TFR1 is highly expressed at the cell surface and will compete with TFR2 for HFE.

Reproduced from: Fisher AL, Babitt JL. Coordination of iron homeostasis by bone morphogenetic proteins: Current understanding and unanswered questions. *Dev Dyn*. 2022;251(1):26-46 with permission from John Wiley and Sons, ©Copyright John Wiley and Sons, 2022. License number: 5443760011537.

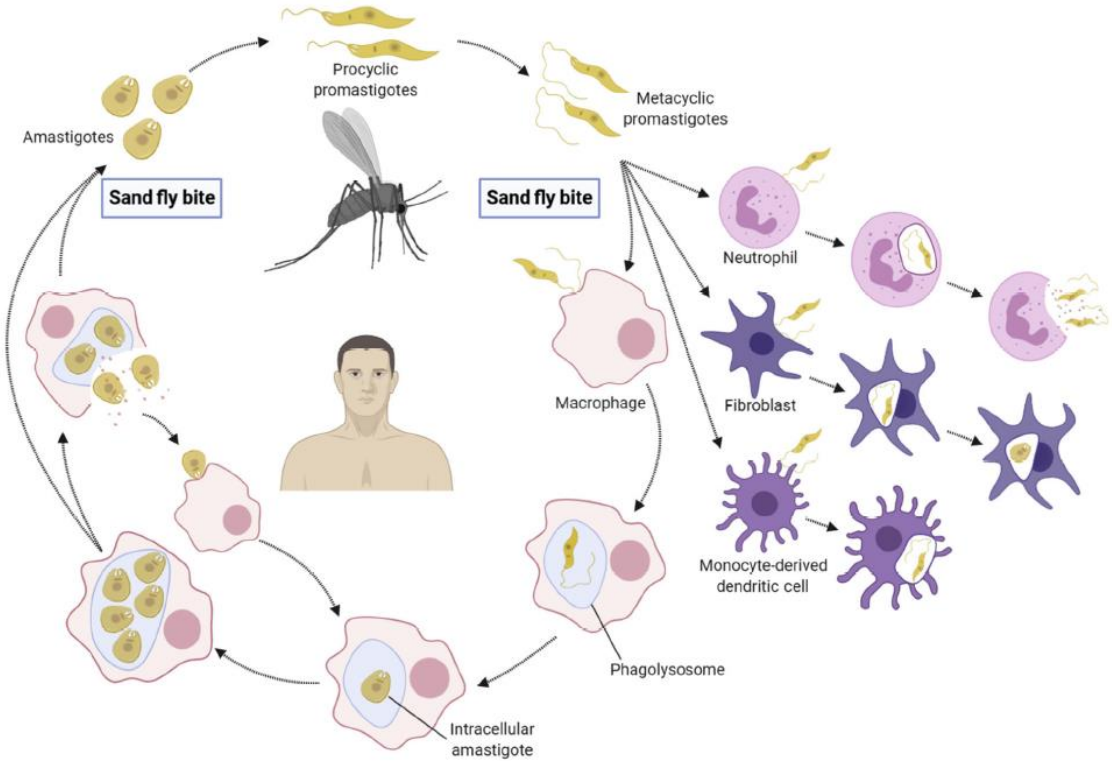

Figure 1.3: *Leishmania*'s life cycle.
The *Leishmania* life cycle begins in the female sand fly midgut where motile promastigotes proliferate. Upon taking a bloodmeal, parasites gain access to the mammalian host's circulation where parasites will be phagocytosed by primarily recruited neutrophils and macrophages, as well as fibroblasts and monocyte-derived dendritic cells. Macrophages are the target cell where parasite can differentiate into immotile amastigotes in parasitophorous vacuoles (phagolysosomes containing parasite). Amastigotes will replicate within macrophages and eventually cause these to burst releasing parasite into the bloodstream where these can reinfect new macrophages. To complete the cycle, sand flies ingest infected macrophages upon taking a bloodmeal where amastigotes will differentiate back to promastigotes upon release.

Reproduced from: Laranjeira-Silva MF, Hamza I, Pérez-Victoria JM. Iron and Heme Metabolism at the Leishmania–Host Interface. *Trends Parasitol*. 2020;36(3):279-289 with permission from Elsevier. ©Copyright Elsevier, 2022. License number: 5444820459718.

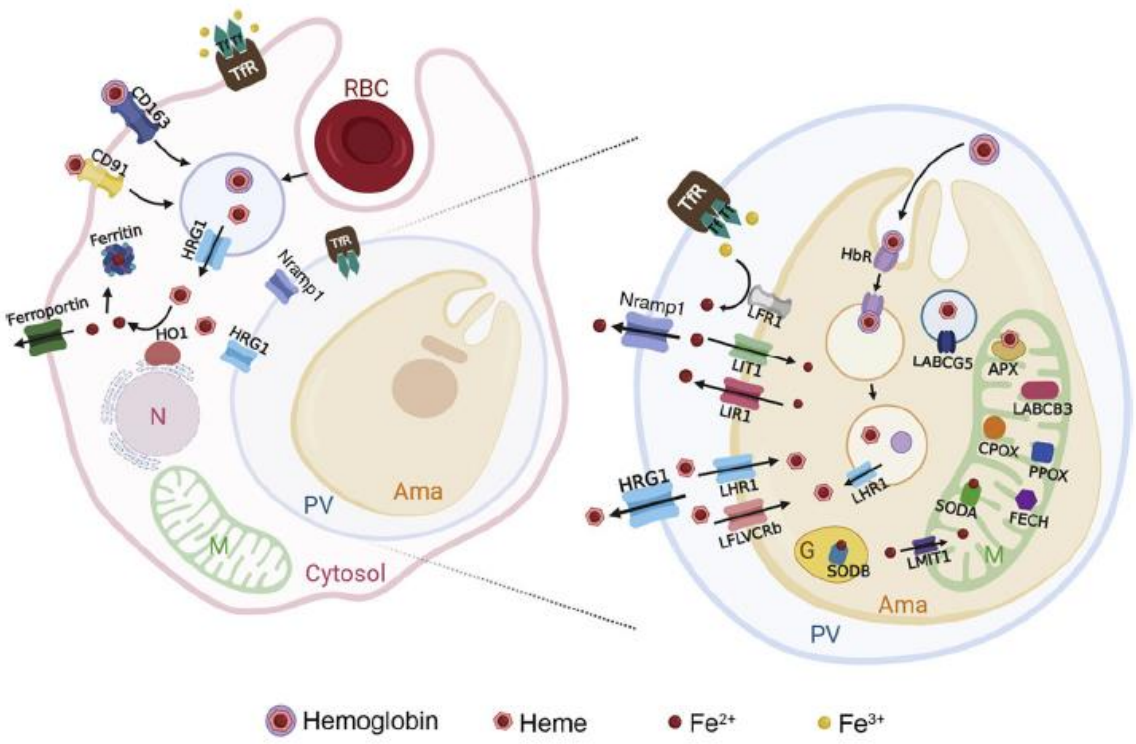

Figure 1.4: Macrophage and *Leishmania* iron transport.
Macrophages will obtain iron from hemoglobin, heme, or transferrin through CD163, CD91, or transferrin receptor 1 (TfR), respectively. Macrophages may export heme from endosomes using heme-responsive gene 1 (HRG1) and will export cellular iron through ferroportin. Endosomes comprised of iron molecules may merge with parasitophorous vacuoles (PV) giving access to iron to amastigotes. Amastigotes can reduce ferric iron to ferrous iron using *Leishmania* ferric reductase 1 (LFR1) to then import it through *Leishmania* iron transporter 1 (LIT1). To protect itself from iron-induced oxidative stress, *Leishmania* may export ferrous iron through *Leishmania* iron regulator 1 (LIR1). Nramp1 at the surface of PVs will export iron and compete with LIT1 for iron acquisition. Similarly, heme may be taken up by amastigotes through *Leishmania* heme receptor 1 (LHR1) or *Leishmania* feline leukemia virus subgroup C cellular receptor b (LFLCVRb) where HRG1 will compete by exporting heme from the PV.

Reproduced from: Laranjeira-Silva MF, Hamza I, Pérez-Victoria JM. Iron and Heme Metabolism at the Leishmania–Host Interface. *Trends Parasitol*. 2020;36(3):279-289 with permission from Elsevier. ©Copyright Elsevier, 2022. License number: 5444820459718.

Preface to chapter 2

There has been phenomenal progress in the field of systemic iron homeostasis over the past two decades. Only now are we beginning to uncover the mechanisms by which higher organisms regulate their iron intake and sense fluxes in iron. From what we know so far, hepcidin, produced by the liver, is the main homeostatic regulator of iron flow through its action of inhibiting and inducing degradation of the cellular iron exporter ferroportin. A large body of work has focused on understanding the intricate regulatory network necessary to properly control the production of this hormone. Recent findings uncovered bone morphogenetic proteins (BMP), namely BMP6 and BMP2, as inducers of hepcidin in response to iron and these are produced by the liver's sinusoidal endothelial cells. One important question that remains and that we have attempted to answer is: what prompts expression of BMPs in endothelial cells? The answer remains elusive due to the numerous forms of iron circulating in organisms and the possibility of other iron-induced signaling molecules. By specifically understanding the trigger for BMP production, novel therapies could be designed to induce hepcidin when it is aberrantly low such as in cases of hereditary hemochromatosis, a broad term used to define diseases of excess body iron due to genetic defects. Hence, this chapter has aimed to uncover whether iron obtained through the primary cellular iron gate, transferrin receptor 1, is of significant importance for production of BMPs in endothelial cells.

This chapter was adapted from: Charlebois E, Fillebeen CC, Presley JF, Cagnone G, Lisi V, Lavallee VP, Joyal JS, & Pantopoulos P. Liver sinusoidal endothelial cells induce BMP6 expression in response to non-transferrin bound iron. *Blood*. 2023.

Chapter 2

Liver sinusoidal endothelial cells induce BMP6 expression in response to non-transferrin bound iron

Running head: BMP6 induction via NTBI

Edouard Charlebois[1,2], Carine Fillebeen[1,2], John Presley[3], Gael Cagnone[4], Véronique Lisi[4], Vincent-Philippe Lavallée[4,5], Jean-Sébastien Joyal[4,5,6] and Kostas Pantopoulos[1,2]*

[1] Lady Davis Institute for Medical Research, Jewish General Hospital

[2] Department of Medicine, McGill University, Montreal, Quebec, Canada

[3] Department of Anatomy and Cell Biology, McGill University, Montreal, Quebec, Canada

[4] Centre de Recherche du Centre Hospitalier Universitaire Sainte-Justine and Departments of Ophthalmology and Pediatrics, University of Montreal, Montreal, Quebec, Canada

[5] Department of Pediatrics, University of Montreal, Montreal, Quebec, Canada

[6] Departments of Ophthalmology, University of Montreal, Montreal, Quebec, Canada

* Corresponding author; tel.: (514) 340-8260 ext. 25293; email: kostas.pantopoulos@mcgill.ca

2.1 Key points

1. NTBI uptake by LSECs is the major signal for Bmp6 induction during iron overload, and Tfr1 contributes mostly under low iron conditions
2. Bmp6 induction in the presence of NTBI is associated with extensive genetic reprogramming of LSECs that involves Nrf2 and Myc pathways

2.2 Abstract

Homeostatic adaptation to systemic iron overload involves transcriptional induction of bone morphogenetic protein 6 (BMP6) in liver sinusoidal endothelial cells (LSECs). BMP6 is then secreted to activate signaling to the iron hormone hepcidin (HAMP) in neighboring hepatocytes. To explore the mechanism for iron sensing by LSECs, we generated $Tfrc^{Tek\text{-}Cre}$ mice with endothelial cell-specific ablation of transferrin receptor 1 (Tfr1). We also used control $Tfrc^{fl/fl}$ mice to characterize LSEC-specific molecular responses to iron by single-cell transcriptomics. $Tfrc^{Tek\text{-}Cre}$ animals tend to have modestly increased liver iron content (LIC) compared to $Tfrc^{fl/fl}$ controls but express physiological *Bmp6* and *Hamp* mRNA. Despite a transient inability to upregulate *Bmp6*, they eventually respond to iron challenges with *Bmp6* and *Hamp* induction, yet occasionally to levels slightly lower relative to LIC. High dietary iron intake triggered accumulation of serum non-transferrin bound iron (NTBI), which significantly correlated with liver *Bmp6* and *Hamp* mRNA levels and elicited more profound alterations in the LSEC transcriptome compared to holo-transferrin injection. These culminated in robust induction of *Bmp6* and other nuclear factor erythroid 2-related factor 2 (Nrf2) target genes, as well as Myc target genes involved in ribosomal biogenesis and protein synthesis. LSECs and midzonal hepatocytes were the most responsive liver cells to iron challenges and exhibited highest expression of *Bmp6* and *Hamp* mRNAs, respectively. Our data suggest that during systemic iron overload, LSECs internalize NTBI, which promotes oxidative stress and thereby transcriptionally induces *Bmp6* via Nrf2. Tfr1 appears to contribute to iron sensing by LSECs mostly under low iron conditions.

Keywords: iron metabolism, hepcidin, Tfr1, transferrin, NTBI

2.3 Introduction

LSECs play a critical role in iron sensing by secreting BMP6 and BMP2, which are potent inducers of the iron regulatory hormone hepcidin[1]. They can form heterodimers and bind to BMP receptors on hepatocytes to activate the SMAD signaling cascade, leading to transcription of the hepcidin-encoding *HAMP* gene. Hepcidin limits iron entry into the bloodstream by binding to the iron exporter ferroportin in target cells such as duodenal enterocytes and tissue macrophages, which are crucial for dietary iron absorption and iron recycling from effete red blood cells, respectively[2]. Hepcidin binding occludes ferroportin's iron channel[3], and also triggers ferroportin internalization and lysosomal degradation[4].

Hepcidin expression is induced in response to elevated serum or tissue iron and serves as a homeostatic adaptation to prevent systemic iron overload and the ensuing complications. Increased transferrin (Tf) saturation in the blood stabilizes transferrin receptor 2 (Tfr2) on hepatocytes, which in turn stimulates SMAD signaling to hepcidin[5]. On the other hand, excessive tissue iron promotes induction of primarily BMP6 and to a lesser extent BMP2 in the liver[1]. LSECs are the major site for hepatic BMP6 and BMP2 production, and endothelial cell-specific ablation of either Bmp6[6] or Bmp2[7,8] in mice causes systemic iron overload (hemochromatosis) due to hepcidin deficiency.

The mechanisms by which LSECs sense iron and respond to increased liver iron stores via BMP6 induction are not well understood. *In vitro*, treatment of primary murine LSECs or LSEC-like cell lines with iron is sufficient to activate *Bmp6* mRNA in a cell autonomous manner[9-11]. Biochemical studies showed that the *BMP6* promoter contains a binding site of the Nrf2 transcription factor and provided evidence that iron-dependent induction of BMP6 in the LSEC culture models involves Nrf2 activation by oxidative stress[9]. In line with this finding, $Nrf2^{-/-}$ mice exhibited a blunted Bmp6 response to oral or parenteral iron challenges[9]. The above data established a role of Nrf2 in iron-mediated induction of *Bmp6* within LSECs, but do not offer a clue on how these cells accumulate excess iron and respond to systemic iron overload *in vivo*.

Most cells acquire iron from circulating Tf by transferrin receptor 1 (Tfr1) via endocytosis[12]. Thus, we hypothesized that Tf/Tfr1-mediated iron uptake may be a crucial component of the iron-sensing pathway by LSECs that results in *Bmp6* induction. To address this, we generated $Tfrc^{Tek\text{-}Cre}$ mice with endothelial cell-specific ablation of the Tfr1-encoding *Tfrc* gene. We show that with minor exceptions, these mice respond to iron challenges with *Bmp6* and

Hamp mRNA induction; however, they tend to have relatively increased liver iron content (LIC). Iron-dependent *Bmp6* and *Hamp* mRNA induction in both $Tfrc^{fl/fl}$ and $Tfrc^{Tek\text{-}Cre}$ mice positively correlated with NTBI, which emerges following high dietary iron intake. Moreover, we show by single-cell transcriptomics that acute dietary iron loading promotes extensive reprogramming of LSEC gene expression in control $Tfrc^{fl/fl}$ mice, characterized by induction of Nrf2 and Myc target genes.

2.4 Methods

2.4.1 Animals

$Tfrc^{fl/fl}$ mice were generated in house[13] and Tek-Cre transgenic mice[14] (B6.Cg-Tg(Tek-cre)^{1Ywa}/J; JAX stock #008863) were purchased from the Jackson Laboratory (Bar Harbor, ME). $Rosa26^{mT\text{-}mG/mT\text{-}mG}$ reporter mice[15] were kindly provided by Dr. Schiffrin. These animals, as well as $Tfrc^{Tek\text{-}Cre}$ and $Rosa26^{mT\text{-}mG/+}$;$Tfrc^{fl/+}$;Tek-Cre progeny were housed in macrolone cages (up to 5 mice/cage, 12:12 h light-dark cycle: 7 am - 7 pm; 22±1°C, 60±5% humidity) and were allowed *ad libitum* access to chow and drinking water. The mice were fed a standard diet (Teklad Global 18% protein 2918; 200 ppm iron) or, when indicated, iron-deficient (TD.80396; 2-6 ppm iron), or high-iron diets (TD.09521; 2% carbonyl iron). Where indicated, the mice were injected intravenously (tail vein) with 0.9 mg ferric ammonium citrate or 10 mg holo-Tf. At the endpoints, the animals were sacrificed by CO_2 inhalation. Experimental procedures were approved by the Animal Care Committee of McGill University (protocol 4966).

2.4.2 Biochemical assays and histology

Serum biochemistry, quantitative real-time (qPCR), immunohistochemistry and quantification of tissue iron were performed as described[16-18]. Details are provided in Supplemental Methods.

2.4.3 Single-cell transcriptomics

Liver cells were isolated from perfused anaesthetized mice for scRNA-Seq analysis. Details are provided in Supplemental Methods. Raw and normalized data have been deposited on GEO accession number GSE215324.

2.5 Results

2.5.1 Tfrc$^{Tek\text{-}Cre}$ mice exhibit Tfr1 ablation in LSECs.

For disruption of Tfr1 in LSECs, Tfrc$^{fl/fl}$ mice were mated with Tek-Cre transgenic animals. The resulting Tfrc$^{Tek\text{-}Cre}$ offspring were born in lower than Mendelian ratios, which is indicative of partial embryonic lethality. Moreover, some newborn pups had a pale appearance and died within a few days after birth. Approximately 25% of the expected Tfrc$^{Tek\text{-}Cre}$ mice (86 out of 342) survived to adulthood without apparent phenotypic abnormalities. There was no sex-specific bias as the male to female ratio among surviving animals was 1:1. Adult Tfrc$^{Tek\text{-}Cre}$ mice did not manifest anemia, but their red blood cells (RBCs) had modestly increased distribution width (RDW) and lower mean corpuscular volume (MCV) compared to those of Tfrc$^{fl/fl}$ littermates (Table S1). Additionally, RBCs from male but not female Tfrc$^{Tek\text{-}Cre}$ mice had lower mean corpuscular hemoglobin (MCH) content (Table S1). There were no differences in serum iron indexes among males and females (Figure S.2.1). These data suggest that endothelial cell-specific ablation of Tfr1 in this Tfrc$^{Tek\text{-}Cre}$ mouse model elicits strong adverse effects during embryogenesis and early postnatal period. Nevertheless, surviving mice develop normally and only exhibit a mild hematological phenotype.

Liver sections of adult Tfrc$^{fl/fl}$ control and Tfrc$^{Tek\text{-}Cre}$ mice were used to validate Tfr1 ablation in LSECs by immunofluorescence. The animals were previously fed an iron-deficient diet to stimulate Tfr1[13]. As expected[13], Tfr1 was strongly expressed in hepatocytes of both genotypes (Figure 2.1A, red color). Staining for the endothelial cell-specific marker CD31 (green) revealed the LSEC lining in sinusoids. In control livers, the Tfr1 signal was present throughout the lining (Figure 2.1A, left), and areas with overlapping CD31 and Tfr1 staining were visible (yellow, see rectangles 1 and 2). By contrast, the Tfr1 signal was absent in the LSEC lining of Tfrc$^{Tek\text{-}Cre}$ mice (Figure 2.1A, right; see rectangles 3 and 4). Thus, the Tfrc$^{Tek\text{-}Cre}$ mouse model bears efficient Tfr1 ablation in LSECs. We further validated this by using a Rosa26$^{mT\text{-}mG/+}$;Tfrc$^{fl/+}$;Tek-Cre reporter mouse, where Cre recombination resulted in replacement of red mT with green mG in the LSEC lining (Figure 2.1B).

2.5.2 Tfrc$^{Tek\text{-}Cre}$ mice express physiological levels of Bmp6 and Hamp mRNAs and induce them in response to iron.

We explored the impact of endothelial cell-specific Tfr1 ablation on sensing of high dietary iron by LSECs (Figure 2.2A). A first group of Tfrc$^{fl/fl}$ and Tfrc$^{Tek\text{-}Cre}$ mice remained on standard diet (SD) and served as control. A second group of animals was switched from SD to a high iron diet (HID) for 18 hours. This dietary manipulation was expected to rapidly increase Tf saturation leading to gradual NTBI accumulation[13]. For acute exposure to NTBI, mice in a third group received an intravenous injection with ferric ammonium citrate (FAC) and sacrificed after 5 h, an optimal time point inferred from a preliminary kinetics experiment (Figure S.2.2).

Intake of HID increased serum iron, Tf saturation and NTBI in both Tfrc$^{fl/fl}$ and Tfrc$^{Tek\text{-}Cre}$ mice within 18 h (Figure 2.2B-E). Similar results were obtained with FAC injection; however, the NTBI increase did not reach statistical significance, presumably due to rapid clearance by liver parenchymal cells, as previously shown[19]. Tfrc$^{Tek\text{-}Cre}$ mice tended to have higher LIC in all experimental settings (Figure 2.2F), but their iron content in spleen, kidney and heart was physiological (Figure S.2.3). Expression of the mRNAs encoding Bmp6, Bmp2, and the BMP target hepcidin (*Hamp*) did not significantly differ in livers of Tfrc$^{fl/fl}$ and Tfrc$^{Tek\text{-}Cre}$ mice on SD (Figure 2.2G-H), and this persisted after normalization to LIC (Figure 2.2K-M). Expression of the BMP target *Id*, as well as *Id1*/LIC ratios were higher in Tfrc$^{Tek\text{-}Cre}$ mice (Figure 2.2J and 2N, respectively). As expected, HID intake induced *Bmp6*, *Hamp* and *Id1* mRNAs in both genotypes, yet the *Hamp*/LIC ratio was lower in Tfrc$^{Tek\text{-}Cre}$ mice. Surprisingly, FAC injection promoted *Bmp6* mRNA induction only in Tfrc$^{fl/fl}$ but not Tfrc$^{Tek\text{-}Cre}$ mice (Figure 2.2G). It also resulted in *Hamp* mRNA upregulation in both genotypes (Figure 2.2I), possibly with the contribution of the inflammatory pathway, since FAC induced expression of the inflammatory marker *Socs3* (Figure S.2.4). Taken together, these data suggest that the responses of Tfr1-deficient LSECs to high dietary iron are intact. However, Tfr1 appears critical for *Bmp6* induction following FAC injection, at least within the 5 h experimental time frame.

2.5.3 Iron-restricted Tfrc$^{Tek\text{-}Cre}$ mice have increased LIC, express relatively lower levels of Bmp6 and Hamp mRNAs, and respond to dietary iron or holo-Tf injection.

In another experiment, we addressed the responses of Tfrc$^{fl/fl}$ and Tfrc$^{Tek\text{-}Cre}$ mice to more physiologically relevant dietary iron intake or holo-Tf injection (Figure 2.3A). All animals were

rendered relatively iron deficient by feeding IDD for one week and then were divided into three experimental groups. In the first group, the mice remained on IDD and served as control. In the second and third groups, the mice were either switched from IDD to SD or injected intravenously with holo-Tf, respectively, and then sacrificed (together with controls) after 18 h.

Under iron-restricted conditions, the $Tfrc^{Tek\text{-}Cre}$ mice exhibited modestly but significantly elevated LIC and reduced *Bmp6*/LIC and *Hamp*/LIC ratios compared to control $Tfrc^{fl/fl}$ littermates (Figure 2.3F, 2.3K and 2.3M). Switch from IDD to SD tended to increase serum iron, Tf saturation and NTBI in both genotypes, while holo-Tf injection did not affect serum iron at the endpoint but increased TIBC and decreased Tf saturation without alterations in NTBI (Figure 2.3B-E). The switch to SD did not alter expression of *Bmp6*, *Bmp2* or *Id1* mRNAs but promoted *Hamp* mRNA induction to levels appropriate relative to LIC in both $Tfrc^{fl/fl}$ and $Tfrc^{Tek\text{-}Cre}$ mice (Figure 2.3G-N). *Hamp* mRNA was also induced following holo-Tf injection, and the response appeared more potent in $Tfrc^{Tek\text{-}Cre}$ mice (Figure 2.3I). The *Hamp*/LIC ratio was lower at baseline (IDD) in $Tfrc^{Tek\text{-}Cre}$ mice (Figure 2.3M), even though *Hamp* mRNA expression was at control levels (Figure 2.3I). Surprisingly, holo-Tf injection promoted induction of *Bmp6*, *Bmp2* and *Id1* mRNAs in both $Tfrc^{fl/fl}$ and $Tfrc^{Tek\text{-}Cre}$ mice (Figure 2.3G-N). Dietary iron manipulations or holo-Tf injection did not affect expression of *Socs3* mRNA (Figure S.2.4).

The expression of *Bmp6* and *Hamp* mRNAs positively and significantly correlated with NTBI (Figure 2.4) but also with Tf saturation and LIC (Figure S.2.5) in both $Tfrc^{fl/fl}$ and $Tfrc^{Tek\text{-}Cre}$ mice. As expected, the correlation between *Bmp6* and *Hamp* mRNA levels was also significant (Figure 2.4E-F). The correlations between NTBI and Tf saturation or LIC were significant only in control $Tfrc^{fl/fl}$ but not in $Tfrc^{Tek\text{-}Cre}$ mice (Figure S.2.5I-L). Together, the above data suggest that Tfr1 ablation in LSECs of $Tfrc^{Tek\text{-}Cre}$ mice is associated with modestly increased LIC but only minimally affects the capacity of these animals to induce *Bmp6* in response to iron challenges.

2.5.4 *Single-cell transcriptomic profiles in the mouse liver following holo-Tf injection or acute dietary iron loading.*

We went on to determine the impact of holo-Tf injection or acute dietary iron loading on the transcriptome of liver cells using scRNA-Seq (Figure 2.5A). Three $Tfrc^{fl/fl}$ mice were fed IDD for one week; one of them was used as control. The other mice were either injected with holo-Tf or switched to HID for 18 h. At the endpoints, livers were dissociated, and single-cell suspensions

were used for scRNA-Seq analysis. This produced good quality datasets (Figure S.2.6A-B), with 2070 cells in the control (IDD) group, 6505 cells in the holo-Tf (IDD+holo-Tf) group and 3134 cells in the HID (IDD→HID) group (Figure 2.5B). Dimensionality reduction followed by clustering and differential gene expression analysis allowed us to annotate 9 distinct cell types: hepatocytes (2 types), macrophages/monocytes, endothelial cells, B lymphocytes, stellate cells, T lymphocytes, dendritic cells, and neutrophils (Figure 2.5B-C and S.2.5C). These cell types expressed known gene markers (Figure 2.5C) and were found at variable proportion in each dataset (Figure 2.5D).

The effects of holo-Tf or dietary iron on liver cell transcriptomes were first investigated using a machine learning algorithm (Augur[20]) implementing a random forest classifier to detect most affected cell types. Compared to control, holo-Tf injection and HID intake showed most impact on endothelial cells (ECs) followed by stellate cells (Figure 2.5E). Yet, when comparing HID to holo-Tf treatments, midzonal hepatocytes were the most divergent, followed by B lymphocytes (BCs). Cell type-specific differential analysis between groups showed important gene expression changes in all cell types (Figure S.2.7). These transcriptomic variations were associated with differential pathway enrichment obtained from the Molecular Signatures Database (Figure S.2.8A). Analysis of iron pathways from this database revealed that both holo-Tf and dietary iron increased expression of iron-related gene sets (Figure 2.5F and S.2.5D). Notably, these changes were more pronounced in the group switched to HID compared to the holo-Tf-treated group. Across the different cell types, ECs and midzonal hepatocytes were the most responsive to the experimental treatments. Interestingly, the observed iron effects in both these cell types were matched with increases in reactive oxygen species (ROS) associated pathways, also observed in macrophages/monocytes and dendritic cells (Figure S.2.8B).

2.5.5 Iron-induced genetic reprogramming in LSECs and midzonal hepatocytes.

Endothelial cells line hepatic arteries, veins, and sinusoids (Figure 2.6A). Sub-clustering of ECs from our scRNA-Seq datasets defined three subtypes expressing specific arterial (periportal), venous (pericentral), and sinusoidal (midzonal) marker genes (Figure 2.6B-C), in line with previous data[21]. The sinusoidal subtype (LSECs) represented most of the detected ECs (Figure 2.6D) and expressed genes involved in Bmp and Tgf signalling, as reported[22] (Figure 2.6E). Among LSECs, *Bmp6* and *Bmp2* were primarily responsive to acute dietary iron loading

(HID vs control: *Bmp6* p=6.8e-23, log2FC=0.46; *Bmp2* p=1.3e-32, log2FC=0.50) and less to holo-Tf (holo-Tf vs control: *Bmp6* p>0.05; *Bmp2* p=1.2e-19, log2FC=0.37). We thus focused on the transcriptomic impact of HID intake or holo-Tf injection on LSECs, which triggered important up-regulation of genes compared to the control group (Figure 2.6F, Table S.2.2). When comparing the transcriptome of LSECs between the HID and holo-Tf groups (Figure 2.6F), we found significant enrichments in Nfe2l2 (Nrf2) and Myc target genes (Figure 2.6G). Correlating with increased expression of iron-related genes in the HID group, LSECs showed indeed greater expression of genes related to Nrf2 and Myc pathways in comparison to the control and holo-Tf groups (Figure 2.6H-I). Among the iron-related genes, HID intake strongly induced expression of *Slc39a8*, *Slc40a1*, *Fth* and *Ftl* encoding the metal-ion (and NTBI) transporter Zip8, the iron exporter ferroportin, and the H- and L-subunits of the iron storage protein ferritin, respectively (Figure 2.6H).

LSECs-derived BMPs activate the SMAD signaling cascade in hepatocytes, which ultimately leads to transcriptional induction of *Hamp*. From our scRNA-Seq datasets, two clusters of hepatocytes were detected (Figure 2.7A). They manifested gene expression differences consistent with transcriptomic patterns associated with liver zonation[23,24] (Figure 2.7B). Pericentral and periportal hepatocytes tended to cluster near each other possibly due to the iron treatment conditions and were thus grouped into “other hepatocytes”. Midzonal hepatocytes represented a smaller fraction (Figure 2.7C) but exhibited greatest response to holo-Tf or HID, notably regarding *Hamp* expression (Figure 2.7D). Moreover, gene set variation analysis showed higher expression of the GO iron binding pathway in midzonal hepatocytes, and more importantly in the HID group (Figure 2.7E). Differential gene expression analysis for the iron manipulations in midzonal hepatocytes revealed greater transcriptomic responses in the HID group (Figure 2.7F), with up-regulation of *Hamp, Crot, Gpx4* and *Gpx1*. Pathway analysis showed significant enrichment in Nrf2 target genes as well as genes involved in ROS and oxidative phosphorylation (OXPHOS) metabolism (Figure 2.7G-H; Table S.2.3).

Collectively, the single-cell transcriptomics data validate the crucial roles of LSECs in iron sensing via Bmp6 (and Bmp2), and of midzonal hepatocytes in *Hamp* induction. Moreover, they demonstrate that acute dietary iron loading triggers more pronounced genetic responses in LSECs compared to holo-Tf injection, which appear to involve Nrf2- and Myc-dependent pathways.

2.6 Discussion

LSECs respond to systemic iron overload by transcriptional induction of BMP6, which in turn activates signaling to hepcidin in neighboring hepatocytes[6]. We hypothesized that iron sensing by LSECs may require uptake of Tf-bound iron via Tfr1. To address this, we utilized an established Tek-Cre mouse strain[14] for endothelial cell-specific disruption of Tfr1 from $Tfrc^{fl/fl}$ mice[13]. The resulting $Tfrc^{Tek\text{-}Cre}$ mice exhibited partial embryonic and neonatal lethality. Considering that Tek-Cre mice manifest variable degrees of aberrant Cre recombinase expression in hematopoietic lineages[25] and that Tfr1 is essential during erythropoiesis[26], this phenotype is likely related to Tfr1 ablation in erythroid cells. It should be noted that adult mice carrying the Tek-Cre^{1Ywa} allele (as the $Tfrc^{Tek\text{-}Cre}$ animals used in this study) appear to express only a small number of Cre-positive blood cells compared to other Tek-Cre mice[25]. This is consistent with the fact that our surviving adult $Tfrc^{Tek\text{-}Cre}$ mice do not develop anemia and only manifest modestly altered hematological indexes such as RDW, MCV and MCH (Table S1). Efficient disruption of Tfr1 in LSECs from our $Tfrc^{Tek\text{-}Cre}$ mice is documented in figure 2.1.

The data in Figures 2-3 demonstrate that $Tfrc^{Tek\text{-}Cre}$ mice efficiently respond to dietary iron intake by inducing *Bmp6* and downstream *Hamp* expression despite Tfr1 ablation in LSECs. While these homeostatic responses are largely preserved, we noted that $Tfrc^{Tek\text{-}Cre}$ animals tended to have modestly increased LIC, while in some instances the iron-dependent upregulation of *Bmp6* and/or *Hamp* mRNAs was relatively reduced when adjusted for LIC. This was more evident in iron-restricted $Tfrc^{Tek\text{-}Cre}$ mice. Similar results were recently reported with $Tfrc^{Stab2\text{-}Cre}$ mice, another model of Tfr1 disruption in LSECs[27]. Together, these data suggest a minor contribution of Tf-bound iron and Tfr1 in the iron sensing pathway that gives rise to *Bmp6* induction in LSECs. Further support to this conclusion is provided by the scRNA-Seq data showing extensive reprogramming of iron pathways in LSECs by holo-Tf (Figure 2.5E-F) with minor *Bmp6* induction compared to that achieved by acute dietary iron loading (Figure 2.6E).

Bmp6 and *Hamp* mRNA expression positively correlated with LIC, Tf saturation and NTBI levels in both $Tfrc^{Tek\text{-}Cre}$ and control $Tfrc^{fl/fl}$ mice (Figure 2.4 and S.2.5). The positive correlation between *Bmp6* mRNA and LIC is in line with earlier findings[28]. Nevertheless, LIC is unlikely to be the driver for *Bmp6* induction in LSECs for following reasons: First, ablation of the NTBI transporter Zip14 from $Hjv^{-/-}$ mice, a model of hemochromatosis, prevented hepatocellular iron overload without compromising appropriate *Bmp6* mRNA induction[29]. Second, $Fpn^{Tek\text{-}Cre}$ mice

(bearing endothelial cell-specific disruption of ferroportin) were anemic and developed iron overload in Kupffer cells and hepatocytes but failed to induce *Bmp6* mRNA[30]. Third, exposure of primary LSECs or LSEC-like cell lines to iron was sufficient to induce *Bmp6*[9-11,27].

In several publications, an acute increase in Tf saturation directly activated hepcidin in hepatocytes without altering *Bmp6* mRNA[13,28,30], likely via Tfr2 stabilization[5]. Thus, the induction of *Bmp6* following holo-Tf injection in both $Tfrc^{Tek\text{-}Cre}$ and control $Tfrc^{fl/fl}$ mice (Figure 2.3G) was unexpected, even though variable responses in control animals may be related to differences in experimental design. Intravenous injection of 10 mg holo-Tf would lead to an input of 250 μM extra iron into the bloodstream, corresponding to a transient but dramatic elevation of total serum iron levels by ~7-fold. Excess iron was cleared after 18 h (Figure 2.3B), and presumably a significant fraction was taken up by liver cells; in fact, our scRNA-Seq data show prominent responses of macrophages/monocytes and stellate cells to holo-Tf injection (Figure 2.5F). We noted that holo-Tf also upregulated *Bmp2* mRNA (Figure 2.3H).

The quantitatively similar *Bmp6* and *Bmp2* mRNA induction in both genotypes (Figure 2.3G-H) argues against a direct effect of Tfr1-mediated uptake of excess Tf, since LSECs of $Tfrc^{Tek\text{-}Cre}$ mice are Tfr1-deficient. Nevertheless, a contribution of alternative uptake of Tf-bound iron by Tfr2 cannot be excluded, especially considering that *Tfrc* and *Tfr2* mRNAs are expressed at comparative levels in liver endothelial cells (Figure S.2.6D). Alternatively, iron-loaded Kupffer and/or stellate cells could secrete an activating signal. A potential candidate is ferritin, which can be released with its iron content by extracellular vesicles from iron-loaded cells[31] and can activate *Bmp6* expression when injected in mice[32]. Moreover, ferritin can also induce *Bmp6* mRNA in cultured primary LSECs[27]. Conceivably, uptake of iron-rich ferritin may offer a backup mechanism for iron sensing by LSECs.

The data from the holo-Tf injection experiment in figure 2.3 seem to exclude an iron sensing function of LSECs Tfr1. However, figure 2.2G shows that control $Tfrc^{fl/fl}$ but not $Tfrc^{Tek\text{-}Cre}$ mice can induce *Bmp6* following FAC injection, which implies a critical role of Tfr1. While the aim of FAC administration was to increase serum NTBI, this procedure also increased transferrin saturation. In fact, at the 5 h endpoint only high transferrin saturation was sustained and most NTBI was cleared. Thus, *Bmp6* induction in $Tfrc^{fl/fl}$ mice was apparently due to uptake of Tf-bound iron by LSECs Tfr1. Conversely, the failure of $Tfrc^{Tek\text{-}Cre}$ mice to induce *Bmp6* could be due to insufficient exposure of Tfr1-deficient LSECs to a sustained NTBI threshold.

The seemingly contradictory data from the holo-Tf and FAC injection experiments are consistent with a model where LSECs initially respond to an iron challenge by taking up Tf-bound iron via Tfr1, which provides an early signal for *Bmp6* induction. Conceivably, once transferrin saturation increases, uptake of emerging NTBI by LSECs becomes a dominant late stimulus for *Bmp6* induction, which could be enhanced by factors secreted from surrounding cells. As iron overload develops, expression of Tfr1 in LSECs and other liver cells is expected to be suppressed by post-transcriptional mechanisms[12].

Our overall data suggest that NTBI is a major driver of prolonged iron-dependent *Bmp6* induction under iron overload. It was detectable under experimental settings of acute dietary iron loading but not following holo-Tf injection. A notable difference in genetic responses of LSECs to HID intake vs holo-Tf injection (reflecting NTBI) was the activation of a battery of Nrf2 target genes, including *Bmp6* (Figure 2.6H). This indicates oxidative stress[33] and activation of iron pathways[34], and is also consistent with the known role of NTBI as inducer of oxidative stress in endothelial cells[35]. The strong induction of *Slc39a8* mRNA by acute iron loading corroborates earlier biochemical data in cell lines[36] and makes Zip8 a good candidate for NTBI uptake by LSECs. This response may not be homeostatic at the cellular level but could contribute to systemic iron homeostasis by upregulating *Bmp6* and *Hamp*. On the other hand, the induction of *Slc40a1*, *Fth* and *Ftl* in LSECs following acute dietary iron loading may contribute to resolution of iron-induced oxidative stress by promoting iron efflux via ferroportin, or iron storage within ferritin.

Our findings support the previously established role of Nrf2 as a Bmp6 regulator[9]. Moreover, they imply that the Nrf2 pathway is not the single contributor to Bmp6 induction, as dietary iron triggered further molecular responses. The most striking was the induction of Myc target genes (Figure 2.6G), primarily encoding ribosomal proteins and translation factors (Figure 2.6I). Considering that Myc regulates ribosomal biogenesis and protein synthesis[37], this finding indicates stimulatory effects of iron on global mRNA translation in LSECs.

The single-cell transcriptomics data reveal the landscape of gene expression profiles in all liver cell types following acute dietary iron loading or holo-Tf injection. Endothelial cells were the primary but not the only responders to iron challenges, and iron pathways were generally more sensitive to dietary iron vs holo-Tf (Figure 2.5F). Nevertheless, it should be emphasized that a single bolus of exogenous holo-Tf was cleared within the time frame of the experiment (Figure 2.3B), while dietary iron loading (and NTBI formation) was continuous.

Midzonal hepatocytes responded to dietary iron by inducing *Hamp* (Figure 2.7D) but also by a general genetic reprogramming of iron, Nrf2, ROS and OXPHOS pathways (Figures 5F, 7G-H). It appears that these cells are the primary producers of hepcidin and are thereby major regulators of systemic iron homeostasis. The zonation of *Hamp* mRNA in midzonal hepatocytes is consistent with earlier data[23,24].

In conclusion, we demonstrate that endothelial Tfr1 contributes to early iron-dependent induction of *Bmp6* by LSECs, especially under low iron conditions. Together with previous literature, our data suggest that under iron overload, LSECs mount transcriptional *Bmp6* induction in response to NTBI via an Nrf2-dependent oxidative stress mechanism. Our single-cell transcriptomics analysis uncovers Zip8 as a potential NTBI transporter. Furthermore, it implies the contribution of additional pathways, such as Myc-dependent ribosomal biogenesis and protein synthesis, to NTBI-induced activation of *Bmp6*.

2.7 Acknowledgments

E. Charlebois was supported by fellowships from the Natural Sciences and Engineering Research Council of Canada (NSERC) and subsequently the *Fonds de recherche du Québec – Santé* (FRQS). G. Cagnone was supported by the FRQS and Vision Research Health Network, which funded the Single Cell Academy. This work was funded by a grant from the Canadian Institutes of Health Research (CIHR; PJT-159730).

Author contributions: EC, CF and JP performed research and analyzed data; VL and VPL performed and supervised the generation of scRNA-Seq libraries; GC performed the bioinformatic analysis, produced figures related to scRNA-Seq analysis and wrote part of the Results and Methods sections; J-S J supervised the scRNA-Seq experiments and data analysis; KP designed and supervised the study and wrote the paper.

Conflicts of interest: The authors declare no competing financial interests.

2.8 References

1. Xiao X, Alfaro-Magallanes VM, Babitt JL. Bone morphogenic proteins in iron homeostasis. *Bone*. 2020;138:115495.
2. Nemeth E, Ganz T. Hepcidin-Ferroportin Interaction Controls Systemic Iron Homeostasis. *Int J Mol Sci*. 2021;22(12).
3. Billesbolle CB, Azumaya CM, Kretsch RC, et al. Structure of hepcidin-bound ferroportin reveals iron homeostatic mechanisms. *Nature*. 2020;586(7831):807-811.
4. Nemeth E, Tuttle MS, Powelson J, et al. Hepcidin regulates cellular iron efflux by binding to ferroportin and inducing its internalization. *Science*. 2004;306:2090-2093.
5. Worthen CA, Enns CA. The role of hepatic transferrin receptor 2 in the regulation of iron homeostasis in the body. *Front Pharmacol*. 2014;5:34.
6. Canali S, Zumbrennen-Bullough KB, Core AB, et al. Endothelial cells produce bone morphogenetic protein 6 required for iron homeostasis in mice. *Blood*. 2017;129(4):405-414.
7. Koch PS, Olsavszky V, Ulbrich F, et al. Angiocrine Bmp2 signaling in murine liver controls normal iron homeostasis. *Blood*. 2017;129(4):415-419.
8. Canali S, Wang CY, Zumbrennen-Bullough KB, Bayer A, Babitt JL. Bone morphogenetic protein 2 controls iron homeostasis in mice independent of Bmp6. *Am J Hematol*. 2017;92(11):1204-1213.
9. Lim PJ, Duarte TL, Arezes J, et al. Nrf2 controls iron homeostasis in haemochromatosis and thalassaemia via Bmp6 and hepcidin. *Nat Metab*. 2019;1(5):519-531.
10. Wang S, Chen C, Yu L, Mueller J, Rausch V, Mueller S. Bone morphogenetic protein 6-mediated crosstalk between endothelial cells and hepatocytes recapitulates the iron-sensing pathway in vitro. *J Biol Chem*. 2021;297(6):101378.
11. Noguchi T, Ikeda M, Murakami M, et al. Regulatory expression of bone morphogenetic protein 6 by 2,2'-dipyridyl. *Biochim Biophys Acta Gen Subj*. 2020;1864(8):129610.
12. Katsarou A, Pantopoulos K. Basics and principles of cellular and systemic iron homeostasis. *Mol Aspects Med*. 2020;75:100866.
13. Fillebeen C, Charlebois E, Wagner J, et al. Transferrin receptor 1 controls systemic iron homeostasis by fine-tuning hepcidin expression to hepatocellular iron load. *Blood*. 2019;133(4):344-355.
14. Kisanuki YY, Hammer RE, Miyazaki J, Williams SC, Richardson JA, Yanagisawa M. Tie2-Cre transgenic mice: a new model for endothelial cell-lineage analysis in vivo. *Dev Biol*. 2001;230(2):230-242.
15. Rautureau Y, Coelho SC, Fraulob-Aquino JC, et al. Inducible human endothelin-1 overexpression in endothelium raises blood pressure via endothelin type A receptors. *Hypertension*. 2015;66(2):347-355.
16. Fillebeen C, Wilkinson N, Charlebois E, Katsarou A, Wagner J, Pantopoulos K. Hepcidin-mediated hypoferremic response to acute inflammation requires a threshold of Bmp6/Hjv/Smad signaling. *Blood*. 2018;132(17):1829-1841.
17. Katsarou A, Gkouvatsos K, Fillebeen C, Pantopoulos K. Tissue-Specific Regulation of Ferroportin in Wild-Type and Hjv-/- Mice Following Dietary Iron Manipulations. *Hepatol Commun*. 2021;5(12):2139-2150.
18. Daba A, Gkouvatsos K, Sebastiani G, Pantopoulos K. Differences in activation of mouse hepcidin by dietary iron and parenterally administered iron dextran: compartmentalization is critical for iron sensing. *J Mol Med (Berl)*. 2013;91:95-102.

19. Craven CM, Alexander J, Eldridge M, Kushner JP, Bernstein S, Kaplan J. Tissue distribution and clearance kinetics of non-transferrin-bound iron in the hypotransferrinemic mouse: a rodent model for hemochromatosis. *Proc Natl Acad Sci U S A*. 1987;84(10):3457-3461.
20. Skinnider MA, Squair JW, Kathe C, et al. Cell type prioritization in single-cell data. *Nat Biotechnol*. 2021;39(1):30-34.
21. Halpern KB, Shenhav R, Massalha H, et al. Paired-cell sequencing enables spatial gene expression mapping of liver endothelial cells. *Nat Biotechnol*. 2018;36(10):962-970.
22. Colucci S, Altamura S, Marques O, et al. Liver Sinusoidal Endothelial Cells Suppress Bone Morphogenetic Protein 2 Production in Response to TGFbeta Pathway Activation. *Hepatology*. 2021;74(4):2186-2200.
23. Ben-Moshe S, Shapira Y, Moor AE, et al. Spatial sorting enables comprehensive characterization of liver zonation. *Nat Metab*. 2019;1(9):899-911.
24. Halpern KB, Shenhav R, Matcovitch-Natan O, et al. Single-cell spatial reconstruction reveals global division of labour in the mammalian liver. *Nature*. 2017;542(7641):352-356.
25. Payne S, De Val S, Neal A. Endothelial-Specific Cre Mouse Models. *Arterioscler Thromb Vasc Biol*. 2018;38(11):2550-2561.
26. Levy JE, Jin O, Fujiwara Y, Kuo F, Andrews NC. Transferrin receptor is necessary for development of erythrocytes and the nervous system. *Nat Genet*. 1999;21:396-399.
27. Fisher AL, Wang CY, Xu Y, et al. Functional role of endothelial transferrin receptor 1 in iron sensing and homeostasis. *Am J Hematol*. 2022;97(12):1548-1559.
28. Corradini E, Meynard D, Wu Q, et al. Serum and liver iron differently regulate the bone morphogenetic protein 6 (BMP6)-SMAD signaling pathway in mice. *Hepatology*. 2011;54(1):273-284.
29. Jenkitkasemwong S, Wang CY, Coffey R, et al. SLC39A14 Is Required for the Development of Hepatocellular Iron Overload in Murine Models of Hereditary Hemochromatosis. *Cell Metab*. 2015;22(1):138-150.
30. Zhang Z, Guo X, Herrera C, et al. Bmp6 expression can be regulated independently of liver iron in mice. *PLoS One*. 2014;9(1):e84906.
31. Yanatori I, Richardson DR, Dhekne HS, Toyokuni S, Kishi F. CD63 is regulated by iron via the IRE-IRP system and is important for ferritin secretion by extracellular vesicles. *Blood*. 2021;138(16):1490-1503.
32. Feng Q, Migas MC, Waheed A, Britton RS, Fleming RE. Ferritin upregulates hepatic expression of bone morphogenetic protein 6 and hepcidin in mice. *Am J Physiol Gastrointest Liver Physiol*. 2012;302(12):G1397-1404.
33. Tonelli C, Chio IIC, Tuveson DA. Transcriptional Regulation by Nrf2. *Antioxid Redox Signal*. 2018;29(17):1727-1745.
34. Kerins MJ, Ooi A. The Roles of NRF2 in Modulating Cellular Iron Homeostasis. *Antioxid Redox Signal*. 2018;29(17):1756-1773.
35. Vinchi F. Non-Transferrin-Bound Iron in the Spotlight: Novel Mechanistic Insights into the Vasculotoxic and Atherosclerotic Effect of Iron. *Antioxid Redox Signal*. 2021;35(6):387-414.
36. Wang CY, Jenkitkasemwong S, Duarte S, et al. ZIP8 is an iron and zinc transporter whose cell-surface expression is up-regulated by cellular iron loading. *J Biol Chem*. 2012;287(41):34032-34043.

37. van Riggelen J, Yetil A, Felsher DW. MYC as a regulator of ribosome biogenesis and protein synthesis. *Nat Rev Cancer*. 2010;10(4):301-309.

2.9 Figures

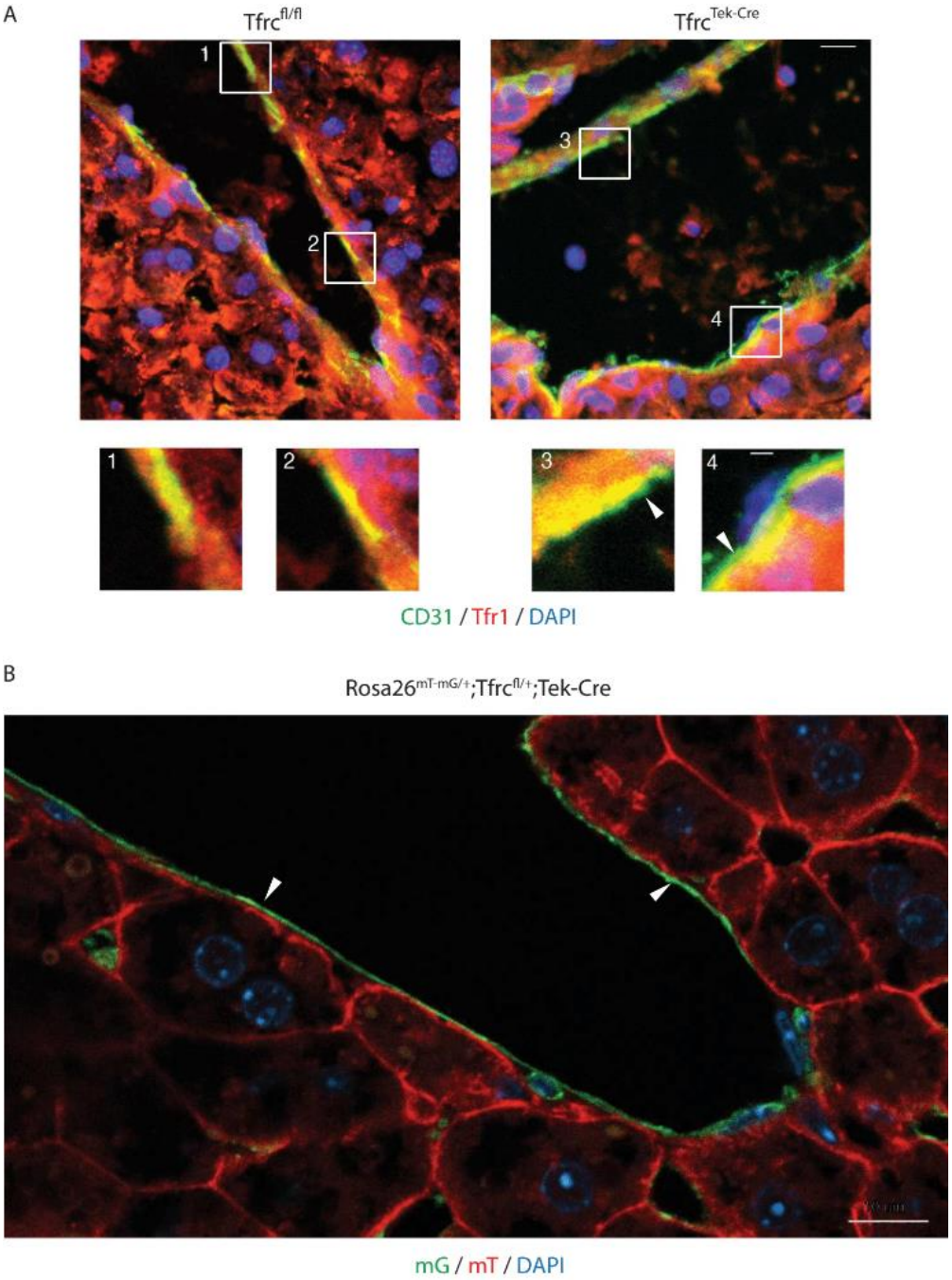

Figure 2.1: Validation of LSECs Tfr1 knockout in the Tfrc$^{Tek\text{-}Cre}$ mouse model.
(A) Frozen liver slices from control Tfrc$^{fl/fl}$ (left) or Tfrc$^{Tek\text{-}Cre}$ mice (right) were processed for immunofluorescence and stained for Tfr1 using a Cy3-labeled secondary antibody (red) and for CD31 using an Alexa488-labeled secondary antibody (green). Overlapping areas of Tfr1 and CD31 expression are shown in yellow. Nuclei were visualized using DAPI staining (blue). Areas in highlighted rectangles are shown in higher magnification at the bottom of the images. Arrows indicate exclusive CD31 expression in the LSEC lining. Scale bar 10 µm (and 2 µm in highlighted rectangles). (B) Frozen liver slices from a Rosa26$^{mT\text{-}mG/+}$;Tfrc$^{fl/+}$;Tek-Cre reporter mouse were processed for confocal microscopy imaging for expression of mT (red) and mG (green); the latter emerges following Cre-mediated recombination. Arrows indicate the LSEC lining. Scale bars 10 µm.

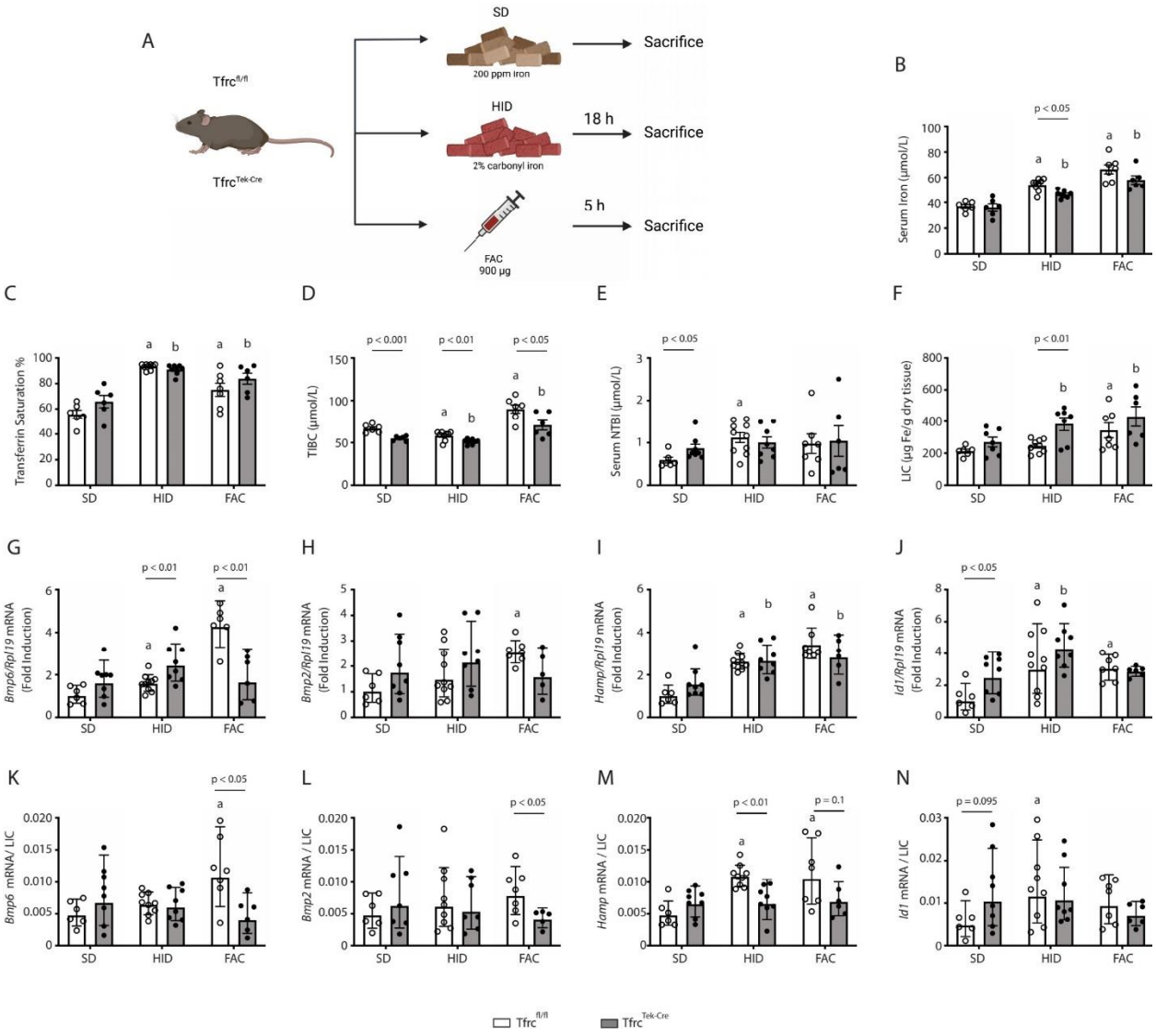

Figure 2.2: Tfrc$^{Tek\text{-}Cre}$ mice express physiological levels of *Bmp6* and *Hamp* mRNAs and induce them in response to high dietary iron but fail to induce *Bmp6* mRNA following FAC injection.

(A) Schematic experimental outline. All mice were 7-8 weeks old males (n=6-10 per group). At the endpoint, the animals were sacrificed; serum was prepared, and livers were harvested for biochemical analysis. (B) Serum iron; (C) transferrin (Tf) saturation; (D) total iron binding capacity (TIBC); (E) non-transferrin bound iron (NTBI); (F) liver iron content (LIC); (G-J) qPCR analysis of mRNAs encoding liver Bmp6, Bmp2, Hamp and Id1, respectively; (K-N) mRNA/LIC ratios for *Bmp6*, *Bmp2*, *Hamp* and *Id1*, respectively. Serum data (B-E) and LIC (F) are represented as mean ± SEM, while gene expression data (G-N) are represented as geometric mean ± geometric standard deviation. Statistical differences ($p<0.05$) were determined using Student's t test on original data (B-E) or log-transformed gene expression data (G-N). Statistically significant differences from Tfrc$^{fl/fl}$ and Tfrc$^{Tek\text{-}Cre}$ mice on standard diet are represented as a or b, respectively. Illustration in A was made with Biorender.com.

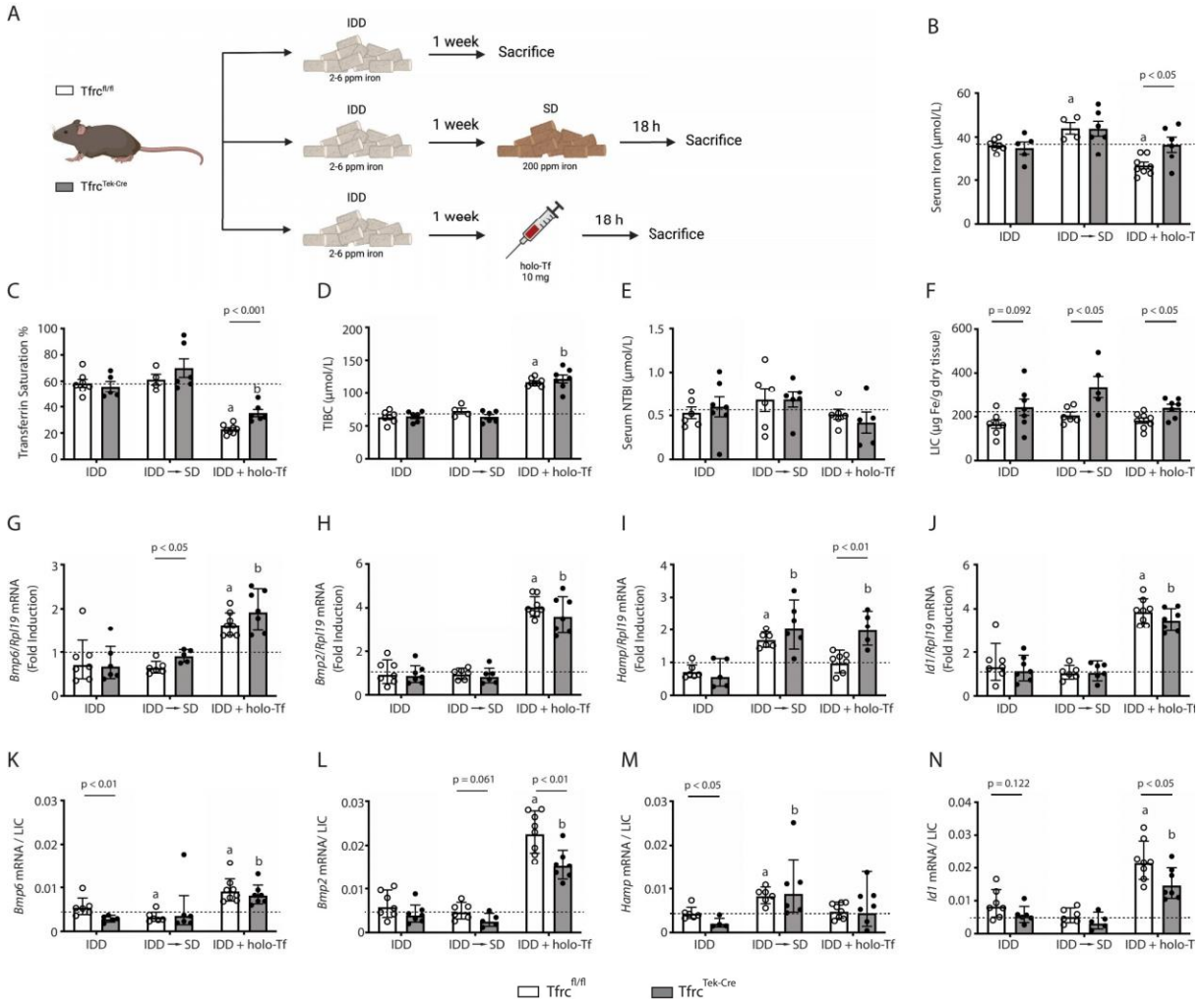

Figure 2.3: Tfrc$^{Tek\text{-}Cre}$ mice on iron-deficient diet have increased liver iron content, express relatively low *Bmp6* and *Hamp* mRNA levels and induce them in response to dietary iron or holo-Tf.

(A) Schematic experimental outline. All mice were 7-8 weeks old males (n=6-10 per group). At the endpoint, the animals were sacrificed; serum was prepared, and livers were harvested for biochemical analysis. (B) Serum iron; (C) transferrin (Tf) saturation; (D) total iron binding capacity (TIBC); (E) non-transferrin bound iron (NTBI); (F) liver iron content (LIC); (G-J) qPCR analysis of mRNAs encoding liver Bmp6, Bmp2, Hamp and Id1, respectively; (K-N) mRNA/LIC ratios for *Bmp6*, *Bmp2*, *Hamp* and *Id1*, respectively. Serum data (B-E) and LIC (F) are represented as mean ± SEM, while gene expression data (G-N) are represented as geometric mean ± geometric standard deviation. Statistical differences ($p<0.05$) were determined using Student's t test on original data (B-E) or log-transformed gene expression data (G-N). Statistically significant differences from Tfrc$^{fl/fl}$ and Tfrc$^{Tek\text{-}Cre}$ mice on standard diet are represented as a or b, respectively. Dotted lines indicate average values obtained from age-matched male Tfrc$^{fl/fl}$ mice on standard diet (n=6). Illustration in A was made with Biorender.com.

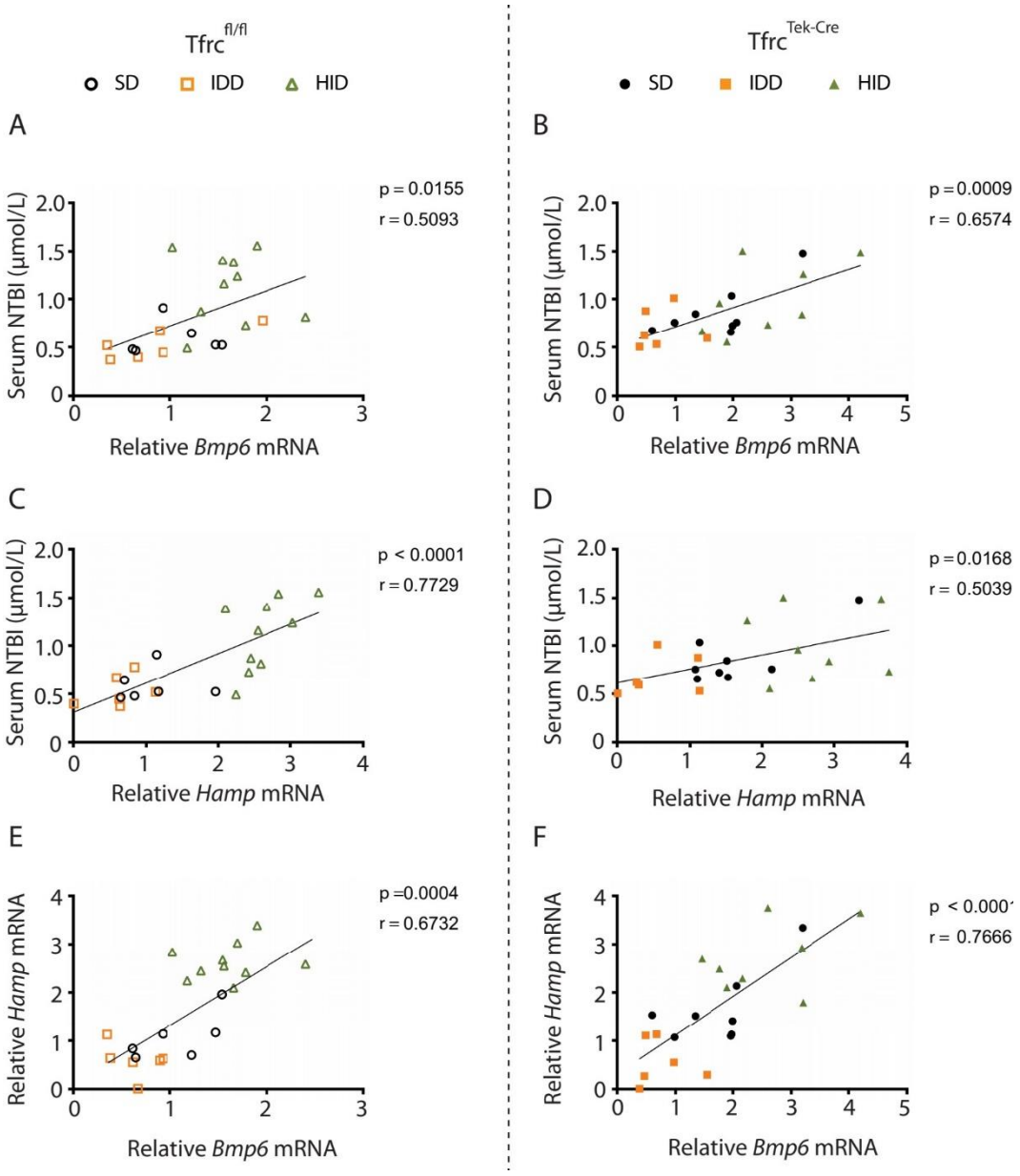

Figure 2.4: Expression of *Bmp6* and *Hamp* mRNAs positively correlates with serum NTBI in both Tfrc$^{fl/fl}$ and Tfrc$^{Tek\text{-}Cre}$ mice.

Pearson correlation analysis of NTBI vs *Bmp6* mRNA (A-B); NTBI vs *Hamp* mRNA (C-D); and *Hamp* mRNA vs *Bmp6* mRNA (E-F). Data are from the experiments shown in Figures 2 and 3 with Tfrc$^{fl/fl}$ and Tfrc$^{Tek\text{-}Cre}$ mice kept on standard diet (SD), exposed to 2% carbonyl iron diet (HID) for 18 hours, or placed on iron-deficient diet (IDD) for 1 week. p values and Pearson's r coefficients are provided for each graph.

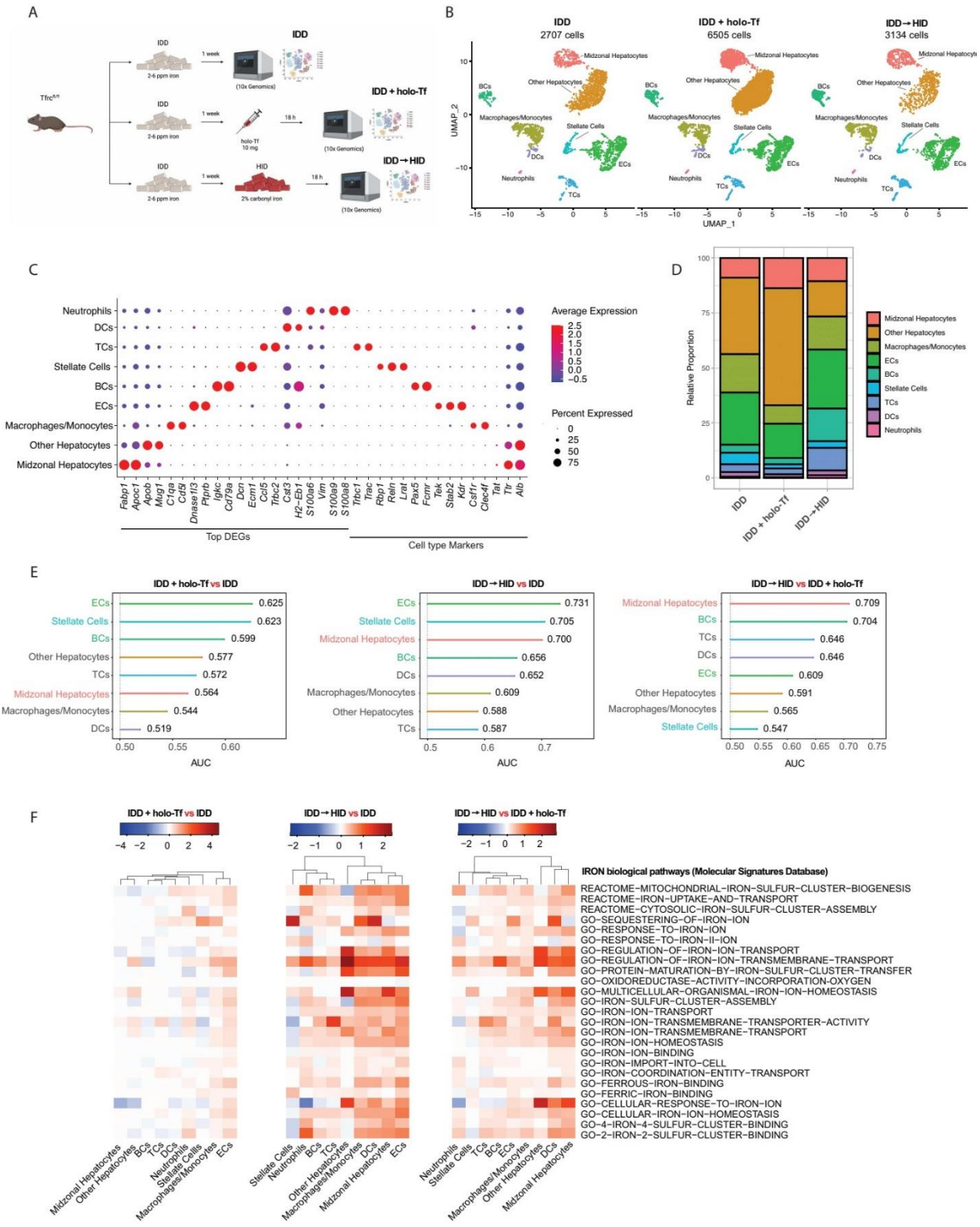
A
IDD
IDD + holo-Tf
IDD→HID
Tfrc^fl/fl
2-6 ppm iron
1 week
(10x Genomics)
holo-Tf 10 mg
18 h
HID
2% carbonyl iron
B
IDD
2707 cells
IDD + holo-Tf
6505 cells
IDD→HID
3134 cells
Midzonal Hepatocytes
Other Hepatocytes
BCs
Macrophages/Monocytes
Stellate Cells
DCs
ECs
Neutrophils
TCs
UMAP_1
UMAP_2
C
Average Expression
Percent Expressed
Top DEGs
Cell type Markers
Fabp1 Apoc1 Apob Mug1 C1qa Cd5l Dnase1l3 Ptprb Igkc Cd79a Dcn Ecm1 Col5 Tfbc2 Cst3 H2−Eb1 S100a6 Vim S100a9 S100a8 Tfrc1 Trac Rbp1 Reln Lrat Pax5 Fcmr Tek Stab2 Kdr Csf1r Clec4f Tat Ttr Alb
D
Relative Proportion
IDD
IDD + holo-Tf
IDD→HID
E
IDD + holo-Tf vs IDD
ECs 0.625
Stellate Cells 0.623
BCs 0.599
Other Hepatocytes 0.577
TCs 0.572
Midzonal Hepatocytes 0.564
Macrophages/Monocytes 0.544
DCs 0.519
IDD→HID vs IDD
ECs 0.731
Stellate Cells 0.705
Midzonal Hepatocytes 0.700
BCs 0.656
DCs 0.652
Macrophages/Monocytes 0.609
Other Hepatocytes 0.588
TCs 0.587
IDD→HID vs IDD + holo-Tf
Midzonal Hepatocytes 0.709
BCs 0.704
TCs 0.646
DCs 0.646
ECs 0.609
Other Hepatocytes 0.591
Macrophages/Monocytes 0.565
Stellate Cells 0.547
AUC
F
IRON biological pathways (Molecular Signatures Database)
REACTOME−MITOCHONDRIAL−IRON−SULFUR−CLUSTER−BIOGENESIS
REACTOME−IRON−UPTAKE−AND−TRANSPORT
REACTOME−CYTOSOLIC−IRON−SULFUR−CLUSTER−ASSEMBLY
GO−SEQUESTERING−OF−IRON−ION
GO−RESPONSE−TO−IRON−ION
GO−RESPONSE−TO−IRON−II−ION
GO−REGULATION−OF−IRON−ION−TRANSPORT
GO−REGULATION−OF−IRON−ION−TRANSMEMBRANE−TRANSPORT
GO−PROTEIN−MATURATION−BY−IRON−SULFUR−CLUSTER−TRANSFER
GO−OXIDOREDUCTASE−ACTIVITY−INCORPORATION−OXYGEN
GO−MULTICELLULAR−ORGANISMAL−IRON−ION−HOMEOSTASIS
GO−IRON−SULFUR−CLUSTER−ASSEMBLY
GO−IRON−ION−TRANSPORT
GO−IRON−ION−TRANSMEMBRANE−TRANSPORTER−ACTIVITY
GO−IRON−ION−TRANSMEMBRANE−TRANSPORT
GO−IRON−ION−HOMEOSTASIS
GO−IRON−ION−BINDING
GO−IRON−IMPORT−INTO−CELL
GO−IRON−COORDINATION−ENTITY−TRANSPORT
GO−FERROUS−IRON−BINDING
GO−FERRIC−IRON−BINDING
GO−CELLULAR−RESPONSE−TO−IRON−ION
GO−CELLULAR−IRON−ION−HOMEOSTASIS
GO−4−IRON−4−SULFUR−CLUSTER−BINDING
GO−2−IRON−2−SULFUR−CLUSTER−BINDING

Figure 2.5: scRNA-Seq identifies endothelial cells and midzonal hepatocytes as the most responsive cell types to acute dietary iron loading or holo-Tf injection.
(A) Schematic experimental outline of scRNA-Seq experiment. All mice were 7-8 weeks old male $Tfrc^{fl/fl}$ (n=1 per group). (B) UMAP plot of most common liver cell types. (C) Dot plot annotation based on differentially expressed genes and previously published cell type markers. (D) Relative proportion of each liver cell population obtained in the experimental settings. (E) Cell type prioritization (lollipop plot) based on Augur-calculated AUC scores for each comparison (IDD vs IDD+holo-Tf, IDD vs IDD→HID, and IDD→HID vs IDD+holo-Tf). (F) Heatmaps with Log2FC (log2 fold changes) of Gene Set Variation Analysis (GSVA) score for iron related biological pathways from the Molecular Signatures Database across cell types identified by scRNA-Seq, highlighting most responsive cell types to different iron manipulations.

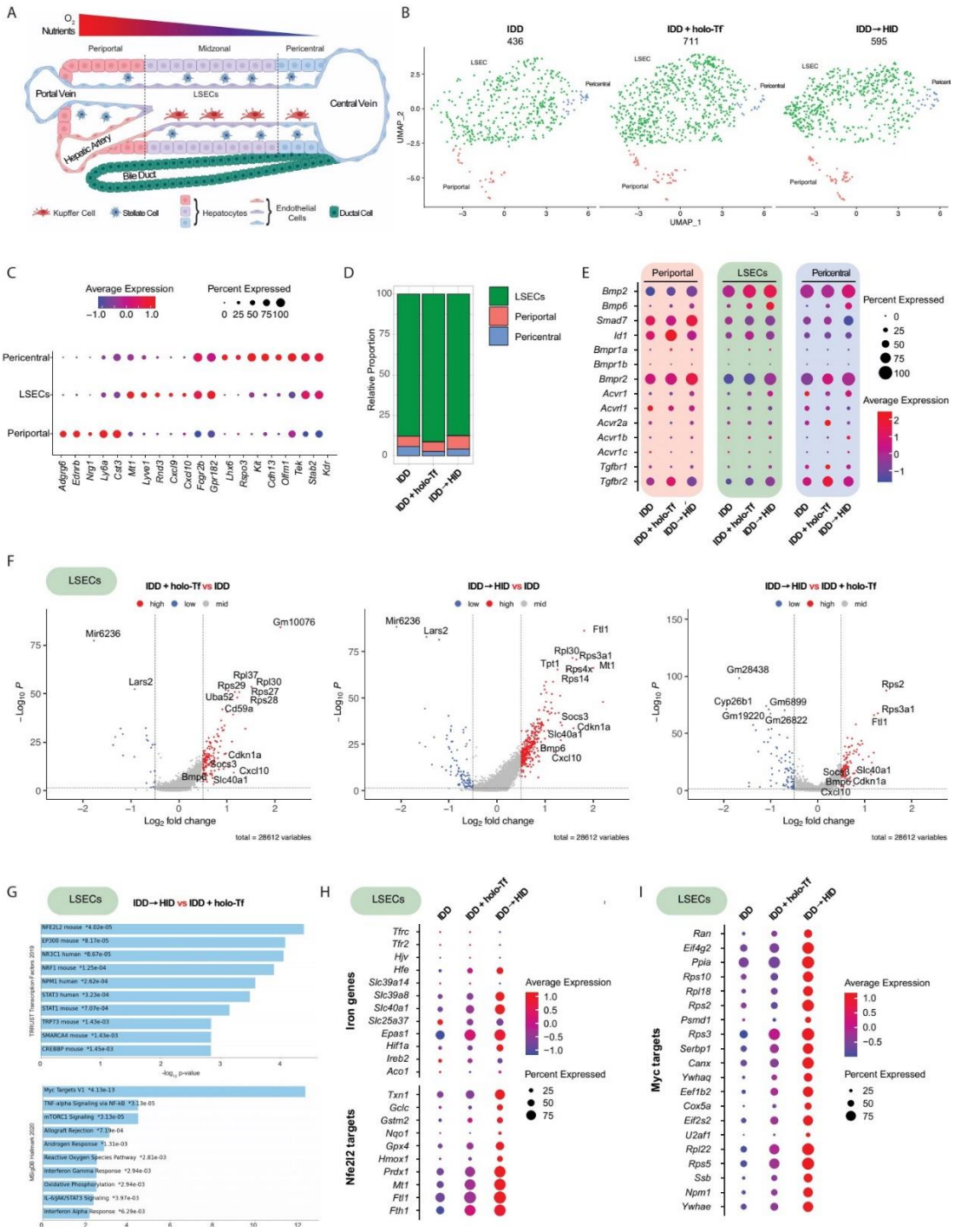

Figure 2.6: Acute dietary iron loading triggers activation of Nfe2l2 and Myc target genes in capillary LSECs. (A) Schematic representation of liver cell architecture. (B-D) The portal and central vein, the artery and the sinusoids of the liver contain distinct endothelial cell (EC) subtypes as identified by scRNA-Seq (UMAP plot, B), which can be annotated based on differentially expressed genes (dot plot, C); with their relative cell subtype proportion in each experimental setting (D). Expression of genes involved in Bmp and Tgf signalling in endothelial cell subtypes in each experimental condition (dot plot, E) and differentially expressed genes (DEGs) in capillary ECs between diet conditions (Volcano plot, F). (G-I) DEGs in capillary LSECs between IDD+holo-Tf and IDD→HID were enriched in the Nfe2l2 and Myc pathways (EnrichR, G), also represented by dot plot (H and I). Illustration in A was made with Biorender.com.

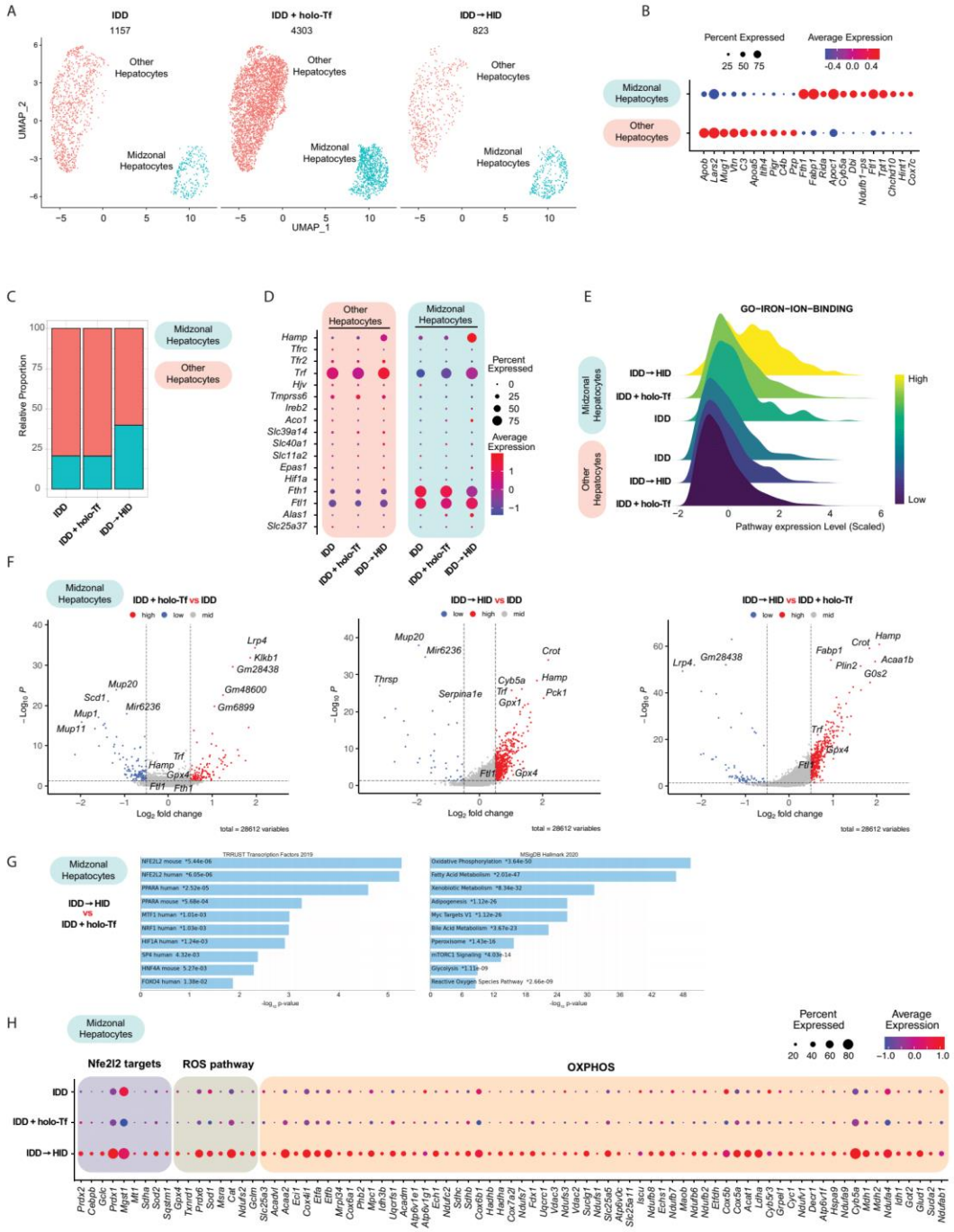

Figure 2.7: Acute dietary iron loading up-regulates Nfe2l2 (Nrf2), ROS and OXPHOS metabolic genes in midzonal hepatocytes.

(A-B) Midzonal hepatocytes are separated from other hepatocyte populations identified by scRNA-Seq (UMAP plot, A), and show a specific gene expression profile (dot plot, B). (C) Relative proportion of midzonal and other hepatocyte subtypes in each experimental condition. (D-E) Expression of genes involved in iron signalling (dot plot, D) and GSVA score for the GO Iron Ion binding pathways (Ridge plot, E) in midzonal and other hepatocyte subtypes in each experimental condition. (F) Volcano plot with differentially expressed genes (DEGs) in midzonal hepatocytes under each experimental condition. (G-H) DEGs in midzonal hepatocytes were enriched in Nfe2l2, ROS and OXPHOS pathways (EnrichR, G), also represented by dot plot (H).

2.10 Supplementary Methods

2.10.1 Immunohistochemistry.

OCT-frozen liver slices (30 μm) were stained using primary antibodies directed against mouse Tfr1 (Invitrogen) or rat CD31 (Novus), and secondary antibodies conjugated to Cy3 (Tfr1) or Alexa488 (CD31). Nuclei were visualized with DAPI. Images were taken with a Zeiss LSM 780 confocal microscope and a Planapochromat 20X 0.8 NA objective. The 488 nm laser line was used to visualize Alexa488 (green, CD31). 568 nm was used to visualize Cy3 (red, transferrin receptor) and DAPI (blue) was visualized using the 405 nm line.

2.10.2 Validation of Cre recombination specificity in reporter mice.

Rosa26$^{mT\text{-}mG/+}$;Tfrc$^{fl/+}$;Tek-Cre mice were anesthetized by intraperitoneal (ip) injection of with 300 to 375 mg/kg avertin. After confirming depth of anesthesia by reflex in hind footpads, the mice were injected ip with heparin (100 USP units). The animals were then perfused through the left ventricle at a constant pressure of 100 mm Hg for 5 minutes with phosphate buffered saline (PBS) to remove the blood, followed by 15 min perfusion with 4% paraformaldehyde (PFA). Liver tissue segments were collected in 4% PFA and incubated for 24 h with gentle agitation at 4°C. Subsequently, the tissues were dehydrated by incubation in 30% sucrose in PBS for 24 h with gentle agitation at 4°C. Tissues were then embedded in VWR Clear Frozen Section Compound (VWR international, Edmonton, Alberta, Canada) and stored at −80°C until use. Expression of membrane-targeted tandem dimer tomato (mT) and membrane-targeted enhanced green fluorescent protein (mG) was assessed by using a Zeiss LSM 800 confocal microscope and a Planapochromat 40X 0.8 NA objective. The 561 nm, 488 nm and 405 nm laser lines were used to visualize mT (red), mG (green) and DAPI (blue), respectively.

2.10.3 Hematological analysis and serum biochemistry.

Blood was collected via cardiac puncture. Hematological parameters were determined with the Scil Vet-ABC hematology analyzer. Serum was prepared by utilizing micro Z-gel tubes with clotting activator (Sarstedt) and was snap-frozen at −80°C. Serum iron and total iron binding capacity (TIBC) were measured on a Roche Hitachi 917 Chemistry Analyzer. Transferrin saturation was calculated from the ratio of serum iron/ TIBC.

2.10.4 NTBI quantification.

NTBI was measured by adapting the method developed by Esposito *et al*[1]. Iron samples of known concentration were created by mixing 70 mM nitrilotriacetate (NTA) (pH 7.0) with 20 mM ferrous ammonium sulfate. Fe^{2+} was allowed to oxidize to Fe^{3+} in ambient air for at least 30 min and then the solution was diluted to 0.2 mM before further serial dilutions to create a ladder. 5 µl of ladder was loaded in a 96-well plate containing 195 µl plasma-like medium with or without 100 µM deferiprone. The composition of the plasma-like medium was: 40 mg/ml bovine serum albumin, 1.2 mM sodium phosphate dibasic, 120 µM sodium citrate, 10 mM sodium bicarbonate in iron-free HEPES-buffered saline (HEPES 20 mM, NaCl 150 mM, treated with Chelex-100 chelating resin [Bio-Rad, Hercules, CA], 0.5 mM NTA, 40 µM ascorbic acid, 50 µM dihydrorhodamine, pH 7.4). 5 µl of sample was loaded in a 96-well plate containing 195 µl of iron-free HEPES-buffered saline with or without 100 µM deferiprone. Microplates were read every 2 minutes at 37°C over 40 min at 485/520 nm (ex/em). Final NTBI was calculated by comparing the oxidation rate of DHR in the presence or absence of the strong chelator deferiprone.

2.10.5 Real-time PCR (qPCR).

Total liver RNA was extracted with the RNeasy kit (Qiagen) and cDNA was synthesized with the OneScript® Plus cDNA Synthesis Kit (Applied Biological Materials Inc.). Gene-specific primers

pairs (Table S.2.4) were validated by dissociation curve analysis and demonstrated amplification efficiency between 90-110 %. SYBR Green (Bioline) and primers were used to amplify products under following cycling conditions: initial denaturation 95°C 10 min, 40 cycles of 95°C 5 s, 58°C 30 s, 72°C 10 s, and final cycle melt analysis between 58°-95°C. Relative mRNA expression was calculated by the $2^{-\Delta\Delta Ct}$ method[2]. Data were normalized to murine ribosomal protein L19 (*Rpl19*) and reported as fold increases compared to samples from control $Tfrc^{fl/fl}$ mice on standard diet (SD).

2.10.6 Quantification of tissue iron.

Tissue non-heme iron was quantified by the ferrozine assay[3].

2.10.7 Statistical analysis of hematological and biochemical data.

The Prism GraphPad software (version 9.3.1) was used for statistics and Pearson's correlation analysis. Pairwise comparisons were performed by the unpaired Student's t test. A probability value $p<0.05$ was considered statistically significant.

2.10.8 Liver cell isolation for scRNA-Seq.

Anaesthetized mice were perfused as previously described[4] with a few modifications[5]. Calcium-free Hank's Balanced Salt Solution (HBSS) buffer containing 0.2 mg/ml EDTA was used to perfuse the liver followed by sequential perfusion with calcium-containing HBSS and 0.5 mg/ml Collagenase D (Roche) for 7 minutes. The liver was excised and minced in 5 ml warm perfusion buffer before addition of 0.5 mg/ml pronase (Sigma; P5147) and 0.1 mg/ml DNase I (Roche) in a total volume of 50 ml. *Ex vivo* digestion was performed at 37°C for 20 min before filtering through a 70 μM filter. Cells were pelleted and collected by spinning at 580 g/10 min/4°C and resuspended in 25 ml DMEM. A series of 4 spins at 50 g/2 min/4°C were performed to pellet hepatocytes and collect non-parenchymal cells (NPCs) in supernatant. NPCs were then pelleted at 580 g/10

min/4°C and treated with RBC lysis buffer (eBioscience™) according to the manufacturer's instructions before resuspension in 5 ml sequencing buffer (phosphate-buffered saline containing 0.04% bovine serum albumin). Hepatocyte viability selection was performed as described[6] on the hepatocyte pellet and cells were resuspended in sequencing buffer. A final mixture of cells was made by mixing 5% of the hepatocyte suspension with 95% of the NPC suspension before adjusting the cell concentration to 4000 cells/μl.

2.10.9 scRNA-Seq analysis.

Single-cell suspensions were processed on the 10X scRNA-Seq platform (Chromium Next GEM Single Cell 3' GEM Kit v3.1) and resulting, quality-controlled libraries were sequenced on Illumina Novaseq S1. Count matrices produced with kb-python[7] (version 0.24.4, Python 3.7.4, reference genome GRCm38) were analyzed individually using Seurat V4[8]. Cells expressing between 100 and 6,000 genes, less than 10,000 total transcripts and less than 25% of mitochondrially-encoded transcripts were retained for further analysis. Briefly, counts were normalized with SCTransform function (regression on nFeature_RNA and percent.mt) then the top 20 principal components based on high variable genes (3000) were used for dimensionality reduction (2D) using Uniform Manifold Approximation and Projection[9]. Graph-based clustering was then performed on reduced UMAP dimensions. Individual datasets were integrated together based on SCT normalized counts followed by UMAP dimensionality reduction on integrated data. Subclustering was done on integrated data as well. Differential gene expression analysis, Gene Set Variation analysis[10] and cell prioritization with Augur[11] was performed on normalised count (NormalizeData). Immune cell subtypes were annotated based on the Immunological Genome Project (ImmGen) database using SingleR[12] which assigned cell identity by correlating single-cell expression profiles to reference data of pure cell types from microarray or RNAseq. Scaled counts

(ScaleData with regression on nFeature_RNA and percent.mt) were used for visualisation purpose. Data visualization in R 4.0.0 (R Core Team 2021, https://www.R-project.org) involved Seurat plotting functions as well as EnhancedVolcano[13] and heatmap.2 functions (https://CRAN.R-project.org/package=gplots). Pathway enrichment analysis from lists of differentially expressed genes was done using EnrichR[14]. Differentially expressed genes/pathways are considered for log2FC > 0.5 and P value<0.05. Heatmaps represent log2FC for the comparisons labeled on top of the graph. MsigDB V7.1 (H, C2 and C5) was used as repository to screen for biological gene sets (12457 gene sets passed the GSVA filter, i.e contained genes detected in our scRNA-Seq).

2.10.10 Supplementary method references

1. Esposito BP, Breuer W, Sirankapracha P, Pootrakul P, Hershko C, Cabantchik ZI. Labile plasma iron in iron overload: redox activity and susceptibility to chelation. *Blood*. 2003;102(7):2670-2677.
2. Livak KJ, Schmittgen TD. Analysis of Relative Gene Expression Data Using Real-Time Quantitative PCR and the 2−ΔΔCT Method. *Methods*. 2001;25(4):402-408.
3. Daba A, Gkouvatsos K, Sebastiani G, Pantopoulos K. Differences in activation of mouse hepcidin by dietary iron and parenterally administered iron dextran: compartmentalization is critical for iron sensing. *J Mol Med (Berl)*. 2013;91:95-102.
4. Fillebeen C, Wilkinson N, Charlebois E, Katsarou A, Wagner J, Pantopoulos K. Hepcidin-mediated hypoferremic response to acute inflammation requires a threshold of Bmp6/Hjv/Smad signaling. *Blood*. 2018;132(17):1829-1841.
5. Xiong X, Kuang H, Ansari S, et al. Landscape of Intercellular Crosstalk in Healthy and NASH Liver Revealed by Single-Cell Secretome Gene Analysis. *Mol Cell*. 2019;75(3):644-660.e645.
6. Kreamer BL, Staecker JL, Sawada N, Sattler GL, Hsia MTS, Pitot HC. Use of a low-speed, iso-density percoll centrifugation method to increase the viability of isolated rat hepatocyte preparations. *In Vitro Cellular & Developmental Biology*. 1986;22(4):201-211.
7. Melsted P, Booeshaghi AS, Liu L, et al. Modular, efficient and constant-memory single-cell RNA-seq preprocessing. *Nat Biotechnol*. 2021;39(7):813-818.
8. Hao Y, Hao S, Andersen-Nissen E, et al. Integrated analysis of multimodal single-cell data. *Cell*. 2021;184(13):3573-3587 e3529.
9. Becht E, McInnes L, Healy J, et al. Dimensionality reduction for visualizing single-cell data using UMAP. *Nat Biotechnol*. 2018.
10. Hanzelmann S, Castelo R, Guinney J. GSVA: gene set variation analysis for microarray and RNA-seq data. *BMC Bioinformatics*. 2013;14:7.
11. Skinnider MA, Squair JW, Kathe C, et al. Cell type prioritization in single-cell data. *Nat Biotechnol*. 2021;39(1):30-34.

12. Aran D, Looney AP, Liu L, et al. Reference-based analysis of lung single-cell sequencing reveals a transitional profibrotic macrophage. *Nat Immunol*. 2019;20(2):163-172.
13. Blighe K, Rana S, Lewis MC. EnhancedVolcano: Publication-ready volcano plots with enhanced colouring and labeling. 2021;R package version 1.12.0:Available online: https://github.com/kevinblighe/EnhancedVolcano.
14. Kuleshov MV, Jones MR, Rouillard AD, et al. Enrichr: a comprehensive gene set enrichment analysis web server 2016 update. *Nucleic Acids Res*. 2016;44(W1):W90-97.

2.11 Supplementary Figures

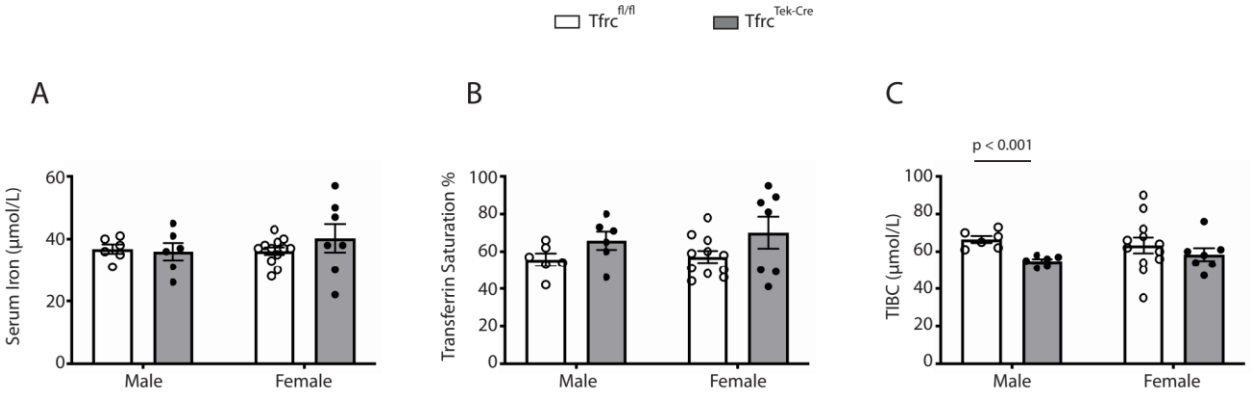

Figure S.2.1: Hematological parameters in male and female Tfrc$^{fl/fl}$ and Tfrc$^{Tek\text{-}Cre}$ mice.
7-8 weeks old male or female Tfrc$^{fl/fl}$ and Tfrc$^{Tek\text{-}Cre}$ mice (n=6-12 per group) on standard diet were sacrificed. Serum was collected for analysis of: (A) Serum iron; (B) transferrin saturation; and (C) total iron binding capacity (TIBC). Statistical differences ($p<0.05$) were determined by using Student's t test.

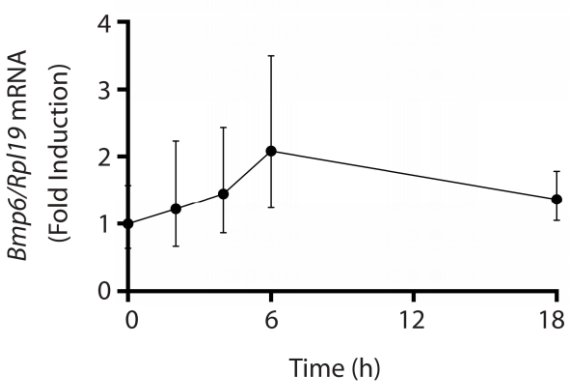

Figure S.2.2: Kinetics of *Bmp6* induction in response to ferric ammonium citrate (FAC) injection.
In this preliminary experiment, 7-8 weeks old male $Tfrc^{fl/fl}$ mice (n=3 per time point) were injected intraperitoneally with 0.9 mg FAC. The animals were sacrificed at the indicated time points and liver *Bmp6* mRNA levels were quantified by qPCR. Under these experimental conditions, maximal *Bmp6* induction was observed 6 h following FAC injection. In the final experiment shown in Figure 2.2, FAC was injected intravenously. We reasoned that direct administration of FAC to the bloodstream via the intravenous route might slightly shift the peak of *Bmp6* induction earlier. Therefore, we chose the 5 h time point as optimal.

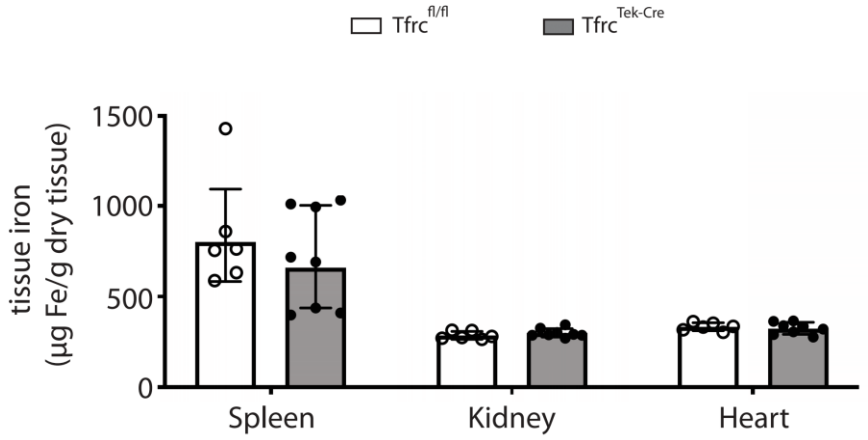

Figure S.2.3: Iron quantification in the spleen, kidney and heart.
7-8 weeks old male $Tfrc^{fl/fl}$ and $Tfrc^{Tek\text{-}Cre}$ mice (n=6-10 mice per group) on standard diet were sacrificed. Spleens, kidneys, and hearts were harvested and used to measure tissue iron content by the ferrozine assay.

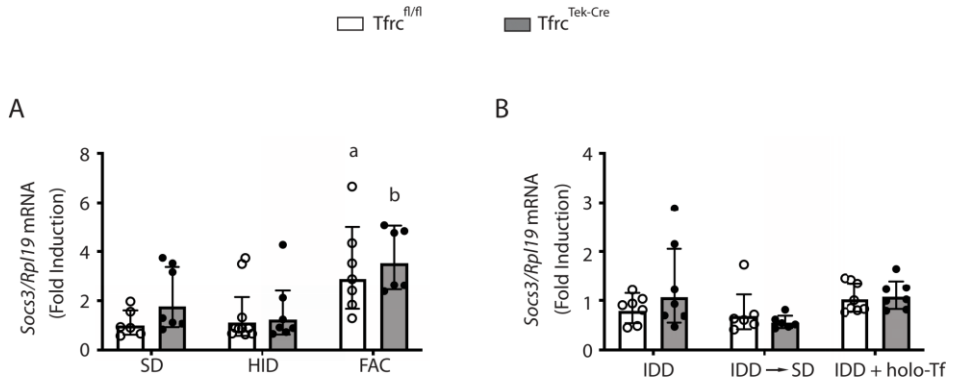

Figure S.2.4: Iron manipulations do not affect expression of the inflammatory marker *Socs3* mRNA in the liver of Tfrc$^{fl/fl}$ or Tfrc$^{Tek\text{-}Cre}$ mice.

Socs3 mRNA expression was quantified using livers from mice described in Figure 2.2 (A) or Figure 2.3 (B). Statistically significant differences ($p<0.05$) from Tfrc$^{Tek\text{-}Cre}$ mice on standard diet are represented as b.

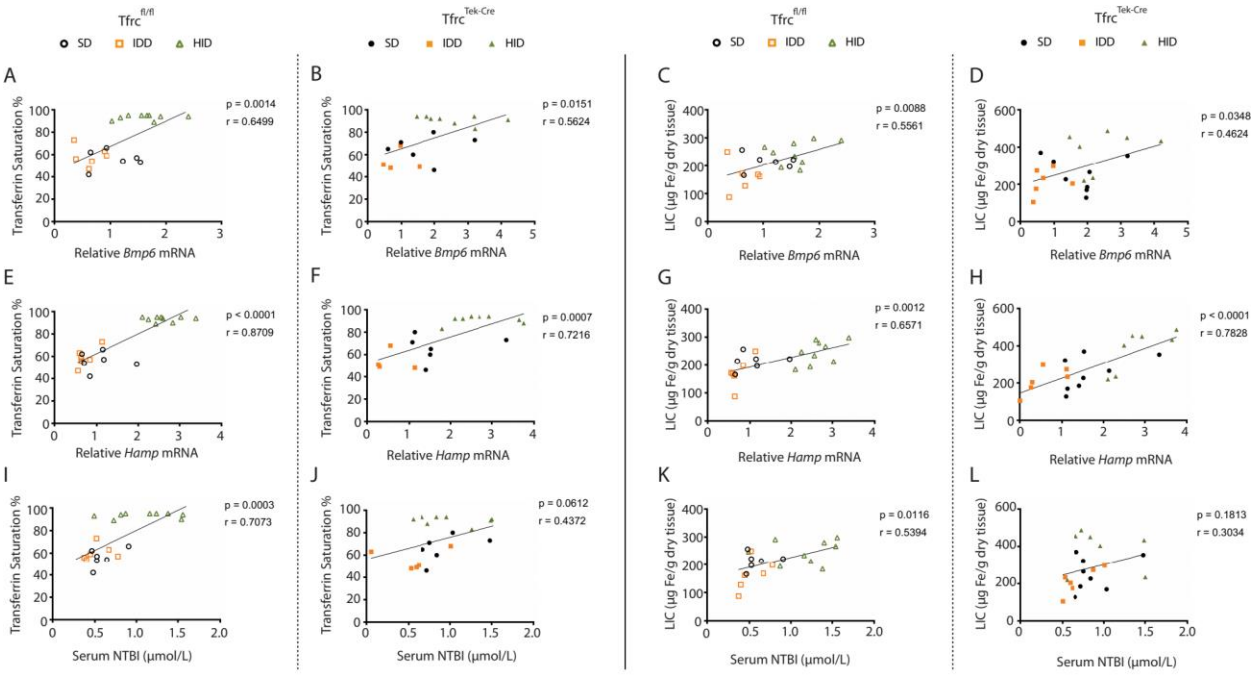

Figure S.2.5: Expression of *Bmp6* and *Hamp* mRNAs positively correlates with Tf saturation and LIC in Tfrc$^{fl/fl}$ and Tfrc$^{Tek-Cre}$ mice.

Pearson correlation analysis of Tf saturation vs *Bmp6* mRNA (A-B); LIC vs *Bmp6* mRNA (C-D); Tf saturation vs *Hamp* mRNA (E-F); LIC vs *Hamp* mRNA (G-H); Tf saturation vs NTBI (I-J); LIC vs NTBI (K-L). Data are from the experiments shown in Figures 2 and 3 with Tfrc$^{fl/fl}$ and Tfrc$^{Tek-Cre}$ mice kept on standard diet (SD), exposed to 2% carbonyl iron diet (HID) for 18 hours, or placed on iron-deficient diet (IDD) for 1 week. p values and Pearson's r coefficients are provided for each graph.

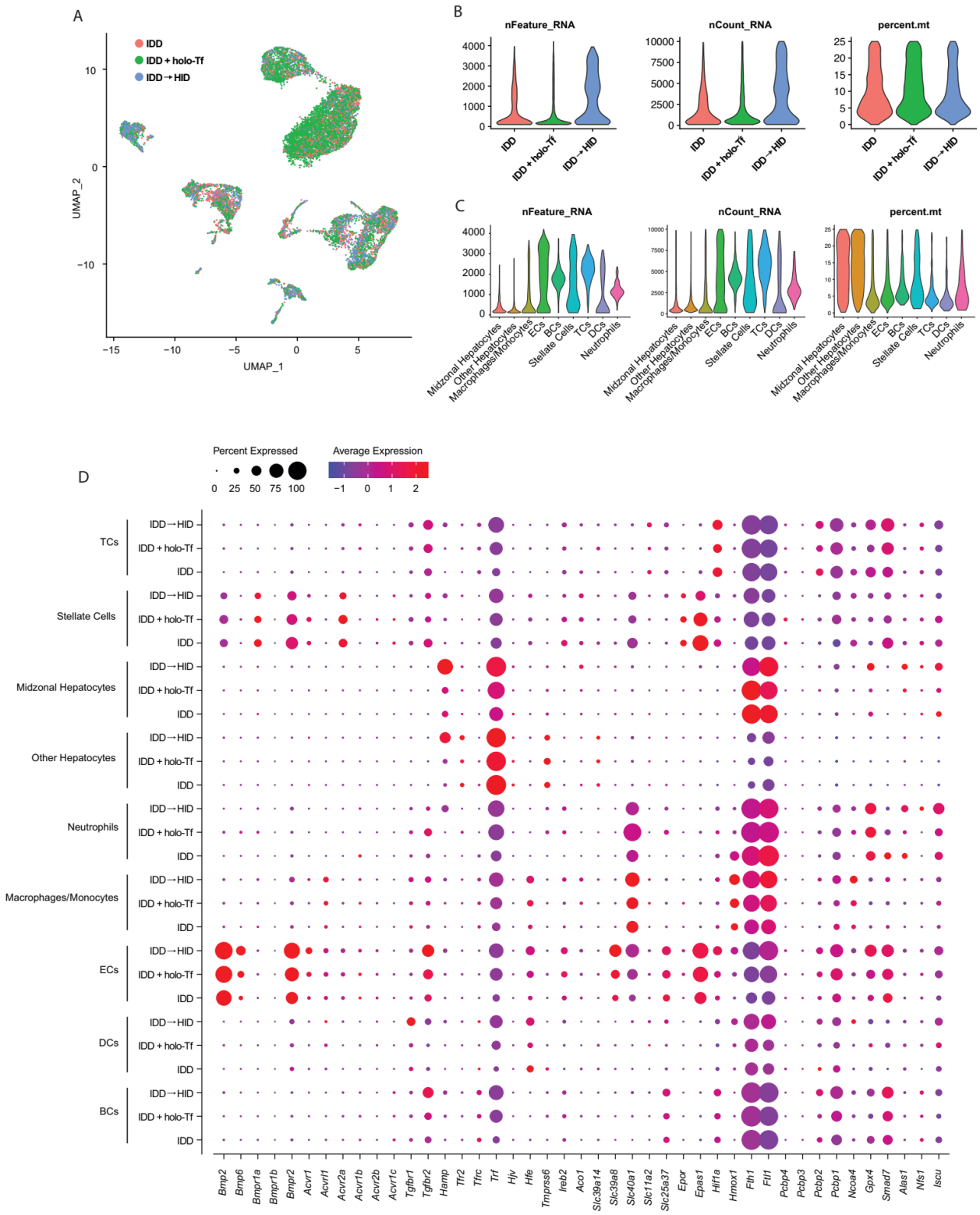

Figure S.2.6: Single-cell RNAseq quality control and cell type expression screen for known iron-related genes. Single-cell RNAseq datasets from mouse livers from the three experimental conditions (UMAP plot, A); with post-filtering single-cell distribution for gene count (nFeature_RNA), transcript count (nCount_RNA), and percent of mitochondrial encoded transcripts (percent.mt), across conditions (B) and annotated cell types (C). Cell type-specific expression of known iron-related genes across conditions (D).

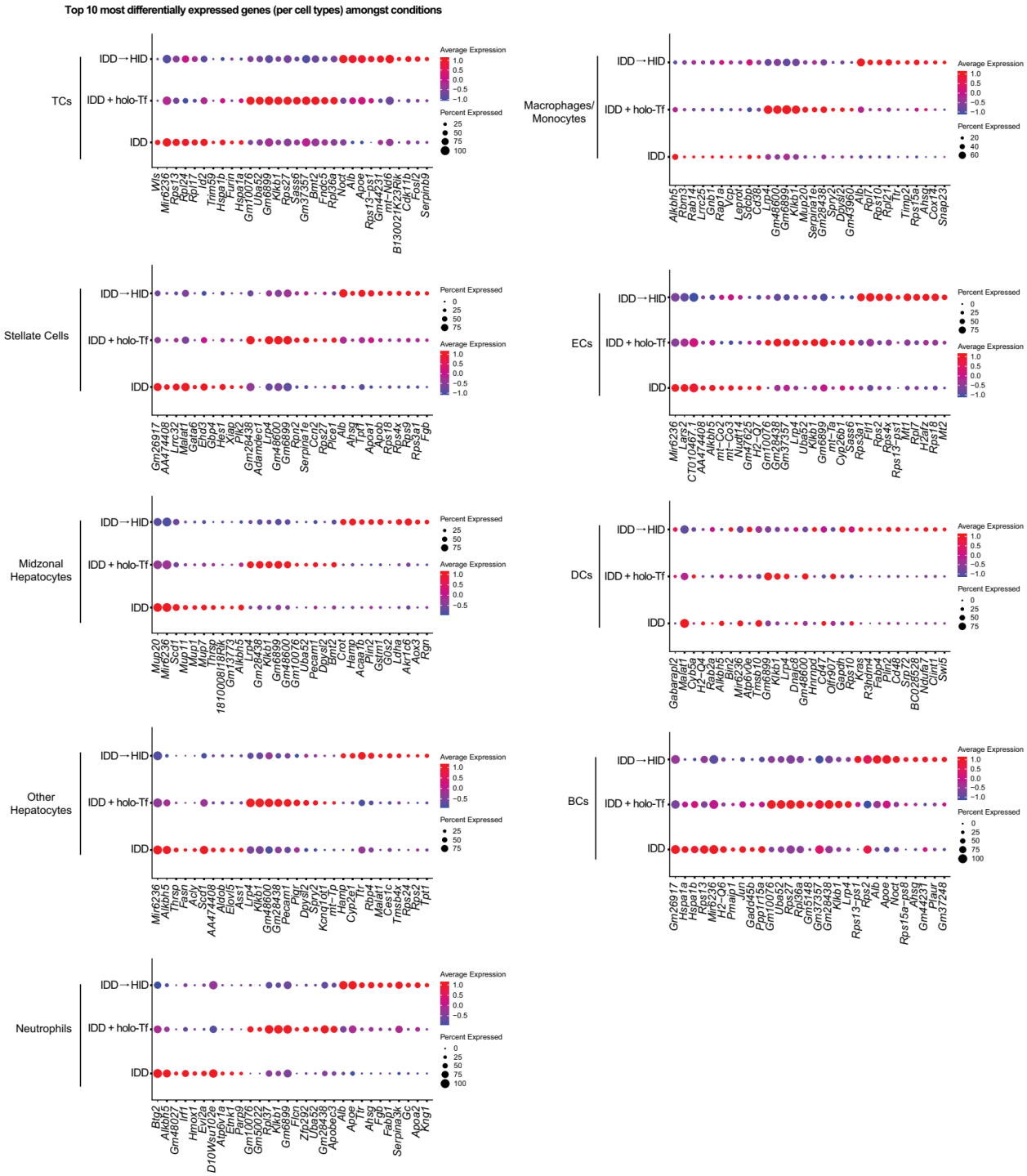

Figure S.2.7: Top 10 most differentially expressed genes amongst experimental conditions across cell types identified by single-cell RNAseq.

For each cell types, dot plot shows the top 10 most differentially expressed genes amongst each of the three experimental conditions, based on p values.

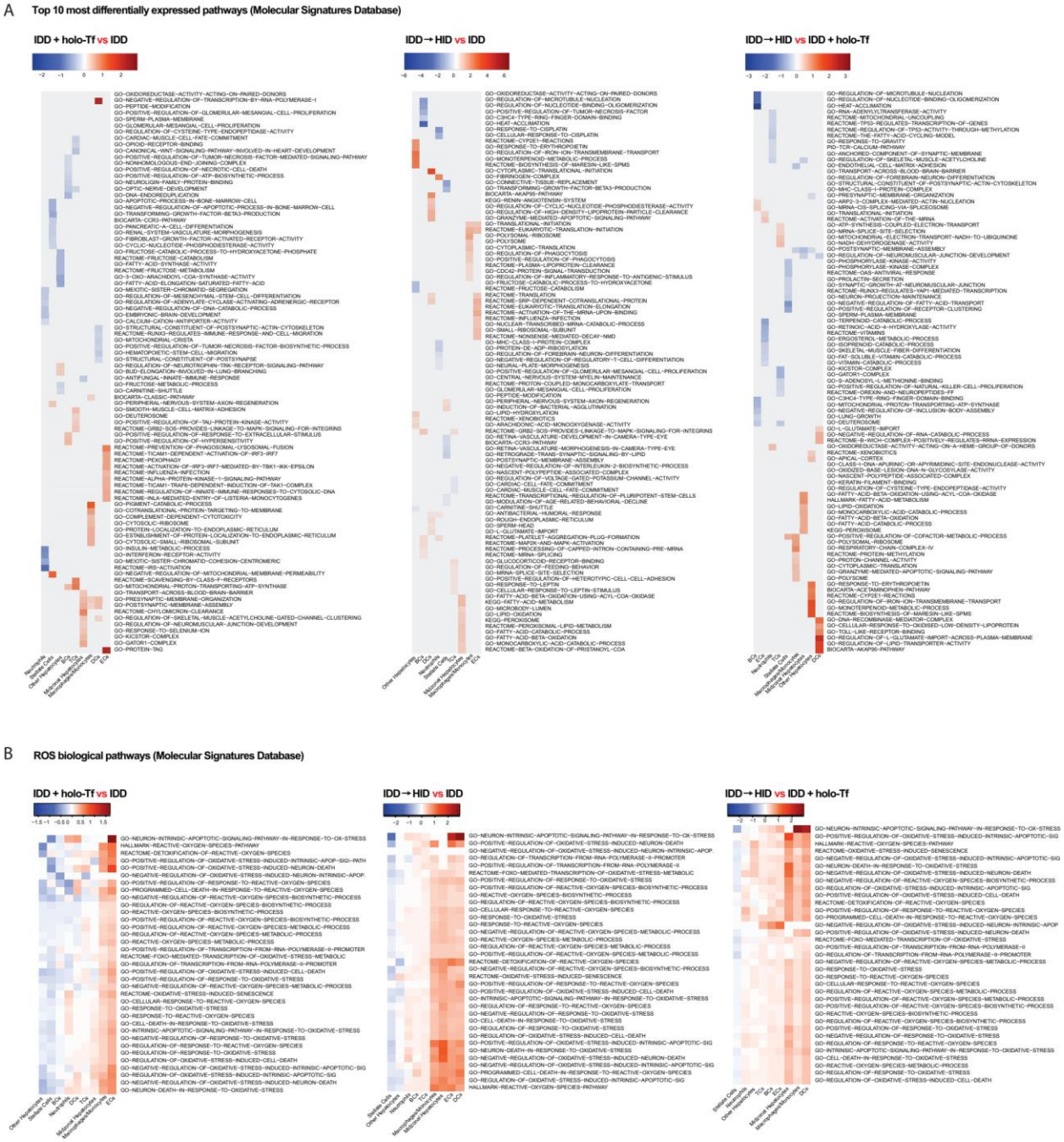

Figure S.2.8: Top 10 most differentially expressed pathways amongst experimental conditions across cell types identified by single-cell RNAseq.

Heatmaps of log2 fold-change for the top 10 most differentially expressed pathways across cell types between each of the experimental conditions, based on P values (A). Log2 fold-change of Gene Set Variation Analysis (GSVA) score for Oxidative stress/ROS related biological pathways from the MsigDB across cell types identified by scRNAseq (heatmap, B)

2.12 Supplementary Tables

*Additional supplementary spreadsheets can be found online at https://doi.org/10.1182/blood.2022016987.

Table S.2.1: Hematological parameters in 8-week mice fed standard diet.

	Male			Female		
Parameter	*Tfrc*$^{fl/fl}$	*Tfrc*$^{Tek\text{-}Cre}$	*p* value	*Tfrc*$^{fl/fl}$	*Tfrc*$^{Tek\text{-}Cre}$	*p* value
Hb (g/dl)	16.0±0.6	15.5±1.2	0.3929	14.6±1.0	13.5±0.9	0.0856
RBC (10^6/µl)	10.1±0.7	10.3±1.1	0.6662	9.0±0.7	7.9±1.5	0.1311
RDW (%)	13.4±0.1	14.7±0.6	*0.0043	13.7±0.5	15.8±0.7	*0.0043
HCT (%)	49.2±3.0	48.2±4.5	0.6623	44.1±3.7	37.1±7.6	0.1255
MCV (fl)	48.8±0.8	46.7±1.2	*0.0089	48.8±0.8	46.6±1.9	*0.0285
MCH (pg)	15.9±0.5	15.0±0.7	*0.0471	16.3±2.1	17.5±2.4	0.4202
MCHC (g/dl)	32.6±0.9	32.3±0.8	0.4966	33.5±4.8	37.4±6.0	0.2588
PLT (10^3/µl)	929.8±60.8	772.5±151.8	0.0589	849.3±58.3	686.8±232.2	0.1305

Table S.2.4: List of primers used for qPCR.

Gene	GenBank accession	Forward primer sequence	Reverse primer sequence
Hamp1	NM_032541.1	*AAGCAGGGCAGACATTGCGAT*	*CAGGATGTGGCTCTAGGCTATGT*
Bmp6	NM_007556.2	*ACTCGGGATGGACTCCACGTCA*	*CACCATGAAGGGCTGCTTGTCG*
Bmp2	NM_007553.3	*CTCTCTCAATGGACGTGCCC*	*ACACTAGAAGACAGCGGGTC*
Id1	NM_010495.2	*GGTACTTGGTCTGTCGGAGC*	*GCAGGTCCCTGATGTAGTCG*
Socs3	NM_007707.3	*TGCGCCTCAAGACCTTCAG*	*GCTCCAGTAGAATCCGCTCTC*
Rpl19	NM_009078.2	*AGGCATATGGGCATAGGGAAGAG*	*TTGACCTTCAGGTACAGGCTGTG*

Preface to chapter 3

The BMPs mentioned in the previous chapter are important signaling molecules which exert their effects in a paracrine fashion on the liver's parenchymal cells, hepatocytes. Binding to their cognate receptor triggers induction of hepcidin through activation of small mothers against decapentaplegic (SMAD) phosphorylation. Yet, hepcidin is also potently induced by inflammation which is primarily triggered by interleukin-6 (IL-6) signaling followed by signal transducers and activators of transcription (STAT) phosphorylation. This is thought to be part of the nutritional immunity response which describes the struggle to withhold nutrients, such as iron, from invading pathogens to prevent their growth. The earliest reports in the field suggested that BMP and IL-6 signaling functioned independently. However, work by our group as well as others has demonstrated that these pathways are synergistic and that BMPs help maintain a basal threshold of hepcidin expression necessary for inflammatory activation of hepcidin. In fact, not only does abrogation of BMP signaling or members of their receptor complexes cause iron overload in animal models and humans, but those suffering from iron overload cannot hope to produce an effective hypoferremia in response to invading pathogens. Thus, the focus of this chapter has been to understand the requirements to induce hypoferremia in organisms that are iron overloaded either dietarily or genetically.

This chapter was adapted from: Charlebois E, Fillebeen C, Katsarou A, Rabinovich A, Wisniewski K, Venkataramani V, Michalke B, Velentza A, & Pantopoulos, P. A crosstalk between hepcidin and IRE/IRP pathways controls ferroportin expression and determines serum iron levels in mice. *eLife*. 2022.

Chapter 3

A crosstalk between hepcidin and IRE/IRP pathways controls ferroportin expression and determines serum iron levels in mice

Edouard Charlebois[1], Carine Fillebeen[1], Angeliki Katsarou[1], Aleksandr Rabinovich[2#], Kazimierz Wisniewski[2†], Vivek Venkataramani[3,4], Bernhard Michalke[5], Anastasia Velentza[2‡] and Kostas Pantopoulos[1]*

[1] Lady Davis Institute for Medical Research, Jewish General Hospital and Department of Medicine, McGill University, Montreal, Quebec, Canada

[2] Ferring Research Institute Inc, San Diego, CA

[3] Department of Medicine II, Hematology/Oncology, University Hospital Frankfurt, Frankfurt, Germany

[4] Institute of Pathology, University Medical Center Göttingen (UMG), Göttingen, Germany

[5] Helmholtz Zentrum München GmbH – German Research Center for Environmental Health, Research Unit Analytical BioGeoChemistry, Neuherberg, Germany

[#] Current address: 8234 Caminito Maritimo La Jolla CA 92037

[†] Current address: Peptide Logic, LLC, 6185 Cornerstone Ct E, Suite 112, San Diego, CA 92121

[‡] Current address: Plexium, 11494 Sorrento Valley Rd, San Diego, CA 92121

* Corresponding author; tel.: (514) 340-8260 ext. 25293; email: kostas.pantopoulos@mcgill.ca

3.1 Abstract

The iron hormone hepcidin is transcriptionally activated by iron or inflammation via distinct, partially overlapping pathways. We addressed how iron affects inflammatory hepcidin levels and the ensuing hypoferremic response. Dietary iron overload did not mitigate hepcidin induction in LPS-treated wt mice but prevented effective inflammatory hypoferremia. Likewise, LPS modestly decreased serum iron in hepcidin-deficient *Hjv*$^{-/-}$ mice, model of hemochromatosis. Synthetic hepcidin triggered hypoferremia in control but not iron-loaded wt animals. Furthermore, it dramatically decreased hepatic and splenic ferroportin in *Hjv*$^{-/-}$ mice on standard or iron-deficient diet, but only triggered hypoferremia in the latter. Mechanistically, iron antagonized hepcidin responsiveness by inactivating IRPs in the liver and spleen, to stimulate ferroportin mRNA translation. Prolonged LPS treatment eliminating ferroportin mRNA permitted hepcidin-mediated hypoferremia in iron-loaded mice. Thus, *de novo* ferroportin synthesis is critical determinant of serum iron and finetunes hepcidin-dependent functional outcomes. Our data uncover a crosstalk between hepcidin and IRE/IRP systems that controls tissue ferroportin expression and determines serum iron levels. Moreover, they suggest that hepcidin supplementation therapy is more efficient combined with iron depletion.

3.2 Introduction

Systemic iron balance is controlled by hepcidin a peptide hormone that is produced by hepatocytes in the liver and operates in target cells by binding to the iron exporter ferroportin[1,2]. This results in ferroportin internalization and lysosomal degradation but also directly inhibits ferroportin function by occluding its iron export channel[3,4]. Ferroportin is highly expressed in duodenal enterocytes and tissue macrophages, which are instrumental for dietary iron absorption and iron recycling from senescent erythrocytes, respectively. Ferroportin is also expressed in hepatocytes, where excess iron is stored and can be mobilized on demand. Hepcidin-mediated ferroportin inactivation inhibits iron entry into plasma. This is a critical homeostatic response against iron overload, but also an innate immune response against infection[5]. Thus, hepcidin expression is induced when systemic iron levels are high to prevent dietary iron absorption, or under inflammatory conditions to promote iron retention within ferroportin-expressing cells and render the metal unavailable to extracellular pathogens.

The hepcidin-encoding *Hamp* gene is transcriptionally induced by iron or inflammatory stimuli via BMP/SMAD[6] or IL-6/STAT3[7] signaling, respectively. These pathways crosstalk at different levels. For instance, the BMP co-receptor hemojuvelin (HJV), a potent enhancer of iron-dependent BMP/SMAD signaling, is also essential for inflammatory induction of hepcidin. Thus, *Hjv*$^{-/-}$ mice, a model of juvenile hemochromatosis characterized by severe iron overload and hepcidin deficiency[8], exhibit blunted inflammatory induction of hepcidin and fail to mount a hypoferremic response following LPS treatment or infection with *E. coli*[9]. Excess iron inhibits hepcidin induction via the BMP/SMAD and IL-6/STAT3 signaling pathways in cultured cells[10,11], but the *in vivo* relevance of these findings is not known.

Hepcidin-dependent inhibition of ferroportin activity and expression is a major but not the sole contributor to inflammatory hypoferremia[12,13]. This is related to the fact that ferroportin expression is regulated by additional transcriptional and post-transcriptional mechanisms[14]. Thus, ferroportin transcription is induced by iron[15] and suppressed by inflammatory signals[16], while translation of *Slc40a1(+IRE)* mRNA, the major ferroportin transcript that harbors an “iron responsive element” (IRE) within its 5’ untranslated regions (5’ UTR) is controlled by “iron regulatory proteins” (IRPs), IRP1 and IRP2. The IRE/IRP system accounts for coordinate post-

transcriptional regulation of iron metabolism proteins in cells[17,18]. In a homeostatic response to iron deficiency, IRPs bind to the IRE within the *Slc40a1(+IRE)* and ferritin (*Fth1* and *Ftl1*) mRNAs, inhibiting their translation. IRE/IRP interactions do not take place in iron-loaded cells, allowing *de novo* ferroportin and ferritin synthesis to promote iron efflux and storage, respectively. The impact of the IRE/IRP system on regulation of tissue ferroportin and serum iron is not well understood.

The aim of this work was to elucidate mechanisms by which systemic iron overload affects hepcidin expression and downstream responses, especially under inflammatory conditions. Utilizing wild type and *Hjv*$^{-/-}$ mice, we demonstrate that serum iron levels reflect regulation of ferroportin in the liver and spleen by multiple signals. We further show that effective hepcidin-mediated hypoferremia is antagonized by compensatory mechanisms aiming to prevent cellular iron overload. Our data uncover a crosstalk between hepcidin and the IRE/IRP system that controls ferroportin expression in the liver and spleen, and thereby determines serum iron levels.

3.3 Results

3.3.1 Dietary iron overload does not prevent further inflammatory Hamp mRNA induction in LPS-treated wt mice, but mitigates hepcidin responsiveness.

In an exploratory experiment, wt mice were subjected to dietary iron loading by feeding a high-iron diet (HID) for short (1 day), intermediate (1 week) or long (5 weeks) time intervals; control animals remained on standard diet (SD). As expected, mice on HID for 1 day manifested maximal increases in serum iron (Figure 3.1A) and transferrin saturation (Figure 3.1B). They retained physiological liver iron content (LIC; (Figure 3.1C) and serum ferritin (Figure 3.1D), a reflection of LIC. Serum iron and transferrin saturation plateaued after longer HID intake, while LIC and serum ferritin gradually increased to peak at 5 weeks. The dietary iron loading promoted gradual upregulation of serum hepcidin (Figure 3.1E) and liver *Hamp* mRNA (Figure 3.1F), with highest values at 5 weeks. This could not prevent chronic dietary iron overload, in agreement with earlier findings[19,20].

LPS triggered appropriate hepcidin induction and a robust hypoferremic response in control mice. Interestingly, LPS-induced inflammation resulted in further proportional increase in hepcidin and *Hamp* mRNA in dietary iron-loaded mice (Figure 3.1E-F). This was accompanied

by significant drops in serum iron and transferrin saturation (Figure 3.1A-B). However, values did not reach the nadir of LPS-treated control animals and were increasing in mice on HID for longer periods, despite significant hepcidin accumulation. These data suggest that hepatic iron overload does not prevent inflammatory induction of hepcidin; however, it impairs its capacity to decrease serum iron.

3.3.2 Uncoupling inflammatory hepcidin induction from hypoferremic response in wt and Hjv$^{-/-}$ mice following dietary iron manipulations.

To further explore the potential of hepcidin to promote hypoferremia under iron overload, wt and *Hjv*$^{-/-}$ mice, a model of hemochromatosis, were subjected to dietary iron manipulations. Wt mice were fed SD or HID, and *Hjv*$^{-/-}$ mice were fed SD or an iron-deficient diet (IDD) for 5 weeks, to achieve a broad spectrum of hepcidin regulation. Wt mice on HID and *Hjv*$^{-/-}$ mice on SD or IDD manifested similarly high serum iron and transferrin saturation (Figure 3.2A-B). Serum non-transferrin bound iron (NTBI) levels appeared modestly elevated in the dietary and genetic iron overload models and seemed to decrease in *Hjv*$^{-/-}$ mice following IDD intake (Figure 3.2C). LIC was substantially reduced in *Hjv*$^{-/-}$ mice in response to IDD, but also compared to wt mice on HID (Figure 3.2D). The quantitative LIC data were corroborated histologically by Perls staining (Figure 3.2E and Figure 3.2-figure supplement 1A). Dietary iron loading increased splenic iron in wt mice and confirmed that *Hjv*$^{-/-}$ mice fail to retain iron in splenic macrophages (Figure 3.2-figure supplement 1B). As expected, serum hepcidin (Figure 3.2F) and liver *Hamp* mRNA (Figure 3.2G) were maximally induced in HID-fed wt mice and were low in *Hjv*$^{-/-}$ mice on SD, and further suppressed to undetectable levels following IDD intake.

LPS reduced serum iron and transferrin saturation in hyperferremic wt mice on HID and *Hjv*$^{-/-}$ mice on SD or IDD, but not below baseline of control wt mice on SD, the only animals that developed a robust hypoferremic response (Figure 3.2A-B); see also ratios of serum iron levels between untreated and LPS-treated mice in Figure 3.2A. The LPS treatment was associated with significant accumulation of hepcidin (Figure 3.2F) and induction of *Hamp* mRNA (Figure 3.2G) in all experimental groups, while NTBI (Figure 3.2C) and LIC (Figure 3.2D) were unaffected. Notably, LPS-treated wt mice on HID and *Hjv*$^{-/-}$ mice on IDD exhibited dramatic differences in *Hamp* mRNA but similar blunted hypoferremic response to the acute inflammatory stimulus. Thus, the profound hepcidin induction in iron-loaded wt mice cannot decrease serum iron below that of

iron-depleted *Hjv*$^{-/-}$ mice with negligible hepcidin, which indicates reduced hepcidin responsiveness. In support to this interpretation, *Id1* and *Socs3* mRNAs (Figure 3.2H-I), which are markers of BMP/SMAD and IL-6/STAT3 signaling, respectively, were appropriately induced by dietary iron loading or LPS treatment in wt mice. Thus, the major hepcidin signaling pathways were intact under these experimental conditions.

Serum iron levels are also controlled by hepcidin-independent mechanisms[12,13]. To explore their possible contribution in our experimental setting, we analyzed expression of genes involved in iron transport in the liver, an organ that contributes to iron sequestration during inflammation. Ferroportin is encoded by two alternatively spliced transcripts, *Slc40a1(+IRE)* and *Slc40a1(-IRE)*[21]. Both of them were significantly increased in the liver of iron-loaded wt mice on HID and *Hjv*$^{-/-}$ mice on SD, which is consistent with transcriptional induction[15], and were strongly suppressed by LPS (Figure 3.2J-K). The LPS treatment induced *Slc11a2*, *Slc39a14* and *Lcn2* mRNAs in all animals (Figure 3.2L-N). These encode the divalent metal transporter DMT1, the NTBI transporter Zip14 and the siderophore-binding protein Lcn2, respectively; *Lcn2* mRNA induction was dramatic. The transferrin receptor 1-encoding *Tfrc* mRNA was largely unaffected by LPS, except for a reduction in *Hjv*$^{-/-}$ mice on IDD (Figure 3.2O). The above data indicate that LPS-induced inflammation triggers transcriptional responses favoring reduced iron efflux from the liver and increased uptake of NTBI by liver cells.

To assess the downstream function of hepcidin, we analyzed tissue ferroportin levels. Immunohistochemical staining of liver sections revealed strong ferroportin expression in Kupffer cells, predominantly in periportal areas, under all experimental conditions (Figure 3.3A and Figure 3.3-figure supplement 1). Hepatocellular ferroportin staining is also evident in the iron overload models, mostly in periportal hepatocytes (Figure 3.3-figure supplement 1), and in line with recent data[22]. LPS triggered redistribution and decreased expression of ferroportin in Kupffer cells from wt but not *Hjv*$^{-/-}$ mice (Figure 3.3-figure supplement 1), as reported[9].

We further analyzed ferroportin in liver homogenates by Western blotting. Levels of biochemically detectable liver ferroportin differed substantially between wt and *Hjv*$^{-/-}$ mice. Thus, they were relatively low in the former and highly induced in the latter (Figure 3.3B), independently of iron load. The differences were more dramatic compared to those observed by

immunohistochemistry (Figure 3.3A and Figure 3.3-figure supplement 1). Conceivably, the strong ferroportin signal in Western blots from *Hjv*$^{-/-}$ liver homogenates reflects high ferroportin expression in hepatocytes, which are the predominant cell population and make up ~80% of the liver cell mass[23]. Yet, hepatocellular ferroportin is less visible by immunohistochemistry because the signal is substantially weaker compared to that in Kupffer cells (see also Figure 3.6E). Interestingly, the LPS treatment visibly suppressed total liver ferroportin in *Hjv*$^{-/-}$ mice on SD but not IDD, and appeared to modestly reduce it in wt mice (Figure 3.3B); albeit, without statistical significance. These data are consistent with negative regulation of ferroportin by residual LPS-induced hepcidin in *Hjv*$^{-/-}$ mice on SD, which could explain the small drop in serum iron and transferrin saturation under these acute inflammatory conditions, as reported[9]. However, liver ferroportin remained detectable and apparently functional, as it did not allow significant iron sequestration and dramatic drop in serum iron. Notably, persistence of relatively high serum iron is also evident in LPS-treated wt mice on HID, despite maximal hepcidin and minimal liver ferroportin levels.

Next, we analyzed ferroportin in the spleen, an organ with erythrophagocytic macrophages that plays an important role in body iron traffic[24]. Immunohistochemical analysis shows that LPS reduced ferroportin in red pulp splenic macrophages from wt mice on SD, but this effect was less evident in wt mice on HID and in *Hjv*$^{-/-}$ mice on SD or IDD (Figure 3.3C and Figure 3.3-figure supplement 2). Western blot analysis shows a stronger ferroportin signal in splenic extracts from *Hjv*$^{-/-}$ animals (Figure 3.3D), consistent with immunohistochemistry. However, in this assay LPS suppressed splenic ferroportin in wt animals and in *Hjv*$^{-/-}$ mice on SD, but not IDD. This could be a result of residual hepcidin upregulation (Figure 3.2F-G), while the lack of significant splenic ferroportin suppression in *Hjv*$^{-/-}$ mice on IDD may denote hepcidin insufficiency. In any case, the relatively high circulating iron levels in dietary iron-loaded and LPS-treated wt mice indicates continuous iron efflux to plasma despite hepcidin excess.

3.3.3 Insufficient hepcidin leads to blunted hypoferremic response in iron overload.

We used human synthetic hepcidin to address whether the failure of mouse models of iron overload to mount an appropriate hypoferremic response to acute inflammation is caused by endogenous hepcidin insufficiency or other mechanisms. Wt and *Hjv*$^{-/-}$ mice subjected to dietary iron manipulations received 2.5 μg/g synthetic hepcidin every two hours for a total of four

intraperitoneal injections. Each dose corresponds to ~200-fold excess over endogenous circulating hepcidin in control wt animals. The treatment caused hypoferremia in wt mice on SD but not HID, where the decrease in serum iron was significant but well above baseline of untreated wt controls (Figure 3.4A-B); see also ratios of serum iron levels between untreated and hepcidin-treated mice in Figure 3.4A. Likewise, synthetic hepcidin significantly decreased serum iron but failed to cause dramatic hypoferremia in hepcidin-deficient *Hjv*$^{-/-}$ mice on SD. Notably, hepcidin administration was much more effective in relatively iron-depleted *Hjv*$^{-/-}$ mice on IDD, and lowered serum iron and transferrin saturation below baseline. The treatments significantly reduced NTBI in *Hjv*$^{-/-}$ mice on SD, with a trend in mice on IDD (Figure 3.4C) but did not affect LIC or splenic iron content (SIC) under any experimental conditions (Figure 3.4D-E and Figure 3.4-figure supplement 1). Serum iron represents <2% of total tissue iron and therefore its acute fluctuations are not expected to dramatically alter LIC or SIC.

Synthetic hepcidin led to significant reduction of endogenous *Hamp* mRNA in wt mice on SD (Figure 3.4F), as earlier reported[25]. Conceivably, this is related to destabilization of the Hamp inducer Tfr2 in the liver (Figure 3.4-figure supplement 2), a known response to hypoferremia[26]. Synthetic hepcidin did not promote inflammation, iron perturbations or alterations in BMP/SMAD signaling in the liver, as judged by the unaltered expression of hepatic *Slc40a1(+IRE)*, *Socs3*, *Id1* and *Bmp6* mRNAs (Figure 3.4-figure supplement 3A-D). Moreover, synthetic hepcidin did not affect *Slc11a2*, *Slc39a14*, *Lcn2* or *Tfrc* mRNAs (Figure 3.4-figure supplement 3E-H), which encode iron transporters; *Slc39a14* and *Lcn2* are also inflammatory markers.

Next, we analyzed liver ferroportin by immunohistochemistry. Figure 3.5A and Figure 3.5-figure supplement 1 show that exogenous hepcidin decreased ferroportin signal intensity in all animal groups to varying degrees. The hepcidin effect was particularly noticeable in hepatocytes from *Hjv*$^{-/-}$ mice (see low magnification images in Figure 3.5-figure supplement 1). Kupffer cells seemed to retain some ferroportin in all groups except *Hjv*$^{-/-}$ mice on IDD. Interestingly, while synthetic hepcidin decreased ferroportin signal intensity in Kupffer cells, it did not alter intracellular ferroportin distribution as would be expected based on the data in LPS-treated wt mice (Figure 3.5A).

Western blotting confirmed that total liver ferroportin is highly induced in *Hjv*$^{-/-}$ mice (Figure 3.5B). Again, the signal intensity can be attributed to protein expressed in hepatocytes. The treatment with synthetic hepcidin did not significantly affect liver ferroportin in wt mice (either on SD or HID), but substantially reduced it in *Hjv*$^{-/-}$ mice, to almost wt levels. The effect appeared more pronounced in *Hjv*$^{-/-}$ mice on IDD; nevertheless, ferroportin remained detectable.

Splenic ferroportin was reduced in all animal groups following hepcidin treatment, with stronger effects visualized by immunohistochemistry in wt mice on SD and *Hjv*$^{-/-}$ mice on IDD (Figure 3.5C and Figure 3.5-figure supplement 2). At the biochemical level, ferroportin expression was again much stronger in the spleen of *Hjv*$^{-/-}$ mice (Figure 3.5D). Synthetic hepcidin did not significantly affect splenic ferroportin in wt mice, but dramatically reduced it in all *Hjv*$^{-/-}$ mice.

Taken together, our data suggest that synthetic hepcidin overcomes endogenous hepcidin deficiency in *Hjv*$^{-/-}$ mice. However, it only triggers hypoferremia in these animals following relative iron depletion. On the other hand, in iron-loaded wt mice with already high endogenous hepcidin, excess synthetic hepcidin fails to promote hypoferremia.

3.3.4 Dietary iron manipulations are sensed by IRPs in the liver and spleen of wt and Hjv$^{-/-}$ *mice.*

The IRE/IRP system orchestrates homeostatic adaptation to cellular iron supply (17, 18). To evaluate the responses of IRPs in the whole liver and spleen to the above-described dietary iron manipulations, we analyzed tissue extracts from wt and *Hjv*$^{-/-}$ mice by an electrophoretic mobility shift assay (EMSA) using a ^{32}P-labelled IRE probe. The data in Figure 3.6A-B show that HID intake tended to decrease the IRE-binding activities of IRP1 and IRP2 in both liver and spleen of wt mice (statistical significance is only reached in the liver); densitometric quantification of IRE/IRP1 and IRE/IRP2 complexes is shown on the right. Conversely, IDD intake significantly induced the IRE-binding activity of IRP2 in the liver and spleen of *Hjv*$^{-/-}$ mice, leaving IRP1 largely unaffected. IRE/IRP2 interactions are better visible in longer exposures (middle panels). EMSAs with tissue extracts previously treated with 2-mercaptoethanol (2-ME) were performed as loading controls (27) and are shown in the bottom panels.

To clarify which cell types of the liver account for the responses of IRPs to dietary iron, separate EMSAs were performed using extracts from isolated hepatocytes or non-parenchymal

liver cells. The data in Figure 3.6C-D uncover that IRP1 and IRP2 in both liver cell populations from wt and *Hjv*$^{-/-}$ mice are sensitive to dietary iron loading or restriction, respectively. The EMSA analysis of non-parenchymal liver cells, which contain Kupffer cells among others, showed a high experimental variability (Figure 3.6D). Nevertheless, the overall results are consistent with those obtained with splenic extracts, which contain red pulp macrophages (Figure 3.6B).

3.3.5 Relative expression of ferroportin in hepatocytes and non-parenchymal liver cells from wt and Hjv$^{-/-}$ *mice.*

We determined the relative abundance of ferroportin in hepatocytes and non-parenchymal liver cells from wt and *Hjv*$^{-/-}$ mice on SD by Western blotting. As expected, ferroportin expression (normalized to β-actin) was ~1.5-2-fold higher in the non-parenchymal cell fraction as compared to hepatocytes in both wt and *Hjv*$^{-/-}$ mice (Figure 3.6E). In comparison across genotypes, ferroportin expression was ~2-fold higher in hepatocytes and ~50% higher in non-parenchymal cells from *Hjv*$^{-/-}$ vs wt mice.

3.3.6 Iron-dependent regulation of ferroportin mRNA translation in the liver.

Having established that dietary iron manipulations trigger IRP responses in the liver and spleen, we hypothesized that the functional outcomes of exogenous hepcidin may not merely depend on its capacity to degrade tissue ferroportin, but also on iron-dependent ferroportin regeneration via *de novo* synthesis. *Slc40a1(+IRE)* mRNA is the predominant ferroportin transcript in the mouse liver and spleen, as well as in hepatoma and macrophage cell lines[21], and is considered as a target of IRPs.

Thus, we assessed the effects of dietary iron on whole liver *Slc40a1(+IRE)* mRNA translation by polysome profile analysis. We focused on the liver because this organ contains the highest number of iron-recycling macrophages[28] and can also export iron to plasma from ferroportin-expressing parenchymal cells. Liver extracts from wt mice on SD or HID, and *Hjv*$^{-/-}$ mice on SD or IDD were fractionated on sucrose gradients to separate translationally inactive light monosomes from translating heavy polysomes (Figure 3.7A). The relative distribution of *Slc40a1(+IRE)*, *Fth1* (positive control for iron regulation) and *Actb* (negative control) mRNAs within the different fractions was quantified by qPCR (Figure 3.7B-D). Dietary iron loading stimulated *Slc40a1(+IRE)* (and *Fth1*) mRNA translation in wt mice (note the shifts from

monosomes to polysomes in Figure 3.7B-C). Conversely, dietary iron depletion inhibited *Slc40a1(+IRE)* (and *Fth1*) mRNA translation in *Hjv*$^{-/-}$ mice. We also attempted to obtain polysome profiles of *Slc40a1(-IRE)* mRNA but it was undetectable after fractionation. These data indicate that in mice subjected to iron overload, iron-stimulated ferroportin synthesis in the liver antagonizes hepcidin-mediated ferroportin degradation and prevents an appropriate hypoferremic response. Considering that levels of *Slc40a1(+IRE)* mRNA are elevated in iron-loaded wt and *Hjv*$^{-/-}$ mice (Figure 3.2J and Figure 3.4-figure supplement 3), it is possible that increased *de novo* ferroportin synthesis is further enhanced by transcriptional induction.

Quantification of liver iron by ICP-MS (Figure 3.7E) validated iron loading of wt mice by HID, and relative iron depletion of *Hjv*$^{-/-}$ mice by IDD intake, respectively (see also Figure 3.2D). Iron redox speciation analysis by CE-ICP-MS revealed a profound increase in Fe^{2+}/Fe^{3+} ratios in livers of *Hjv*$^{-/-}$ mice on SD, which was corrected by dietary iron depletion (Figure 3.7F). Nevertheless, there was no difference in Fe^{2+}/Fe^{3+} ratios among livers of wt mice on SD or HID, and *Hjv*$^{-/-}$ mice on IDD. We conclude that a relative increase in total iron content, rather than excessive accumulation of redox active Fe^{2+} drives *Slc40a1(+IRE)* (and *Fth1*) mRNA translation in the liver.

3.3.7 Restoration of effective hypoferremic response under iron overload following maximal Slc40a1 mRNA suppression.

We reasoned that complete inactivation of ferroportin mRNA would restore hepcidin-induced hypoferremia despite iron overload. An 8-hour treatment of mice with LPS suppressed liver *Slc40a1(+IRE)* mRNA below detection levels (Figure 3.8A), as reported[9]. The same holds true for the *Slc40a1(-IRE)* isoform (Figure 3.8B), which was 290 times less abundant in control mouse livers compared to *Slc40a1(+IRE)* (ΔCt=8.18), in agreement with published data[21]. We went on to examine the effects of synthetic hepcidin on serum iron under these conditions of maximal *Slc40a1* mRNA suppression. Importantly, the prolonged LPS treatment decreased serum iron in wt mice on HID below the control baseline (Figure 3.8C). Furthermore, when combined with synthetic hepcidin, it promoted an effective hypoferremic response in wt mice on HID and *Hjv*$^{-/-}$ mice on SD (or IDD) (Figure 3.8C-D) and tended to decrease NTBI (Figure 3.8E). These data strongly suggest that the expression of actively translating *Slc40a1* mRNA in iron-exporting tissues under systemic iron overload mitigates hepcidin-induced drop in serum iron.

3.4 Discussion

We sought to analyze how iron overload affects hepcidin-mediated inflammatory responses. We and others reported that excess iron inhibits the major hepcidin signaling pathways (BMP/SMAD and IL-6/STAT3) in cultured cells[10,11]. To explore the physiological relevance of these findings, wt mice were subjected to variable degrees of dietary iron loading and then treated with LPS. All iron-loaded mice could further upregulate hepcidin in response to LPS-induced acute inflammation (Figure 3.1). This is consistent with other relevant findings[29] and apparently contradicts the *in vitro* data. While experimental iron loading of cultured cells is rapid, dietary iron loading of mice is gradual[20] and most of excess iron is effectively detoxified within ferritin, which is highly induced[30]. By contrast, the suppression of hepcidin preceded ferritin induction in cultured cells[10], which may explain the discrepancy with the *in vivo* data.

The unimpaired inflammatory induction of hepcidin in iron-loaded wt mice correlated with significant drops in serum iron, but these appeared inversely proportional to the degree of systemic iron loading (Figure 3.1). Thus, LPS-treated mice on 5 weeks HID developed relative hypoferremia but could not further reduce serum iron below a baseline of untreated control mice on SD. This can be attributed to mechanisms antagonizing hepcidin action. To explore how iron modulates the capacity of hepcidin to trigger inflammatory hypoferremia, we established conditions of iron overload using wt and *Hjv*$^{-/-}$ mice with extreme differences in hepcidin expression. Figures 2 and 3 demonstrate that iron overload prevents effective inflammatory hypoferremia independently of hepcidin and tissue ferroportin levels.

We used a ~200-fold excess of synthetic hepcidin to directly assess its capacity to divert iron traffic in iron-loaded mice. Hepcidin injection caused hypoferremia in control wt mice on SD and significantly reduced serum iron in wt mice on HID and *Hjv*$^{-/-}$ mice on SD, but not below baseline (Figure 3.4). Thus, synthetic hepcidin failed to drastically drop serum iron levels in iron overload models with either high or low endogenous hepcidin. Importantly, synthetic hepcidin promoted robust hypoferremia in relatively iron-depleted *Hjv*$^{-/-}$ mice on IDD, with undetectable endogenous hepcidin. It should be noted that synthetic hepcidin had similar effects on tissue ferroportin among wt or *Hjv*$^{-/-}$ mice, regardless of iron diet (Figure 3.5). It reduced intensity of the ferroportin signal in Kupffer cells and splenic macrophages of wt mice without significantly

affecting biochemically detectable total protein levels. In addition, it dramatically reduced total ferroportin in the liver and spleen of *Hjv*$^{-/-}$ mice. However, in all experimental settings there was residual tissue ferroportin, which appears to be functionally significant.

We reasoned that at steady-state, tissue ferroportin may consist of fractions of newly synthesized protein, and protein that is *en route* to hepcidin-mediated degradation. Conceivably, the former may exhibit more robust iron export activity, at least before its iron channel gets occluded by hepcidin. Increased *de novo* synthesis of active ferroportin could explain why synthetic hepcidin cannot drastically drop serum iron levels under iron overload. In fact, Figure 3.7 demonstrates that dietary iron overload augments *Slc40a1(+IRE)* mRNA translation in the liver of wt mice. Conversely, relative dietary iron depletion inhibits *Slc40a1(+IRE)* mRNA translation in the liver of *Hjv*$^{-/-}$ mice, in line with the restoration of hepcidin-mediated hypoferremic response (Figure 3.4).

Our data are consistent with translational control of liver ferroportin expression via the IRE/IRP system and do not exclude the possibility for an additional contribution of iron-dependent transcriptional regulation of *Slc40a1(+IRE)* mRNA. Direct evidence for activation of IRP responses in the liver and spleen to dietary iron manipulations is provided in Figure 3.6. While translational control of ferritin in tissues is established[31], regulation of ferroportin by the IRE/IRP system is less well characterized and has hitherto only been documented in cell models[32,33], the mouse duodenum[34], and the rat liver[35]. Moreover, the physiological relevance of this mechanism remained speculative. The data in Figures 6 and 7 show that the IRE/IRP system is operational and controls *Slc40a1(+IRE)* mRNA translation in both fractions of hepatocytes and non-parenchymal liver cells. Presumably, this offers a compensatory mechanism to protect the cells from iron overload and iron-induced toxicity. On the other hand, this mechanism attenuates hepcidin responsiveness and promotes a state of hepcidin resistance, as higher amounts of hepcidin are required to achieve effective hypoferremia. Because hepcidin has a short plasma half-life, it is reasonable to predict that the use of more potent hepcidin analogs[36] will overcome the antagonistic effects of increased ferroportin mRNA translation under iron overload.

The critical role of *de novo* ferroportin synthesis in fine-tuning hepcidin-dependent functional outcomes is also highlighted in Figure 3.8. Thus, synthetic hepcidin was highly effective

as promoter of hypoferremia in dietary iron-loaded wt mice when administered together with LPS. LPS is known to suppress *Slc40a1* mRNA in cell lines[16] and mouse tissues, with a nadir in the liver reached at 8 h[9]. The recovery of hepcidin effectiveness in mouse models of iron overload was only possible when *Slc40a1* mRNA was essentially eliminated. Under these conditions, LPS treatment alone was sufficient to decrease serum iron in dietary iron-loaded wt mice below baseline.

Tissue iron uptake may be another important determinant of the hypoferremic response to inflammation. LPS did not affect *Tfrc* mRNA levels in the liver (Figure 3.2O), which argues against increased uptake of transferrin-bound iron via TfR1. On the other hand, LPS induced *Slc39a14*, *Slc11a2* and *Lcn2* mRNAs (Figure 3.2L-N). Zip14 is the NTBI transporter accounting for hepatocellular iron overload in hemochromatosis[37] and is upregulated by inflammatory cues in hepatocytes[38]. DMT1 is dispensable for NTBI uptake by hepatocytes[39], and its inflammatory induction might promote iron acquisition by macrophages[16,40]. Nevertheless, considering that the fraction of NTBI represents <2% of total serum iron even in the iron overload models (Figure 3.2A and C), it is implausible that NTBI uptake by Zip14 and/or DMT1 substantially contributes to inflammatory hypoferremia. Lcn2 is an acute phase protein that can sequester intracellular iron bound to catecholate siderophores[41], and is more likely to transport iron to tissues during infection. In any case, synthetic hepcidin did not affect expression of iron transporters (Figure 3.4-figure supplement 3E-H). This excludes the possibility for a synergistic effect on LPS-induced tissue iron uptake that could promote effective hypoferremia in the iron overload models.

Our study has some limitations. While the data highlight the importance of translational regulation of liver ferroportin as a determinant of serum iron, they do not accurately dissect the specific role of ferroportin expressed in hepatocytes and Kupffer cells; the latter were not separated from other non-parenchymal cells in biochemical assays. The involvement of the IRE/IRP system has been established indirectly, while the relative contributions of IRP1 and IRP2 in the mechanism are not fully defined. The possible role of iron-dependent transcriptional induction of ferroportin in counterbalancing hepcidin actions requires further clarification. The use of diets with variable iron content may have triggered responses to iron availability independent of hepcidin signaling and Hjv functionality. Finally, the physiological implications of translational regulation of ferroportin in the broader setting of inflammation and/or infection have not been explored.

In conclusion, our data reveal a crosstalk between the hepcidin pathway and the IRE/IRP system in the liver and spleen for the control of tissue ferroportin and serum iron levels. Furthermore, they suggest that application of hepcidin therapeutics for treatment of iron overload disorders should be combined with iron depletion strategies to mitigate *Slc40a1* mRNA translation and increase hepcidin efficacy. Future work is expected to clarify whether optimizing the hypoferremic response to inflammation under systemic iron overload decreases susceptibility to pathogens.

3.5 Materials and Methods

3.5.1 Animals.

Wild type C57BL/6J and isogenic *Hjv*$^{-/-}$ mice[42] were housed in macrolone cages (up to 5 mice/cage, 12:12 h light-dark cycle: 7 am - 7 pm; 22 ± 1°C, 60 ± 5% humidity). The mice were fed either a standard diet (200 ppm iron), an iron-deficient diet (2-6 ppm iron) or a high-iron diet (2% carbonyl iron)[43]. Where indicated, mice were injected intraperitoneally with 1 μg/g LPS (serotype 055:B5; Sigma-Aldrich) or subcutaneously with 2.5 μg/g synthetic hepcidin; control mice were injected with phosphate-buffered saline. At the endpoints, animals were sacrificed by CO_2 inhalation and cervical dislocation. Experimental procedures were approved by the Animal Care Committee of McGill University (protocol 4966).

3.5.2 Serum biochemistry.

Blood was collected via cardiac puncture. Serum was prepared by using micro Z-gel tubes with clotting activator (Sarstedt) and was kept frozen at −20°C until analysis. Serum iron, total iron binding capacity (TIBC) and, where indicated serum ferritin, were determined at the Biochemistry Department of the Montreal Jewish General Hospital using a Roche Hitachi 917 Chemistry Analyzer. Transferrin saturation was calculated from the ratio of serum iron and TIBC. Serum hepcidin was measured by using an ELISA kit (HMC-001; Intrinsic LifeSciences).

3.5.3 Quantification of serum non-transferrin bound iron (NTBI).

NTBI was measured by adapting the method developed by Esposito *et al*[44]. Briefly, iron samples of known concentration were created by mixing 70 mM nitrilotriacetate (NTA) (pH = 7.0) with 20 mM ferrous ammonium sulfate. Fe^{2+} was allowed to oxidize to Fe^{3+} in ambient air for at

least 30 min and then the solution was diluted to 0.2 mM before further serial dilutions to create a ladder. 5 µl of ladder was loaded in a 96-well plate containing 195 µl plasma-like medium with or without 100 µM deferiprone. The composition of the plasma-like medium was: 40 mg/ml bovine serum albumin, 1.2 mM sodium phosphate dibasic, 120 µM sodium citrate, 10 mM sodium bicarbonate in iron-free HEPES-buffered saline (HEPES 20 mM, NaCl 150 mM, treated with Chelex-100 chelating resin [Bio-Rad, Hercules, CA], 0.5 mM NTA, 40 µM ascorbic acid, 50 µM dihydrorhodamine, pH=7.4). 5 µl of sample was loaded in a 96-well plate containing 195 µl of iron-free HEPES-buffered saline with or without 100 µM deferiprone. Microplates were read every 2 minutes at 37°C over 40 min at 485/520 nm (ex/em). Final NTBI was calculated by comparing the oxidation rate of DHR in the presence or absence of the strong chelator deferiprone.

3.5.4 Hepcidin synthesis.

Human hepcidin (DTHFPICIFCCGCCHRSKCGMCCKT) was synthesized at Ferring Research Institute, San Diego, CA. The linear peptide was assembled on Rink amide resin using Tribute peptide synthesizer and the peptide was cleaved from the resin with the TFA/TIS/EDT/H_2O 91:3:3:3 (v/v/v/v) cocktail. The solvents were evaporated, and the crude peptide was precipitated with diethyl ether, reconstituted in 50% aqueous acetonitrile and lyophilized. The lyophilizate was dissolved in 30% aqueous acetonitrile at the concentration of 0.05 mM and the pH of the solution was adjusted to 7.8 with 6 M ammonium hydroxide. Folding was achieved within 4 hours using the cysteine/cystine redox (peptide/Cys/Cys_2 1:6:6 molar ratio). The reaction mixture was acidified to pH 3, loaded onto HPLC prep column and purified in a TFA based gradient. The identity of the peptide was confirmed by mass spectrometry and by coelution with a commercially available sample (Peptide International, #PLP-3771-PI).

3.5.5 Quantitative real-time PCR (qPCR).

RNA was extracted from livers by using the RNeasy kit (Qiagen). cDNA was synthesized from 1 µg RNA by using the OneScript® Plus cDNA Synthesis Kit (Applied Biological Materials Inc.). Gene-specific primers pairs (Table S.3.1) were validated by dissociation curve analysis and demonstrated amplification efficiency between 90-110 %. SYBR Green (Bioline) and primers were used to amplify products under following cycling conditions: initial denaturation 95°C 10 min, 40 cycles of 95°C 5 s, 58°C 30 s, 72°C 10 s, and final cycle melt analysis between 58°-95°C.

Relative mRNA expression was calculated by the $2^{-\Delta\Delta Ct}$ method[45]. Data were normalized to murine ribosomal protein L19 (*Rpl19*). Data are reported as fold increases compared to samples from wild type mice on standard diet (SD).

3.5.6 Polysome fractionation.

RNA was freshly prepared from frozen livers. Linear sucrose gradients were prepared the day before the experiment by using 5% (w/v) and 50% (w/v) sucrose solutions with 10x gradient buffer (200 mM HEPES pH=7.6, 1 M KCl, 50 mM $MgCl_2$, 0.1 mg/ml Cycloheximide, 1 tablet cOmplete™, Mini, EDTA-free Protease Inhibitor Cocktail (Roche), 200 U/mL Recombinant RNasin® Ribonuclease Inhibitor (Promega), 2 mM DTT). Linear gradients were prepared in Polyallomer Centrifuge Tubes (Beckman Coulter). Tubes were marked using a gradient cylinder (BioComp), and 5% sucrose solution was added using a syringe with a layering needle (BioComp) until solution level reached the mark. Then, 50% sucrose solution was layered underneath the 5% solution until the interface between the two solutions reached the mark. Tubes were capped with rate zonal caps (BioComp) and linearized using a Gradient Master 108 (Biocomp). All reagents were nuclease-free and all solutions were kept on ice or at 4°C. Sample preparation was adapted from Liang *et al.*[46]. Briefly, livers were flash frozen upon collection. Roughly 30-80 mg of tissue was crushed using a mortar and pestle in the presence of liquid nitrogen to prevent thawing. Tissues were lysed in up to 1 ml of hypotonic lysis buffer (5 mM Tris-Hcl pH=7.5, 1.5 mM KCl, 2.5 mM $MgCl_2$, 2 mM DTT, 1 mg/ml Cycloheximide, 200 U/ml Recombinant RNasin® Ribonuclease Inhibitor (Promega), 1 tablet cOmplete™, Mini, EDTA-free Protease Inhibitor Cocktail (Roche), 0.5% (v/v) Triton X-100, 0.5% (v/v) Sodium Deoxycholate) and homogenized using Dounce homogenizers (60 movements with both loose and tight pestles) on ice. Samples were centrifuged at 4°C, 16,060g for 4 minutes and supernatants were collected. Sample optical density was measured at 260 nM and samples were normalized to either the lowest value or 30 ODs. 450 µl of sucrose gradient was removed from the top and replaced with normalized sample. Tube weights were balanced by weight before centrifugation at 200,000g for 2 h at 4°C in a SW 41 Ti rotor and a Beckman Optima L-60 Ultracentrifuge. Samples were fractionated using a BR-188 Density Gradient Fractionation System (Brandel). Immediately upon collection, 800 µl of samples were mixed with 1 ml of TRIzol™ and kept on ice before storage at -80°C. Polysomal RNA was

processed according to the manufacturer's protocol. mRNA distribution was analyzed as previously described[47].

3.5.7 Electrophoretic mobility shift assay (EMSA).

IRE-binding activities from liver and spleen were analyzed by EMSA using a radioactive ^{32}P-labelled IRE probe, according to established procedures[27]. EMSAs were also performed in extracts from hepatocytes and non-parenchymal cells, which were separated by using a 2-step collagenase perfusion technique, as previously described[9].

3.5.8 Western blotting.

Livers were washed with ice-cold PBS and dissected into pieces. Aliquots were snap frozen at liquid nitrogen and stored at −80ºC. Protein lysates were obtained as described[22]. Lysates containing 40 μg of proteins were analyzed by SDS-PAGE on 9-13% gels and proteins were transferred onto nitrocellulose membranes (BioRad). The blots were blocked in non-fat milk diluted in tris-buffered saline (TBS) containing 0.1% (v/v) Tween-20 (TBS-T), and probed overnight with antibodies against ferroportin[48] (1:1000 diluted monoclonal rat anti-mouse 1C7, kindly provided by Amgen Inc), β-actin (1:2000 diluted; Sigma), or Tfr2 (1:1000 diluted rabbit polyclonal; Alpha Diagnostics). Following a 3x wash with TBS-T, the membranes were incubated with peroxidase-coupled secondary antibodies for 1 h. Immunoreactive bands were detected by enhanced chemiluminescence with the Western Lightning ECL Kit (Perkin Elmer).

3.5.9 Immunohistochemistry.

Tissue specimens were fixed in 10% buffered formalin and embedded in paraffin. Samples from 3 different mice for each experimental condition were cut at 4-μm, placed on SuperFrost/Plus slides (Fisher) and dried overnight at 37°C. The slides were then loaded onto the Discovery XT Autostainer (Ventana Medical System) for automated immunohistochemistry. Slides underwent de-paraffinization and heat-induced epitope retrieval. Immunostaining was performed by using 1:500 diluted rabbit polyclonal antibodies against ferroportin[49] and an appropriate detection kit (Omnimap rabbit polyclonal HRP, #760-4311 and ChromoMap-DAB #760-159; Roche). Negative controls were performed by the omission of the primary antibody. Slides were counterstained with hematoxylin for four minutes, blued with Bluing Reagent for four minutes, removed from the

autostainer, washed in warm soapy water, dehydrated through graded alcohols, cleared in xylene, and mounted with Permount (Fisher). Sections were analyzed by conventional light microscopy and quantified by using the Aperio ImageScope software (Leica Biosystems)[9].

3.5.10 Perls Prussian blue staining.

To visualize non-heme iron deposits, deparaffinized tissue sections were stained with Perls' Prussian blue using the Accustain Iron Stain kit (Sigma).

3.5.11 Quantification of liver iron content (LIC).

Total liver iron was quantified by using the ferrozine assay[20] or inductively coupled plasma mass spectrometry (ICP-MS)[50].

3.5.12 Iron speciation analysis.

Iron redox speciation analysis in the liver was performed by capillary electrophoresis (CE) coupled to ICP-MS (CE-ICP-MS). Dynamic reaction cell (DRC) technology (ICP-DRC-MS) with NH_3 as DRC-gas was applied for non-interfered monitoring of the iron isotopes. A "PrinCe 706" CE system (PrinCe Technologies B.V., Emmen, Netherlands) was employed for separation of iron species at +20 kV. Temperature settings for sample/buffer tray and capillary were set to 20°C. An uncoated capillary (100 cm x 50 µm ID; CS-Chromatographie Service GmbH, Langerwehe, Germany) was used for separation and hyphenation to the ICP–DRC-MS. A CE-ICP-MS interface[50,51] was installed which provided the electrical connection between CE capillary end and outlet electrode. The self-aspiration mode allowed for best flow rate adjustment and avoided suction flow. Electrolytes for sample stacking and electrophoretic separation were 10% HCl = leading electrolyte, 0.05 mM HCl= terminating electrolyte and 50 mM HCl = background electrolyte. The Fe^{2+}/Fe^{3+} ratio was calculated from quantitative determined concentrations of Fe-species.

3.5.13 Statistics.

Statistical analysis was performed by using the Prism GraphPad software (version 9.1.0). Lognormally distributed data including qPCR and ELISA results were first log transformed before analysis with ordinary two-way ANOVA (Tukey's multiple comparisons test) for comparisons

within same treatment groups (denoted by a or b on figures) or with multiple unpaired t tests using the Holm-Sidak method to compare effects between treatments. Normally distributed data was analyzed by two-way ANOVA using either Sidak's method for comparisons between treatment groups or Tukey's multiple comparisons test within treatments groups. Where indicated, pairwise comparisons were done with unpaired Student's t test. Probability value $p<0.05$ was considered statistically significant.

3.6 Acknowledgments

We thank Dr. Naciba Benlimame and Lilian Canetti for assistance with histology and immunohistochemistry. This work was supported by a grant from the Canadian Institutes of Health Research (CIHR; PJT-159730). EC was funded by a fellowship from the Natural Sciences and Engineering Research Council of Canada (NSERC) and is currently a recipient of a fellowship from the *Fonds de recherche du Québec – Santé* (FRQS). The work of VV and BM was financially supported by the Deutsche Forschungsgemeinschaft (DFG) through the Priority Program "Ferroptosis: from Molecular Basics to Clinical Applications" (SPP 2306).

3.7 Competing interests

The authors declare no competing financial interests.

3.8 References

1. Camaschella C, Nai A, Silvestri L. Iron metabolism and iron disorders revisited in the hepcidin era. *Haematologica*. 2020;105(2):260-272.
2. Katsarou A, Pantopoulos K. Basics and principles of cellular and systemic iron homeostasis. *Mol Aspects Med*. 2020;75:100866.
3. Aschemeyer S, Qiao B, Stefanova D, et al. Structure-function analysis of ferroportin defines the binding site and an alternative mechanism of action of hepcidin. *Blood*. 2018;131(8):899-910.
4. Billesbolle CB, Azumaya CM, Kretsch RC, et al. Structure of hepcidin-bound ferroportin reveals iron homeostatic mechanisms. *Nature*. 2020;586(7831):807-811.
5. Ganz T, Nemeth E. Iron homeostasis in host defence and inflammation. *Nat Rev Immunol*. 2015;15(8):500-510.
6. Wang CY, Babitt JL. Liver iron sensing and body iron homeostasis. *Blood*. 2019;133(1):18-29.
7. Schmidt PJ. Regulation of Iron Metabolism by Hepcidin under Conditions of Inflammation. *J Biol Chem*. 2015;290(31):18975-18983.
8. Huang FW, Pinkus JL, Pinkus GS, Fleming MD, Andrews NC. A mouse model of juvenile hemochromatosis. *J Clin Invest*. 2005;115(8):2187-2191.
9. Fillebeen C, Wilkinson N, Charlebois E, Katsarou A, Wagner J, Pantopoulos K. Hepcidin-mediated hypoferremic response to acute inflammation requires a threshold of Bmp6/Hjv/Smad signaling. *Blood*. 2018;132(17):1829-1841.
10. Charlebois E, Pantopoulos K. Iron overload inhibits BMP/SMAD and IL-6/STAT3 signaling to hepcidin in cultured hepatocytes. *PLoS One*. 2021;16(6):e0253475.
11. Yu LN, Wang SJ, Chen C, Rausch V, Elshaarawy O, Mueller S. Direct modulation of hepatocyte hepcidin signaling by iron. *World J Hepatol*. 2021;13(10):1378-1393.
12. Guida C, Altamura S, Klein FA, et al. A novel inflammatory pathway mediating rapid hepcidin-independent hypoferremia. *Blood*. 2015;125(14):2265-2275.
13. Deschemin JC, Vaulont S. Role of hepcidin in the setting of hypoferremia during acute inflammation. *PLoS One*. 2013;8(4):e61050.
14. Drakesmith H, Nemeth E, Ganz T. Ironing out Ferroportin. *Cell Metab*. 2015;22(5):777-787.
15. Aydemir F, Jenkitkasemwong S, Gulec S, Knutson MD. Iron loading increases ferroportin heterogeneous nuclear RNA and mRNA levels in murine J774 macrophages. *J Nutr*. 2009;139(3):434-438.
16. Ludwiczek S, Aigner E, Theurl I, Weiss G. Cytokine-mediated regulation of iron transport in human monocytic cells. *Blood*. 2003;101:4148-4154.
17. Wang J, Pantopoulos K. Regulation of cellular iron metabolism. *Biochem J*. 2011;434(3):365-381.
18. Muckenthaler MU, Galy B, Hentze MW. Systemic iron homeostasis and the iron-responsive element/iron-regulatory protein (IRE/IRP) regulatory network. *Annu Rev Nutr*. 2008;28:197-213.
19. Corradini E, Meynard D, Wu Q, et al. Serum and liver iron differently regulate the bone morphogenetic protein 6 (BMP6)-SMAD signaling pathway in mice. *Hepatology*. 2011;54(1):273-284.

20. Daba A, Gkouvatsos K, Sebastiani G, Pantopoulos K. Differences in activation of mouse hepcidin by dietary iron and parenterally administered iron dextran: compartmentalization is critical for iron sensing. *J Mol Med (Berl)*. 2013;91:95-102.
21. Zhang DL, Hughes RM, Ollivierre-Wilson H, Ghosh MC, Rouault TA. A ferroportin transcript that lacks an iron-responsive element enables duodenal and erythroid precursor cells to evade translational repression. *Cell Metab*. 2009;9(5):461-473.
22. Katsarou A, Gkouvatsos K, Fillebeen C, Pantopoulos K. Tissue-Specific Regulation of Ferroportin in Wild-Type and Hjv-/- Mice Following Dietary Iron Manipulations. *Hepatol Commun*. 2021;5(12):2139-2150.
23. Schulze RJ, Schott MB, Casey CA, Tuma PL, McNiven MA. The cell biology of the hepatocyte: A membrane trafficking machine. *J Cell Biol*. 2019;218(7):2096-2112.
24. Kurotaki D, Uede T, Tamura T. Functions and development of red pulp macrophages. *Microbiol Immunol*. 2015;59(2):55-62.
25. Laftah AH, Ramesh B, Simpson RJ, et al. Effect of hepcidin on intestinal iron absorption in mice. *Blood*. 2004;103:3940-3944.
26. Johnson MB, Enns CA. Diferric transferrin regulates transferrin receptor 2 protein stability. *Blood*. 2004;104:4287-4293.
27. Fillebeen C, Wilkinson N, Pantopoulos K. Electrophoretic mobility shift assay (EMSA) for the study of RNA-protein interactions: the IRE/IRP example. *J Vis Exp*. 2014(94).
28. Krenkel O, Tacke F. Liver macrophages in tissue homeostasis and disease. *Nat Rev Immunol*. 2017;17(5):306-321.
29. Enculescu M, Metzendorf C, Sparla R, et al. Modelling Systemic Iron Regulation during Dietary Iron Overload and Acute Inflammation: Role of Hepcidin-Independent Mechanisms. *PLoS Comput Biol*. 2017;13(1):e1005322.
30. Kent P, Wilkinson N, Constante M, et al. Hfe and Hjv exhibit overlapping functions for iron signaling to hepcidin. *J Mol Med (Berl)*. 2015;93(5):489-498.
31. Wilkinson N, Pantopoulos K. The IRP/IRE system in vivo: insights from mouse models. *Front Pharmacol*. 2014;5:176.
32. Lymboussaki A, Pignatti E, Montosi G, Garuti C, Haile DJ, Pietrangelo A. The role of the iron responsive element in the control of ferroportin1/IREG1/MTP1 gene expression. *J Hepatol*. 2003;39:710-715.
33. Nairz M, Ferring-Appel D, Casarrubea D, et al. Iron Regulatory Proteins Mediate Host Resistance to Salmonella Infection. *Cell Host Microbe*. 2015;18(2):254-261.
34. Galy B, Ferring-Appel D, Becker C, et al. Iron regulatory proteins control a mucosal block to intestinal iron absorption. *Cell Rep*. 2013;3(3):844-857.
35. Garza KR, Clarke SL, Ho YH, et al. Differential translational control of 5' IRE-containing mRNA in response to dietary iron deficiency and acute iron overload. *Metallomics*. 2020;12(12):2186-2198.
36. Katsarou A, Pantopoulos K. Hepcidin Therapeutics. *Pharmaceuticals (Basel)*. 2018;11(4).
37. Jenkitkasemwong S, Wang CY, Coffey R, et al. SLC39A14 Is Required for the Development of Hepatocellular Iron Overload in Murine Models of Hereditary Hemochromatosis. *Cell Metab*. 2015;22(1):138-150.
38. Liuzzi JP, Lichten LA, Rivera S, et al. Interleukin-6 regulates the zinc transporter Zip14 in liver and contributes to the hypozincemia of the acute-phase response. *Proc Natl Acad Sci USA*. 2005;102:6843-6848.

39. Wang CY, Knutson MD. Hepatocyte divalent metal-ion transporter-1 is dispensable for hepatic iron accumulation and non-transferrin-bound iron uptake in mice. *Hepatology*. 2013;58(2):788-798.
40. Wardrop SL, Richardson DR. Interferon-gamma and lipopolysaccharide regulate the expression of Nramp2 and increase the uptake of iron from low relative molecular mass complexes by macrophages. *Eur J Biochem*. 2000;267(22):6586-6593.
41. Xiao X, Yeoh BS, Vijay-Kumar M. Lipocalin 2: An Emerging Player in Iron Homeostasis and Inflammation. *Annu Rev Nutr*. 2017;37:103-130.
42. Gkouvatsos K, Fillebeen C, Daba A, Wagner J, Sebastiani G, Pantopoulos K. Iron-dependent regulation of hepcidin in Hjv-/- mice: evidence that hemojuvelin is dispensable for sensing body iron levels. *PLoS One*. 2014;9(1):e85530.
43. Fillebeen C, Charlebois E, Wagner J, et al. Transferrin receptor 1 controls systemic iron homeostasis by fine-tuning hepcidin expression to hepatocellular iron load. *Blood*. 2019;133(4):344-355.
44. Esposito BP, Breuer W, Sirankapracha P, Pootrakul P, Hershko C, Cabantchik ZI. Labile plasma iron in iron overload: redox activity and susceptibility to chelation. *Blood*. 2003;102(7):2670-2677.
45. Livak KJ, Schmittgen TD. Analysis of Relative Gene Expression Data Using Real-Time Quantitative PCR and the 2−ΔΔCT Method. *Methods*. 2001;25(4):402-408.
46. Liang S, Bellato HM, Lorent J, et al. Polysome-profiling in small tissue samples. *Nucleic Acids Res*. 2018;46(1):e3-e3.
47. Panda A, Martindale J, Gorospe M. Polysome Fractionation to Analyze mRNA Distribution Profiles. *BIO-PROTOCOL*. 2017;7(3).
48. Ross SL, Biswas K, Rottman J, et al. Identification of Antibody and Small Molecule Antagonists of Ferroportin-Hepcidin Interaction. *Front Pharmacol*. 2017;8:838.
49. Maffettone C, Chen G, Drozdov I, Ouzounis C, Pantopoulos K. Tumorigenic properties of iron regulatory protein 2 (IRP2) mediated by its specific 73-amino acids insert. *PLoS One*. 2010;5(4):e10163.
50. Michalke B, Willkommen D, Venkataramani V. Iron Redox Speciation Analysis Using Capillary Electrophoresis Coupled to Inductively Coupled Plasma Mass Spectrometry (CE-ICP-MS). *Front Chem*. 2019;7:136.
51. Michalke B, Willkommen D, Venkataramani V. Setup of Capillary Electrophoresis-Inductively Coupled Plasma Mass Spectrometry (CE-ICP-MS) for Quantification of Iron Redox Species (Fe(II), Fe(III)). *J Vis Exp*. 2020(159).

3.9 Figures

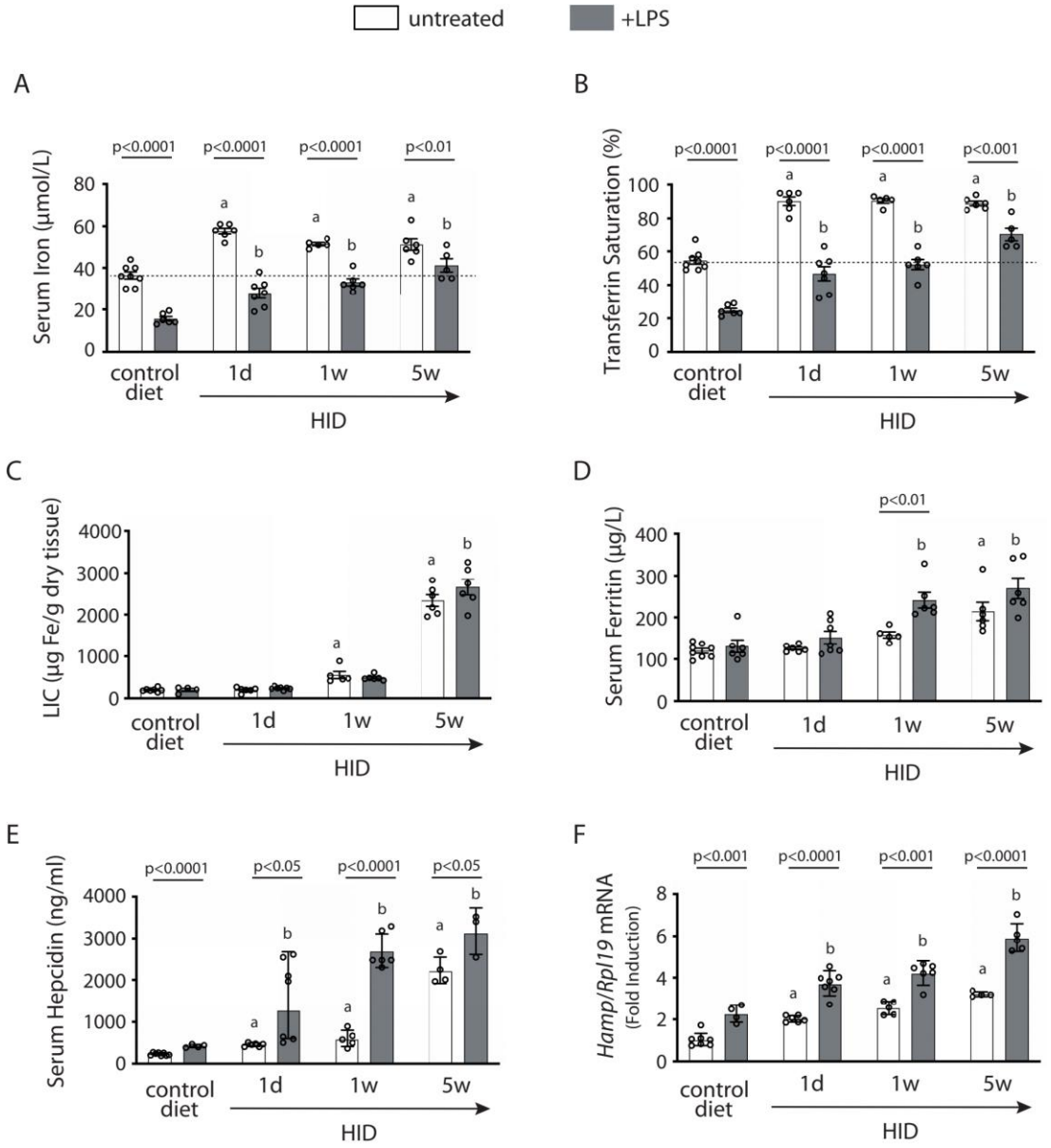

Figure 3.1: Dietary iron loading does not disrupt inflammatory hepcidin induction in LPS-treated wild type mice but blunts hepcidin-mediated hypoferremia.
Nine-week-old male mice (n=12-14 per group) were fed SD or HID for one day, one week, or five weeks prior to sacrifice. Half of the mice were injected intraperitoneally with saline and the other half with 1 µg/g LPS 4 hours before sacrifice. Sera were collected by cardiac puncture and analyzed for: (A) iron, (B) transferrin saturation, (D) ferritin, and (E) hepcidin. Livers were dissected and processed for biochemical analysis of: (C) liver iron content (LIC) by the ferrozine assay and (F) *Hamp* mRNA by qPCR. The dotted line in (A) and (B) indicates baseline serum iron and transferrin saturation, respectively, of control mice on SD. Data (A-E) are presented as the mean±SEM and in (F) as geometric mean±SD. Statistically significant differences ($p<0.05$) over time compared to values from saline- or LPS-treated control mice are indicated by a or b, respectively.

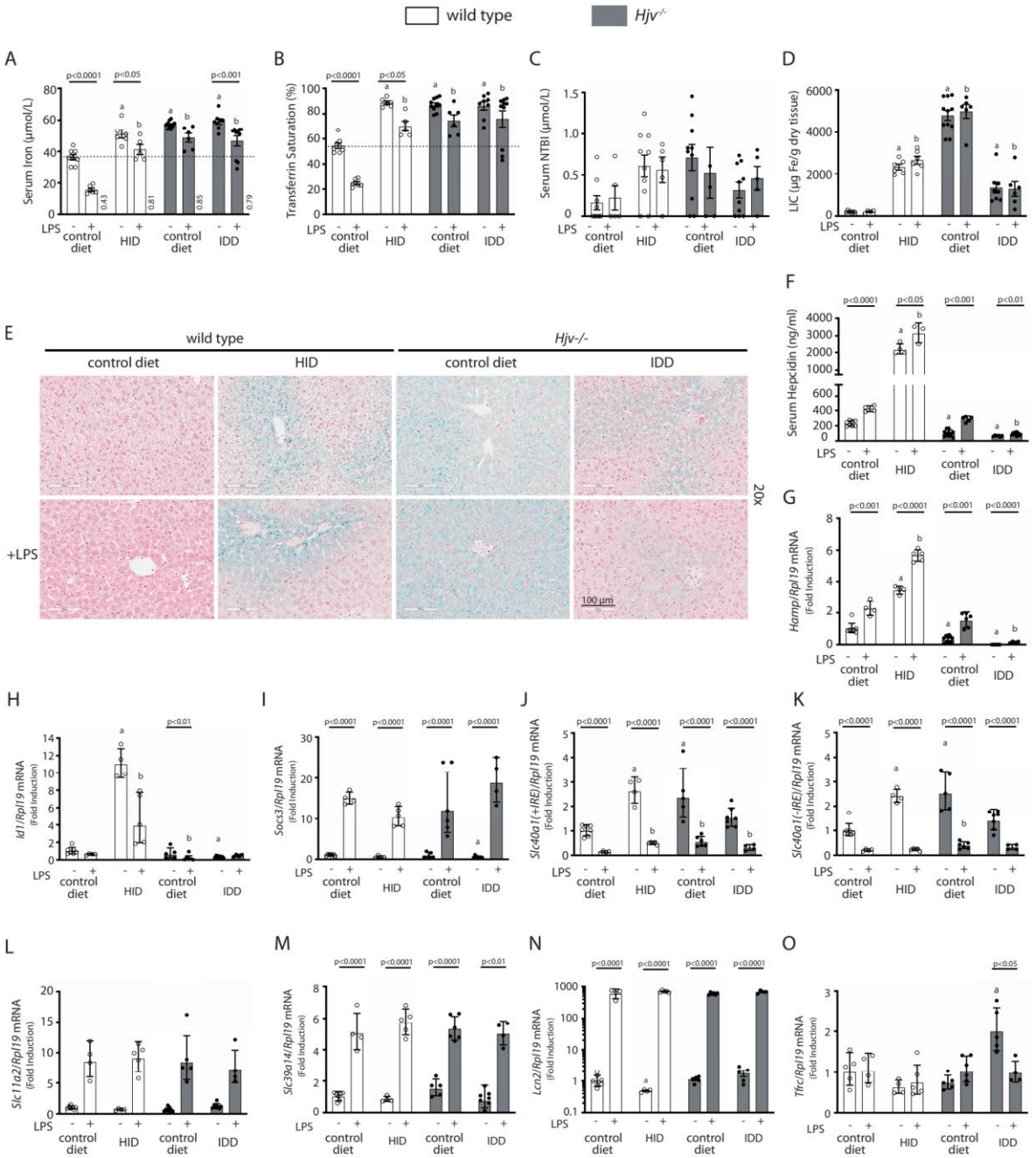

Figure 3.2: Iron overload blunts hepcidin responsiveness to LPS-induced inflammation.
Four-week-old male wt mice (n=12-14 per group) were placed on HID for five weeks. Conversely, age- and sex-matched isogenic *Hjv*$^{-/-}$ mice (n=12-14 per group) were placed on IDD for five weeks to prevent excessive iron overload. Controls from both genotypes were kept on SD. Half of the mice were injected with saline and the other half with 1 µg/g LPS; all animals were sacrificed 4 hours later. Sera were collected by cardiac puncture and analyzed for: (A) iron, (B) transferrin saturation, (C) NTBI, and (F) hepcidin. Livers were dissected and processed for LIC quantification by the ferrozine assay (D) and for histological detection of iron deposits by Perls' staining (E; magnification: 20x). Livers were also used for qPCR analysis of following mRNAs: (G) *Hamp*, (H) Id1, (I) Socs3, (J) *Slc40a1(+IRE)*, (K) *Slc40a1(-IRE)*, (L) *Slc11a2*, (M) *Slc39a14*, (N) *Lcn2* and (O) *Tfrc*. The dotted line in (A) and (B) indicates baseline serum iron and transferrin saturation, respectively, of control wt mice on SD. Values in (A) represent ratios of serum iron levels between untreated and LPS-treated mice. Data in (A-F) are presented as the mean±SEM while in (G-O) are presented as geometric mean±SD. Statistically significant differences ($p<0.05$) compared to values from saline- or LPS-treated wt control mice are indicated by a or b, respectively.

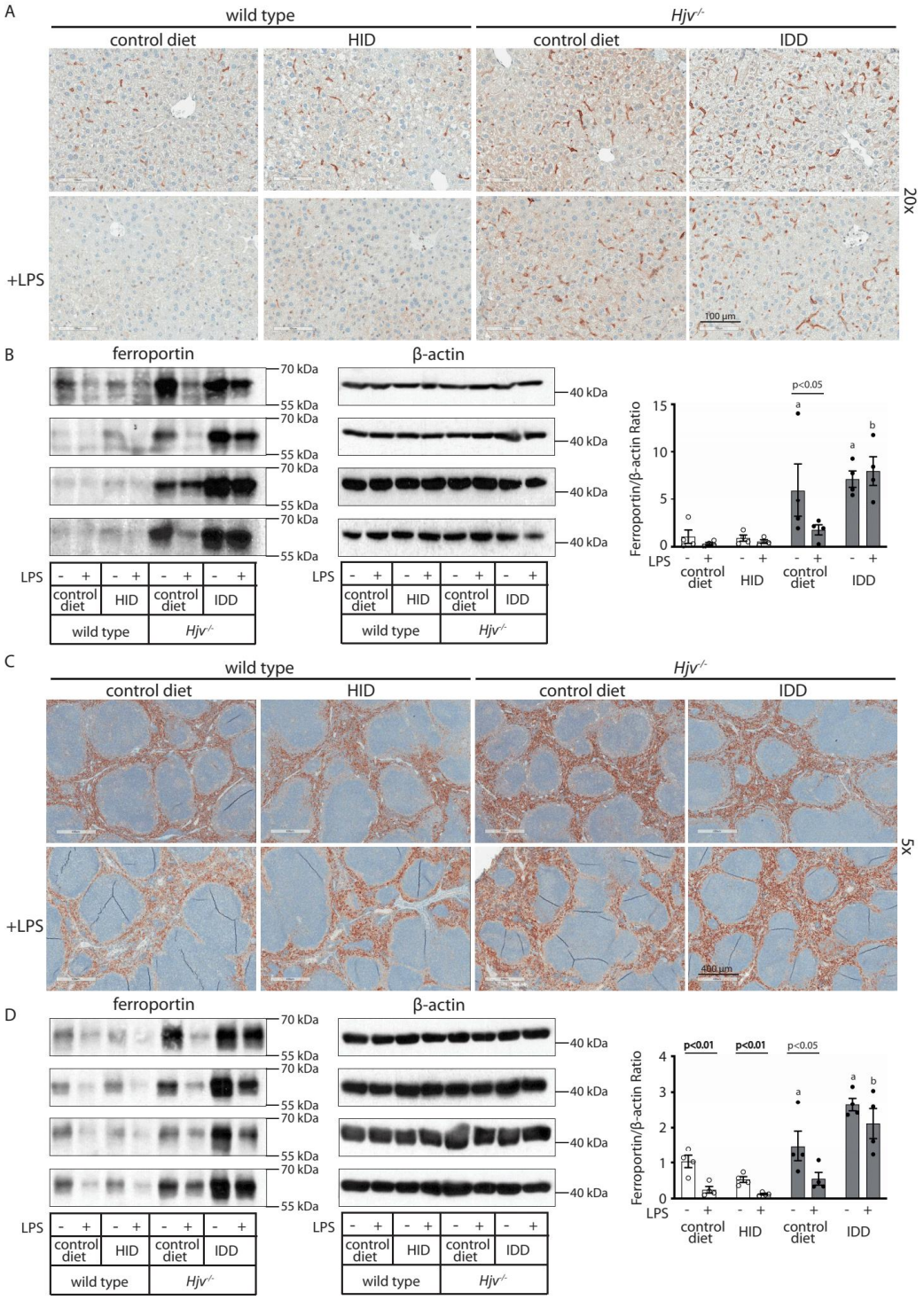

Figure 3.3: Effects of LPS on hepatic and splenic ferroportin of iron-manipulated wt and *Hjv*$^{-/-}$ mice.
Livers and spleens from mice described in Figure 2 were dissected and processed for immunohistochemical and biochemical analysis of ferroportin. Immunohistochemical staining of ferroportin in liver (A) and spleen (C) sections (magnification for liver is 20x and for spleen 5x). Western blot for ferroportin and β-actin in liver (B) and spleen (D) extracts from four representative mice in each condition. Blots were quantified by densitometry and ferroportin/β-actin ratios are shown on the right. Densitometric data are presented as the mean±SEM. Statistically significant differences ($p<0.05$) compared to values from saline- or LPS-treated wt control mice are indicated by a or b, respectively. Statistics in bold were performed using unpaired Student's t test.

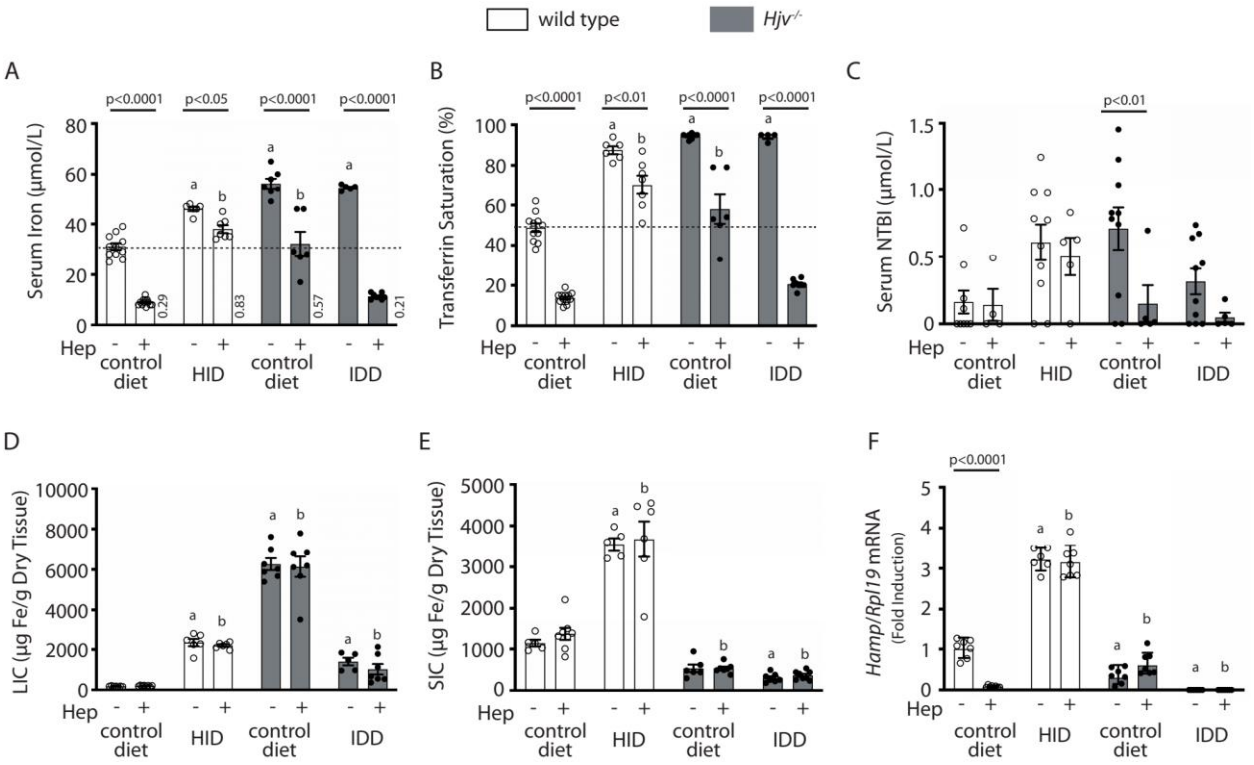

Figure 3.4: Iron depletion of *Hjv*$^{-/-}$ mice improves the efficacy of synthetic hepcidin to promote hypoferremia. Four-week-old wt male mice (n=12-14 per group) were placed on HID for five weeks. Conversely, age- and sex-matched isogenic *Hjv*$^{-/-}$ mice (n=12-14 per group) were placed on IDD for five weeks to prevent excessive iron overload. Controls from both genotypes were kept on SD. Half of the mice were injected every 2 hours for a total of 4 injections with saline, and the other half with 2.5 µg/g synthetic hepcidin. Sera were collected by cardiac puncture and analyzed for: (A) iron, (B) transferrin saturation, and (C) NTBI. Livers and spleens were dissected and processed for analysis of: (D) LIC and (E) SIC by the ferrozine assay. (F) qPCR analysis of liver *Hamp* mRNA. The dotted line in (A) and (B) indicates baseline serum iron and transferrin saturation, respectively, of control wt mice on SD. Values in (A) represent ratios of serum iron levels between untreated and hepcidin-treated mice. Data in (A-E) are presented as the mean±SEM and in (F) as geometric mean±SD. Statistically significant differences ($p<0.05$) compared to values from saline- or hepcidin-treated wt control mice are indicated by a or b, respectively.

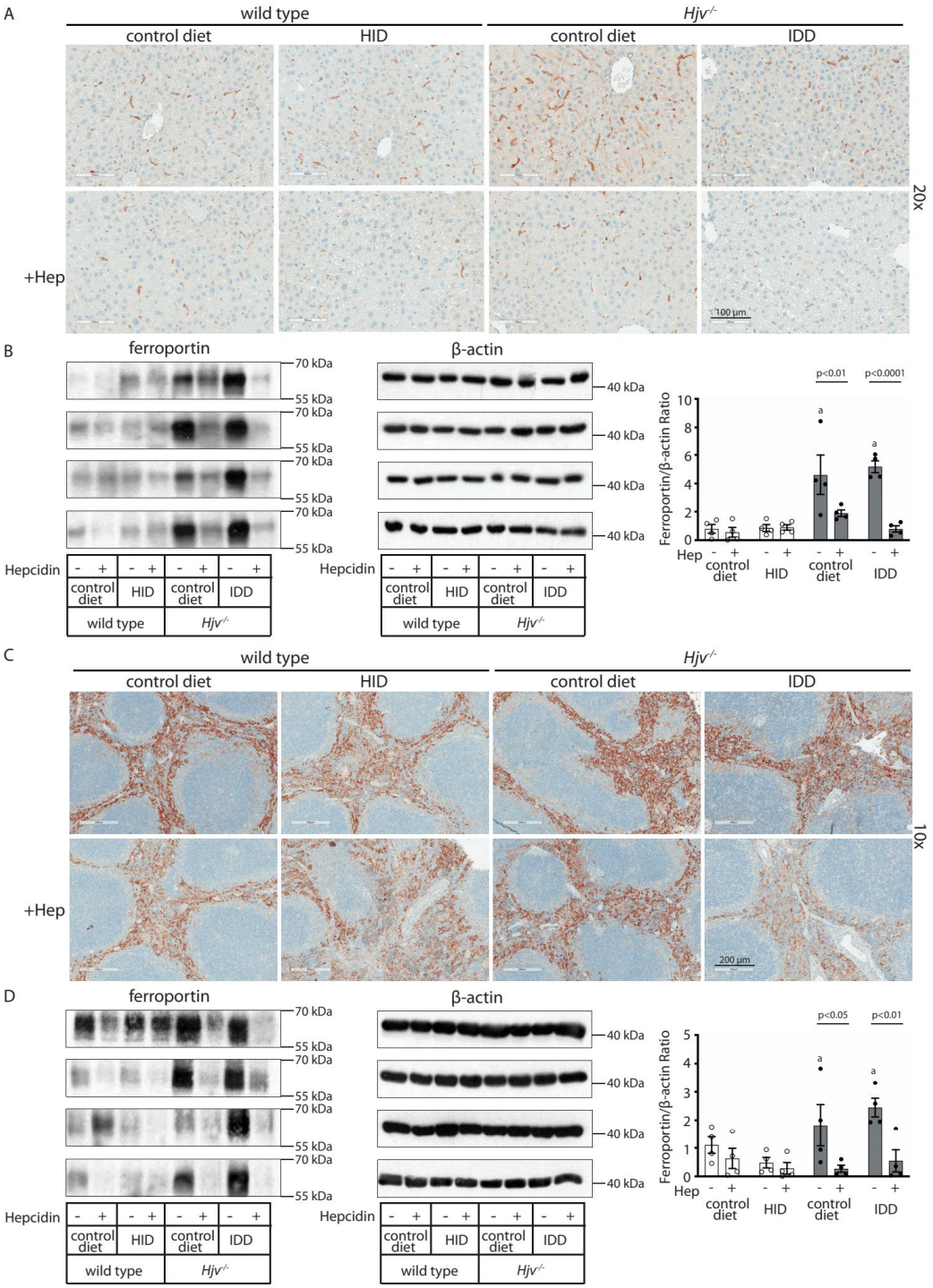

Figure 3.5: Effects of synthetic hepcidin on hepatic and splenic ferroportin of iron-manipulated wt and *Hjv*$^{-/-}$ mice.

Livers and spleens from mice described in Figure 4 were dissected and processed for immunohistochemical and biochemical analysis of ferroportin. Immunohistochemical staining of ferroportin in liver (A) and spleen (C) sections (magnification for liver is 20x and for spleen 10x). Western blot for ferroportin and β-actin in liver (B) and spleen (D) extracts from four representative mice in each condition. Blots were quantified by densitometry and ferroportin/β-actin ratios are shown on the right. Densitometric data are presented as the mean±SEM. Statistically significant differences ($p<0.05$) compared to values from saline- or hepcidin-treated wt control mice are indicated by a or b, respectively.

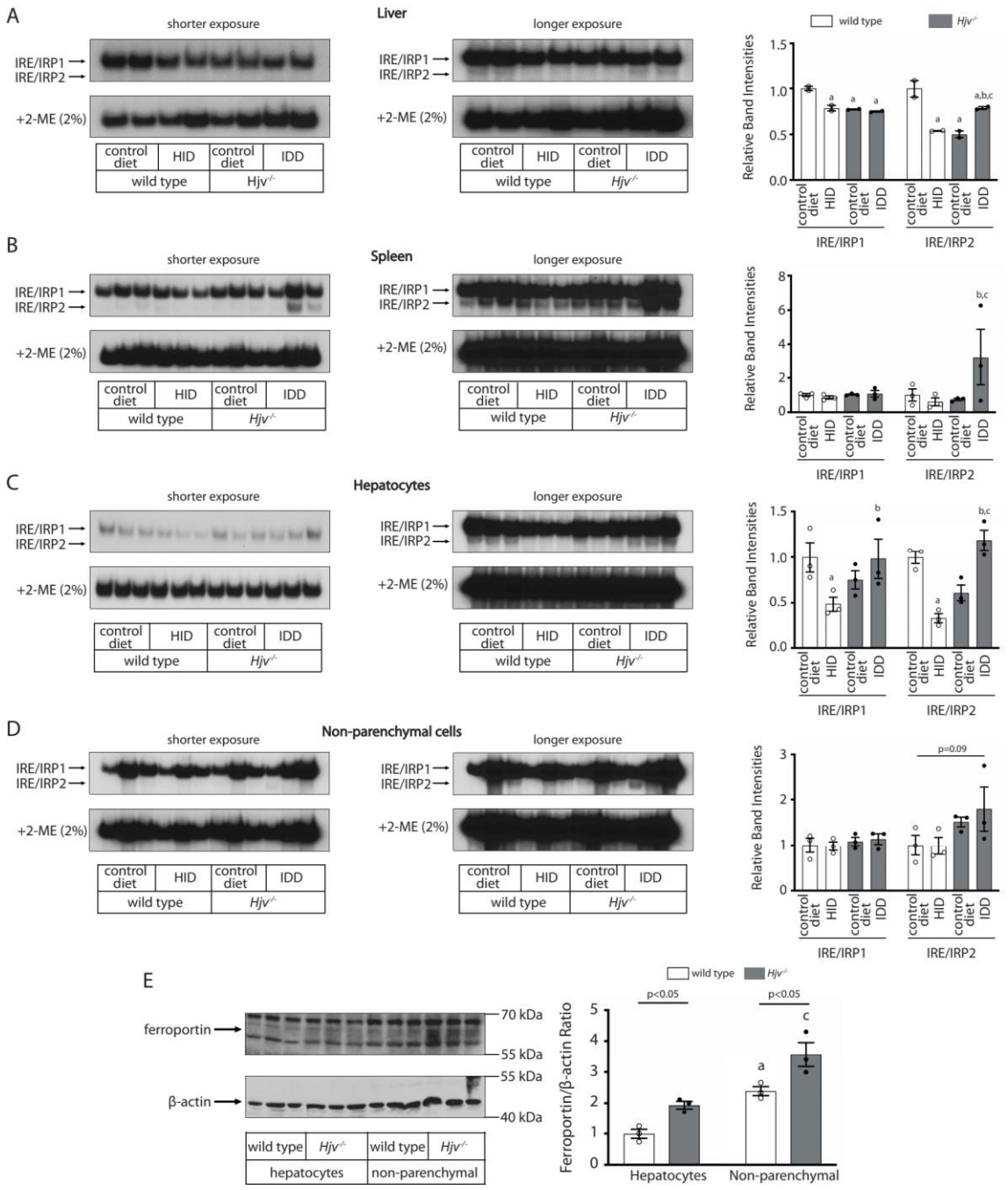

Figure 3.6: Dietary iron manipulations trigger IRP responses in the liver and spleen, as well as in primary hepatocytes and non-parenchymal liver cells of wt and *Hjv*$^{-/-}$ mice.

Whole liver (A), whole spleen (B), isolated hepatocytes (C) or isolated non-parenchymal liver cells (D) from the mice described in Figure 4 were analyzed for IRE-binding activity by EMSA with a ^{32}P-labelled IRE probe in the absence (top) or presence (bottom) of 2% mercaptoethanol (2-ME). Two or three representative samples from each condition are shown. The positions of IRE/IRP1 and IRE/IRP2 complexes are indicated by arrows. Shorter and longer exposures of the autoradiograms are shown in the left and middle panels, respectively. Relative band intensities were quantified by densitometry and shown on the right panels. (E) Isolated hepatocytes and isolated non-parenchymal liver cells were analyzed by Western blotting for expression of ferroportin and β-actin. Blots were quantified by densitometry and ferroportin/β-actin ratios are shown on the right. Densitometric data are presented as the mean±SEM. Statistically significant differences ($p<0.05$) in values from control wt mice on SD are indicated by a, from wt mice on HID by b, and from *Hjv*$^{-/-}$ mice on SD by c.

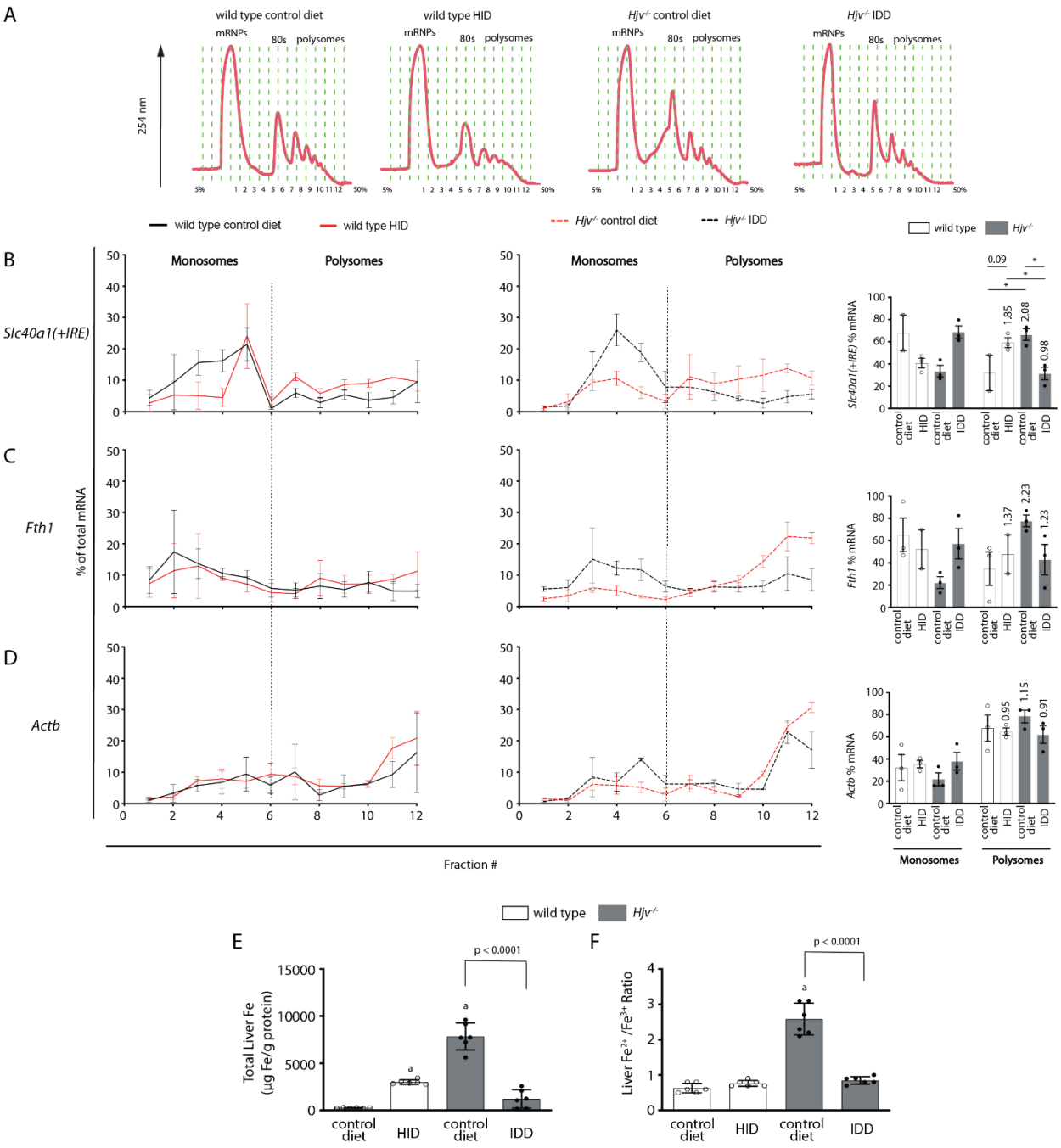

Figure 3.7: Iron regulation of Slc40a1(+IRE) mRNA translation in the mouse liver.
Four-week-old wt male mice (n=10-14 per group) were placed on HID for five weeks. Conversely, age- and sex-matched isogenic *Hjv*$^{-/-}$ mice (n=10-14 per group) were placed on IDD for five weeks to prevent excessive iron overload. Controls from both genotypes were kept on SD. At the endpoint, the mice were sacrificed, and livers were used for polysome profile analysis and iron assays. (A) Recording of absorbance at 254 nm of representative samples. Fraction numbers and direction of the gradient are indicated. (B-D) Liver polysome profiles from n=3 mice in each experimental group. Distribution of (B) *Slc40a1(+IRE)*, (C) *Fth1* and (D) *Actb* mRNAs among light monosomal and heavy polysomal fractions (separated by dashed line) was analyzed by qPCR. Bar graph comparisons of pooled fractions are shown on the right. Numbers indicate the fold change compared to wt mice on SD. (E and F) Analysis of total iron (E), and redox iron speciation (F) in the liver by CE-ICP-MS. Data are presented as the mean±SEM. Statistical analysis in (A) was performed by two-way ANOVA and in (B, C) by one-way ANOVA. Statistically significant differences ($p<0.05$) compared to values from wt control mice on SD are indicated by a.

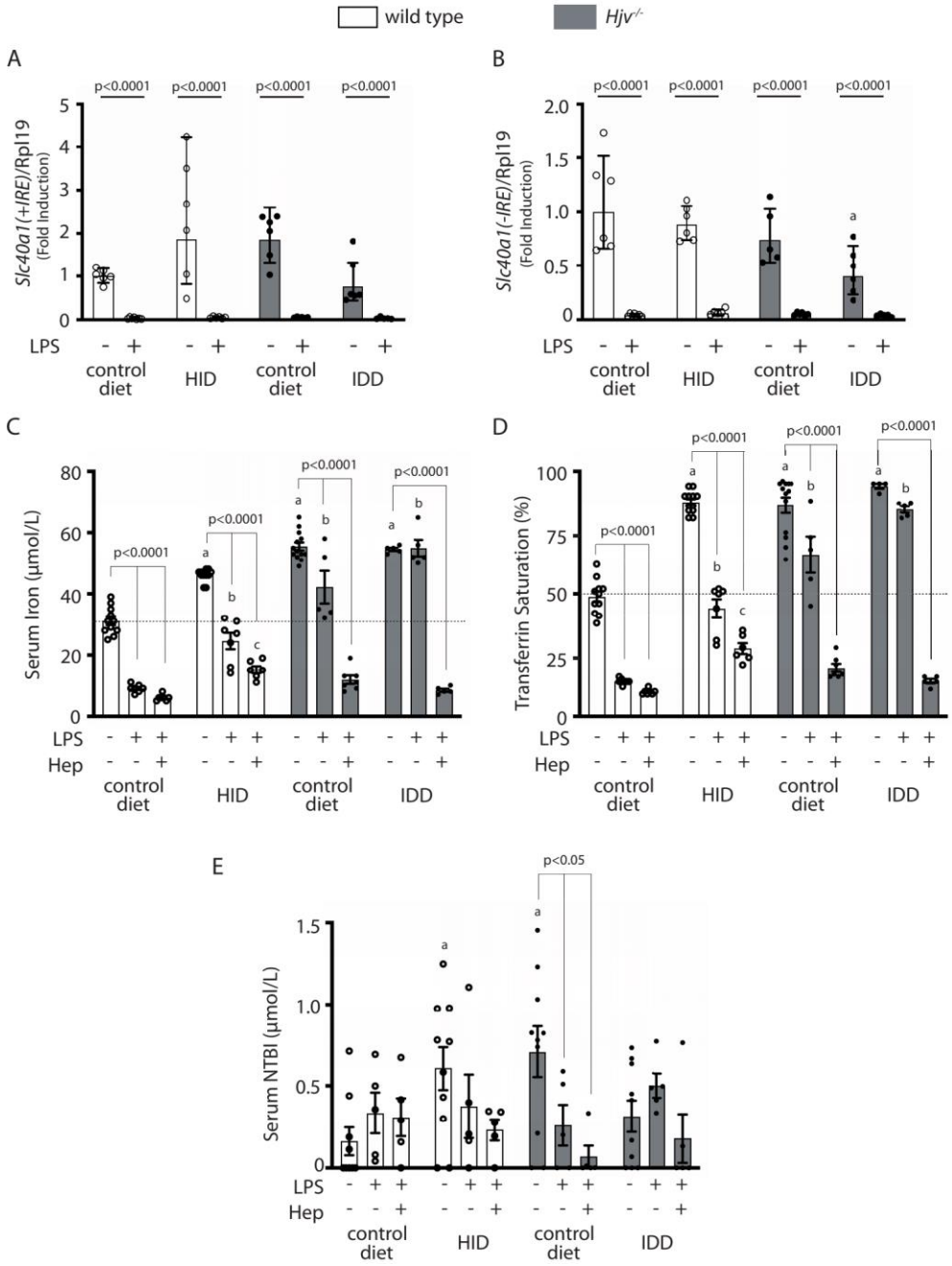

Figure 3.8: Elimination of ferroportin mRNA by prolonged LPS treatment potentiates hepcidin-induced hypoferremia in mouse models of iron overload.

Four-week-old wt male mice (n=10-14 per group) were placed on HID for five weeks. Conversely, age- and sex-matched isogenic *Hjv*$^{-/-}$ mice (n=10-14 per group) were placed on IDD for five weeks to prevent excessive iron overload. Controls from both genotypes were kept on SD. (A and B) Half of the mice were injected with saline and the other half with 1 µg/g LPS and sacrificed after 8 h. Livers were dissected and processed for qPCR analysis of *Slc40a1(+IRE)* (A) and *Slc40a1(-IRE)* (B) mRNAs. (C-E) All mice were injected with 1 µg/g LPS. Half of the animals were subsequently injected with saline, and the other half with 2.5 µg/g synthetic hepcidin every two hours for a total of 4 injections. At the endpoint the mice were sacrificed. Sera were collected by cardiac puncture and analyzed for: (C) iron, (D) transferrin saturation, and (E) NTBI. The dotted line in (C) and (D) indicates baseline serum iron and transferrin saturation, respectively, of control wt mice on SD. Data are presented as (A-B) geometric mean±SD or (C-E) mean±SEM. Statistically significant differences ($p<0.05$) compared to values from saline-, LPS- or hepcidin-treated wt control mice on SD are indicated by a, b or c, respectively.

3.10 Supplementary Figures

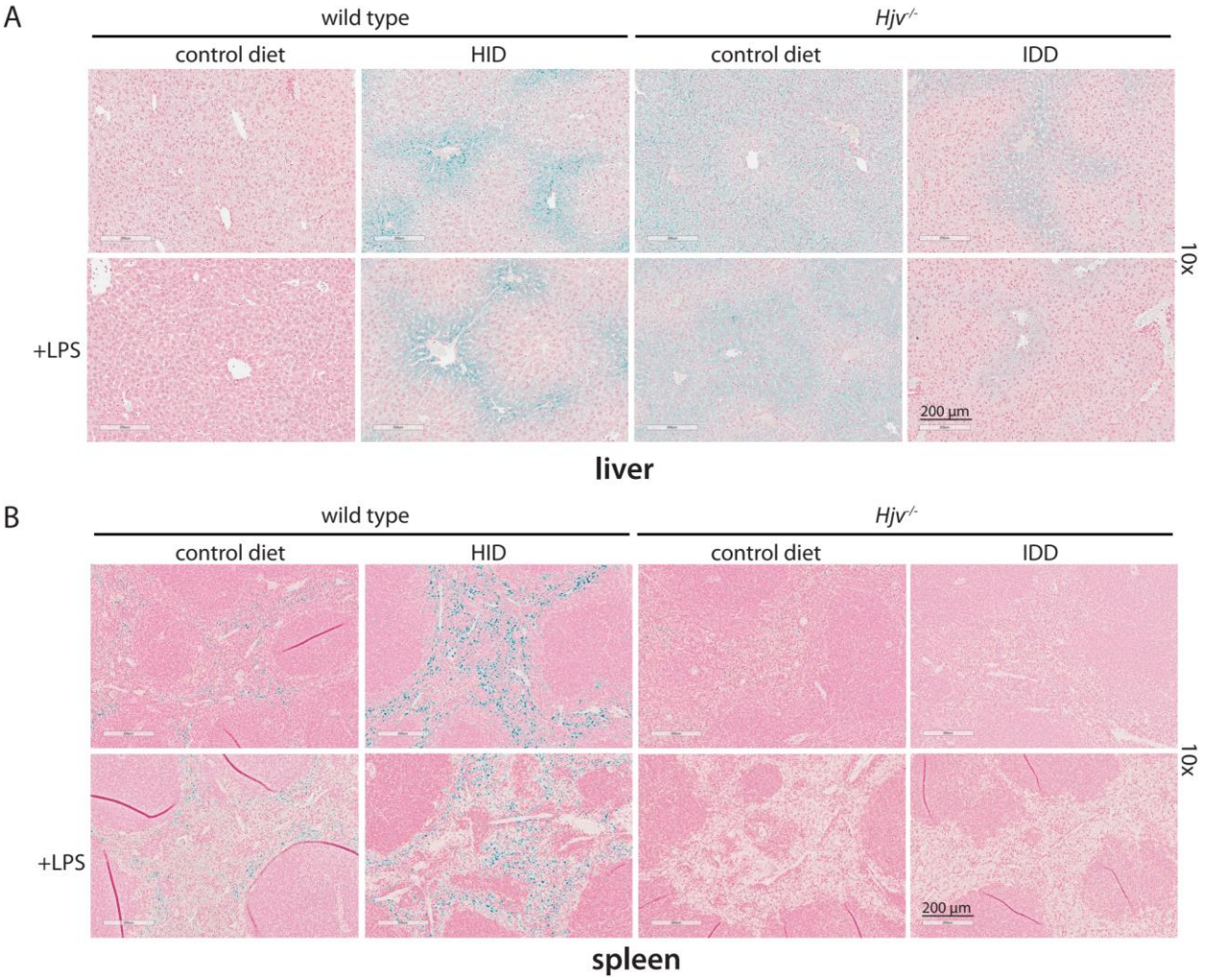

Figure 3.2-figure supplement 1: Effects of dietary iron manipulations in hepatic and splenic iron of wt and *Hjv*$^{-/-}$ mice.
(A) Liver and (B) spleen sections from mice described in Figure 2 were analyzed histologically for iron deposits by Perls staining (magnification: 10x).

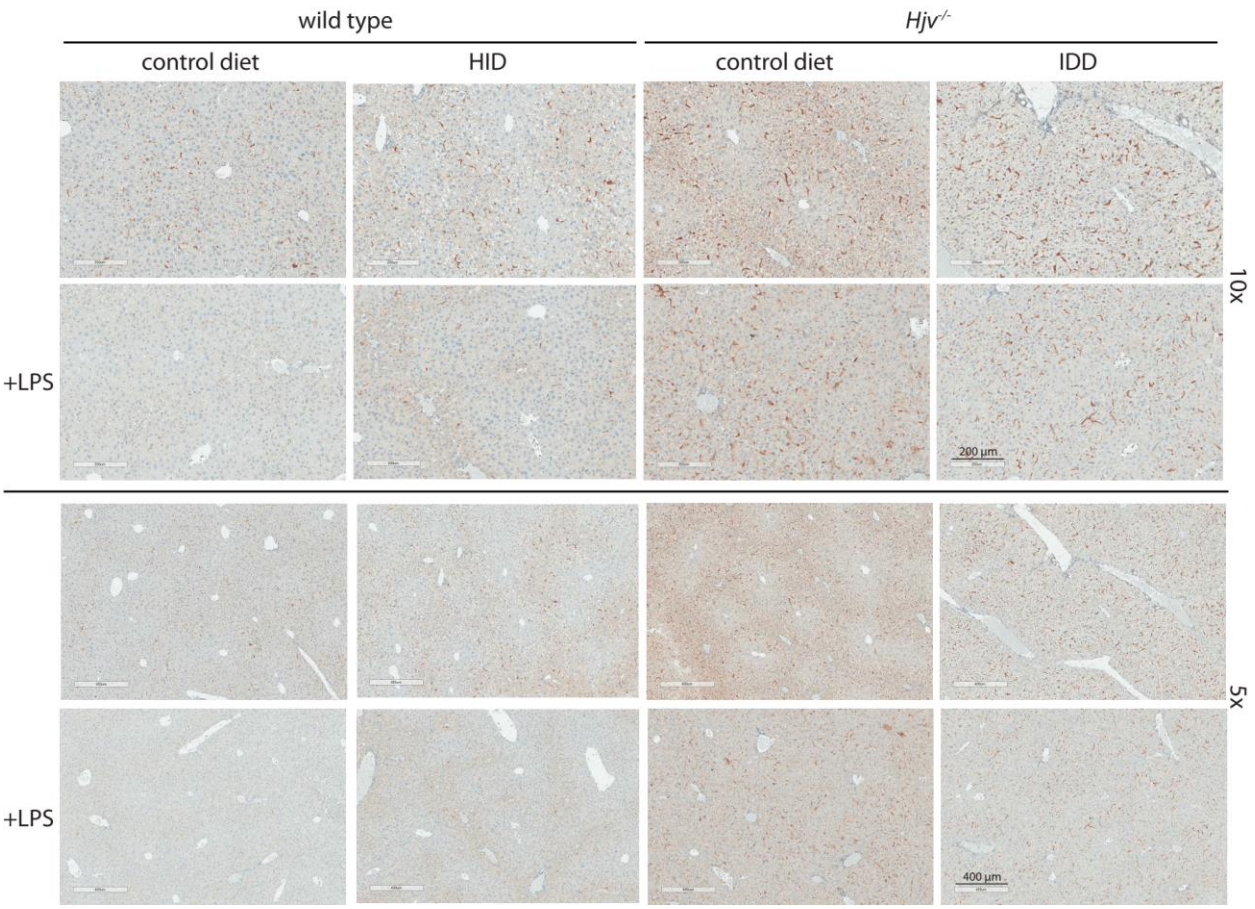

Figure 3.3-figure supplement 1: Low magnification immunohistochemical images of ferroportin in liver sections of dietary iron-manipulated wild type and *Hjv*$^{-/-}$ mice following LPS treatment.
Liver sections from mice described in Figure 2 were used for immunohistochemical analysis of ferroportin (magnifications: 10x and 5x).

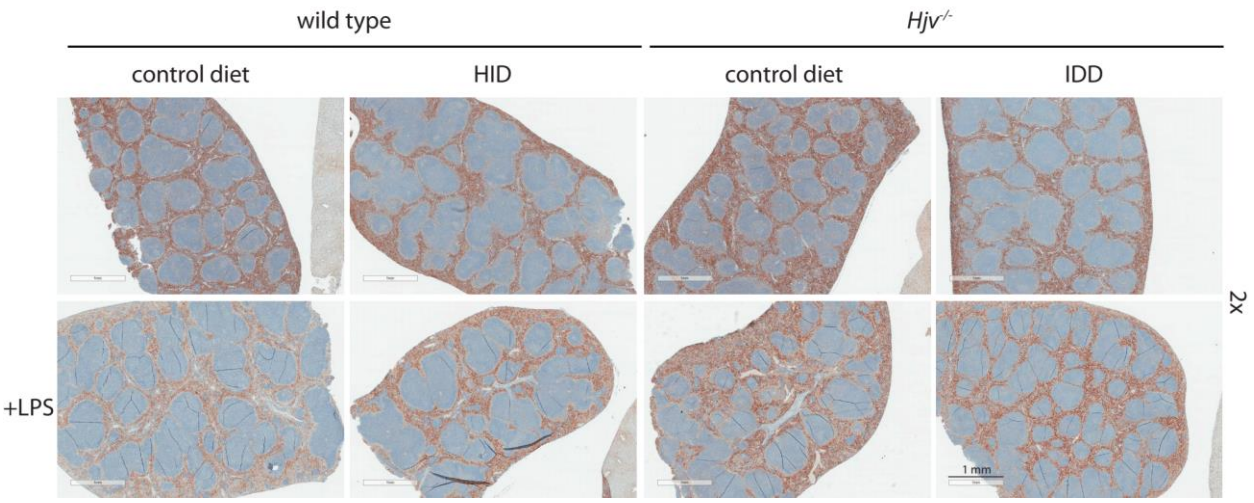

Figure 3.3-figure supplement 2: Low magnification immunohistochemical images of ferroportin in spleen sections of dietary iron-manipulated wild type and *Hjv*$^{-/-}$ mice following LPS treatment.

Spleen sections from mice described in Figure 2 were used for immunohistochemical analysis of ferroportin (magnification: 2x).

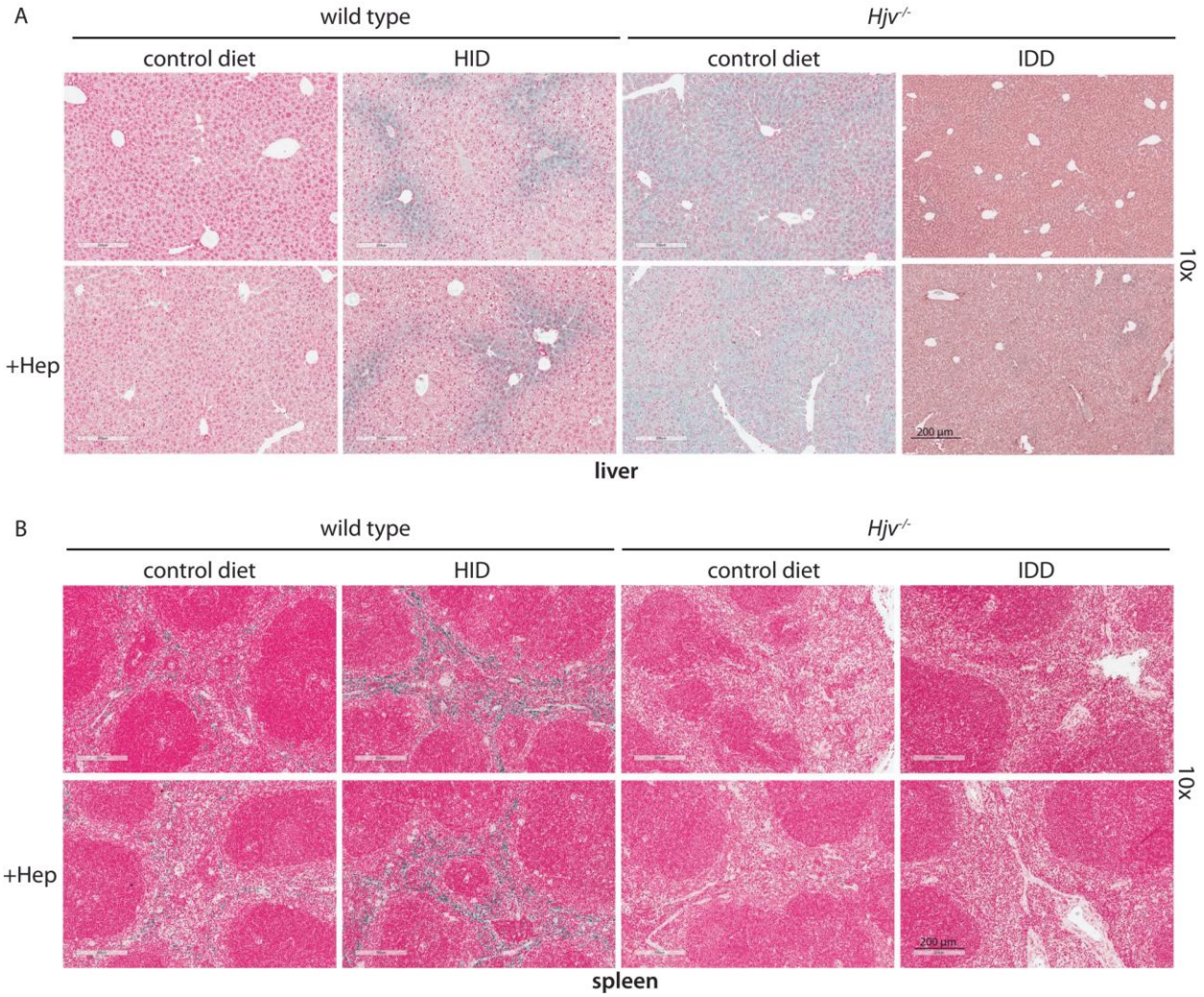

Figure 3.4-figure supplement 1: Perls staining for iron deposits in liver and spleen sections of dietary iron-manipulated wild type and *Hjv*$^{-/-}$ mice following treatment with synthetic hepcidin.
(A) Liver and (B) spleen sections from mice described in Figure 4 were stained with Perls Prussian blue (magnification: 10x).

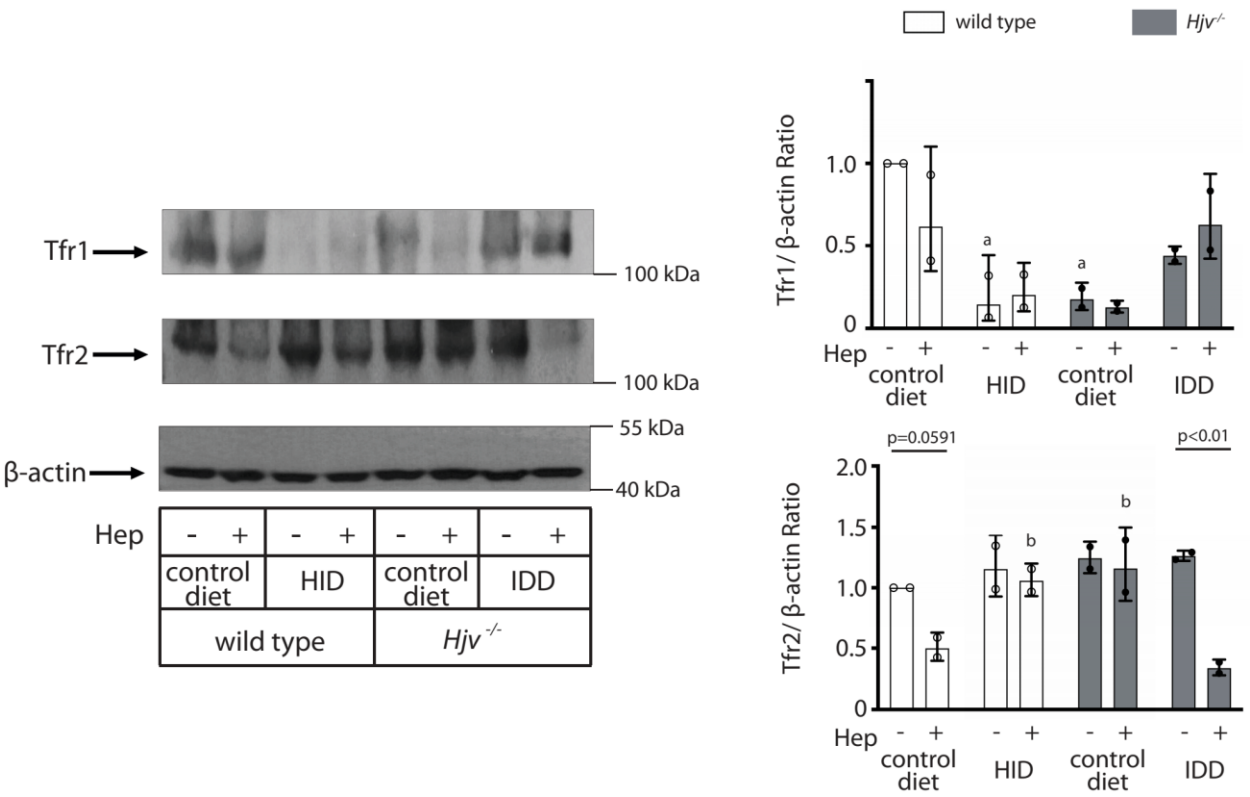

Figure 3.4-figure supplement 2: Western analysis of transferrin receptors of dietary iron-manipulated wild type and *Hjv*$^{-/-}$ mice following treatment with synthetic hepcidin.

Livers from mice described in Figure 4 were analyzed by Western blot for expression of Tfrc, Tfr2, and β-actin; a representative image (out of n=2 samples) is shown on the left. The blots were quantified by densitometry and Tfrc/β-actin or Tfr2/β-actin ratios are shown on the right.

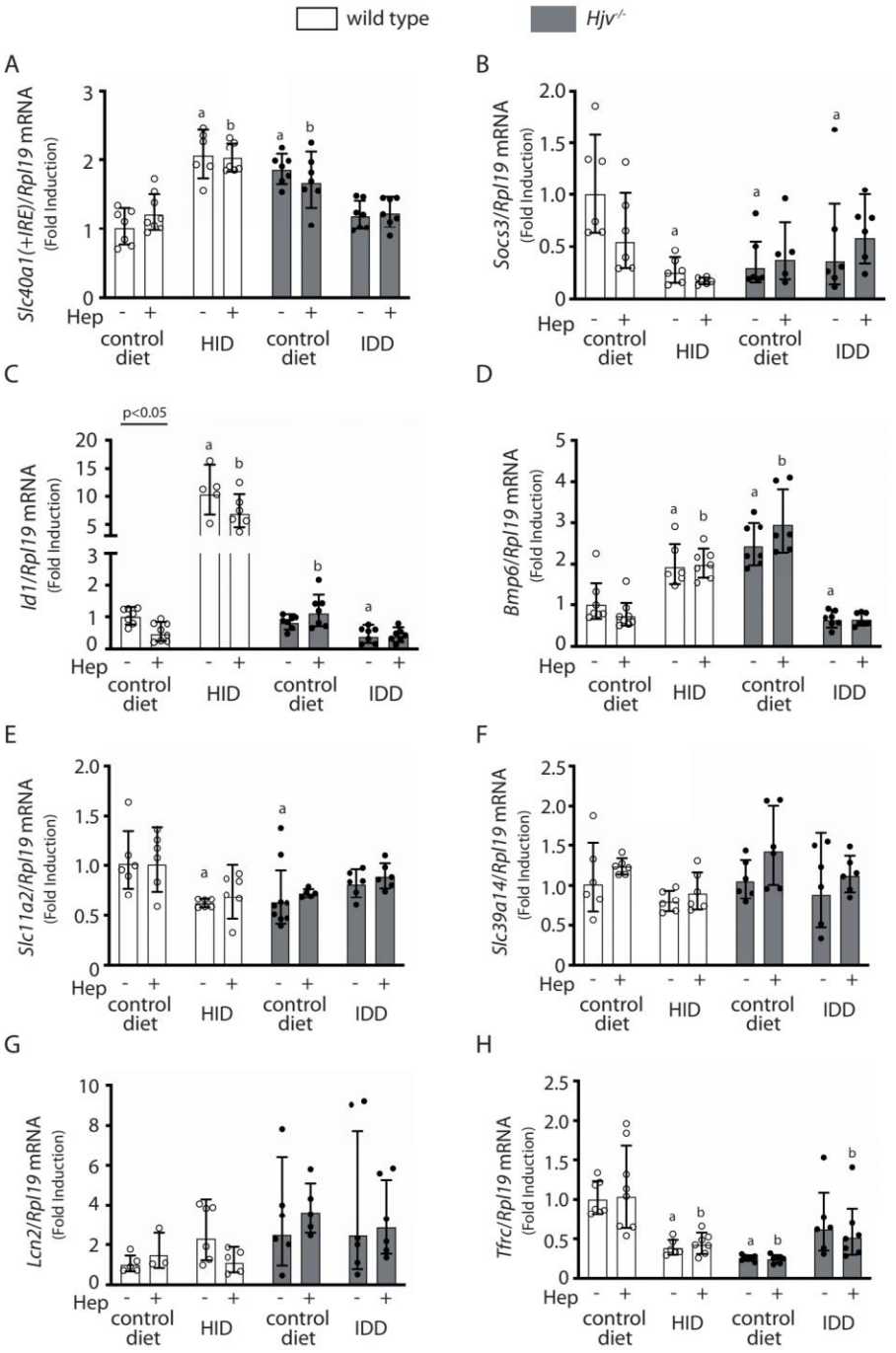

Figure 3.4-figure supplement 3: Effects of LPS treatment on expression of mRNAs encoding iron transport proteins and signaling endpoints in the liver of dietary iron-manipulated wild type and *Hjv*$^{-/-}$ mice.

Livers from mice described in Figure 4 were dissected and processed for qPCR analysis of mRNAs encoding iron transport proteins and signaling endpoints. (A) *Slc40a1(+IRE)*, (B) *Socs3*, (C) *Id1*, (D) *Bmp6*, (E) *Slc11a2*, (F) *Slc39a14*, (G) *Lcn2* and (H) *Tfrc*. All data are presented as the geometric mean ± SD. Statistically significant differences ($p<0.05$) compared to values from saline- or hepcidin-treated control mice are indicated by a or b, respectively.

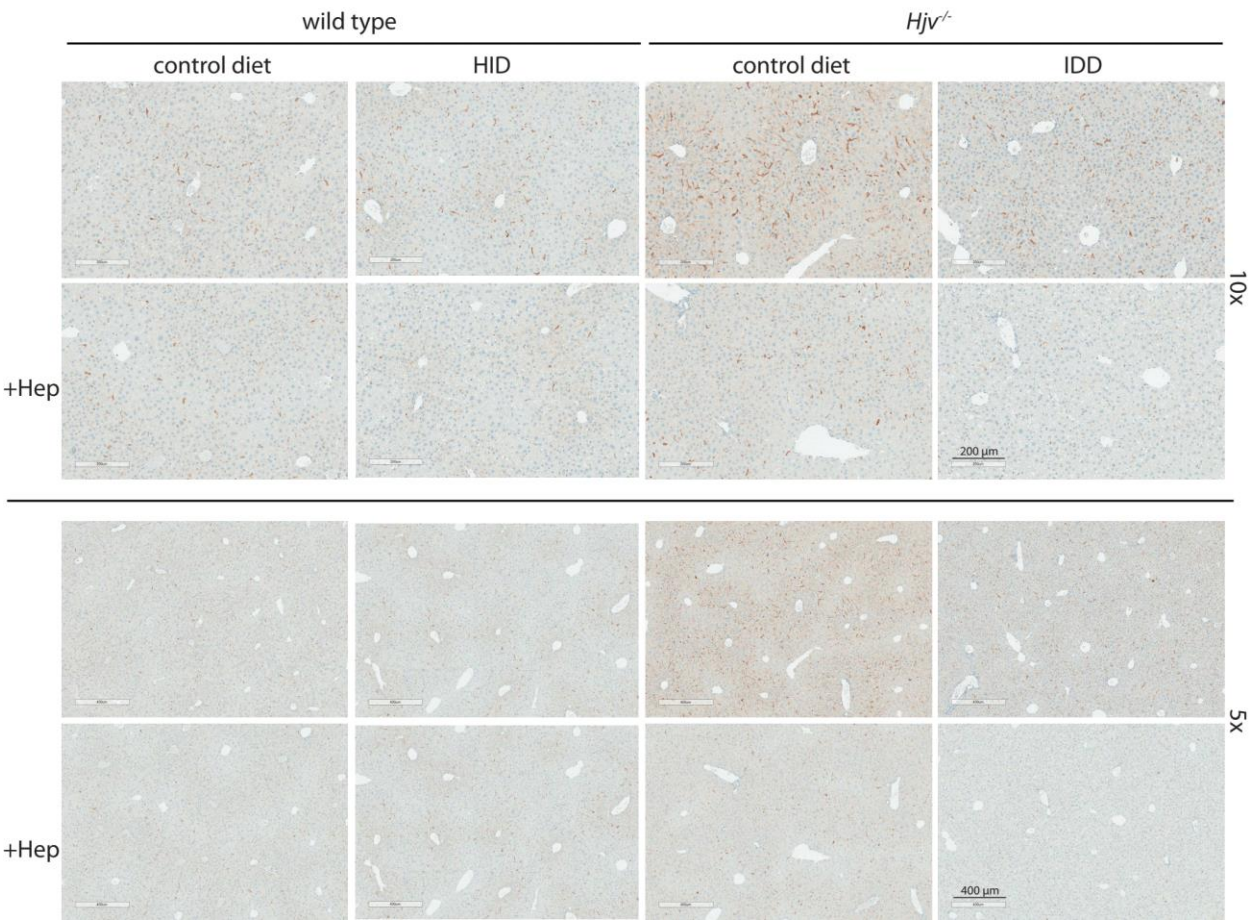

Figure 3.5-figure supplement 1: Low magnification immunohistochemical images of ferroportin in liver sections of dietary iron-manipulated wild type and *Hjv*$^{-/-}$ mice following treatment with synthetic hepcidin.
Liver sections from mice described in Figure 4 were used for immunohistochemical analysis of ferroportin (magnifications: 10x and 5x).

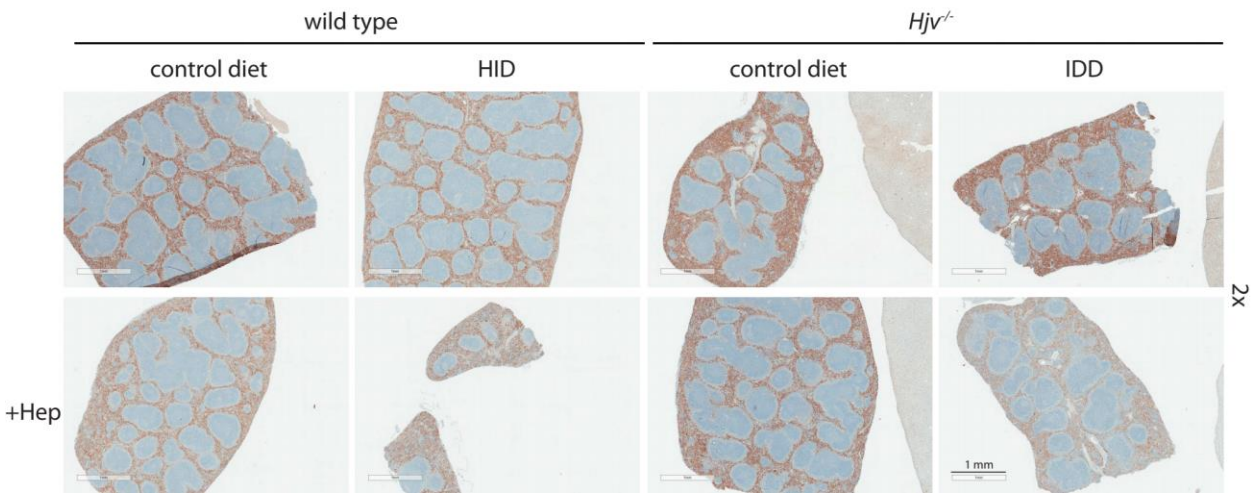

Figure 3.5-figure supplement 2: Low magnification immunohistochemical images of ferroportin in spleen sections of dietary iron-manipulated wild type and *Hjv*$^{-/-}$ mice following treatment with synthetic hepcidin.
Spleen sections from mice described in Figure 4 were used for immunohistochemical analysis of ferroportin (magnification: 2x).

3.11 Supplementary Tables

Table S.3.1: List of primers used for qPCR.

Gene	GenBank accession	Forward primer sequence	Reverse primer sequence
Hamp1	NM_032541.1	*AAGCAGGGCAGACATTGCGAT*	*CAGGATGTGGCTCTAGGCTATGT*
Slc40a1(+IRE)	NM_016917.2	*GGCATAAGGCTGTTGTGCTT*	*TCATGACACCAGGCGTTCTC*
Slc40a1(-IRE)	XM_006496137.4	*GCCGGTTGGAGTTTCAATGT*	*TCATGACACCAGGCGTTCTC*
Slc11a2	NM_001146161.1	*CTTGGGATACTGACGGTGAC*	*GATTTGCAGTCTGGAGCAGT*
Slc39a14	NM_001135151.1	*TGGATAGTGAGGCTGCGTGG*	*ATGGTGAGGCCAAGGCTAAT*
Lcn2	NM_008491	*GGCCAGTTCACTCTGGGAAA*	*TGGCGAACTGGTTGTAGTCC*
Tfrc	NM_011638.4	*AGCCAGATCAGCATTCTCTAACT*	*GCCTTCATGTTATTGTCGGCAT*
Bmp6	NM_007556.2	*ACTCGGGATGGACTCCACGTCA*	*CACCATGAAGGGCTGCTTGTCG*
Id1	NM_010495.2	*GGTACTTGGTCTGTCGGAGC*	*GCAGGTCCCTGATGTAGTCG*
Socs3	NM_007707.3	*TGCGCCTCAAGACCTTCAG*	*GCTCCAGTAGAATCCGCTCTC*
Fth1	NM_010239.2	*AAGTGCGCCAGAACTACCAC*	*AGCCACATCATCTCGGTCAA*
Rpl19	NM_009078.2	*AGGCATATGGGCATAGGGAAGAG*	*TTGACCTTCAGGTACAGGCTGTG*
Actb	NM_007393.3	*GACGACATGGAGAAGATCTG*	*GTGAAGCTGTAGCCACGCTC*

Preface to chapter 4

The work in chapter 3 demonstrated the critical importance of maintaining proper hepcidin levels for immunity against invading pathogens. However, this work focused on lipopolysaccharide (LPS)-induced inflammation which is a constituent of gram-negative bacteria which are typically extracellular pathogens. Organisms must trigger completely different immune responses to intracellular pathogens where it is preferred to export cellular iron to starve invaders. *Leishmania*, being an intra-macrophage protozoan parasite, was an ideal subject for study considering studies had shown it heavily relies on iron for differentiation and growth. Infection with this parasite can result in disfiguring cutaneous lesions or lethal visceral disease. Yet, excess iron can overwhelm *Leishmania*'s antioxidant mechanisms and absence of iron can inhibit its growth. Areas that are endemic for leishmaniasis are also commonly encumbered by conditions of iron-deficiency either due to dietary insufficiency or chronic infections. As a result, it is important to know if iron therapies are safe under these conditions or if they may aggravate leishmaniasis. The model of genetic iron overload discussed in the previous chapter provides a unique iron environment within macrophages which can be used to better understand *Leishmania*'s iron requirements. In the absence of systemic hepcidin, macrophages retain ferroportin at the cell surface for extended periods of time. This results in an intracellular deficiency of iron stores. Therefore, this chapter aims to explore the effects of relative macrophage iron deficiency on development of leishmaniasis. Both models of cutaneous and visceral leishmaniasis were studied.

This chapter was adapted from: Charlebois E, Li Y, Wagner V, Pantopoulos K, & Olivier M. Genetic iron overload hampers development of cutaneous leishmaniasis in mice. *International Journal of Molecular Sciences*. 2023.

Chapter 4

Genetic iron overload hampers development of cutaneous leishmaniasis in mice

Edouard Charlebois[1,2], Yupeng Li[1,2], Victoria Wagner[3,4], Kostas Pantopoulos[1,2]* and Martin Olivier[2,4]*

Copyright: © 2022 by the authors. Submitted for possible open access publication under the terms and conditions of the Creative Commons Attribution (CC BY) license (https://creativecommons.org/licenses/by/4.0/).

[1] Lady Davis Institute for Medical Research, Jewish General Hospital, Montreal, QC H3T 1E2, Canada

[2] Department of Medicine, McGill University, Montreal, QC H4A 3J1, Canada

[3] Université de Montréal Faculté de Médecine Vétérinaire, Montreal, QC J2S 2M2, Canada

[4] Research Institute of the McGill University Health Centre, Montreal, QC H4A 3J1, Canada

* Correspondence: MO martin.olivier@mcgill.ca; Tel.: +1-514-934-1934 (ext. 76356) and KP kostas.pantopoulos@mcgill.ca; Tel.: +1-514-340-8260 (ext. 25293)

4.1 Abstract

Survival, growth, and virulence of *Leishmania* spp., a group of protozoan parasites, depends on proper access and regulation of iron. Macrophages, *Leishmania*'s host cell, may divert iron traffic by reducing uptake or by increasing efflux of iron via the exporter ferroportin. The parasite has adapted by inhibiting synthesis and by inducing degradation of ferroportin. To study the role of iron in leishmaniasis, we employed *Hjv*$^{-/-}$ mice, a model of hemochromatosis. Disruption of hemojuvelin (Hjv) abrogates expression of the iron hormone hepcidin. This allows unrestricted iron entry into plasma from ferroportin-expressing intestinal epithelial cells and tissue macrophages, resulting in systemic iron overload. Mice were injected with *Leishmania major* in hind footpads or intraperitoneally. Compared to wild type controls, *Hjv*$^{-/-}$ mice displayed transient delayed growth of *L. major* in hind footpads, with a significant difference in parasite burden 4 weeks post-infection. Following acute intraperitoneal exposure to *L. major*, *Hjv*$^{-/-}$ peritoneal cells manifested increased expression of inflammatory cytokines and chemokines (*Il1b*, *Tnfa*, *Cxcl2*, *Ccl2*). In response to infection with *L. infantum*, causative agent of visceral leishmaniasis, *Hjv*$^{-/-}$ and control mice developed similar liver and splenic parasite burden despite vastly different tissue iron content and ferroportin expression. Thus, genetic iron overload due to hemojuvelin deficiency appears to mitigate early development of only cutaneous leishmaniasis.

Keywords: Leishmaniasis; iron; hemojuvelin; hepcidin; hemochromatosis; macrophages.

4.2 Introduction

Leishmania spp. are sandfly-transmitted trypanosomatid protozoan parasites endemic to tropical and sub-tropical regions including the Mediterranean area, which rely on iron for growth and differentiation[1-3]. Pathology of this disease can range from self-healing cutaneous lesions to lethal visceralizing disease depending on *Leishmania* species and strain. Infection with *Leishmania major* results in cutaneous leishmaniasis, while *Leishmania infantum* will spread into organs. Propagation of this disease is increasing due to environmental changes and socio-economic conflicts, with an estimated 0.7-1 million new cases annually[4]. In humans, parasites infect macrophages or neutrophils, later to be engulfed by macrophages infecting them in a trojan horse mechanism[5,6]. Macrophages are equipped with multiple mechanisms to combat this intracellular infection, including diverting iron flux to starve invaders[7,8]. Iron efflux is mediated by the sole cellular iron exporter ferroportin (gene name *Slc40a1*). Leishmania spp. have adapted to this challenge by inhibiting *Slc40a1* mRNA translation and by promoting ferroportin degradation[9,10].

Iron is an essential micronutrient for practically all living organisms and a central component of heme groups, iron-sulfur clusters, and key enzymes involved in mitochondrial respiration and DNA synthesis. Heme is of particular importance as *Leishmania* spp. are heme-auxotrophs[11]. Furthermore, parasite differentiation from promastigote to amastigote is dependent on iron, whose availability drastically differs between vector and host[12]. Susceptibility to *Leishmania* infection has been associated with Nramp1 (gene name *Slc11a1*), an iron transporter on the parasitophorous vacuole membrane, suggesting an important role of host iron metabolism for parasite growth[13-15]. In experiments with rodent models, pharmacological treatments with the iron chelator desferrioxamine had either no effect[16] or suppressed[17-19] intra-macrophagic growth, depending on parasite species. Pre-treatment of mice with desferrioxamine only seemed to cause a slight delay in growth of cutaneous lesions[20]. Comparably, dietary iron restriction had very little impact on proliferation of the visceral disease-causing species *L. infantum*[21].

Conversely, iron loading may cause parasite killing due to formation of reactive oxygen species (ROS) which may overwhelm parasite defenses. Thus, iron administration in murine models limited growth of both cutaneous[20,22,23] and visceral[21] disease-causing strains of *Leishmania*. Iron loading may also play a role on host immunity which can modulate NF-κB

signaling in macrophages[24,25]. This pathway would then induce differentiation of IFNγ-producing CD4+ T cells crucial for parasite restriction[26].

In general, iron is an important regulator of immune responses. Excess iron may either impair[27,28] or induce[29] pro-inflammatory cytokine production in macrophages. In cell culture experiments, iron supplementation favored Th2 activation and antagonized IFNγ responses[30]. Yet, iron was also shown to directly drive T helper cell pathogenicity through interactions with the iron chaperone poly(rC)-binding protein 1[31]. Nitric oxide production necessary for intracellular pathogen killing greatly affects cellular iron homeostasis and promotes iron accumulation[28,32]. Iron negatively regulates transcription of the inducible nitric oxide synthase providing a feedback mechanism[33].

Systemic iron metabolism is primarily controlled by hepcidin (gene name *Hamp*), a hepatocyte-derived peptide hormone[34]. Hepcidin binds to ferroportin, occludes its opening[35], and targets it for lysosomal degradation[36]. The result of this process is restricted dietary iron import and reduced export from erythrophagocytic macrophages to the bloodstream. Hepcidin expression is predominantly regulated at the transcriptional level in response to iron fluctuations through BMP/SMAD signaling, or in response to inflammatory cues via JAK/STAT signaling, initiated largely by IL-6[37].

Hemojuvelin (Hjv) is a bone morphogenetic protein (BMP) co-receptor that enhances BMP/SMAD signaling to hepcidin on hepatocytes. Disruption of the *HJV* gene causes juvenile hereditary hemochromatosis in humans[38] and a similar phenotype is observed in *Hjv*$^{-/-}$ mice[39]. Hereditary hemochromatosis comprises a group of genetically heterogenous disorders of systemic iron overload caused by hepcidin suppression[40]. Paradoxically, tissue macrophages are unable to retain iron[41] due to unrestricted expression of ferroportin on the cell surface[39,42]; this results in lower splenic iron content. Macrophage iron deficiency combined with concurrent systemic iron overload provides a unique environment to study leishmaniasis. Herein, we sought to explore whether the hemochromatosis phenotype favors resistance to *Leishmania* as has been previously reported for other intra-macrophage pathogens[43,44].

4.3 Results

4.3.1. Growth of Leishmania major is transiently delayed in Hjv$^{-/-}$ mice during early infection

We first sought to assess the susceptibility of genetically iron overloaded mice to cutaneous leishmaniasis. We injected wild type (*Hjv*$^{+/+}$) control and *Hjv*$^{-/-}$ mice with *L. major* in hind footpads. Footpad swelling was followed over a period of 8 weeks (Figure 4.1A). Statistical differences in swelling between both groups were observed for all but the final week (Figure 4.1A), indicating that *Hjv*$^{-/-}$ mice are at least less sensitive to infection with *L. major*. A limiting dilution assay revealed that parasite load was significantly reduced in footpads of *Hjv*$^{-/-}$ mice 4 weeks post-infection, but not at 7 weeks (Figure 4.1B-C). These data suggest that parasite load recovers before swelling.

Popliteal lymph nodes, the draining lymph nodes that are accessible to parasite during footpad infections, were collected and evaluated for cytokine and chemokine gene expression. In both mouse models, cytokine gene expression appeared to increase over time. It was significantly higher than in mesenteric lymph nodes (MLN) used as uninfected control tissues, except for *Il6* expression which remained at baseline (Figure 4.2 A-D). Chemokine expression remained largely unaffected in lymph nodes with only a slight increase in *Ccl2* expression at 7 weeks post-infection (Figure 4.2E-H). No genotype-specific differences were observed, suggesting that cytokine and chemokine expression in the draining lymph node is not the cause of delayed parasite growth observed in footpads.

4.3.2 Cytokine acute response to Leishmania major is altered in Hjv$^{-/-}$ mice

Considering that lymph node cytokine gene expression was similar across both genotypes, we hypothesized that early parasite establishment within the host could be a main factor in the observed relative resistance of *Hjv*$^{-/-}$ mice to *L. major*. To study this, we injected mice intraperitoneally with *L. major* and collected serum, liver, and peritoneal lavage 6 hours post-infection. Iron parameters in the circulation were measured to better understand the systemic effects of *Leishmania* infection on iron distribution. The bacterial endotoxin lipopolysaccharide (LPS) was used as a control for inflammation. Serum iron from mice infected with *L. major* was unaffected compared to the drop observed by LPS in wild type animals (Figure 4.3A), which is known as hypoferremic response to inflammation[8]. Transferrin saturation, another marker of

circulating iron levels, displayed a similar trend (Figure 4.3B). Characteristically, iron levels were largely unchanged throughout all inflammatory treatments in *Hjv*$^{-/-}$ mice, and transferrin saturation was at maximal levels with only a slight reduction observed after LPS treatment (Figure 4.3A-B), as previously described[45]. *Leishmania* infection did not alter total iron binding capacity (TIBC) in either wild type or *Hjv*$^{-/-}$ mice (Figure 4.3C).

The liver plays an important role in immune response to pathogens by being the major producer of hepcidin to control systemic iron traffic. Invading extracellular bacterial pathogens will typically activate expression of *Hamp* mRNA due to IL-6 driven inflammation[46]. The ensuing hypoferremic response is thought to inhibit growth of pathogens by depriving them of iron. Yet, for intracellular pathogens, this would be deleterious as iron levels would consequently increase within infected cells. In fact, host macrophages are known to upregulate ferroportin in order to reduce their iron content in response to intracellular pathogens such as *S. typhimurium*[47]. However, this has not been observed in the context of leishmaniasis as parasites will suppress ferroportin synthesis and will also increase hepcidin expression over the course of infection[9,10]. Interestingly, *Hamp* mRNA levels were measured and were increased in response to LPS but not to *L. major* in wild-type mice, in this experimental time frame (Figure 4.3D). *Hamp* expression was significantly reduced in *Hjv*$^{-/-}$ mice (Figure 4.3D), as expected. Expression of the inflammatory cytokine-encoding *Il6*, *Il1b* and *Tnfa* mRNAs was unresponsive to *L. major* infection compared to endotoxin exposure, whereas *Ifng* expression was induced by the parasite (Figure 4.3E-H). Curiously, liver expression of the latter cytokine was significantly lower in *Hjv*$^{-/-}$ mice (Figure 4.3H). Levels of *Il6*, *Il1b* and *Tnfa* mRNAs did not differ in the livers of LPS-treated wild type and *Hjv*$^{-/-}$ mice, as previously reported[45].

We then assessed cytokine gene expression in the peritoneal lavage. LPS-treated animals responded as anticipated with increased expression of all tested cytokine and chemokine genes except for *Ifng* (Figure 4.4). A similar trend was observed in *L. major*-infected animals with the additional lack of response in *Il6* (Figure 4.4A). Interestingly, there was an overall trend towards upregulation of cytokine and chemokine gene expression in *Hjv*$^{-/-}$ mice (Figure 4.4). *L. major* infection produced a less pronounced effect overall, without any remarkable differences between genotypes in expression of *Il6*, *Ifng*, *Ccl3*, and *Ccl4* mRNAs (Figure 4.4). However, it should be

noted that IL-6 and CCL2 protein levels were elevated in knockout mice in peritoneal lavage supernatants when measured by a multiplex assay (Figure S.4.1).

Analysis of the cell suspension by cytospin centrifugation revealed that the peritoneal lavage 6 hours post-infection mostly consisted of neutrophils and macrophages (Figure 4.5A). We utilized these cell populations to assess the rate of infection and parasite load per cell immediately following separation (Figure 4.5B-C), or after allowing collected cells to grow in culture for 24, 48, and 72 hours (Figure 4.5 D-E). Under these conditions, the cultured cells were primarily macrophages, which clear neutrophils by phagocytosis. No genotype-specific differences were observed in infection rate or cellular parasite burden at any timepoint measured, suggesting that *Hjv*$^{-/-}$ cells do not exhibit altered phagocytosis, consistent with another report[48]. In addition, there was no increased intracellular parasite killing at these timepoints.

4.3.3. Genetic iron overload does not impact visceral disease progression by Leishmania infantum despite induction of the iron exporter ferroportin

L. infantum causes visceral leishmaniasis affecting primarily the liver and spleen. To assess the role of genetic iron overload in progression of visceral disease, wild type and *Hjv*$^{-/-}$ mice were infected with *L. infantum* and sacrificed 1-, 2-, or 3-weeks post-infection. Organs were collected, weighed, and used for limiting dilution assay (Figure 4.6A-D). No differences in organ weight were observed between genotypes (Figure 4.6A and C) and organ parasite burden was similar at the measured timepoints (Figure 4.6B and D). Splenic iron content was characteristically low in knockouts as previously reported[39,42] (Figure 4.6E), and ferroportin protein expression was significantly elevated (Figure 4.6F). Nevertheless, parasite growth and disease progression were largely unaffected.

4.4 Discussion

Hemochromatosis resulting from disruption of *Hjv* produces a unique iron environment where enterocytes and macrophages cannot retain iron and release it to the bloodstream. Thus, excessive amounts of the metal accumulate in plasma and are eventually taken up by tissue parenchymal cells. In the present work, we sought to understand how this iron environment would affect growth of *L. major* and *L. infantum*, the parasites causing cutaneous and visceral leishmaniasis, respectively. The delayed swelling of *L. major*-infected *Hjv*$^{-/-}$ mice (Figure 4.1)

closely resembles results with desferrioxamine pre-treated mice, showing a several week delay in parasite growth[20]. Consequently, it is likely that the microenvironment within *Hjv*$^{-/-}$ murine macrophages mimics that of macrophages from desferrioxamine-pretreated mice and is characterized by relative iron deficiency. Furthermore, inappropriately low circulating hepcidin results in excessive ferroportin expression at the cell surface of macrophages, as observed in splenic extracts in figure 4.6F. Despite having decreased iron stores, macrophages from *Hjv*$^{-/-}$ mice exhibit physiological clearance of senescent red blood cells (erythrophagocytosis), which implies high iron turnover. In another model of iron overload, involving iron dextran injection into wild type mice, macrophages become extremely iron loaded. Under these conditions, *L. major* growth was inhibited due to increased parasite killing[20], which is possibly enhanced by ROS-mediated shift of immunity toward a T helper type 1 (Th1) response[23]. Thus, it is difficult to directly compare data from the genetic and pharmacological models of iron overload since they differ significantly in tissue iron distribution.

Notably, the genetic background of mice may also affect immune responses and leishmaniasis progression. Herein, we used C57BL/6 mice, which tend to favor a Th1 response resulting in resistance to persistent infection; on the other hand, BALB/c mice favor Th2 responses leading to susceptibility[49,50]. These effects are also dependent on *Leishmania* spp. that modulate macrophage immunity, adding another level of complexity. For instance, in a recent study, infection with *L. panamensis* induced a potent activation of classical M1 macrophages in C57BL/6 mice, but only an intermediate response in BALB/c mice[51]. Hence, it would be of interest to study effects of genetic iron overload using different mouse and *Leishmania* spp. strains.

We did not observe any induction of the *Ifng* gene by either LPS treatment or *L. major* infection in the macrophages and neutrophils collected from peritoneal lavage of both wild type and *Hjv*$^{-/-}$ mice 6 hours post-treatment, suggesting that these cells are not major producers of IFNγ (Figure 4.4D). This result somewhat contradicts previous data, where a marked reduction in IFNγ levels was observed 6 hours post-E. coli infection in sera as well as in cultured thioglycolate-elicited peritoneal macrophages from *Hjv*$^{-/-}$ vs wild type mice[48]. The disparity between these findings may lie in the different sections (peritoneal cells vs. sera) analyzed as well as the mouse model used. Interestingly, in our experiments, liver *Ifng* expression was significantly diminished 6 hours post-infection in *Hjv*$^{-/-}$ mice (Figure 4.3H) suggesting that perhaps tissue-resident Th1 or

NK T cells could be an important source of IFNγ, which then enters the circulation. In fact, Th1 cells[52] and NK T cells[53] are considered the primary producers of IFNγ. Whether macrophages and neutrophils can produce IFNγ remains contentious, and *in vitro* experiments with primary cells may not always be physiologically relevant[54]. Taken together, our data do not provide any evidence that macrophages or neutrophils can produce IFNγ, at least in our experimental setting. However, we cannot rule out the possibility that circulating IFNγ produced elsewhere is an important determinant for establishment of *Leishmania* infection in footpads.

We noted a marked increase in expression of many cytokine and chemokine genes in peritoneal cells of *Hjv*$^{-/-}$ mice (Figure 4.4). Cytokines play a differential role in infection depending on mouse strain as well as parasite species. *Tnfa* expression has been linked to protection against cutaneous leishmaniasis during early stages of infection[55], whereas it can lead to immunopathology when it persists later in disease[56]. This makes it a strong candidate for the delayed parasite growth observed during the early weeks of infection in knockout animals. A multiplex assay was performed to measure GM-CSF, IFNγ, IL-1β, IL-2, IL-4, IL-6, IL-10, IL-12p70, CCL2, and TNFα. Only IL-6 and CCL2 were consistently expressed in lavage supernatants of infected mice, and their levels were significantly higher in *Hjv*$^{-/-}$ mice (Figure S.4.1). IL-6 has been reported to play a dual role in leishmaniasis. It may downregulate macrophage leishmanicidal effects[57], while it may also induce the growth of IL-10+ CD4+ T cells[58]. Considering the different species of *Leishmania* studied in these analyses, it is difficult to specify the exact role of IL-6 in the development of cutaneous lesions from *L. major* infection in our study. Given its effects on macrophages, it is unlikely that IL-6 accounts for the observed delayed growth of cutaneous lesions in *L. major*-infected *Hjv*$^{-/-}$ mice. CCL2 is an important chemoattractant for monocytes. Yet, it may be involved in Th2 polarization as *Ccl2*$^{-/-}$ mice are resistant to *L. major* and do not have abnormal naïve T cell migration[59]. This is in contrast to its cognate receptor CCR2, which plays a crucial role in protection against cutaneous leishmaniasis[29]. Thus, we rationalize that CCL2 would be protective during early *L. major* infection by recruiting monocytes but may later be detrimental. Taken together, *Hjv*$^{-/-}$ mice may be protected by production of TNFα, even though this cytokine could not be directly measured in lavage supernatants, and by enhanced expression of CCL2.

Remarkably, *Hjv*$^{-/-}$ mice were not protected from visceral disease resulting from *L. infantum* infection despite having greatly increased ferroportin levels in the spleen, as well as

reduced splenic iron content (Figure 4.6E-F). These results corroborate earlier data showing that dietary iron restriction did not affect parasite load in the mouse liver and spleen, 60 days post *L. infantum* infection[21]. The stark difference in these two models is that dietary iron deficiency does not induce, and rather post-transcriptionally suppresses tissue ferroportin[60], the expression of which is reported to be protective[9]. Interestingly, pharmacological iron deficiency induced by a two-week pre-treatment of BALB/c mice with desferrioxamine[61] led to a significant decrease in splenic parasite load 6 weeks post *L. chagasi* infection. Taken together, these results suggest that the severity and timeframe of iron-deficiency may be important for parasite replication, particularly at later stages of infection. Nevertheless, iron-restriction does not appear an optimal strategy for the control of visceral leishmaniasis.

Leishmaniasis is a complicated disease considering that iron supplementation seems to protect the host against the parasite[20-23], while iron deprivation appears to have little to no effect[20,21], contrary to most other pathogens[7,8]. The hemochromatosis phenotype of systemic iron overload with macrophage iron deficiency and high iron turnover did not further increase vulnerability to *Leishmania* infection as has been reported with several other bacteria, fungi, and even viruses[62]. Previous publications showed that *Leishmania* spp. express many different receptors and transporters for iron[63-67], yet it remains to be clarified which form of iron is the most important for amastigote development and replication. Herein, we provide evidence that transient iron pools in macrophages are sufficient for parasite replication, even with enhanced iron export resulting in a net iron deficiency. Our work cannot differentiate between systemic effects of *Hjv* deficiency on iron metabolism and possible local immunological effects in macrophages. This remains to be addressed in future studies.

4.5 Materials and Methods

4.5.1 Animals and ethics

Mouse experiments were performed in the McGill University Health Centre research institute in containment level 2 housing facilities. Wild type C57BL/6J and isogenic *Hjv*$^{-/-}$ mice[68] were housed under pathogen-free conditions in macrolone cages (up to 5 mice/cage, 12:12 h light-dark cycle: 7 am - 7 pm; 22 ± 1°C, 60 ± 5% humidity). At the endpoints, animals were sacrificed by CO_2 inhalation and cervical dislocation. All mice used in experiments were male. Animal experiments were performed in compliance with the Canadian Council on Animal Care (CCAC)

Guidelines, and McGill University Animal Care Committee (UACC). The approved animal use protocol number is 7791. Isoflurane was used for anesthesia prior to euthanasia to alleviate suffering.

4.5.2 Parasite culture

L. major (strain MHOM/SN/74/Seidman) were generously supplied by Dr. Robert McMaster (University of British Columbia, Canada). All parasites were cultured at 25˚C, 5% CO2 in Schneider's Drosophila Medium (SDM) supplemented with 10% heat-inactivated fetal bovine serum (FBS, Wisent, St-Bruno, QC, Canada), and 5 mg/ml hemin and passaged every 3 to 4 days. Cultures of promastigotes growing at logarithmic phase (day 3–4 post passage) were passaged bi-weekly and were grown to stationary phase (day 6–8 post passage) before being used in infections for all experiments[69].

4.5.3 Footpad infections

Groups of ten 6-week-old mice per genotype were each injected with $5x10^6$ *L. major* promastigotes into one hind footpad. 5 mice per genotype were sacrificed at 4 and 7 weeks and footpads were used to measure parasite burden by limiting dilution assay. Popliteal lymph nodes were also collected, snap frozen in liquid nitrogen, and later analyzed by qPCR. A group of 5 mice per genotype was kept and footpads were measured at 8 weeks post-infection. Mice in each group were housed in the same cage for the duration of the experiment. The uninfected footpad was used as the negative control for measurement purposes. Lesion development was monitored weekly by the difference of footpad thickness between the infected and uninfected footpad, measured by digital calipers. Experiments were repeated up to three times.

4.5.4 Limiting dilution assay

Footpads were sterilized with ethanol, excised, and washed with phosphate buffered saline (PBS). Next, tissue was disrupted manually using a glass tissue homogenizer in sterile PBS under a BSL2 tissue culture hood. 50 mL total volume of footpad homogenate was recovered and 100 µL of each sample was added to 96-well plates (Sarstedt, Germany) containing 100 µL complete SDM per well, in duplicate. A minimum of 24 2-fold serial dilutions were performed for each sample. Plates were kept at 25 °C until microscopic examination 10 days later, when the highest dilutions at which promastigotes were observed were recorded.

4.5.5 Acute intraperitoneal infections

Groups of 3 mice each were injected intraperitoneally with PBS, 1 μg/g LPS (serotype 055:B5; Sigma-Aldrich), or 10^8 *L. major* promastigotes before sacrifice 6 hours later. Mice in each group were housed in the same cage for the duration of the experiment. In total, 9 mice were analyzed per genotype per treatment group. Mice were lavaged with 5 ml of ice-cold endotoxin-free PBS at endpoints. The number of live cells present in the lavages was counted using a hemocytometer. Cells were prepared for microscopy using the Cytospin 4 cytocentrifuge (Thermo Scientific, Waltham, MA, USA). The cells were fixed and stained using the Differential Quik (Diff-Quik) Stain Kit (Ral Diagnostics, Martillac, France). The percentage of cell types found in the lavage was counted. Next, the percent of cells infected and the number of *Leishmania* amastigotes found within the cells were counted. 150 μl of the lavages were plated in 4 well chamber slides (Corning, USA) and incubated at 37°C for 1 hr before the addition of Dulbecco's modified eagle medium (Wisent, St-Bruno, QC, Canada) with 10% FBS and 1% penicillin-streptomycin-glutamine. Cells were kept at 37℃ in 5% CO2. 24, 48, and 72 hours post plating, media was removed, cells were then air dried, fixed, and stained using the Diff-Quik Stain Kit. The percent of cells infected and the number of *Leishmania* amastigotes found within the cells were counted. From the total 300 cells counted from each slide, the percentage was calculated, and the number of amastigotes found in individual cells was counted as well. Total lavage was centrifuged at 1500 rpm for 10 mins to separate cells and supernatant. These fractions were kept at -80℃ until processing.

4.5.6 Visceral leishmaniasis infection

8-week-old mice (n=5-10) were infected intraperitoneally with 10^8 *L. infantum* promastigotes (MHOM/MA/67/ITMAP-263). Control mice were injected with PBS. Mice were weighed and sacrificed 1-, 2-, and 3-weeks post-infection. Whole livers and spleens were collected, weighed, and snap frozen in liquid nitrogen. A piece of liver and spleen was weighed and directly used without freezing for limiting dilution assay. Spleens were later used for Western blotting and iron quantification.

4.5.7 Serum biochemistry

Blood was collected via cardiac puncture. Serum was prepared by using micro Z-gel tubes with clotting activator (Sarstedt) and was kept frozen at −20°C until analysis. Serum iron and total iron binding capacity (TIBC) were determined at the Biochemistry Department of the Montreal Jewish General Hospital using a Roche Hitachi 917 Chemistry Analyzer. Transferrin saturation was calculated from the ratio of serum iron and TIBC.

4.5.8 Quantitative real-time PCR (qPCR)

RNA was extracted from organs and cells by using the RNeasy kit (Qiagen). cDNA was synthesized from 1 μg RNA by using the OneScript® Plus cDNA Synthesis Kit (Applied Biological Materials Inc.). Gene-specific primers pairs (Table S.4.1) were validated by dissociation curve analysis and demonstrated amplification efficiency between 90-110 %. SYBR Green (Bioline) and primers were used to amplify products under following cycling conditions: initial denaturation 95°C 10 min, 40 cycles of 95°C 5 s, 58°C 30 s, 72°C 10 s, and final cycle melt analysis between 58°-95°C. Relative mRNA expression was calculated by the $2^{-\Delta\Delta Ct}$ method[70]. Data were normalized to murine ribosomal protein L19 (*Rpl19*). Data are reported as fold increases compared to samples from wild type mice.

4.5.9 Multiplex cytokine/chemokine quantification assay

100μl of the lavage supernatant were analyzed by a Mouse Cytokine Proinflammatory Focused 10-Plex Discovery Assay® Array (MDF10) (Eve Technologies, Calgary, AB, Canada). These include GM-CSF, IFNγ, IL-1β, IL-2, IL-4, IL-6, IL-10, IL-12p70, CCL2, and TNFα. The multiplex laser bead technology utilizes antibodies that are coupled to color-coded polystyrene beads where lasers activate the fluorescent dye and excites the fluorescent conjugate, which is then quantified for the concentration of the target analyte.

4.5.10 Western blotting

Spleens were washed with ice-cold PBS and dissected into pieces. Aliquots were snap frozen at liquid nitrogen and stored at −80oC. Protein lysates were obtained as described[42]. Lysates containing 40 μg of proteins were analyzed by SDS-PAGE on 9-13% gels and proteins were

transferred onto nitrocellulose membranes (BioRad). The blots were blocked in non-fat milk diluted in tris-buffered saline (TBS) containing 0.1% (v/v) Tween-20 (TBS-T), and probed overnight with antibodies against ferroportin[71] (1:1000 diluted monoclonal rat anti-mouse 1C7, kindly provided by Amgen Inc), β-actin (1:2000 diluted; Sigma). Following a 3x wash with TBS-T, the membranes were incubated with peroxidase-coupled secondary antibodies for 1.5 h. Immunoreactive bands were detected by enhanced chemiluminescence with the Western Lightning ECL Kit (Perkin Elmer). Blot images were quantified using ImageJ software.

4.5.11 Tissue iron quantification

Splenic iron content (SIC) was quantified by using the ferrozine assay[72].

4.5.12 Statistics

Statistical analysis was performed by using the Prism GraphPad software (version 9.1.0). Lognormally distributed data including qPCR results were first log transformed before analysis with unpaired Student's t test. Normally distributed data was analyzed by unpaired Student's t test. Comparisons within same genotype are denoted by a or b on figures. Probability value $p<0.05$ was considered statistically significant.

4.6 Author Contributions

Conceptualization, E.C., K.P. and M.O.; methodology, M.O.; sample collection and formal analysis, E.C., Y.L. and V.W.; investigation, E.C.; writing—original draft preparation, E.C.; writing—review and editing, K.P. and M.O.; supervision, M.O.; funding acquisition, K.P. and M.O. All authors have read and agreed to the published version of the manuscript.

4.7 Funding

This research was funded by the Canadian Institutes of Health Research (CIHR), grant number PJT-159730. E.C. was funded by a fellowship from the Natural Sciences and Engineering Research Council of Canada (NSERC) and is currently a recipient of a fellowship from the *Fonds de recherche du Québec – Santé* (FRQS).

4.8 Institutional Review Board Statement

All animal experiments were performed in accordance with the Canadian Council on Animal Care (CCAC) Guidelines, approved by the Institutional Animal Care and Use Committees at the McGill University under ethics protocol 7791.

4.9 Data Availability Statement

All data are contained within the manuscript and the supporting information.

4.10 Conflicts of Interest

The authors declare no conflict of interest.

4.11 References

1. Khan YA, Andrews NW, Mittra B. ROS regulate differentiation of visceralizing Leishmania species into the virulent amastigote form. *Parasitology Open*. 2018;4.
2. Kumar A, Chauhan N, Singh S. Understanding the Cross-Talk of Redox Metabolism and Fe-S Cluster Biogenesis in Leishmania Through Systems Biology Approach. *Frontiers in Cellular and Infection Microbiology*. 2019;9.
3. Kevric I, Cappel MA, Keeling JH. New World and Old World Leishmania Infections. 2015;33(3):579-593.
4. Burza S, Croft SL, Boelaert M. Leishmaniasis. *The Lancet*. 2018;392(10151):951-970.
5. Laskay T, van Zandbergen G, Solbach W. Neutrophil granulocytes as host cells and transport vehicles for intracellular pathogens: Apoptosis as infection-promoting factor. *Immunobiology*. 2008;213(3):183-191.
6. Van Zandbergen G, Klinger M, Mueller A, et al. Cutting Edge: Neutrophil Granulocyte Serves as a Vector for *Leishmania* Entry into Macrophages. *The Journal of Immunology*. 2004;173(11):6521-6525.
7. Weiss G, Schaible UE. Macrophage defense mechanisms against intracellular bacteria. *Immunol Rev*. 2015;264(1):182-203.
8. Ganz T. Iron and infection. *Int J Hematol*. 2018;107(1):7-15.
9. Ben-Othman R, Flannery AR, Miguel DC, Ward DM, Kaplan J, Andrews NW. Leishmania-Mediated Inhibition of Iron Export Promotes Parasite Replication in Macrophages. 2014;10(1):e1003901.
10. Das NK, Sandhya S, G VV, et al. Leishmania donovani inhibits ferroportin translation by modulating FBXL5-IRP2 axis for its growth within host macrophages. *Cell Microbiol*. 2018:e12834.
11. Chin Shen C, Kwang-Poo C. Heme requirement and acquisition by extracellular and intracellular stages of Leishmania mexicana amazonensis. *Molecular and Biochemical Parasitology*. 1985;16(3):267-276.
12. Mittra B, Cortez M, Haydock A, Ramasamy G, Myler PJ, Andrews NW. Iron uptake controls the generation of Leishmania infective forms through regulation of ROS levels. *J Exp Med*. 2013;210(2):401-416.
13. Bucheton B, Abel L, Kheir MM, et al. Genetic control of visceral leishmaniasis in a Sudanese population: candidate gene testing indicates a linkage to the NRAMP1 region. *Genes & Immunity*. 2003;4(2):104-109.
14. Blackwell JM, Fakiola M, Ibrahim ME, et al. Genetics and visceral leishmaniasis: of mice and man. *Parasite Immunol*. 2009;31(5):254-266.
15. Castellucci L, Jamieson SE, Miller EN, et al. CXCR1 and SLC11A1polymorphisms affect susceptibility to cutaneous leishmaniasis in Brazil: a case-control and family-based study. *BMC Med Genet*. 2010;11(1):10.
16. Murray HW, Granger AM, Teitelbaum RF. Gamma interferon-activated human macrophages and Toxoplasma gondii, Chlamydia psittaci, and Leishmania donovani: antimicrobial role of limiting intracellular iron. *Infection and Immunity*. 1991;59(12):4684-4686.
17. Das NK, Biswas S, Solanki S, Mukhopadhyay CK. Leishmania donovani depletes labile iron pool to exploit iron uptake capacity of macrophage for its intracellular growth. *Cell Microbiol*. 2009;11(1):83-94.

18. Segovia M, Navarro A, Artero JM. The effect of liposome-entrapped desferrioxamine on *Leishmania donovani in vitro*. *Annals of Tropical Medicine & Parasitology*. 1989;83(4):357-360.
19. Borges VM, Vannier-Santos MA, De Souza W. Subverted transferrin trafficking in Leishmania- infected macrophages. *Parasitol Res*. 1998;84(10):811-822.
20. Bisti S, Konidou G, Papageorgiou F, Milon Ge, Boelaert JR, Soteriadou K. The outcome of Leishmania major experimental infection in BALB / c mice can be modulated by exogenously delivered iron. *Eur J Immunol*. 2000;30(12):3732-3740.
21. Vale-Costa S, Gomes-Pereira S, Teixeira CM, et al. Iron Overload Favors the Elimination of Leishmania infantum from Mouse Tissues through Interaction with Reactive Oxygen and Nitrogen Species. *PLoS Negl Trop Dis*. 2013;7(2):e2061.
22. Bisti S, Konidou G, Boelaert J, Lebastard M, Soteriadou K. The prevention of the growth of Leishmania major progeny in BALB/c iron-loaded mice: a process coupled to increased oxidative burst, the amplitude and duration of which depend on initial parasite developmental stage and dose. *Microb Infect*. 2006;8(6):1464-1472.
23. Bisti S, Soteriadou K. Is the reactive oxygen species-dependent-NF-κB activation observed in iron-loaded BALB/c mice a key process preventing growth of Leishmania major progeny and tissue-damage? *Microb Infect*. 2006;8(6):1473-1482.
24. Xiong S, She H, Takeuchi H, et al. Signaling Role of Intracellular Iron in NF-κB Activation. *J Biol Chem*. 2003;278(20):17646-17654.
25. Galaris D, Pantopoulos K. Oxidative Stress and Iron Homeostasis: Mechanistic and Health Aspects. *Crit Rev Clin Lab Sci*. 2008;45(1):1-23.
26. Artis D, Speirs K, Joyce K, et al. NF-κB1 Is Required for Optimal $CD4^+$ Th1 Cell Development and Resistance to *Leishmania major*. *The Journal of Immunology*. 2003;170(4):1995-2003.
27. Olynyk JK, Clarke SL. Iron overload impairs pro-inflammatory cytokine responses by Kupffer cells. *J Gastroenterol Hepatol*. 2001;16(4):438-444.
28. Nairz M, Schleicher U, Schroll A, et al. Nitric oxide-mediated regulation of ferroportin-1 controls macrophage iron homeostasis and immune function in Salmonella infection. *J Exp Med*. 2013;210(5):855-873.
29. Quinones MP, Estrada CA, Jimenez F, et al. CCL2-independent role of CCR2 in immune responses against Leishmania major. *Parasite Immunol*. 2007;29(4):211-217.
30. Weiss G, Fuchs D, Hausen A, et al. Iron modulates interferon-gamma effects in the human myelomonocytic cell line THP-1. *Exp Hematol*. 1992;20(5):605-610.
31. Wang Z, Yin W, Zhu L, et al. Iron Drives T Helper Cell Pathogenicity by Promoting RNA-Binding Protein PCBP1-Mediated Proinflammatory Cytokine Production. *Immunity*. 2018;49(1):80-92.e87.
32. Pantopoulos K, Weiss G, Hentze MW. Nitric oxide and the post-transcriptional control of cellular iron traffic. *Trends in Cell Biology*. 1994;4(3):82-86.
33. Weiss G, Werner-Felmayer G, Werner ER, Grünewald K, Wachter H, Hentze MW. Iron regulates nitric oxide synthase activity by controlling nuclear transcription. *J Exp Med*. 1994;180(3):969-976.
34. Nemeth E, Ganz T. Hepcidin-Ferroportin Interaction Controls Systemic Iron Homeostasis. *Int J Mol Sci*. 2021;22(12).
35. Billesbølle CB, Azumaya CM, Kretsch RC, et al. Structure of hepcidin-bound ferroportin reveals iron homeostatic mechanisms. *Nature*. 2020.

36. Nemeth E, Tuttle MS, Powelson J, et al. Hepcidin regulates cellular iron efflux by binding to ferroportin and inducing its internalization. *Science*. 2004;306(5704):2090-2093.
37. Rishi G, Subramaniam VN. Signaling pathways regulating hepcidin. *Vitam Horm*. 2019;110:47-70.
38. Papanikolaou G, Samuels ME, Ludwig EH, et al. Mutations in HFE2 cause iron overload in chromosome 1q–linked juvenile hemochromatosis. *Nat Genet*. 2004;36(1):77-82.
39. Huang FW, Pinkus JL, Pinkus GS, Fleming MD, Andrews NC. A mouse model of juvenile hemochromatosis. *J Clin Invest*. 2005;115(8):2187-2191.
40. Pantopoulos K. Inherited Disorders of Iron Overload. *Front Nutr*. 2018;5:103.
41. Cairo G, Recalcati S, Montosi G, Castrusini E, Conte D, Pietrangelo A. Inappropriately High Iron Regulatory Protein Activity in Monocytes of Patients With Genetic Hemochromatosis. *Blood*. 1997;89(7):2546-2553.
42. Katsarou A, Gkouvatsos K, Fillebeen C, Pantopoulos K. Tissue-Specific Regulation of Ferroportin in Wild-Type and Hjv-/- Mice Following Dietary Iron Manipulations. *Hepatol Commun*. 2021;5(12):2139-2150.
43. Olakanmi O, Schlesinger LS, Britigan BE. Hereditary hemochromatosis results in decreased iron acquisition and growth by Mycobacterium tuberculosis within human macrophages. *J Leukoc Biol*. 2007;81(1):195-204.
44. Nairz M, Theurl I, Schroll A, et al. Absence of functional Hfe protects mice from invasive Salmonella enterica serovar Typhimurium infection via induction of lipocalin-2. *Blood*. 2009;114(17):3642-3651.
45. Fillebeen C, Wilkinson N, Charlebois E, Katsarou A, Wagner J, Pantopoulos K. Hepcidin-mediated hypoferremic response to acute inflammation requires a threshold of Bmp6/Hjv/Smad signaling. *Blood*. 2018;132(17):1829-1841.
46. Nemeth E, Rivera S, Gabayan V, et al. IL-6 mediates hypoferremia of inflammation by inducing the synthesis of the iron regulatory hormone hepcidin. *J Clin Invest*. 2004;113(9):1271-1276.
47. Nairz M, Theurl I, Ludwiczek S, et al. The co-ordinated regulation of iron homeostasis in murine macrophages limits the availability of iron for intracellular Salmonella typhimurium. *Cell Microbiol*. 2007;9(9):2126-2140.
48. Wu Q, Shen Y, Tao Y, et al. Hemojuvelin regulates the innate immune response to peritoneal bacterial infection in mice. *Cell discovery*. 2017;3:17028-17028.
49. Scott P, Natovitz P, Coffman RL, Pearce E, Sher A. Immunoregulation of cutaneous leishmaniasis. T cell lines that transfer protective immunity or exacerbation belong to different T helper subsets and respond to distinct parasite antigens. *J Exp Med*. 1988;168(5):1675-1684.
50. Heinzel FP, Sadick MD, Holaday BJ, Coffman RL, Locksley RM. Reciprocal expression of interferon gamma or interleukin 4 during the resolution or progression of murine leishmaniasis. Evidence for expansion of distinct helper T cell subsets. *J Exp Med*. 1989;169(1):59-72.
51. Restrepo CM, Llanes A, Herrera L, Ellis E, Lleonart R, Fernández PL. Gene expression patterns associated with Leishmania panamensis infection in macrophages from BALB/c and C57BL/6 mice. *PLoS Negl Trop Dis*. 2021;15(2):e0009225.
52. Kasahara T, Hooks JJ, Dougherty SF, Oppenheim JJ. Interleukin 2-mediated immune interferon (IFN-gamma) production by human T cells and T cell subsets. *The Journal of Immunology*. 1983;130(4):1784-1789.

53. Scharton TM, Scott P. Natural killer cells are a source of interferon gamma that drives differentiation of CD4+ T cell subsets and induces early resistance to Leishmania major in mice. *J Exp Med*. 1993;178(2):567-577.
54. Schleicher U, Hesse A, Bogdan C. Minute numbers of contaminant CD8+ T cells or CD11b+CD11c+ NK cells are the source of IFN-γ in IL-12/IL-18-stimulated mouse macrophage populations. *Blood*. 2005;105(3):1319-1328.
55. Titus RG, Sherry B, Cerami A. Tumor necrosis factor plays a protective role in experimental murine cutaneous leishmaniasis. *J Exp Med*. 1989;170(6):2097-2104.
56. Ribeiro-De-Jesus A, Almeida RP, Lessa H, Bacellar O, Carvalho EM. Cytokine profile and pathology in human leishmaniasis. *Brazilian Journal of Medical and Biological Research*. 1998;31(1):143-148.
57. Hatzigeorgiou DE, He S, Sobel J, Grabstein KH, Hafner A, Ho JL. IL-6 down-modulates the cytokine-enhanced antileishmanial activity in human macrophages. *The Journal of Immunology*. 1993;151(7):3682-3692.
58. Stäger S, Maroof A, Zubairi S, Sanos SL, Kopf M, Kaye PM. Distinct roles for IL-6 and IL-12p40 in mediating protection against *Leishmania donovani* and the expansion of IL-10+ CD4+ T cells. *Eur J Immunol*. 2006;36(7):1764-1771.
59. Gu L, Tseng S, Horner RM, Tam C, Loda M, Rollins BJ. Control of TH2 polarization by the chemokine monocyte chemoattractant protein-1. *Nature*. 2000;404(6776):407-411.
60. Charlebois E, Fillebeen C, Katsarou A, et al. A crosstalk between hepcidin and IRE/IRP pathways controls ferroportin expression and determines serum iron levels in mice. *Elife*. 2022;11:e81332.
61. Malafaia G, Marcon LdN, Pereira LdF, Pedrosa ML, Rezende SA. Leishmania chagasi: Effect of the iron deficiency on the infection in BALB/c mice. *Exp Parasitol*. 2011;127(3):719-723.
62. Khan FA, Fisher MA, Khakoo RA. Association of hemochromatosis with infectious diseases: expanding spectrum. *Int J Infect Dis*. 2007;11(6):482-487.
63. Huynh C, Yuan X, Miguel DC, et al. Heme Uptake by Leishmania amazonensis Is Mediated by the Transmembrane Protein LHR1. *PLoS Pathogens*. 2012;8(7):e1002795.
64. Cabello-Donayre M, Orrego LM, Herráez E, et al. Leishmania heme uptake involves LmFLVCRb, a novel porphyrin transporter essential for the parasite. *Cellular and Molecular Life Sciences*. 2020;77(9):1827-1845.
65. Sarkar A, Andrews NW, Laranjeira-Silva MF. Intracellular iron availability modulates the requirement for Leishmania Iron Regulator 1 (LIR1) during macrophage infections. *Int J Parasitol*. 2019;49(6):423-427.
66. Laranjeira-Silva MF, Wang W, Samuel TK, et al. A MFS-like plasma membrane transporter required for Leishmania virulence protects the parasites from iron toxicity. *PLOS Pathogens*. 2018;14(6):e1007140.
67. Huynh C, Sacks DL, Andrews NW. A Leishmania amazonensis ZIP family iron transporter is essential for parasite replication within macrophage phagolysosomes. *J Exp Med*. 2006;203(10):2363-2375.
68. Gkouvatsos K, Fillebeen C, Daba A, Wagner J, Sebastiani G, Pantopoulos K. Iron-dependent regulation of hepcidin in Hjv-/- mice: evidence that hemojuvelin is dispensable for sensing body iron levels. *PLoS One*. 2014;9(1):e85530.
69. Silva Rd, Sacks DL. Metacyclogenesis is a major determinant of Leishmania promastigote virulence and attenuation. *Infection and Immunity*. 1987;55(11):2802-2806.

70. Livak KJ, Schmittgen TD. Analysis of Relative Gene Expression Data Using Real-Time Quantitative PCR and the 2−ΔΔCT Method. *Methods*. 2001;25(4):402-408.
71. Ross SL, Biswas K, Rottman J, et al. Identification of Antibody and Small Molecule Antagonists of Ferroportin-Hepcidin Interaction. *Front Pharmacol*. 2017;8:838.
72. Daba A, Gkouvatsos K, Sebastiani G, Pantopoulos K. Differences in activation of mouse hepcidin by dietary iron and parenterally administered iron dextran: compartmentalization is critical for iron sensing. *J Mol Med (Berl)*. 2013;91(1):95-102.

4.12 Figures

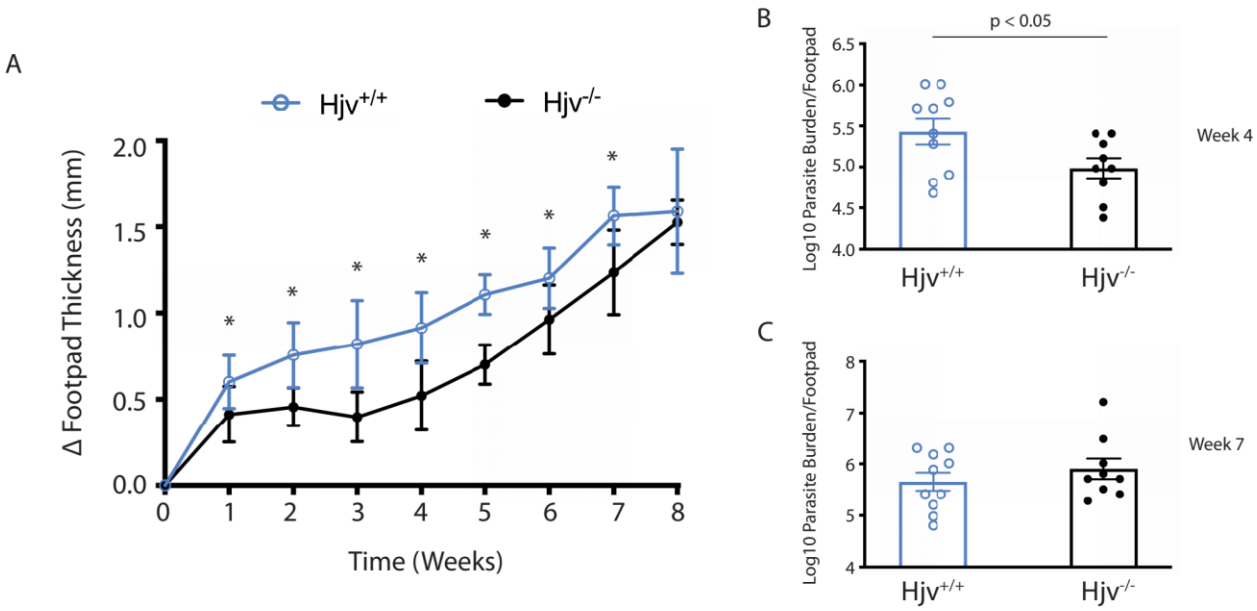

Figure 4.1: *Hjv*$^{-/-}$ mice exhibit relative resistance to *L. major* footpad infection.
Hjv$^{+/+}$ and *Hjv*$^{-/-}$ mice (n=5-24 per group) were injected in hind footpads with 5x10^{6} *L major* parasites. (A) Footpads were measured weekly over 7 weeks, and thickness of uninfected versus infected footpads was compared. Footpads were collected at endpoints and used to perform a limiting dilution assay of parasite growth at 4 weeks (B), or 7 weeks (C) post-infection. Time course data are presented as mean ± SD while $\log_{10}$ number of parasites per footpad are presented as mean ± SEM.

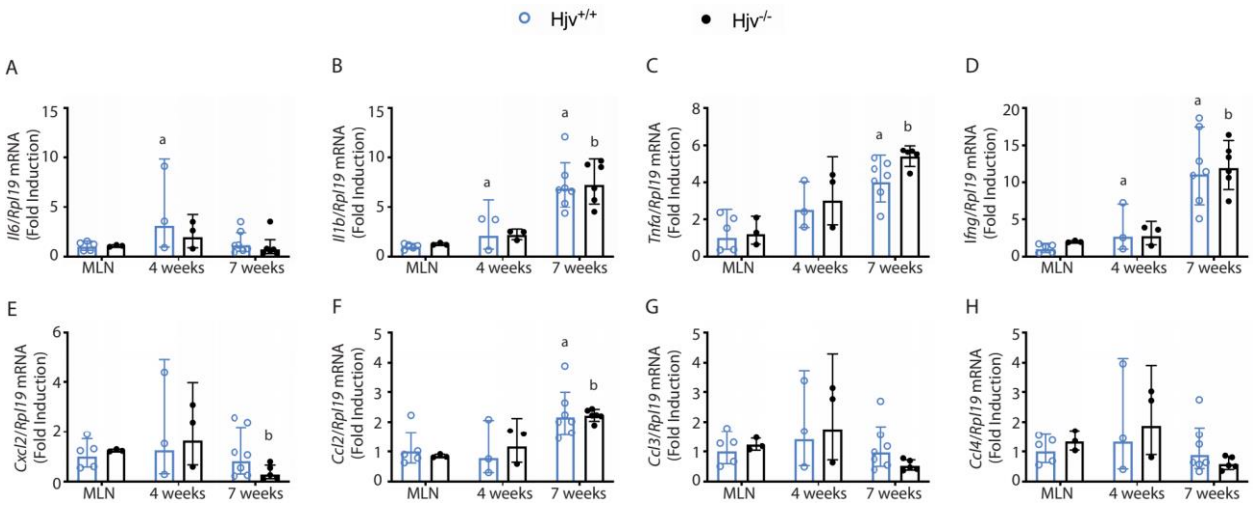

Figure 4.2: Popliteal lymph node cytokine expression following footpad infection.
Popliteal lymph nodes were collected from *Hjv*$^{+/+}$ and *Hjv*$^{-/-}$ mice infected with 5x10^{6} *L. major* in hind footpads 4- or 7- weeks post-infection. Mesenteric lymph nodes (MLN) were also collected as uninfected control organs. RNA was extracted, reverse transcribed and used for qPCR analysis of (A) *Il6*, (B) *Il1b*, (C) *Tnfa*, (D) *Ifng*, (E) *Cxcl2*, (F) *Ccl2*, (G) *Ccl3*, and (H) *Ccl4* mRNAs. Data are presented as geometric mean ± geometrical SD. Statistical differences compared to MLN from *Hjv*$^{+/+}$ or *Hjv*$^{-/-}$ mice are indicated by a or b, respectively.

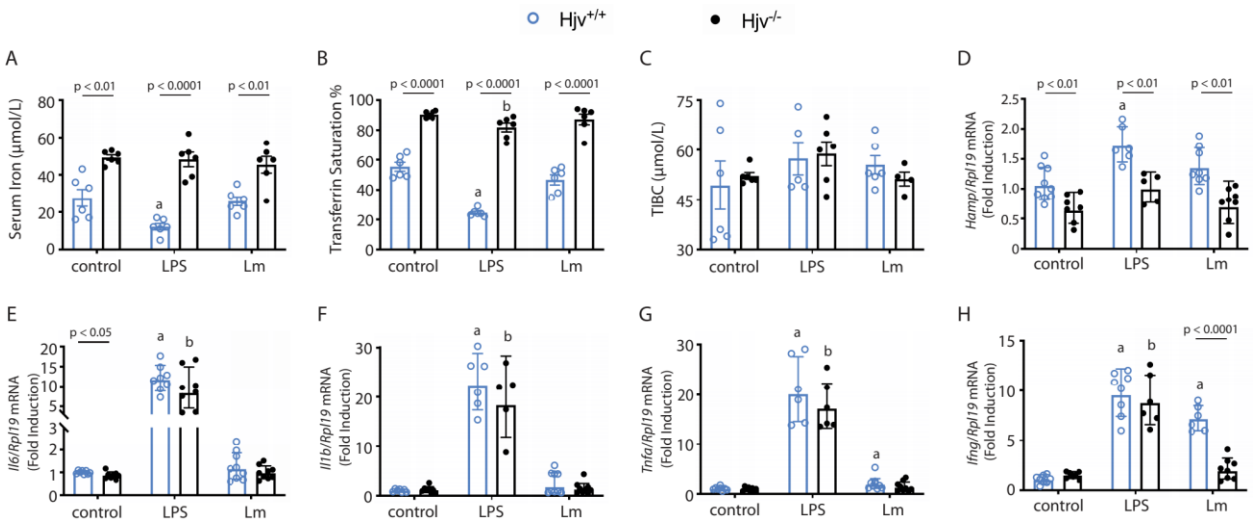

Figure 4.3: *Leishmania major* acute infection does not trigger a hypoferremic response.
Hjv$^{+/+}$ and *Hjv*$^{-/-}$ mice were injected intraperitoneally with either phosphate-buffered saline (control), the endotoxin LPS, or 10^8 *L. major* stationary phase parasites (Lm). 6 hours post-infection, blood was collected by cardiac puncture. Serum was separated from whole blood and used for analysis of: (A) serum iron, (B) transferrin saturation, and (C) total iron binding capacity (TIBC). Liver samples were collected; RNA was extracted and used for analysis of: (D) *Hamp*, (E) *Il6*, (F) *Il1b*, (G) *Tnfa*, and (H) *Ifng* mRNAs by qPCR. Data in (A-C) are presented as mean ± SEM, while data in (D-H) are presented as geometric mean ± geometrical SD. Statistical differences compared to untreated Hjv$^{+/+}$ or Hjv$^{-/-}$ mice are indicated by a or b, respectively.

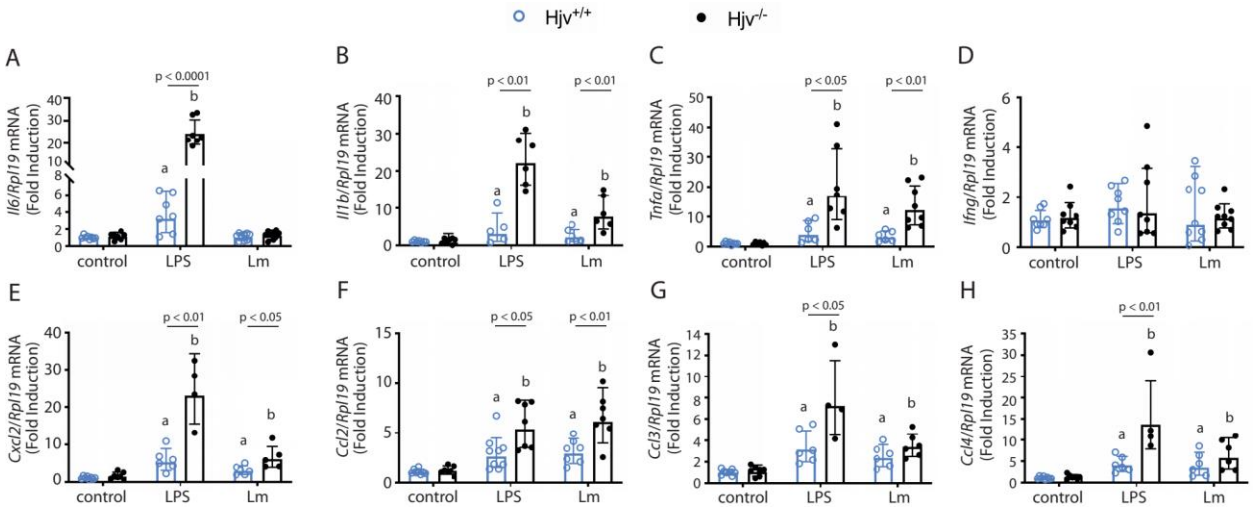

Figure 4.4: Cytokine expression in peritoneal lavage following acute infection with *L. major*.
Hjv$^{+/+}$ and *Hjv*$^{-/-}$ mice were injected intraperitoneally with either phosphate-buffered saline (control), the endotoxin LPS, or 10^8 *L. major* stationary phase parasites (Lm). 6 hours post-infection, peritoneum was lavaged and peritoneal cells were collected. RNA was extracted, reverse transcribed and used for qPCR analysis of: (A) *Il6*, (B) *Il1b*, (C) *Tnfa*, (D) *Ifng*, (E) *Cxcl2*, (F) *Ccl2*, (G) *Ccl3*, and (H) *Ccl4* mRNAs. Data are presented as geometric mean ± geometrical SD. Statistical differences compared to untreated *Hjv*$^{+/+}$ or *Hjv*$^{-/-}$ mice are indicated by a or b, respectively.

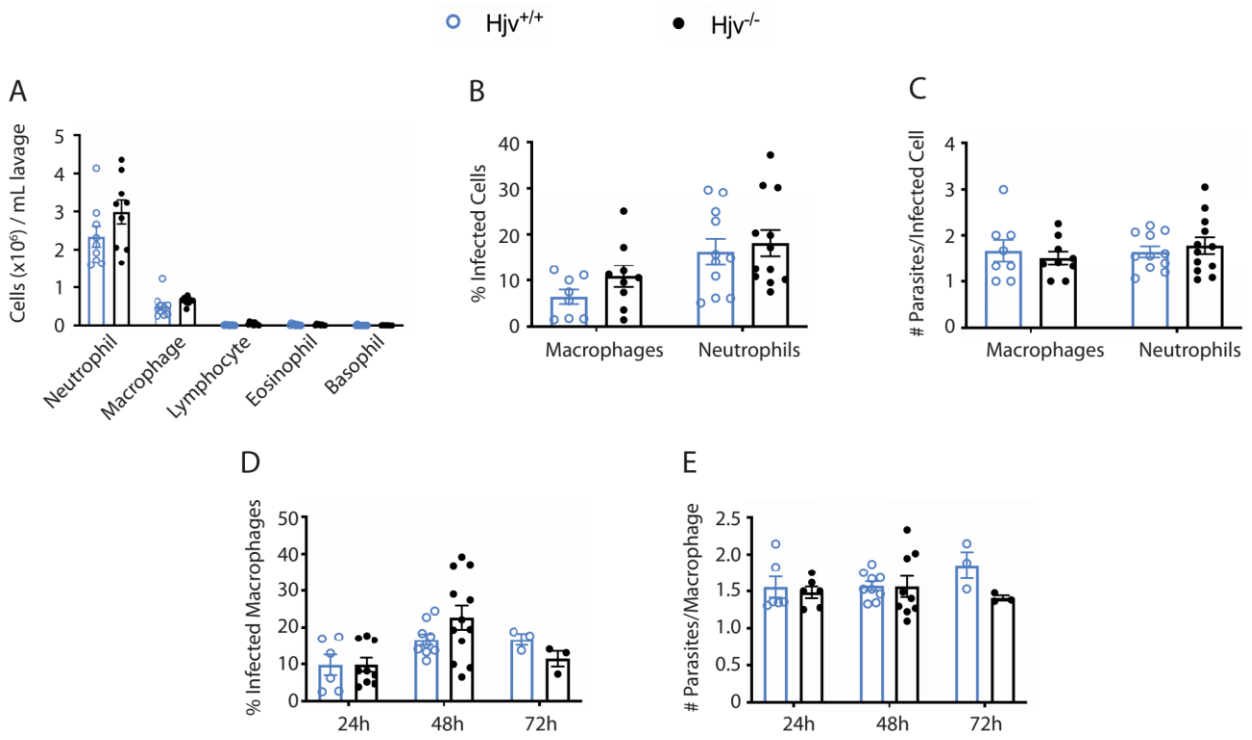

Figure 4.5: Analysis of intraperitoneal macrophages and neutrophils recovered post-infection.
Hjv$^{+/+}$ and *Hjv*$^{-/-}$ mice were injected intraperitoneally with 10^8 *L. major* stationary phase parasites. 6 hours post-infection, peritoneum was lavaged, peritoneal cells were counted, and 50 µl from the suspension was used for Cytospin centrifugation. Cells were fixed onto slides and stained using Diff-Quik. Numbers of separated cell types are shown in (A). Percentage of infected macrophages and neutrophils (B), and number of parasites per infected cell (C) were assessed. (E-E) 10^5 cells following lavage were plated in 4-well chambers. Cells were cultured over 24, 48, and 72 hours before removal of media, drying, and staining with Diff-Quik. Percentage of infected cells (macrophages) (D), and number of parasites per infected cell (E) were assessed. Data are presented as mean ± SEM.

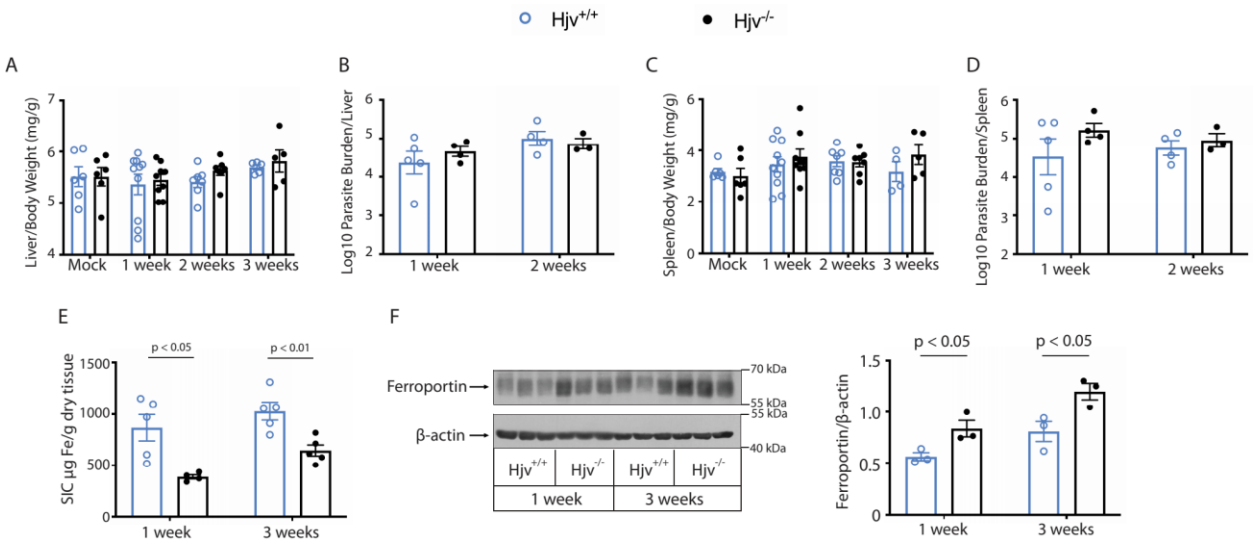

Figure 4.6: Severe genetic iron overload does not affect visceral leishmaniasis disease progression.
Hjv$^{+/+}$ and *Hjv*$^{-/-}$ mice were injected intraperitoneally with phosphate buffered saline or 10^8 *L. infantum* parasite. Mice were sacrificed 1-, 2-, or 3-weeks post-infection. (A) Liver/body weight; (B) parasite burden in the liver; (C) spleen/body weight; (D) parasite burden in the spleen; (E) splenic iron content (SIC). (F) A representative Western blot of splenic ferroportin; data from n=3 experiments were quantified by densitometry and are shown on the right. Data are presented as mean ± SEM.

4.13 Supplementary Figures

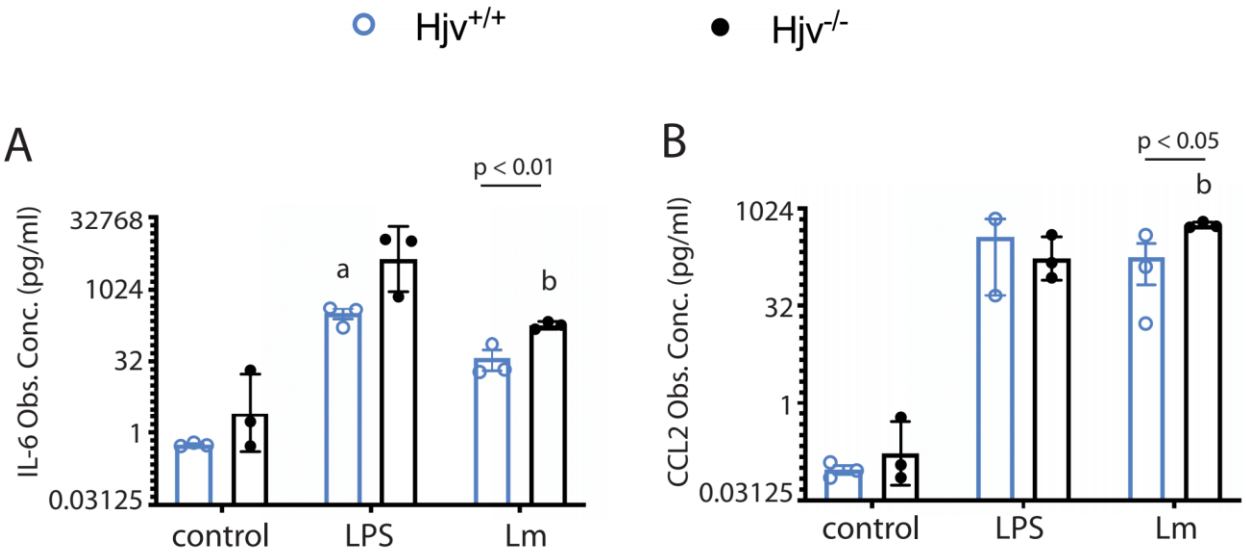

Figure S.4.1: Multiplex cytokine expression of intraperitoneal lavage.
Lavage supernatant was collected from mice described in figure 4. Supernatant were analysed for expression of (A) IL-6 and (B) CCL2 by multiplex assay. Data are presented as mean ± SEM. Statistical differences compared to untreated *Hjv*$^{+/+}$ or *Hjv*$^{-/-}$ mice are indicated by a or b, respectively.

4.14 Supplementary Tables

Table S.4.1: List of primers used for qPCR.

Gene	GenBank accession	Forward primer sequence	Reverse primer sequence
Rpl19	NM_009078.2	*AGGCATATGGGCATAGGGAAGAG*	*TTGACCTTCAGGTACAGGCTGTG*
Hamp1	NM_032541.1	*AAGCAGGGCAGACATTGCGAT*	*CAGGATGTGGCTCTAGGCTATGT*
Il6	NM_031168.2	*AGCCAGAGTCCTTCAGAGAGA*	*GGTCTTGGTCCTTAGCCACTC*
Il1b	NM_008361.4	*GCCACCTTTTGACAGTGATGA*	*AGCTTCTCCACAGCCACAAT*
Tnfa	NM_013693.3	*TACTGAACTTCGGGGTGATCG*	*GGTGGTTTGCTACGACGTG*
Cxcl2	NM_009140.2	*CTCTCAAGGGCGGTCAAAAAG*	*GAGGCACATCAGGTACGATCC*
Ccl2	NM_011333.3	*TGCCCTAAGGTCTTCAGCAC*	*AAGGCATCACAGTCCGAGTC*
Ccl3	NM_011337.2	*TGCGCTGACTCCAAAGAGAC*	*CTCGATGTGGCTACTTGGCA*
Ccl4	NM_013652.2	*TGTGCAAACCTAACCCCGAG*	*GCCGGGAGGTGTAAGAGAAA*
Ifng	NM_008337.4	*CAGCAACAGCAAGGCGAAAAAGG*	*TTTCCGCTTCCTGAGGCTGGAT*

Chapter 5: General Discussion

The past two decades have brought about a wealth of knowledge regarding mammalian iron metabolism. The discovery of the liver-derived iron hormone hepcidin has revolutionized our understanding of iron flux between the circulation and cells. Yet, iron deficiency remains one of the leading contributors to global burden of disease[1]. Anemias affected roughly a quarter of the world's population in 2005 with iron deficiency anemia accounting for about half of cases[2]. Many of these cases are linked to malnutrition in impoverished regions. Little progress has been made since then as, in 2016, iron deficiency anemia was one of the top five causes of years lived with disability with over 1.2 billion cases reported[3]. On the other hand, hereditary hemochromatosis, an inherited disease of iron overload characterized by increased dietary iron absorption due to hepcidin deficiency, is one of the most common autosomal recessive disorders in Caucasians of northern European descent[4]. Roughly 1 in 200 people of this background will be affected[5] and treatment options remain crude involving phlebotomy which may be contraindicated if patients present with cellulitis, abscesses, hematoma, venous fibrosis to name a few. Importantly, iron dysregulation will alter immune responses when faced with pathogens. Leishmaniasis has been studied as an example since it is a neglected tropical disease reported to have affected 4.8 million people in 2016[3]. The work presented herein has used genetically manipulated mouse models ablating endothelial transferrin receptor 1 (TFR1) or global hemojuvelin (HJV) to study the corresponding mechanisms behind iron sensing and hemochromatosis. This thesis has generated new knowledge with respect to mammalian iron sensing, describing novel mechanisms for the control of serum iron levels in hemochromatosis. In addition, the work of the thesis strengthened our understanding on the infection susceptibility by the protozoan parasite *Leishmania* as a function of macrophage ability to retain iron.

5.1 Main Findings, Limitations, Future perspectives

5.1.1 Ablation of the cellular iron gate, transferrin receptor 1, only modestly influences endothelial iron sensing

As demonstrated, $Tfrc^{Tek\text{-}Cre}$ mice efficiently produce bone morphogenetic protein 6 (BMP6), the main driver of iron-mediated hepcidin expression, in response to dietary iron when

given in large doses (2% carbonyl iron) over 18 hours. Notably, they transiently fail to do so in a 5-hour timeframe, where kinetic studies revealed the largest increase in BMP expression, when non-transferrin bound iron (NTBI) is injected intravenously in the form of ferric ammonium citrate (FAC) (Figure 2.2). Knockout animals respond appropriately to holo-transferrin, the primary regulated form of systemic iron delivery. As mentioned, these results suggest a modest role for TFR1 early in endothelial cell iron sensing. The major driver is proposed to be NTBI which may enter endothelial cells through the metal-ion transporter ZIP8. Furthermore, we rationalize that the 18-hour holo-transferrin injection causes BMP expression under these experimental conditions due to cell autonomous factors. Although regulated export of ferritin may be a possible candidate for iron signaling from macrophages[6], it should be noted that Tek expression is also found in a significant portion of tissue-resident macrophages as these may originate from the yolk-sac-derived erythron-myeloid progenitors[7,8]. Thus, while some macrophages may still be able to obtain iron from transferrin, a more likely explanation would be that stellate cells signal to endothelial cells in response to transferrin-bound iron. Hepatocytes are an unlikely candidate due to the observed physiological production of BMP6 even in the absence of hepatocytic TFR1[9]. It would be of great interest to disrupt the newly described CD63 pathway of ferritin-exosome signaling, which may be responsible for paracrine iron signaling, and measure the pathway's role on BMP6 expression[6].

It remains unclear why liver iron content is elevated in mice lacking endothelial TFR1 expression. These results were corroborated in $Tfrc^{Stab2\text{-}cre}$ mice, generating liver sinusoidal specific TFR1 ablation, which demonstrated a similar trend[10]. Attempts to visualize liver iron by Perls' staining revealed no obvious differences between genotypes, and hematoxylin and eosin staining excluded extramedullary hematopoiesis. Thus, it is difficult to conclude the localization and speciation of these extra iron stores.

5.1.2 Proposed regulatory pathways of endothelial BMP6 expression

A recent study suggested that a hepatocyte-derived factor may be necessary for liver sinusoidal endothelial cell (LSEC) BMP6 production as primary cultures of these cells appear incapable of producing BMP6 in response to a variety of iron treatments[11]. The authors conclude that only under conditions of co-cultures with hepatocytes and LSECs can the latter respond to iron treatments in contrast to previous reports[12]. The disparity in these results may stem from the

use of established cell lines in previous reports which may not fully recapitulate the complex LSEC phenotype[13]. Difficulty in isolating and culturing endothelial cells has been a significant barrier for many studying LSECs in this field. The study by Colucci *et al.* claims that their primary LSEC cultures are more physiologically relevant by the appearance of fenestrae *in vitro*[11]. Nevertheless, these results provide an alternative method of activation for LSEC BMP6 production which may complement NFE2L2-driven gene activation observed in our studies. Identification of the hepatocyte-derived factor is of critical importance if conclusions are to be made about LSEC iron sensing.

In fact, recent reports suggest that endothelial BMP6 production is linked to NFE2L2, the ROS-regulated transcription factor responsible for activating antioxidant response elements (AREs), since an ARE is present in intron 1 of the BMP6 gene[14]. NFE2L2 is kept suppressed as a complex with KEAP1 and BACH1. In this model, mitochondrial lipid peroxidation would cause release of electrophilic lipids which may interact with residues on KEAP1 to activate NFE2L2[14]. However, one important limitation of this study is that *NFE2L2* knockout mice retain basal levels of BMP6 when on normal diet and express hepcidin mRNA to similar extents when fed a 2% carbonyl iron diet suggesting that there may be other mechanisms of BMP regulation at play. Moreover, endothelial cell iron loading does not seem to be directly linked to BMP6 production as endothelial-specific ferroportin knockout mice have reduced BMP6 expression despite liver iron overload[15]. Thus, although NFE2L2 seems to play a distinct role in the regulation of BMP6 expression, the possibility of other factors influencing BMP6 expression cannot be discounted.

5.1.3 Apo-transferrin injections reveal limiting factor for dietary iron uptake

Initial experiments in this study placed mice on iron-deficient diet for one week followed by injection with apo-transferrin (transferrin lacking iron) followed by feeding mice with 0.25% carbonyl iron diet for 6 hours. The rationale for this experimental setting was to reduce and prevent formation of NTBI in the bloodstream of mice by reducing iron acquisition from the diet followed by injecting them with additional transferrin to act as a buffer. The diet used to trigger iron uptake was 0.25% carbonyl, nearly a tenth of the iron compared to the high iron diet used in the experiments shown in Figure 2.2 (2% carbonyl iron diet). However, injection with apo-transferrin had the unexpected effect of rapidly increasing iron absorption from the diet resulting in a massive increase in serum iron, transferrin saturation, and presence of NTBI. Due to the complexity of

these results, they were excluded from the final manuscript in favor of intravenous FAC injections which directly model an acute increase in NTBI. Apo-transferrin injection did reveal that $Tfrc^{Tek\text{-}Cre}$ animals could produce a robust BMP response and highlight that abundance of transferrin may be a limiting factor for dietary iron absorption. Saturation of the transferrin buffer remains unavoidable and is a limiting factor in iron studies. Thus, differentiating between the effects of holo-transferrin and NTBI remains difficult. This can be addressed by measuring results at early timepoints since NTBI absorption is more rapid, on the order of seconds, than holo-transferrin, on the order of minutes[16]. Moreover, FAC injection have primarily been used in animal models to investigate bacterial infection and brain iron accumulation[17,18]. The dosage used in these experimental conditions is proposed to induce a transient hyperferremia[17]. We inferred from a preliminary experiment using intraperitoneal FAC injection that hepcidin was activated after 6 hours and, consequently, rationalized that intravenous injection would act earlier on hepcidin expression at 5 hours (Figure S.2.2). FAC was used as an alternative to iron-dextran since the latter is known to be directly taken up by macrophages for processing and is therefore less physiologically relevant[19].

5.1.4 Lessons from liver single cell transcriptomics

Using a scRNA-seq approach, we identified the key effects of iron uptake on endothelial cell mRNA expression profiles. The Augur[20] machine learning algorithm revealed that the most profoundly altered cell types in response to either dietary iron loading or holo-transferrin injection within liver cell populations were endothelial cells (Figure 2.5). Interestingly, these were closely followed by stellate cells, which have been typically associated with carbohydrate regulation, mitochondrial, lipid, and retinoid homeostasis, and drive hepatic fibrosis[21]. Cell crosstalk analysis using CellChat[22] performed on this dataset suggests that stellate cells may be communicating with endothelial cells to a greater degree than expected although the relevance of this communication in the context of iron metabolism is not certain. Endothelial cells were revealed to highly induce NFE2L2 target genes in response to dietary iron and, unexpectedly, activate expression of many MYC and mammalian target of rapamycin (mTOR) targets (Figure 2.6). It would be of interest to examine the family of small MAF proteins commonly associated with NFE2L2 to elucidate any possible function they may play in BMP signaling. The activation of mTOR and MYC targets suggests changes in translation regulation which need to be validated experimentally. Interestingly,

iron deficiency in mammals triggers cellular reprogramming involving the IRE/IRP system but also tristetraprolin (TTP) which binds AU-rich elements and promotes their turnover[23]. TTP may control the expression of TFR1, for example, and is inhibited by mTOR[24]. Moreover, MYC is another target of TTP linking iron status to expression of these targets[25]. To summarize, iron deficiency would inhibit mTOR consequently activating TTP which would function to degrade target genes such as MYC to regulate cellular translation. Work in the plant *Arabidopsis thaliana* demonstrated that up to 81 ribosomal proteins were differentially expressed in response to iron deficiency[26] with significant reduction in the mRNA transcripts as observed in RNA-seq studies[27]. Conceivably, the observed activation of MYC and mTOR targets by single cell sequencing could reflect the recovery from the week-long iron-deficient diet fed to mice despite this timeframe being relatively short and incapable of significantly altering serum iron parameters and draining liver iron stores (Figure 2.3). This highlights the swiftness of adaptation to shortage of iron in the diet.

Importantly, midzonal hepatocytes, the hepatocytes responsible for most hepcidin expression[28], were the most profoundly perturbed when comparing both treatment groups. This comparison may reveal, in part, the effects of non-transferrin bound iron as one is studying the difference between an animal given holo-transferrin and one obtaining all forms of iron through the diet. One should consider this as a reductionist explanation considering holo-transferrin is given at one timepoint while diet is provided *ad libitum*. Nevertheless, these findings reveal the possibility of a midzonal hepatocyte response to NTBI which was characterized by increased oxidative phosphorylation, fatty acid metabolism, and, to a lesser extent, ROS signaling (Figure 2.7).

Single cell analysis of heme-regulated eIF2α kinase (HRI), a translational regulator during iron deficiency, demonstrated an upregulation at the mRNA level after dietary iron intake in both macrophages and endothelial cell populations (data not shown). HRI translationally regulates production of globin genes in erythroid precursors by phosphorylating the α-subunit of the eukaryotic translation initiation factor 2 (eIF2α) to prevent an imbalance of globin synthesis in the absence of heme[29,30]. Yet, bone marrow-derived macrophages lacking HRI display impaired erythrophagocytosis and attenuated responses to LPS[31]. Thus, validating and exploring this protein's role in translational regulation of both macrophages and endothelial cells would be of interest.

5.1.5 Functional crosstalk between inflammatory and iron signaling to hepcidin

Production of BMPs is the first step in expression of hepcidin and helps control its basal levels. When this cascade is disrupted, inflammation cannot successfully produce hypoferremia[32]. The hypoferremic response is believed to be protective against invading extracellular pathogens preventing them from acquiring necessary iron for replication[33]. Previous *in vitro* work by our group demonstrated that inorganic iron treatment of Huh7 cells and primary murine hepatocytes abrogated hepcidin gene expression and small mothers against differentiation (SMAD) phosphorylation[34]. This suggested that iron overload may, at least in part, play a role in hepcidin's downregulation in hemochromatosis. Thus, the experiments in chapter 3 aimed to dissect the mechanisms of hepcidin regulation in response to iron loading and to clarify the mechanisms which interfere with inflammatory hypoferremia in models of iron overload. Our data demonstrated that hepcidin is progressively induced in response to iron loading and that LPS works synergistically with iron to further induce hepcidin expression (Figure 3.1). Yet, dietary iron loading overwhelms hepcidin's capacity to produce hypoferremia despite its intense production.

It should be mentioned that there is no clearly defined threshold for hypoferremia as a protective mechanism. That is, we have previously shown that infection with live *Escherichia coli* causes a progressive decrease in serum iron over 24 hours post-infection but determining how protective this response is on its own is difficult considering the numerous other mechanisms activated during infection[32]. Particularly, mammals have a multitude of responses that are employed to withhold iron from pathogens. For bacterial infections, lipocalin-2 works to sequester bacterial siderophores responsible for iron acquisition within hosts[35]. Although cases of iron overload have been associated with worse outcomes for many infections[36], and iron supplementation can be detrimental in areas endemic with infectious diseases[37], iron deficiency has been more difficult to study. Host iron status may be difficult to determine prior to infection[38], and iron deficiency has pleiotropic effects on the host immune system[39]. Herein, we have analyzed the hypoferremic response as a binary phenomenon which may not fully recapitulate the protective response mounted by the host but does shed light on many mechanisms of inflammatory iron flux.

Injection with LPS, a potent endotoxin and toll-like receptor 4 agonist, revealed that iron overload, whether dietary or genetic, mitigated reduction in serum iron preventing effective hypoferremia. Moreover, these results revealed that LPS triggered a hepcidin-independent

response due to the observed modest drop in serum iron even in complete absence of hepcidin expression (Figure 3.2). The possibility of hepcidin-independent mechanisms for serum iron regulation has been proposed previously[40-43] and linked to downregulation of ferroportin expression in macrophages of the reticuloendothelial system. Yet, the mechanism of ferroportin's mRNA regulation by endotoxin-produced inflammation remains unclear. Clarifying whether the ferroportin promoter contains a binding element for a negative regulator, whether these effects are epigenetic, or even posttranscriptional could guide us toward novel avenues for ferroportin regulation in hemochromatosis.

One major limitation discussed was determining which fraction of cells express the most ferroportin transcripts and protein in the liver, namely hepatocytes or Kupffer cells, the liver's tissue-resident macrophages. We have attempted to isolate pure fractions of Kupffer cells without success which has hindered our ability to address this question. However, we used the approach of separating hepatocytes from non-parenchymal cell fractions and measuring IRE/IRP binding activity and ferroportin expression (Figure 3.6). Based on the immunohistochemical data in Figure 3.3, it is assumed that macrophages would produce the most ferroportin out of non-parenchymal cell populations, mainly endothelial cells, stellate cells, and few tissue resident immune cells. As expected, non-parenchymal fractions had elevated IRP binding activity in *Hjv*$^{-/-}$ mice and expressed greater ferroportin protein suggesting that liver ferroportin may be predominantly in Kupffer cells. Nevertheless, it would be beneficial to isolate pure fractions of Kupffer cells and hepatocytes for direct comparison.

This study demonstrated that *de novo* ferroportin synthesis appears to be the critical component of serum iron levels under iron overload. By disrupting ferroportin synthesis with LPS treatment, synthetic hepcidin's capacity to induce degradation of ferroportin and reduced serum iron was greatly enhanced (Figure 3.8). Thus, future work should focus on designing targeted therapies disrupting ferroportin transcription combined with synthetic hepcidin treatment. Designing small interfering RNA targeting ferroportin combined with an adenoviral vector or a lipid nanoparticle for specific cellular targeting in hemochromatosis animal models would be an appealing approach. This approach combined with small hepcidin mimetics known as minihepcidins[44,45] designed to improve serum half-life could be an effective strategy for long term control of iron overload[46]. This method would require differentiating the contribution to serum

iron of cell types as mentioned. Since macrophages of the reticuloendothelial system are typically major contributors to serum iron levels through the process of erythrophagocytosis and iron storage[47,48], the spleen would be a natural target for iron therapies.

5.1.6 Discoveries in Leishmania iron acquisition

The protozoan parasites of genus *Leishmania* reside within parasitophorous vacuoles of macrophages where they must compete with their hosts for iron. The primary form of iron acquisition for these dangerous parasites remains an important question. We investigated whether macrophages lacking iron stores due to increased cell surface ferroportin could harbor *Leishmania* efficiently. Our study revealed that growth of cutaneous leishmaniasis in footpads was transiently delayed (Figure 4.1). One important caveat of these measurements is that they measure inflammation in footpads which reflect cellular recruitment to the site of inoculation as well as parasite replication. Dysregulated iron metabolism can have pleiotropic effects on both cellular recruitment and immune responses[49] of which only the latter was examined. For example, Th1 T cells are sensitive to perturbations in iron where holo-transferrin may impair autocrine and paracrine IFNγ signaling, while iron chelation may increase IFNγ sensitivity but will impair cell proliferation and IFNγ output[50-52]. In macrophages, function is highly dependent on iron. Iron may inhibit transcription of major histocompatibility complex (MHC) -II impairing interaction with Th1 cells[53]. Still, models of iron overload *in vitro* do not reflect macrophages in models of hereditary hemochromatosis where macrophages are deficient in iron stores. Interestingly, macrophages from *Hfe*$^{-/-}$ mice, which develop a relatively mild form of hemochromatosis, displayed reduced capacity to produce TNFα and IL-6 in response to *Salmonella* and LPS stimulation suggesting that reduced macrophage iron stores play a role in cytokine expression[54]. These results differ with the observed increase in TNFα gene expression in peritoneal cells from *Hjv*$^{-/-}$ mice, as well as IL-6 in lavage supernatant in response to *Leishmania* (Figure 4.4, S.4.1). Thus, it is possible that observed changes in cytokine expression is primarily a result of other cells present in collected lavages such as neutrophils.

Our data on infection with *Leishmania major* reveal the interesting possibility that IFNγ is not produced locally at the site of infection. It remains controversial whether IFNγ can be produced by infiltrating macrophages or neutrophils in response to infection. One study claimed that IFNγ could be produced by macrophages *in vitro* in response to *E. coli*[55]. Yet, claims have been made

that primary macrophage cultures may be contaminated with minute quantities of CD8+ T cells and NK cells producing IFNγ[56]. Nonetheless, in this experimental setting, IFNγ expression from collected intraperitoneal cells and from supernatants of intraperitoneal lavage could not be measured to any appreciable extent. However, acute infection with *L. major* revealed that liver production of IFNγ was significantly lower in *Hjv*$^{-/-}$ animals 6 hours post-infection suggesting that circulating IFNγ may play a role in the course of infection.

One key limitation of this study was the use of complete *Hjv* knockout animals. HJV belongs to the RGM family of BMP co-receptors which were initially defined for their roles as adhesion proteins guiding the development of neurons[57,58]. These are now known to have a diverse set of functions in regulating biological processes through intracellular signaling[59]. Yet, very few studies have investigated the role of RGM family of proteins in immunity. One such study demonstrated a putative role for RGMa in leukocyte migration[60]. Another study revealed that disruption of RGMb in macrophages resulted in increased IL-6 expression[61]. The only study disrupting HJV in macrophages investigated its role in bacterial infection and found increased susceptibility to bacterial infection in knockout macrophages[55]. Thus, it would be of critical importance to determine if the observed effects in growth of cutaneous leishmaniasis were due to absence of HJV on macrophages or from impaired iron stores.

Finally, to determine the extent of the effects of iron in this model, it would be necessary to manipulate dietary iron in *Hjv*$^{-/-}$ mice. We have shown in chapter 3 that a 5-week course of iron-deficient diet can successfully reduce iron stores by about 70% (Figure 3.2). This seemingly reprograms the liver by increasing TFR1 and reducing ferroportin gene expression. Thus, it would be of interest to manipulate dietary iron by both depriving *Hjv*$^{-/-}$ mice of iron or feeding them a high-iron diet. These may exacerbate the observed phenotype in footpads and indicate whether the lack of iron stores or increased iron flow through macrophages is responsible for delayed footpad swelling.

5.2 Concluding remarks

This thesis sought to address outstanding problems in the field of iron metabolism. By studying iron sensing, we have clarified one of the key signals that triggers redistribution of systemic iron and, in doing so, have provided invaluable knowledge for treatment of iron

deficiency. In addition, our work on iron overload and inflammation has helped address questions regarding control of hemochromatosis and nutritional immunity. These issues are united by the underlying challenge of providing iron treatments to iron-deficient individuals in areas endemic with infectious diseases such as leishmaniasis. This dissertation has provided vital insights in the careful balancing act of iron in both health and disease.

5.3 References

1. Pasricha S-R, Tye-Din J, Muckenthaler MU, Swinkels DW. Iron deficiency. *The Lancet*. 2021;397(10270):233-248.
2. De Benoist B, Cogswell M, Egli I, McLean E. Worldwide prevalence of anaemia 1993-2005; WHO global database of anaemia. 2008.
3. Vos T, Abajobir AA, Abate KH, et al. Global, regional, and national incidence, prevalence, and years lived with disability for 328 diseases and injuries for 195 countries, 1990–2016: a systematic analysis for the Global Burden of Disease Study 2016. *The Lancet*. 2017;390(10100):1211-1259.
4. Powell LW, Seckington RC, Deugnier Y. Haemochromatosis. *Lancet*. 2016;388(10045):706-716.
5. Bacon BR, Powell LW, Adams PC, Kresina TF, Hoofnagle JH. Molecular medicine and hemochromatosis: At the crossroads. *Gastroenterology*. 1999;116(1):193-207.
6. Yanatori I, Richardson DR, Dhekne HS, Toyokuni S, Kishi F. CD63 is regulated by iron via the IRE-IRP system and is important for ferritin secretion by extracellular vesicles. *Blood*. 2021;138(16):1490-1503.
7. Canali S, Zumbrennen-Bullough KB, Core AB, et al. Endothelial cells produce bone morphogenetic protein 6 required for iron homeostasis in mice. *Blood*. 2017;129(4):405-414.
8. Gomez Perdiguero E, Klapproth K, Schulz C, et al. Tissue-resident macrophages originate from yolk-sac-derived erythro-myeloid progenitors. *Nature*. 2015;518(7540):547-551.
9. Fillebeen C, Charlebois E, Wagner J, et al. Transferrin receptor 1 controls systemic iron homeostasis by fine-tuning hepcidin expression to hepatocellular iron load. *Blood*. 2019.
10. Fisher AL, Wang CY, Xu Y, et al. Functional role of endothelial transferrin receptor 1 in iron sensing and homeostasis. *Am J Hematol*. 2022.
11. Colucci S, Altamura S, Marques O, et al. Iron-dependent BMP6 Regulation in Liver Sinusoidal Endothelial Cells Is Instructed by Hepatocyte-derived Secretory Signals. *HemaSphere*. 2022;6(10):e773.
12. Wang S, Chen C, Yu L, Mueller J, Rausch V, Mueller S. Bone morphogenetic protein 6–mediated crosstalk between endothelial cells and hepatocytes recapitulates the iron-sensing pathway in vitro. *J Biol Chem*. 2021;297(6):101378.
13. Poisson J, Lemoinne S, Boulanger C, et al. Liver sinusoidal endothelial cells: Physiology and role in liver diseases. *J Hepatol*. 2017;66(1):212-227.
14. Lim PJ, Duarte TL, Arezes J, et al. Nrf2 controls iron homoeostasis in haemochromatosis and thalassaemia via Bmp6 and hepcidin. *Nature Metabolism*. 2019;1(5):519-531.
15. Zhang Z, Guo X, Herrera C, et al. Bmp6 Expression Can Be Regulated Independently of Liver Iron in Mice. *PLoS One*. 2014;9(1):e84906.
16. Craven CM, Alexander J, Eldridge M, Kushner JP, Bernstein S, Kaplan J. Tissue distribution and clearance kinetics of non-transferrin-bound iron in the hypotransferrinemic mouse: a rodent model for hemochromatosis. *Proceedings of the National Academy of Sciences*. 1987;84(10):3457-3461.
17. Michels KR, Zhang Z, Bettina AM, et al. Hepcidin-mediated iron sequestration protects against bacterial dissemination during pneumonia. *JCI Insight*. 2017;2(6).
18. You LH, Li F, Wang L, et al. Brain iron accumulation exacerbates the pathogenesis of MPTP-induced Parkinson's disease. *Neuroscience*. 2015;284:234-246.

19. Richter GW. THE CELLULAR TRANSFORMATION OF INJECTED COLLOIDAL IRON COMPLEXES INTO FERRITIN AND HEMOSIDERIN IN EXPERIMENTAL ANIMALS. *J Exp Med*. 1959;109(2):197-216.
20. Squair JW, Skinnider MA, Gautier M, Foster LJ, Courtine G. Prioritization of cell types responsive to biological perturbations in single-cell data with Augur. *Nat Protoc*. 2021;16(8):3836-3873.
21. Trivedi P, Wang S, Friedman SL. The Power of Plasticity—Metabolic Regulation of Hepatic Stellate Cells. *Cell Metab*. 2021;33(2):242-257.
22. Jin S, Guerrero-Juarez CF, Zhang L, et al. Inference and analysis of cell-cell communication using CellChat. *Nature Communications*. 2021;12(1):1088.
23. Ramos-Alonso L, Romero AM, Polaina J, Puig S, Martínez-Pastor MT. Dissecting mRNA decay and translation inhibition during iron deficiency. *Curr Genet*. 2019;65(1):139-145.
24. Bayeva M, Khechaduri A, Puig S, et al. mTOR Regulates Cellular Iron Homeostasis through Tristetraprolin. *Cell Metab*. 2012;16(5):645-657.
25. Brooks SA, Blackshear PJ. Tristetraprolin (TTP): Interactions with mRNA and proteins, and current thoughts on mechanisms of action. *Biochim Biophys Acta*. 2013;1829(6-7):666-679.
26. Wang J, Lan P, Gao H, Zheng L, Li W, Schmidt W. Expression changes of ribosomal proteins in phosphate- and iron-deficient Arabidopsis roots predict stress-specific alterations in ribosome composition. *BMC Genomics*. 2013;14(1):783.
27. Rodriguez-Celma J, Pan I-C, Li W, Lan P, Buckhout T, Schmidt W. The transcriptional response of Arabidopsis leaves to Fe deficiency. *Frontiers in Plant Science*. 2013;4.
28. Halpern KB, Shenhav R, Matcovitch-Natan O, et al. Single-cell spatial reconstruction reveals global division of labour in the mammalian liver. *Nature*. 2017;542(7641):352-356.
29. Han A-P, Yu C, Lu L, et al. Heme-regulated eIF2α kinase (HRI) is required for translational regulation and survival of erythroid precursors in iron deficiency. *The EMBO Journal*. 2001;20(23):6909-6918.
30. Liu S, Bhattacharya S, Han A, et al. Haem-regulated eIF2α kinase is necessary for adaptive gene expression in erythroid precursors under the stress of iron deficiency. *Br J Haematol*. 2008;143(1):129-137.
31. Liu S, Suragani RNVS, Wang F, et al. The function of heme-regulated eIF2α kinase in murine iron homeostasis and macrophage maturation. *The Journal of Clinical Investigation*. 2007;117(11):3296-3305.
32. Fillebeen C, Wilkinson N, Charlebois E, Katsarou A, Wagner J, Pantopoulos K. Hepcidin-mediated hypoferremic response to acute inflammation requires a threshold of Bmp6/Hjv/Smad signaling. *Blood*. 2018;132(17):1829-1841.
33. Ganz T. Iron and infection. *Int J Hematol*. 2018;107(1):7-15.
34. Charlebois E, Pantopoulos K. Iron overload inhibits BMP/SMAD and IL-6/STAT3 signaling to hepcidin in cultured hepatocytes. *PLoS One*. 2021;16(6):e0253475.
35. Sia AK, Allred BE, Raymond KN. Siderocalins: Siderophore binding proteins evolved for primary pathogen host defense. *Curr Opin Chem Biol*. 2013;17(2):150-157.
36. Doherty CP. Host-Pathogen Interactions: The Role of Iron. *The Journal of Nutrition*. 2007;137(5):1341-1344.
37. Sazawal S, Black RE, Ramsan M, et al. Effects of routine prophylactic supplementation with iron and folic acid on admission to hospital and mortality in preschool children in a high malaria transmission setting: community-based, randomised, placebo-controlled trial. *The Lancet*. 2006;367(9505):133-143.

38. Chandra RK. Nutritional deficiency and susceptibility to infection. *Bull World Health Organ*. 1979;57(2):167-177.
39. Cherayil BJ. Iron and Immunity: Immunological Consequences of Iron Deficiency and Overload. *Arch Immunol Ther Exp (Warsz)*. 2010;58(6):407-415.
40. Yang F, Liu X-b, Quinones M, Melby PC, Ghio A, Haile DJ. Regulation of Reticuloendothelial Iron Transporter MTP1 (Slc11a3) by Inflammation *. *J Biol Chem*. 2002;277(42):39786-39791.
41. Liu X-B, Nguyen N-BH, Marquess KD, Yang F, Haile DJ. Regulation of hepcidin and ferroportin expression by lipopolysaccharide in splenic macrophages. *Blood Cells Mol Dis*. 2005;35(1):47-56.
42. Ludwiczek S, Aigner E, Theurl I, Weiss Gn. Cytokine-mediated regulation of iron transport in human monocytic cells. *Blood*. 2003;101(10):4148-4154.
43. Guida C, Altamura S, Klein FA, et al. A novel inflammatory pathway mediating rapid hepcidin-independent hypoferremia. *Blood*. 2015;125(14):2265-2275.
44. Preza GC, Ruchala P, Pinon R, et al. Minihepcidins are rationally designed small peptides that mimic hepcidin activity in mice and may be useful for the treatment of iron overload. *J Clin Invest*. 2011;121(12):4880-4888.
45. Ramos E, Ruchala P, Goodnough JB, et al. Minihepcidins prevent iron overload in a hepcidin-deficient mouse model of severe hemochromatosis. *Blood*. 2012;120(18):3829-3836.
46. Katsarou A, Pantopoulos K. Hepcidin Therapeutics. *Pharmaceuticals*. 2018;11(4):127.
47. Knutson M, Wessling-Resnick M. Iron Metabolism in the Reticuloendothelial System. *Critical Reviews in Biochemistry and Molecular Biology*. 2003;38(1):61-88.
48. Yiannikourides A, Latunde-Dada GO. A Short Review of Iron Metabolism and Pathophysiology of Iron Disorders. *Medicines*. 2019;6(3):85.
49. Nairz M, Weiss G. Iron in infection and immunity. *Mol Aspects Med*. 2020;75:100864.
50. Thorson JA, Smith KM, Gomez F, Naumann PW, Kemp JD. Role of iron in T cell activation: TH1 clones differ from TH2 clones in their sensitivity to inhibition of DNA synthesis caused by IgG Mabs against the transferrin receptor and the iron chelator deferoxamine. *Cell Immunol*. 1991;134(1):126-137.
51. Regis G, Bosticardo M, Conti L, et al. Iron regulates T-lymphocyte sensitivity to the IFN-γ/STAT1 signaling pathway in vitro and in vivo. *Blood*. 2005;105(8):3214-3221.
52. Regis G, Conti L, Boselli D, Novelli F. IFNγR2 trafficking tunes IFNγ–STAT1 signaling in T lymphocytes. *Trends Immunol*. 2006;27(2):96-101.
53. Oexle H, Kaser A, Möst J, et al. Pathways for the regulation of interferon-γ-inducible genes by iron in human monocytic cells. *Journal of Leukocyte Biology*. 2003;74(2):287-294.
54. Wang L, Johnson EE, Shi HN, Walker WA, Wessling-Resnick M, Cherayil BJ. Attenuated inflammatory responses in hemochromatosis reveal a role for iron in the regulation of macrophage cytokine translation. *The Journal of Immunology*. 2008;181(4):2723-2731.
55. Wu Q, Shen Y, Tao Y, et al. Hemojuvelin regulates the innate immune response to peritoneal bacterial infection in mice. *Cell discovery*. 2017;3:17028-17028.
56. Schleicher U, Hesse A, Bogdan C. Minute numbers of contaminant CD8+ T cells or CD11b+CD11c+ NK cells are the source of IFN-γ in IL-12/IL-18-stimulated mouse macrophage populations. *Blood*. 2005;105(3):1319-1328.

57. Wu Q, Sun CC, Lin HY, Babitt JL. Repulsive Guidance Molecule (RGM) Family Proteins Exhibit Differential Binding Kinetics for Bone Morphogenetic Proteins (BMPs). *PLoS One*. 2012;7(9):e46307.
58. Niederkofler V, Salie R, Sigrist M, Arber S. Repulsive Guidance Molecule (RGM) Gene Function Is Required for Neural Tube Closure But Not Retinal Topography in the Mouse Visual System. *The Journal of Neuroscience*. 2004;24(4):808-818.
59. Corradini E, Babitt JL, Lin HY. The RGM/DRAGON family of BMP co-receptors. *Cytokine Growth Factor Rev*. 2009;20(5):389-398.
60. Mirakaj V, Brown S, Laucher S, et al. Repulsive guidance molecule-A (RGM-A) inhibits leukocyte migration and mitigates inflammation. *Proceedings of the National Academy of Sciences*. 2011;108(16):6555-6560.
61. Xia Y, Cortez-Retamozo V, Niederkofler V, et al. Dragon (Repulsive Guidance Molecule b) Inhibits IL-6 Expression in Macrophages. *The Journal of Immunology*. 2011;186(3):1369-13